



## Review

## Review of solar energetic particle models

Kathryn Whitman<sup>a,b,\*</sup>, Ricky Egeland<sup>c</sup>, Ian G. Richardson<sup>d,e</sup>, Clayton Allison<sup>f</sup>, Philip Quinn<sup>f</sup>, Janet Barzilla<sup>f</sup>, Irina Kitiashvili<sup>g</sup>, Viacheslav Sadykov<sup>h</sup>, Hazel M. Bain<sup>i,j</sup>, Mark Dierckxsens<sup>k</sup>, M. Leila Mays<sup>d</sup>, Tilaye Tadesse<sup>f</sup>, Kerry T. Lee<sup>c</sup>, Edward Semones<sup>c</sup>, Janet G. Luhmann<sup>l</sup>, Marlon Núñez<sup>m</sup>, Stephen M. White<sup>n</sup>, Stephen W. Kahler<sup>n</sup>, Alan G. Ling<sup>o</sup>, Don F. Smart<sup>p</sup>, Margaret A. Shea<sup>p</sup>, Valeriy Tenishev<sup>l</sup>, Soukaina F. Boubrahimi<sup>r</sup>, Berkay Aydin<sup>h</sup>, Petrus Martens<sup>h</sup>, Rafal Angryk<sup>h</sup>, Michael S. Marsh<sup>s</sup>, Silvia Dalla<sup>t</sup>, Norma Crosby<sup>k</sup>, Nathan A. Schwadron<sup>u</sup>, Kamen Kozarev<sup>v</sup>, Matthew Gorby<sup>w</sup>, Matthew A. Young<sup>u</sup>, Monica Laurenza<sup>x</sup>, Edward W. Cliver<sup>y</sup>, Tommaso Alberti<sup>x</sup>, Mirko Stumpo<sup>z,x</sup>, Simone Benella<sup>x</sup>, Athanasios Papaioannou<sup>aa</sup>, Anastasios Anastasiadis<sup>aa</sup>, Ingmar Sandberg<sup>ab</sup>, Manolis K. Georgoulis<sup>ac</sup>, Anli Ji<sup>h</sup>, Dustin Kempton<sup>h</sup>, Chetraj Pandey<sup>h</sup>, Gang Li<sup>ad</sup>, Junxiang Hu<sup>ad</sup>, Gary P. Zank<sup>ad</sup>, Eleni Lavasa<sup>ae,aa</sup>, Giorgos Giannopoulos<sup>af</sup>, David Falconer<sup>ad,ag</sup>, Yash Kadadi<sup>ah</sup>, Ian Fernandes<sup>ai</sup>, Maher A. Dayeh<sup>aj,al</sup>, Andrés Muñoz-Jaramillo<sup>ak</sup>, Subhamoy Chatterjee<sup>ak</sup>, Kimberly D. Moreland<sup>al,aj</sup>, Igor V. Sokolov<sup>q</sup>, Iliia I. Roussev<sup>l</sup>, Aleksandre Taktakishvili<sup>am</sup>, Frederic Effenberger<sup>an</sup>, Tamas Gombosi<sup>q</sup>, Zhenguang Huang<sup>q</sup>, Lulu Zhao<sup>q</sup>, Nicolas Wijzen<sup>ao</sup>, Angels Aran<sup>ap</sup>, Stefaan Poedts<sup>ao,aq</sup>, Athanasios Kouloumvakos<sup>ar</sup>, Miikka Paassilta<sup>as</sup>, Rami Vainio<sup>as</sup>, Anatoly Belov<sup>at</sup>, Eugenia A. Eroshenko<sup>at,1</sup>, Maria A. Abunina<sup>at</sup>, Artem A. Abunin<sup>at</sup>, Christopher C. Balch<sup>j</sup>, Olga Malandraki<sup>aa</sup>, Michalis Karavolos<sup>aa</sup>, Bernd Heber<sup>au</sup>, Johannes Labrenz<sup>au</sup>, Patrick Kühl<sup>au</sup>, Alexander G. Kosovichev<sup>av,g</sup>, Vincent Oria<sup>av</sup>, Gelu M. Nita<sup>av</sup>, Egor Illarionov<sup>aw,ax</sup>, Patrick M. O'Keefe<sup>av</sup>, Yucheng Jiang<sup>av</sup>, Sheldon H. Ferreira<sup>av</sup>, Aatiya Ali<sup>h</sup>, Evangelos Paouris<sup>ay,az</sup>, Sigiava Aminalragia-Giamini<sup>ab,ae</sup>, Piers Jiggins<sup>ba</sup>, Meng Jin<sup>bb</sup>, Christina O. Lee<sup>l</sup>, Erika Palmerio<sup>bc</sup>, Alessandro Bruno<sup>d,am</sup>, Spiridon Kasapis<sup>q</sup>, Xiantong Wang<sup>q</sup>, Yang Chen<sup>q</sup>, Blai Sanahuja<sup>ap</sup>, David Lario<sup>d</sup>, Carla Jacobs<sup>bd</sup>, Du Toit Strauss<sup>be</sup>, Ruhann Steyn<sup>be</sup>, Jabus van den Berg<sup>be,bf</sup>, Bill Swalwell<sup>t</sup>, Charlotte Waterfall<sup>t</sup>, Mohamed Nedal<sup>v</sup>, Rositsa Miteva<sup>v</sup>, Momchil Dechev<sup>v</sup>, Pietro Zucca<sup>bg</sup>, Alec Engell<sup>bh</sup>, Brianna Maze<sup>bh</sup>, Harold Farmer<sup>bh</sup>, Thuha Kerber<sup>bh</sup>, Ben Barnett<sup>bh</sup>, Jeremy Loomis<sup>bh</sup>, Nathan Grey<sup>bh</sup>, Barbara J. Thompson<sup>d</sup>, Jon A. Linker<sup>bc</sup>, Ronald M. Caplan<sup>bc</sup>, Cooper Downs<sup>bc</sup>, Tibor Török<sup>bc</sup>, Roberto Lionello<sup>bc</sup>, Viacheslav Titov<sup>bc</sup>, Ming Zhang<sup>bi</sup>, Pouya Hosseinzadeh<sup>r</sup>

\* Corresponding author at: KBR, 601 Jefferson Street, Houston, TX 77002, USA.

E-mail address: [kathryn.whitman@nasa.gov](mailto:kathryn.whitman@nasa.gov) (K. Whitman).

<sup>1</sup> Deceased.

- <sup>a</sup> University of Houston, 4800 Calhoun Rd, Houston, TX 77204, USA  
<sup>b</sup> KBR, 601 Jefferson Street, Houston, TX 77002, USA  
<sup>c</sup> NASA Johnson Space Center, 2101 E NASA Pkwy, Houston, TX 77058, USA  
<sup>d</sup> NASA Goddard Space Flight Center, 8800 Greenbelt Rd, Greenbelt, MD 20771, USA  
<sup>e</sup> Department of Astronomy, University of Maryland, 4296 Stadium Dr., College Park, MD 20742, USA  
<sup>f</sup> Leidos, Inc., 555 Forge River Rd, Ste 150A, Webster, TX 77598, USA  
<sup>g</sup> NASA Ames Research Center, Mail Stop 204-14 Moffett Field, CA 94035, USA  
<sup>h</sup> Georgia State University, 25 Park Place NE, Atlanta, GA 30303, USA  
<sup>i</sup> CIRES, University of Colorado Boulder, 216 UCB, Boulder, CO 80309, USA  
<sup>j</sup> NOAA Space Weather Prediction Center, 325 Broadway, Boulder, CO 80305, USA  
<sup>k</sup> Royal Belgian Institute for Space Aeronomy, Ringlaan 3, B-1180 Brussels, Belgium  
<sup>l</sup> Space Sciences Laboratory, University of California at Berkeley, 7 Gauss Way, Berkeley, CA 94720, USA  
<sup>m</sup> University of Malaga, Av. de Cervantes, 2, 29016 Malaga, Spain  
<sup>n</sup> Air Force Research Laboratory, Space Vehicles Directorate, 3550 Aberdeen Avenue, Kirtland AFB, NM 87117, USA  
<sup>o</sup> Atmospheric Environmental Research, 3550 Aberdeen Ave. SE, Albuquerque, NM 87110, USA  
<sup>p</sup> SSSRC, 100 Tennyson Avenue, Nashua, NH 03062, USA  
<sup>q</sup> University of Michigan, 500 S. State Street, Ann Arbor, MI 48109, USA  
<sup>r</sup> Utah State University, 0500 Old Main Hill, Logan, UT 84322-0500, USA  
<sup>s</sup> Met Office, FitzRoy Road, Exeter, DevonEX1 3PB, UK  
<sup>t</sup> University of Central Lancashire, Fylde Rd, Preston, Lancashire PR1 2HE, UK  
<sup>u</sup> University of New Hampshire, 105 Main St, Durham, NH 03824, USA  
<sup>v</sup> Institute of Astronomy and National Astronomical Observatory, Bulgarian Academy of Sciences, 72 Tsarigradsko Chaussee Blvd., 1784 Sofia, Bulgaria  
<sup>w</sup> Cray Inc., 2131 Lindau Ln 1000, Bloomington, MN 55425, USA  
<sup>x</sup> INAF, Institute for Space Astrophysics and Planetology, via del Fosso del Cavaliere 100, 00133 Roma, Italy  
<sup>y</sup> National Solar Observatory, 3665 Discovery Dr 3rd, Boulder, CO 80303, USA  
<sup>z</sup> Università di Roma Tor Vergata, Via Cracovia, 50, 00133 Roma, Italy  
<sup>aa</sup> National Observatory of Athens, Institute for Astronomy, Astrophysics, Space Applications and Remote Sensing, Vas. Pavlou & I. Metaxa, GR-15 236 Penteli, Athens, Greece  
<sup>ab</sup> Space Applications & Research Consultancy (SPARC), Aiolou St. 73, 10551 Athens, Greece  
<sup>ac</sup> RCAAM of the Academy of Athens, 4 Soranou Efessiou Street, 115 27 Athens, Greece  
<sup>ad</sup> University of Alabama at Huntsville, 301 Sparkman Drive, Huntsville, AL 35899, USA  
<sup>ae</sup> National and Kapodistrian University of Athens, Athens 157 72, Greece  
<sup>af</sup> Athena Research Center, Επιδιοροφου και Αρτεμιδος, Marousi 151 25, Greece  
<sup>ag</sup> NASA Marshall Space Flight Center, Martin Rd SW, Huntsville, AL 35812, USA  
<sup>ah</sup> Stanford University, 450 Serra Mall, Stanford, CA 94305, USA  
<sup>ai</sup> Princeton University, P.O. Box 430, Princeton, NJ 08544, USA  
<sup>aj</sup> Southwest Research Institute, 6220 Culebra Road, San Antonio, TX 78238, USA  
<sup>ak</sup> Southwest Research Institute Boulder, 1050 Walnut St 300, Boulder, CO 80302, USA  
<sup>al</sup> University of Texas at San Antonio, 1 UTSA Circle, San Antonio, TX 78249, USA  
<sup>am</sup> Catholic University of America, 620 Michigan Ave NE, Washington, DC 20064, USA  
<sup>an</sup> University of California at Los Angeles, 405 Hilgard Avenue, Los Angeles, CA 90095, USA  
<sup>ao</sup> Department of Mathematics/Centre for Mathematical Plasma Astrophysics, KU Leuven, Celestijnenlaan 200 B 3001 Leuven, Leuven, Belgium  
<sup>ap</sup> Departament de Física Quàntica i Astrofísica, Institut de Ciències del Cosmos (ICCUB), Universitat de Barcelona, UB-IEEC, Martí i Franquès, 1 Barcelona, Spain  
<sup>aq</sup> Institute of Physics, University of Maria Curie-Skłodowska, ul.Radziszewskiego 10, 20-031 Lublin, Poland  
<sup>ar</sup> IRAP, 9 Av.du Colonel Roche, 31400 Toulouse, France  
<sup>as</sup> Department of Physics and Astronomy, FI-20014 University of Turku, Finland  
<sup>at</sup> Pushkov Institute of Terrestrial Magnetism, Ionosphere, and Radio Wave Propagation (IZMIRAN), Russian Academy of Sciences, 108840 Moscow Troitsk, Russia  
<sup>au</sup> IEAP, Christian-Albrechts-Universitaet, Leibnizstraße 11-19, 24118 Kiel, Germany  
<sup>av</sup> New Jersey Institute of Technology, 323 Dr Martin Luther King Jr Blvd, Newark, NJ 07102, USA  
<sup>aw</sup> Department of Mechanics and Mathematics, Moscow State University, Ulitsa Kolmogorova, 1, Moscow 119991, Russia  
<sup>ax</sup> Moscow Center of Fundamental and Applied Mathematics, Moscow 119234, Russia  
<sup>ay</sup> George Mason University, 4400 University Dr, Fairfax, VA 22030, USA  
<sup>az</sup> The Johns Hopkins University Applied Physics Laboratory, 11100 Johns Hopkins Rd, Laurel, MD 20723, USA  
<sup>ba</sup> European Space Research and Technology Centre (ESTEC), Space Environment and Effects Section Keplerlaan 1, 2200AG Noordwijk, the Netherlands  
<sup>bb</sup> Lockheed Martin Solar & Astrophysics Laboratory, 3176 Porter Dr, Palo Alto, CA 94304, USA  
<sup>bc</sup> Predictive Science Inc., , 9990 Mesa Rim Rd, Ste 170, San Diego, CA 92121, USA  
<sup>bd</sup> Space Applications Systems, 1932 Zaventem, Belgium  
<sup>be</sup> Centre for Space Research, North-West University, Building G5, Potchefstroom Campus, North-West University, Potchefstroom, South Africa  
<sup>bf</sup> South African National Space Agency, Hospital St, Hermanus 7200, South Africa  
<sup>bg</sup> ASTRON, The Netherlands Institute for Radio Astronomy, Oude Hoogeveensedijk 4, 7991 PD Dwingeloo, the Netherlands  
<sup>bh</sup> NextGen Federal Systems, 1399 Stewartstown Road, Suite 350, Morgantown, WV 26505, USA  
<sup>bi</sup> Florida Institute of Technology, 150 W University Blvd, Melbourne, FL 32901, USA

Received 31 March 2022; received in revised form 29 July 2022; accepted 3 August 2022

## Abstract

Solar Energetic Particle (SEP) events are interesting from a scientific perspective as they are the product of a broad set of physical processes from the corona out through the extent of the heliosphere, and provide insight into processes of particle acceleration and transport that are widely applicable in astrophysics. From the operations perspective, SEP events pose a radiation hazard for aviation, electronics in space, and human space exploration, in particular for missions outside of the Earth's protective magnetosphere including to the Moon and Mars. Thus, it is critical to improve the scientific understanding of SEP events and use this understanding to develop and improve SEP forecasting capabilities to support operations. Many SEP models exist or are in development using a wide variety of approaches and with differing goals. These include computationally intensive physics-based models, fast and light empirical models, machine learning-based models, and mixed-model approaches. The aim of this paper is to summarize all of the SEP models currently developed in the scientific community, including a description of model approach, inputs and outputs, free parameters, and any published validations or comparisons with data.

© 2022 COSPAR. Published by Elsevier B.V. This is an open access article under the CC BY license (<http://creativecommons.org/licenses/by/4.0/>).

**Keywords:** Space radiation; Solar energetic particles; Space weather models; Space weather forecasting; SEP models

## 1. Introduction

Solar Energetic Particle (SEP) events are transient injections into the heliosphere of protons, electrons, and higher mass charged particles with a wide range of energies (tens of keVs to GeVs), spectra, composition, and intensities. They follow energetic solar eruptions that are generally associated with flares and Coronal Mass Ejection (CME) s. They are apparently accelerated by processes associated with flares, such as wave-particle interactions and reconnection, as well as by acceleration at CME-driven shocks (for reviews, see e.g., [Shea and Smart, 1990](#); [Reames, 2004](#); [Reames, 2017](#); [Desai and Giacalone, 2016](#); [Klein and Dalla, 2017](#)). As has long been recognized since at least the Apollo era ([Hilberg, 1969](#)), SEP events are hazardous to electronics (e.g., [Iucci et al., 2005](#)) and humans in space. As humans pursue space exploration outside of low Earth orbit, the understanding, monitoring, and forecasting of SEP events becomes increasingly important (e.g., [Kim et al., 2011](#)). SEPs are also hazardous to aircraft crews, in particular on polar routes ([Jones et al., 2005](#)), and to modern technological systems ([Eastwood et al., 2017](#)). Thus, in the last two decades, government agencies around the world have developed policies related to space weather, including the need for improved forecasting of SEP events ([Guarnieri et al., 2005](#); [Opgenoorth et al., 2019](#); [National Science & Technology Council, 2019](#)). Plans for the National Aeronautics and Space Administration (NASA) Artemis missions to send astronauts back to the Moon in the mid-2020s are providing further motivation to improve SEP forecasting.

Efforts to predict SEP events have a long history (e.g., [Smart et al., 1979](#)). At present, three dozen SEP models have been or are being developed in the scientific research community, as listed in [Table 1](#). These models use a variety of approaches: Empirical models are based on the identifi-

cation of correlations and other relationships in observational data that may be related to the underlying physical processes. They typically give rapid forecasts and are easily incorporated into forecasting and operations. Such models might give a binary “all clear” or “not all clear” prediction, representing the confidence that an event of a given magnitude *will not* or *will* occur during a given forecast window, the probability that an event of a certain intensity will occur, or deterministic quantities (e.g., onset time, the peak flux at a certain energy). Physics-based models use our current understanding of the processes of particle acceleration and transport at the Sun and in interplanetary space to model these processes and predict the properties of the associated SEP event. Most of these models are computationally intensive, and the ability to produce a prediction “in real time” may be limited by the resources available, so they may not be readily incorporated into a forecasting workflow. In addition, fundamental parameters required by the model may be poorly characterized. However, these complex models hold the promise of modeling the complete distribution of SEP events with time in 2- or 3-dimensional space. Machine Learning (ML) approaches are now being investigated in the hope that they will yield a new class of SEP models that will produce fast forecasts with improved accuracy. Lastly, multi-module forecasting systems link existing models of multiple types to create a chain that feeds forecasts from one module to the next that can be updated as real time measurements become available, e.g. a flare forecast module passes information to a CME forecast module which then passes parameters to produce a final SEP forecast. All of the models described here focus on the prediction of SEP protons, as these are the most abundant particles and the largest contributors to space radiation. Many of the physics-based models have the added capability to investigate the behavior of SEP ions and electrons, which allows them to probe the details of

Table 1

Solar energetic particle models. For any models without an entry in the Access column, we encourage interested readers to contact the model developer. RoR stands for Runs on Request available through CCMC. \*Deployment to CCMC in progress, \*\*Will be available on SEP Scoreboard and RoR.

Model	Model Type	Access to Model	Reference
ADEPT	Empirical	-	Kahler and Ling (2017)
AFRL PPS	Empirical	-	Smart et al. (1979, 1989, 1992)
Aminalragia-Giamini model	ML	-	Aminalragia-Giamini et al. (2021)
AMPS	Physics-based	CCMC RoR	Tenishev et al. (2021)
Boubrahimi model	ML	-	Boubrahimi et al. (2017)
COMESSEP SEPFforecast	Empirical & Physics-based	Web	Dierckxens et al. (2015), Marsh et al. (2015)
EPREM	Physics-based	-	Schwadron et al. (2010)
ESPERTA	Empirical & ML	-	Laurenza et al. (2009, 2018), Stumpo et al. (2021)
FORSPEF	Empirical	Web	Anastasiadis et al. (2017)
Georgia State University	ML	Web	Ji et al. (2020.)
iPATH	Physics-based	CCMC RoR**	Hu et al. (2017)
Lavasa Model	ML	-	Lavasa et al. (2021)
MAG4	Empirical	Web, CCMC RoR, SEP Scoreboard	Falconer et al. (2011, 2014)
MagPy	Empirical	-**	Tadesse, T., Fernandes, I., Kadadi, Y., Lee, K. T., and Falconer, D.
MEMPSEP	ML	-	Moreland et al. 2022, Chatterjee et al. 2022, Dayeh et al. 2022 (all in preparation)
M-FLAMPA	Physics-based	CCMC RoR*	Sokolov et al. (2004), Borovikov et al. (2015)
PARADISE	Physics-based	Web	Wijzen (2020, 2022)
PCA (Papaioannou) model	Empirical	-	Papaioannou et al. (2018)
PHSVM	ML	-	Pouya Hosseinzadeh, Soukaina Filali Boubrahimi
PROTONS	Empirical	-	Balch (1999, 2008)
REleASE	Empirical	Web, SEP Scoreboard	Posner, 2007; Malandraki et al., 2020
Sadykov et al. (2021) model	ML	-	Sadykov et al. (2021)
SAWS-ASPECS	Empirical	Web, SEP Scoreboard	Anastasiadis et al. (2017), Georgoulis et al. (2021), Papaioannou et al. (2022)
SEPCaster	Physics-based	-*	Li et al. (2021)
SEPMOD	Physics-based	CCMC RoR, SEP Scoreboard	Luhmann et al. (2007)
SEPSTER	Empirical	SEP Scoreboard	Richardson et al. (2018)
SEPSTER2D	Empirical	SEP Scoreboard	Bruno and Richardson (2021)
SMARP Model	ML	-	Kasapis et al. (2022)
SOLPENCO(2)	Physics-based	-	Aran et al. (2006), Aran et al. (2011), Aran et al. (2017)
South African model	Physics-based	Web	Strauss and Fichtner (2015)
SPARX	Physics-based	Web	Marsh et al. (2015)
SPREAdFAST	Physics-based	Web	Kozarev et al. (2017), Kozarev et al. (2022)
SPRINTS	ML	SEP Scoreboard	Engell et al. (2017)
STAT	Physics-based	CCMC RoR	Linker et al. (2019)
UMASEP	Empirical & ML	Web, SEP Scoreboard	Núñez (2011, 2015), Núñez et al. (2017), Malandraki et al. (2020)
Zhang model	Physics-based	-	Zhang and Zhao (2017)

particle acceleration and transport. The aim of this paper is to bring together brief summaries of these models in order to provide a comprehensive survey of the current state of SEP event prediction.

In general terms, SEP models have been motivated either by research aimed at understanding the physical processes related to SEPs or by operational forecasting needs. Science-oriented models typically use all historical measurements available to fine-tune their model parameters with the goal of reproducing all aspects of a specific event as accurately as possible. The tuned model parameters then provide insight into the underlying physics.

Models built with a forecasting focus attempt to produce a rapid forecast with high levels of skill and reliability in a statistical sense. The model inputs are restricted to data streams that are available in real time, and typically, forecasts are made using only information that is accessible before or at the start of an SEP event. *For this reason, it is critical that operationally supported, high-cadence, reliable and accurate space weather data streams for all phenomena relevant to SEP production are publicly available for operations and the deployment and development of forecasting models.* The measurements used by the models discussed in this paper include: solar magnetograms, optical imaging,

extreme ultraviolet (EUV) imaging, Soft X-ray (SXR) measurements, coronagraph imaging of CMEs from single or multiple vantage points, ground and space-based radio observations in the wavelengths that measure Type II, III, and IV radio bursts, in situ energetic proton and electron observations, and in situ measurements of solar wind density, temperature, velocity, and magnetic field. See [Vourlidas et al. \(2021\)](#) for a description of the current state of space weather measurements and anticipated gaps in the future.

[Table 1](#) lists all of the SEP models that the authors are aware of at the time of writing. An overview of different model types will be described in the Overview (Section 2). The models will be described in further detail in Model Descriptions (Section 3). The paper concludes with a comprehensive summary and outlook for future model development (Section 4). [Appendix A](#) defines the acronyms used throughout this paper.

## 2. Overview of current SEP prediction models and their approaches

### 2.1. Typical model inputs

SEP events originate with eruptions within the solar corona that are typically associated with filament eruptions, flares, and CMEs. As noted above, particle acceleration appears to occur both via processes associated with flares low in the corona and by diffusive shock acceleration at the shock fronts of CMEs as they propagate outward into the heliosphere; acceleration at CME-driven shocks appears to dominate in the large SEP events that are of most space weather concern (e.g., [Desai and Giacalone, 2016](#)). The most prompt and most intense SEP events measured at Earth, and hence the most important to forecast, are usually associated with strong flares and fast CMEs at western longitudes that are well-connected to Earth by the spiral interplanetary magnetic field ([Parker, 1965](#)). Magnetic connectivity to the particle source (flare/CME shock) also strongly influences the development and intensity of an SEP event (e.g., [Cane et al., 1988](#); [Cane and Lario, 2006](#); [Richardson et al., 2014](#); [Bain et al., 2016](#)). The intensity of an SEP event is also generally correlated with parameters (e.g., intensity, duration) of the associated SXR flare and speed of the CME (e.g. [Kahler et al., 1984](#); [Cane et al., 2010](#), etc). Hence, flare or CME parameters are frequently used as inputs into SEP prediction models. Flare parameters are particularly widely used as solar X-rays are continually monitored and available in near-real time, for example from the Geosynchronous Orbit Earth observing Satellite (GOES) spacecraft, and the onset of a flare is well-defined and may be closely associated with the eruption of a CME and onset of particle acceleration. The flare location may be identified for example in EUV observations. However, SEP events detected at Earth occasionally originate on the far side of the Sun, in particular behind the west

limb [e.g.,  $\sim 25\%$  of the SEP events discussed by [Richardson et al. \(2014\)](#)] and therefore the flare will not be observed in these cases. While the CMEs from such events may be detected by spacecraft coronagraphs, currently, images from coronagraphs on scientific spacecraft such as Solar and Heliospheric Observatory (SOHO)/Large Angle and Spectrometric Coronagraph Experiment (LASCO) and Solar TERrestrial RELations Observatory (STEREO)/Sun Earth Connection Coronal and Heliospheric Investigation (SECCHI) are not available sufficiently rapidly for real-time forecasting; delays in receiving and analyzing these images to obtain CME parameters may range from hours to even days. Even though models using CME parameters as input may not be suitable for predicting the onsets of prompt SEP events, they are valuable for assessing the use of future near-real time white light coronagraph observations, such as the Compact Coronagraph (CCOR) on the National Oceanic and Atmospheric Administration (NOAA) Space Weather Follow On - Lagrange 1 (SWFO-L1) spacecraft scheduled to launch in 2025, for SEP prediction.

Solar radio observations result from nonthermal electrons and provide another indication of particle acceleration. Bursts at frequencies below a few hundred MHz generally result from plasma emission, which occurs at a frequency related to the plasma density (e.g., [Wild et al., 1963](#); [Nelson and Melrose, 1985](#)). In particular, Type II radio emission that slowly drifts downward in frequency with time is believed to indicate particle acceleration at a shock moving away from the Sun towards lower densities (e.g., [Nelson and Melrose, 1985](#)). Type III radio bursts with much faster drift rates are signatures of energetic electron beams traveling out from the Sun, having been accelerated at a flare site lower in the corona. Both type II and type III emissions are found to be strongly correlated with the occurrence of SEP events (e.g., [Cane et al., 2002](#); [Cliver et al., 2004](#); [Laurenza et al., 2009](#); [Richardson et al., 2014](#); [Papaioannou et al., 2016](#); [Richardson et al., 2018](#)). Solar radio emissions at frequencies above the ionospheric cutoff at about 10 MHz are monitored in real time from the ground by a world-wide network of observatories. However, observations below  $\sim 20$  MHz are difficult due to the ionospheric cut-off, terrestrial interference, and emission from lightning (e.g., [Erickson, 1997](#)). Observations from space-based satellite radio science instruments such as those on WIND, STEREO, Parker Solar Probe (PSP) and Solar Orbiter (SO) can extend to lower frequencies. Unfortunately, data from these scientific spacecraft are not generally available in real time since they were not designed to be operational instruments, and often have very limited telemetry. Because the emission frequency of radio bursts tends to decrease with distance from the Sun, ground-based radio observations provide information on particle acceleration close to the Sun, while spacecraft instruments cover emissions produced in the high corona and solar wind out to the distance of the observing spacecraft.

Models may also use near-real time energetic particle observations as an input. For example, near-relativistic/relativistic SEP electrons may arrive at Earth tens of minutes earlier than, and provide a warning of the impending arrival of, protons with energies of tens of MeV that are of space weather interest (Posner, 2007; Malandraki et al., 2020). The initial rise of the SEP proton intensity may also be used as an early predictor that the intensity may cross a specific threshold of concern (Núñez, 2011).

As will be evident from the model descriptions in Section 3, many SEP forecasting models use one or a combination of these phenomena as inputs into the model. Predicting the largest events of most concern also benefits from what has historically been called the “big flare syndrome”, originally stated by (Kahler, 1982) as “statistically, energetic flare phenomena are more intense in larger flares, regardless of the detailed physics”. In other words (and with less emphasis specifically on flares), the most energetic eruptions are associated with the most intense signatures in a range of related phenomena which may be predictive of a large SEP event even if they have no direct physical connection with the particle acceleration process.

## 2.2. Empirical models

Empirical models are based on approaches that use samples of existing data (e.g., for many historical SEP events) such as those discussed above to discover and characterize (e.g., as mathematical expressions) patterns or relationships between the properties of SEP events and other observable parameters. These models implement correlative relationships that are often guided by the known physical processes behind SEP generation (e.g., Posner, 2007; Richardson et al., 2018). Empirical models may produce:

- probabilistic forecasts, e.g., indicating the probability that an SEP event of a certain intensity will occur in a particular time frame (e.g., Falconer et al., 2011; Papaioannou et al., 2018),
- categorical forecasts, such as the NOAA S-scale<sup>2</sup> with defined thresholds for peak  $\geq 10$  MeV proton flux intensity (e.g., Laurenza et al., 2009),
- binary (yes/no) “all clear” forecasts that an event exceeding a specified threshold will or will not occur (e.g., Boubrahimi et al., 2017; Sadykov et al., 2021), or
- deterministic quantities, e.g., time of event onset or peak in a certain energy range, SEP peak intensity/flux, or the event-integrated intensity (fluence) (e.g., Balch, 1999; Bruno and Richardson, 2021).

Because the relationships established from previous data are generally mathematical functions that can be computed quickly, predictions can be made rapidly by applying them

to current observations. Validation statistics and skill scores for many empirical models have been reported in the literature. As is evident from Table 1, a large fraction of current SEP prediction models are based on empirical methods.

## 2.3. Physics-based models

Physics-based SEP models have typically been developed with the primarily scientific motivation to understand the physical processes that produce SEP events, rather than to generate a fast forecast. Some physics-based model developers have begun research to operations efforts to modify their models for real time forecasting purposes, but this work is still in the early stages. In general, these models aim to numerically reproduce the relevant physics related to particle acceleration: the magnetic structure of the low corona, eruption mechanisms for flares and CMEs, particle acceleration associated with flares and at CME-driven shocks, magnetic field connections in the inner heliosphere to the solar event and shock, the properties of the evolving CME shock, and the transport of particles near the Sun and in the heliosphere. Each of these processes may in itself be the subject of intense study, and not fully understood, so combining them into a full model of SEP prediction is extremely challenging, and modelers may choose to simplify certain aspects of the problem or incorporate an empirical component. In addition, fundamental parameters for these processes may be unknown, for example, because they are difficult to observe (in particular when close to the Sun), are difficult to estimate (e.g., from theory), or apparently vary in time and space (e.g., from event to event) in a way that cannot be predicted before an event occurs.

A physics-based SEP modeling method might (1) define the magnetic field connectivity from the corona through the heliosphere to the observer, (2) simulate the source region responsible for particle acceleration, (3) inject test particles or a particle distribution function into the system, and (4) transport the particles from the source to the observer. The magnetic connectivity modeling system may consist of two main parts: An inner coronal module including a semi-empirical near-Sun model, such as Wang-Sheeley-Arge (WSA) (Arge and Pizzo, 2000) or Magneto-hydrodynamic Algorithm outside a Sphere (MAS) (Linker et al., 2019), that approximates the outflow at the base of the solar wind; and a heliospheric module including a sophisticated three-dimensional magneto-hydrodynamic numerical model, like ENLIL (Odstrcil, 2003), Alfvén-wave-turbulence-based solar atmosphere Model (AWSoM) (Sokolov et al., 2021) or European Heliospheric FORecasting Information Asset (EUHFORIA) (Pomoell and Poedts, 2018), that simulates the resulting solar wind flow evolution out to some outer boundary. The inner coronal module may be driven by observations of the solar surface magnetic field accumulated over a solar rotation and composited into a synoptic

<sup>2</sup> <https://www.swpc.noaa.gov/noaa-scales-explanation>.

map. CMEs can be included in time-dependent heliospheric models, such as ENLIL + Cone (Odstrcil et al., 2004) or AWSOM + Eruptive Event Generator using Gibson-Low configuration (EEGGL) (Jin et al., 2017), with the parameters of the injected CMEs derived from coronagraph images. Such models may be used to simulate the shock driven by a CME, including how the shock parameters vary along the shock as it moves out through the corona and solar wind, and to infer the connectivity between the shock and the observer.

Understanding particle acceleration at shocks is still an area of active research and, because of the complexity of the problem, SEP prediction models often make certain assumptions. Some physics-based models, like Solar Energetic Particle MODel (SEPMOD) (Luhmann et al., 2007), assume that the compression regions and shocks that form ahead of CMEs are the only acceleration regions for SEPs. Models such as Multiple Field Line Advection Model for Particle Acceleration (M-FLAMPA) (Sokolov et al., 2004) may require the injection of a suprathermal seed particle population into the shock that is then accelerated according to diffusive shock acceleration theory. However, the seed particle population, especially near the Sun, is poorly characterized (see Tylka and Lee, 2006; Neergaard Parker and Zank, 2012), though observations of suprathermal ion populations observed at 1 AU prior to an SEP event might be used (with suitable scaling) as a proxy for those closer to the Sun. The shock-accelerated particles may then be transported along magnetic field lines, for example by solving the focused-transport equation (Zhang, 2006; Schwadron et al., 2010) or by using a numerical simulation of particle transport that might include parallel and cross-field diffusion, advection with the solar wind, adiabatic cooling, and drifts (e.g., Zhang and Zhao, 2017; Hu et al., 2017). Alternately, a model may assume that particles are detected by an observer only when directly magnetically connected to the shock, as seen in SEPMOD (Luhmann et al., 2007). Physics-based models also face challenges in reproducing SEP intensity profiles both in time and 2- or 3-dimensional space. Some models attempt to reproduce the Energetic Storm Particle (ESP) component of the event that occurs when a CME shock front passes the observer tens of hours after the solar eruption (e.g., SEPMOD), while others may focus on the early stages of the SEP event when particle acceleration occurs close to the Sun and the onset of the SEP event might be modeled by a simple particle injection at the Sun (e.g., Linker et al., 2019).

An issue with all physics-based SEP models is that they have many poorly constrained free parameters such as the choice of particle diffusion coefficients, the seed population spectral shape and normalization, how to “tune” the solar wind model solution to match measurements (e.g., at Earth), and which specific magnetic field line to select to produce a prediction of the particle spectrum at the observer’s location. New observations may help to constrain some of these parameters. For example, an improved

knowledge of the suprathermal seed population in the inner heliosphere and in particular close to the Sun prior to an SEP event would benefit all physics-based models. Measurements close to the sun by PSP (Desai et al., 2020) and at high latitudes by SO should help to characterize the suprathermal ion population and its variability in these regions, at least in a statistical sense, since these observations will not be available in real time to contribute to SEP predictions.

The placement of the inner boundary of the coronal/solar wind model is also a limitation in some physics-based models. Particle acceleration at the beginning of an SEP event is known to happen deep down in the solar corona, below  $2 R_{\odot}$  (Mäkelä et al., 2015) whereas many model inner boundaries are located further from the Sun, e.g., at  $10 R_{\odot}$  for ZEUS or  $21.5 R_{\odot}$  for ENLIL. Hence, it is not feasible for such models to predict the onset phase of an SEP event. Coronal and solar wind models that are computationally tractable lower in the solar corona would benefit all physics-based SEP models.

Because of their complexity, physics-based models may face significant computational challenges in terms of the resources needed to store the large amount of data generated during the simulation and the time needed to complete a model run. Hence, reported simulations are generally aimed at reproducing a limited number of past events, with a focus on understanding the physics involved and the reasons for event-to-event variations. There are rather few cases where physics-based models have been used without “tuning” to make predictions of future events, i.e., without prior information on the properties of the SEP that results. Also, comparisons with measurements reported in the literature have generally been qualitative rather than quantitative.

#### 2.4. Machine learning models

ML approaches to SEP prediction use a variety of ML/Artificial Intelligence (AI) techniques to identify specific combinations of observed parameters, such as those in Section 2.1, that are associated with/precede an SEP event. As such, they are similar to empirical models in that they are based on existing data, but rely on ML/AI to identify relationships between SEP events and other parameters in (ideally) large data sets without any a priori knowledge of the physics involved. The aim is to discover relationships that might not otherwise be evident from a simple analysis of these data. Typically, the data are divided into a “training set”, used to develop the ML/AI model, and a “validation set” which is used to assess, for example, whether the model reliably reproduces the observed properties of SEPs in this set. As for empirical models, the outputs may be probabilistic, categorical, binary or deterministic. Examples of ML models for binary predictions of whether an SEP event will exceed certain energy and particle flux thresholds (e.g.,  $>100$  MeV,  $>1$  pfu) utilize the X-ray and proton channels, and proton channel cross-correlations

from GOES (Boubrabimi et al., 2017), solar radio flux measurements using statistical analysis, neural networks, and genetic algorithms (Kim et al., 2018), and the properties of SXR flares and CMEs employing an ensemble of forecasts (Huang et al., 2012). Many current research efforts are focused on validating ML algorithms to perform reliable SEP nowcasts and forecasts. The cross-comparison of operational forecasts of SEP events also can provide additional validation of ML-driven models. This capability has become available recently through the Community Coordinated Modeling Center (CCMC) SEP Scoreboard<sup>3</sup>, which aims to bring together forecasts from a range of prediction models for current and historical events (although ML models have yet to be onboarded). Studies comparing ML-driven model predictions with the NOAA Space Weather Prediction Center (SWPC) daily operational forecasts and warnings for SEP events may identify weak points in the models and point to potential improvements (e.g., Jeong et al., 2014; Sadykov et al., 2021).

ML/AI-based models face unique challenges related to the preparation of reliable, uniform observational databases for model development and validation, and the efficient validation and verification of new models. Such considerations have motivated the development of publicly-available frameworks and ML-ready data sets (Engell et al., 2017; Martens et al., 2018). Other problems are related to the statistics and physics of SEP events. While ML/AI can harness the predictive power of massive multidimensional data analysis, a major challenge is the rarity of SEP events, leading to a significant imbalance of days with enhanced SEP proton fluxes and ‘quiet’ days. For example, during Solar Cycle (SC) 24, the number of days when the >10 MeV proton flux was above a threshold of 10 pfu (101 days) was about 34 times less than the number of days with a non-enhanced proton flux (3400 days) (Sadykov et al., 2021). This class imbalance ratio eliminates the possibility of using data-hungry ML algorithms directly and requires additional strategies for model training (Ahmadzadeh et al., 2021). Other challenges may include the widespread time delay (from minutes to hours) between the first detection of the SEP event and the onset of the preceding associated solar flare, which may lead to incorrect SEP-flare associations resulting in inaccurate model training or validation, missing information about host active regions in models using active region parameters, and the lack of observations of the sources of SEP events originating on the far side of the Sun.

### 2.5. Multi-module forecasting systems

Some models take an approach that chains multiple forecast modules together, with the prediction from each module feeding into the next. For example, the first module might use magnetograms or EUV imagery of an active

region to generate a prediction of the likelihood that a flare of a certain class will occur in that region. This prediction, together with the flare information, is passed to a module that predicts the likely parameters of the CME that might accompany the flare. The CME information is then input into a final module that predicts parameters of the potential SEP event. When an eruptive event does occur, each module ingests the required flare, CME, or proton flux observations as they become available and updates the prediction that is passed to the downstream module.

Multi-module systems tend to take advantage of mature models that are already developed and can be linked together so that the output from one model can trigger another. They may also combine models of different types, e.g., empirical, machine learning, and physics-based, exploiting the strengths of each type of model and providing a broader-based prediction of an event.

### 2.6. Model validation

In the “Validation” subsection for each model described in Section 3, published validation results are summarized. Some models have performed extensive quantitative validation studies, while others may have simply performed qualitative comparisons with observations for a few test cases. Some models have not yet published any validation. In the Conclusions (Section 4), we will describe our vision for steps that can facilitate more consistent validation across the SEP modeling field.

Throughout the validation sections, there are mentions of many types of metrics and plots typically used for validation. We refer the reader to papers by Liemohn et al. (2021) and Bain et al. (2021) for descriptions and explanations of the commonly used metrics and skill scores and their application and interpretation.

## 3. Model descriptions

This section summarizes the 36 SEP prediction models in Table 1 presented in alphabetical order. For each model, we specify the model developers, an overall description of the model, inputs, outputs, any free parameters, limitations and caveats related to the model, how data or predictions from the model may be accessed, and a summary of any validation efforts. The descriptions and results given here are intentionally brief and contain a limited number of figures or data tables. Interested readers should refer to the cited references for more details.

The terms “forecasting” and “nowcasting” are regularly used throughout the model descriptions. “Forecasting” typically indicates a model prediction that is made prior to any eruptive event on the Sun, e.g. a flare or CME, although it may mean a prediction issued prior to an increase in particle flux. “Nowcasting” is typically applied when predictions have been made directly following a flare, CME, or observed increase in particle flux at 1 AU. “Prediction” is used as a general term that is equivalent to a

<sup>3</sup> <https://ccmc.gsfc.nasa.gov/challenges/sep.php>.



model producing output. “Prediction” may indicate model output for a historical event or in the context of forecasting or nowcasting.

### 3.1. ADEPT - Air Force Dynamic Energetic Particle Tool

**Model developers:** Stephen M. White and Stephen W. Kahler (Air Force Research Laboratory), Alan G. Ling (Atmospheric Environmental Research).

**Model description:** The Air Force Dynamic Energetic Particle Tool (ADEPT) predicts the peak flux from solar particle events by fitting functional forms to the rise phase once energetic protons start arriving at Earth (or any other location). Either Weibull or log-normal functions can be used, as discussed by Kahler and Ling (2017). The current version uses Weibull functions. The fits consistently tend to under-predict the peak during the early rise phase, but an empirical analysis has determined factors as a function of time that can correct for the under-prediction in real time.

**Inputs:** Current inputs are the GOES 5-min measurements of energetic protons: the initial version focuses on >10 MeV protons, and fits for >30, >50 and >100 MeV protons are being implemented. The longitude of the associated solar event is also used, if available, to determine the parameters of the functional form during the rise phase. Fitting starts once the proton flux exceeds a threshold (0.6 pfu for >10 MeV) and is  $5\sigma$  above the background trend.

**Outputs:** On receipt of a new data point every 5 min, a new functional fit is carried out, providing an estimate of the peak flux and fluence together with an estimate of the uncertainty in the prediction. Once the peak of the event has been reached, the overall timescale for the event is also predicted.

**Free parameters:** The functional forms both have 4 free parameters: 2 shape parameters, a “zero” time (since the functions are distribution functions that are only valid for non-negative arguments), and an amplitude. The shape parameters of the functions need to be fixed in the rise phase in order to achieve successful fits, so for the first 2 h the only free parameter is the amplitude of the event. Thereafter the zero time is also fitted, which allows improved fits for irregular light curves. Once the event has peaked, a shape parameter that reflects the timescale of the event can also be fitted.

**Limitations and caveats:** The intent of ADEPT is to provide a prediction as soon as possible after a solar proton event starts, and to improve that prediction as more data is acquired. This drives the fitting choices described above. Thus, ADEPT provides a prediction of the peak flux of an event that continuously evolves with time during the rise phase.

**Access to model output or forecasts:** This model is under development and is not available to the public.

**Model validation:** A sample of 82 SEP events chosen from the 1986–2017 period was used to determine the empirical correction factor as a function of time. The cur-

rent metric for validation is the uncertainty in the predicted peak, determined from the spread of the predictions for the event sample. This metric also evolves with time, ranging from a factor of 5 at the 1-h point after event onset, down to a factor of less than 2 at the 6-h point. Validation is being carried out on new-cycle SEP events as they occur.

### 3.2. AFRL PPS - Air Force Research Laboratory Proton Prediction System

**Model developers:** Don F. Smart and Margaret A. Shea (developed at the Air Force Geophysics Laboratory).

**Model description:** The Air Force Research Laboratory (AFRL) Proton Prediction System (PPS) model is a post-eruption model that uses the flare fluence, peak time, peak intensity, and location in order to predict the SEP onset time, peak time, peak intensity, and end time (Smart et al., 1979, 1989, 1992). The predictions are made for 1 AU and for proton energies of >5 MeV, >10 MeV, and >50 MeV. From these quantities, a simplistic time profile prediction can be created. The goal in developing this model was to provide a forecast of the expected solar proton flux within 10 min after the data became available to the operator in the forecast center.

The basis of the PPS model are correlations between SEP events from Interplanetary Monitoring Platform (IMP) satellites and associated flares Smart et al. (1979, 1989, 1992). SEPs are assumed to be accelerated at the flare location 0.25 h after the flare onset. The time between the flare onset and SEP onset is predicted based on the results from Barouch et al. (1971) which found a relation to flare longitude. The time to peak intensity is also based on a relationship with flare longitude which was reported in Van Hollebeke et al. (1975). For protons of  $E > 10$  MeV, this relationship is given in Kahler et al. (2007) as:

$$T_{max}(h) = A \times \Theta^2 + 2.7. \quad (1)$$

where  $\Theta$  is the longitudinal angular displacement in radians of the flare site from the Earth’s magnetic footpoint and  $A$  is an asymmetric factor dependent upon flare longitude. The end time is based on Roelof. (1969) which discussed the transport of particles in interplanetary space. A few simplifying assumptions are made here.

- The particles travel along the Interplanetary Magnetic Field (IMF) with a velocity which is a function of particle energy.
- Perpendicular diffusion is ignored.
- The minimum distance to travel from the Sun to Earth is along the Parker spiral.

From these assumptions and results, the model uses a  $1/e$  decay function to predict the end time.

PPS calculates the peak intensity of the proton flux, at the optimum connection at  $W57.3^\circ$  (Kahler et al., 2007), as

$$J(E > 10MeV) = 30.67 \times (F_{XW} \times \Delta T)^{1.327} \quad (2)$$

where  $F_{XW}$  is the GOES peak 1–8 Å X-ray flare flux in ergs and  $\Delta T$  is the X-ray flare rise time from onset to peak in min. The same value can be found using the flare half-power fluence,  $F_x$ , as

$$J(E > 10\text{MeV}) = 347 \times (F_x)^{0.941}. \quad (3)$$

**Inputs:** The inputs for the PPS model are flare fluence or peak flux, flare location, flare onset time, and flare peak time.

- Radio burst flux from US Air Force Radio Solar Telescope Network (RSTN) for the original PPS76 model
- GOES Soft X-ray flux for the current version (flare fluence, peak flux)
- Optical H-alpha imagery from the Solar Observing Optical Network (SOON) for flare location
- Solar wind speed, if available (default of 404 km/s if not available)

**Outputs:** The PPS model predicts the SEP onset time, peak time, peak intensity, end time, and fluence. From these outputs, a simplistic time profile can also be derived. All output is for >5 MeV, >10 MeV, and >50 MeV integral intensities. The model has non-SEP output as well (i.e., polar riometer absorption at Thule, Greenland, dose rate at polar altitudes), but they will not be discussed here.

**Free parameters:** None.

**Limitations and caveats:** The onset time prediction is defined as the time between the flare peak and when >10 MeV proton flux reaches 10 pfu as observed by GOES. Similarly, the peak time prediction is defined as the time between the flare peak and the SEP peak intensity. The flare peak should be identified as the peak in radio (original version) and X-rays (later versions).

The intensity time profile, if constructed from the timing quantities, tends to be simplistic (i.e., straight lines connecting the onset time, peak time, and end time).

PPS was developed with the capability to update the prediction as additional flare data are received. If a second event occurs while a previous event is in progress, the program has the capability to predict a “summation” event (Margaret Shea, personal communication).

**Access to model output or forecasts:** The PPS model was specifically made for use by the 557th Weather Wing of the US Air Force.

**Model validation:** Kahler et al. (2007) considers 78 GOES X-ray flares between 1997 and 2001. Only flares with known locations and peaks greater than M5 were chosen. A comparison was made between PPS predictions and all SEP events during this time period where GOES >10 MeV proton intensity reaches 10 pfu. Correlation coefficients were calculated between the PPS log peak intensity and GOES log peak intensity ( $r = 0.55$ ), PPS log rise time and GOES log rise time ( $r = 0.36$ ), and PPS log rise time and GOES log rise time ( $r$  not given). The study also calculates the Percent Correct as 73%.

Table 2

Ratios and skill scores for four cases of >50 MeV predictions and one case of >10 MeV predictions for the AFRL PPS model.

Solar variable	POD	FAR	TSS	HSS
>M5 flares	0.49	0.66	0.40	0.33
8800-MHz bursts with >M5 flares	0.66	0.82	0.34	0.16
All 8800 MHz bursts >500 sfu	0.66	0.83	0.29	0.13
All 8800 MHz bursts >5000 sfu	0.40	0.49	-0.15	-0.14
>10 MeV with >M5 flares	0.40	0.50	0.08	0.09

Kahler et al. (2017) did a similar validation of PPS but for >50 MeV predictions. The study considered SEP events between 1986 and 2016 where GOES >50 MeV intensity reaches 1 pfu. The PPS model is run for four different cases: all flares greater than M5, all >200 sfu 8800-MHz bursts with associated >M5 flares, all >500 sfu 8800-MHz bursts, and all >5000 sfu 8800-MHz bursts. The results are in the table below and also include results for the >10 MeV predictions. The Probability of Detection (POD), Alarm Ratio (FAR), True Skill Score (TSS), and Heidke Skill Score (HSS) are reported (see Table 2).

### 3.3. Aminimalragia-Giamini Model

**Model developers:** Sigiava Aminimalragia-Giamini (Space Applications and Research Consultancy (SPARC), National and Kapodistrian University of Athens (NKUA)).

**Model description:** The Aminimalragia-Giamini model (Aminimalragia-Giamini et al., 2021) was designed with a focus on operability that will be as uninterrupted as possible, the use of minimal and consistently available inputs, and the minimization of post-eruptive prediction time. The model uses X-ray GOES measurements for the prediction of SEP occurrence during and immediately after the eruption of a solar flare. During the evolution of the flare a probability  $P \in [0, 1]$  that an SEP will occur is provided, and this value is continuously updated by taking into account the real-time X-ray measurement updates of the on-going flare. The probability estimation is finalized after the end of the solar flare eruption. The predictor used is an ensemble of deep feedforward Neural Network (NN) where the final output is the mean of the individual NN predictions. The number of members (N) in the ensemble is set prior to training but the modular implementation used also allows the addition of more NNs; we have used and tested successfully  $N = 3$  and  $N = 10$ . The NNs are trained on 25 years of data, from 1988–2013, which cover the largest part of SC22, the whole SC23, and the rising phase of SC24. This includes several thousands of solar flares (NOAA GOES solar flare catalogue) and more than 200 identified and catalogued SEPs taken and processed from the Solar Energetic Particle Environment Modeling (SEP-EM) Reference Event List<sup>4</sup>. The approach employed has a few noteworthy points:

<sup>4</sup> [http://sepem.eu/help/event\\_ref.html](http://sepem.eu/help/event_ref.html).

- The use of solely X-ray measurements makes for a robust and future-proof model. GOES X-ray Sensor (XRS) measurements have been continuously available in near-real-time for decades and the GOES missions are not envisioned to be discontinued in the foreseeable future. Additionally, the data from different GOES satellites over the years are curated and harmonized from NOAA providing coherent inputs.
- The use of solely X-ray measurements does not require the detection/characterization of CMEs which can potentially delay the output of an occurrence prediction by several hours.
- Regarding the classic dichotomy, the model performs well for both impulsive events, typically associated with solar flares, as well as gradual events, typically associated with solar flares and CMEs.
- Different ensembles of nets have been trained to consider solar flares of certain magnitudes and above, e.g.,  $\geq C1$  and  $\geq M2$ , to emphasize the large range of solar flare intensities, which is of prime Space Weather interest.

**Inputs:** X-ray measurements from the XRS instrument on-board GOES satellites. The X-ray time-series of a solar flare are used to calculate 24 features that are fed as input in the NN ensemble. These features are primarily derived from the peak flux and fluence (time-integrated flux) values of the long and short wavelength GOES X-ray channels. Additionally, when available, the heliolongitude of the solar flare associated active region is also used as an input.

**Outputs:** Probability of an SEP occurring during and after a solar flare, regardless of CME occurrence. This can be also collapsed to a categorical yes/no prediction with a thresholding value (typically 0.5).

**Free parameters:** Operationally none. The internal (weights and biases) parameters of the NNs as well as their hyperparameters can be considered as free, however these are set after training and not user-defined.

**Limitations and caveats:** The GOES XRS measurements cannot distinguish different solar flares if they occur concurrently and the measured X-rays are aggregated. This could potentially affect the NN performance, however as of yet we have not found evidence of this.

**Access to model output or forecasts:** The model will be made operational at the start of 2023. After a pilot operational period, its outputs will be available through a dedicated section in the SPARC webpage ([www.sparc.gr](http://www.sparc.gr)). The model outputs will be also accessible to users by connecting to the SPARC Application Programming Interface (API) through a publicly available Python module (<https://pypi.org/project/sapiadapter>).

**Model validation:** The model has been validated using a 25-year dataset of X-ray measurements and SEPs. Multiple random train/test divisions were used for an overall evaluation. The validation was performed using very strict criteria on a leave-one-out process using all the historical flares

Table 3

Aminalragia-Giamini model True Positive rates, False Positive rates, and TSS from the validation of the model on the full 25 years of available historical data.

	True Positive Rate (%)	False Positive Rate (%)	True Skill Score
Flares $\geq C1$	86.81	7.77	0.790
Flares $\geq M2$	78.36	19.60	0.587

and SEPs. Table 3 and Fig. 1 present the validation outcomes.

### 3.4. AMPS - Adaptive Mesh Particle Simulator

**Model developers:** Valeriy Tenishev (University of Michigan).

**Model description:** Adaptive Mesh Particle Simulator (AMPS) is a 3-dimensional physics-based kinetic Monte Carlo particle model for simulating the dynamics of neutral and charged particles. The energy range of ions and electrons simulated with AMPS varies starting from fractions of eV and up to multiple GeVs. In previous applications, the model was successfully applied to study the planetary, magnetospheric, and heliospheric environments (Tenishev et al., 2021).

AMPS is a fully integrated component of the Space Weather Modeling Framework (SWMF). AMPS incorporates two approaches for modeling transport of SEPs in the heliosphere: (1) simulating SEPs transport when they move along a set of evolving magnetic field lines, and (2) simulating SEPs transported in full 3D. The evolving magnetic field lines are derived from the concurrently conducted magnetohydrodynamic (MHD) modeling of solar wind in the inner heliosphere. AMPS also can be used as a stand-alone SEPs transport model. An analytical representation of the magnetic field line (e.g., Parker spiral) is used in the latter case.

AMPS solves the Parker and Focused transport equations in full 3D and along a set of magnetic field lines (e.g., Tenishev et al., 2005). Model particles are injected at the front of a moving shock. Simulated effects include pitch-angle diffusion (Focused transport equation), spatial diffusion in the direction of the magnetic field line (Parker equation), stochastic accelerations, adiabatic cooling and focusing, and particle drift. The latter is included when modeling is conducted in full 3D. The parameters of the Alfvén turbulence, solar wind, and IMF are derived from concurrently performed MHD modeling of plasma in the inner heliosphere.

**Inputs:** AMPS derives solar wind, IMF, and turbulence parameters from MHD modeling of the inner heliosphere via the coupling infrastructure of the SWMF.

**Outputs:** When simulating SEP transport moving along a set of magnetic field lines, AMPS calculates the flux, density, and energy spectrum of SEPs for a set of the

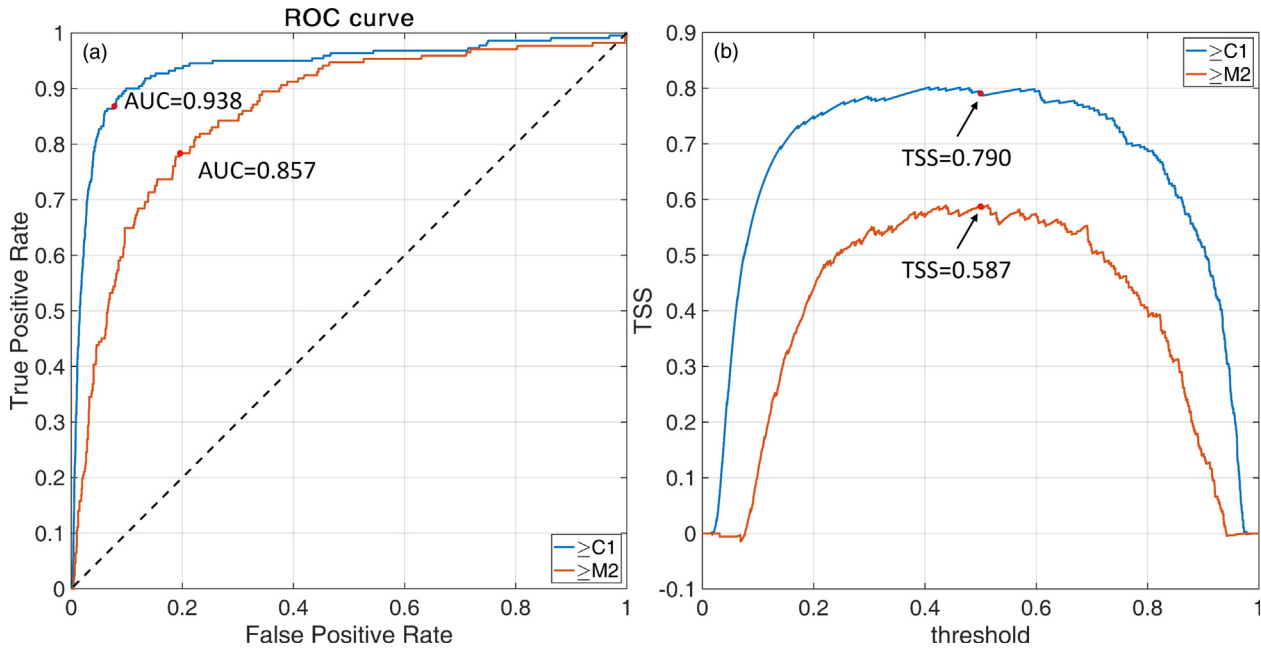


Fig. 1. AminaIragia-Giamini model ROC curves derived from the probabilistic outputs of the model showing the relation of true positive rates and false-positive rates for all thresholds values  $\in [0, 1]$ . Two curves are shown for both the  $SF \geq C1$  and  $SF \geq M2$  cases. The dashed line denotes the random classifier behavior. (b) Evolution of the TSS score for the same range of applied thresholds. Red circles mark the points for threshold equal to 0.5.

user-defined heliocentric distances for each simulated field line. When modeling SEPs transport in 3D, AMPS calculates (1) the integrated density and flux of SEPs at the corners of the grid covering the simulated domain and (2) the energy spectrum of SEPs in a set of user-defined locations.

**Free parameters:** Free parameters include an energy spectrum and a distribution of the source of SEPs. When transporting SEPs along magnetic field lines, AMPS can track the location of the shock that determines where new particles are injected in the model. In the latter case, the solar wind plasma parameters are derived from a concurrently conducted MHD model of the solar wind in the inner heliosphere. In that case, the injection efficiency is an additional free parameter. The choice of the pitch-angle diffusion coefficient is also a free model parameter.

**Limitations and caveats:** AMPS needs to be executed as a component of the SWMF to use evolving magnetic field lines and the solar wind and turbulence parameters.

**Access to model output or forecasts:** AMPS is available in the CCMC at [https://ccmc.gsfc.nasa.gov/requests/PP/user\\_registration.php?model=AMPS](https://ccmc.gsfc.nasa.gov/requests/PP/user_registration.php?model=AMPS). It is also available in source code as a component of the SWMF developed at the University of Michigan.

**Model validation:** Modeling SEP populations is one of the multiple prior applications of AMPS. The core of AMPS is a Monte Carlo solver of kinetic equations. AMPS was extensively validated by comparing with observations when solving the Boltzmann equation in planetary environments and against analytical solutions of plasma wave propagation when solving Vlasov + Maxwell equations. There was no significant validation of the SEP population model when solving Parker or Focused Transport equations conducted so far.

### 3.5. Boubrahimi Model

**Model developers:** Soukaina Filali Boubrahimi, Berkay Aydin, Petrus Martens, Rafal Angryk (developed at Georgia State University).

**Model description:** This model, described in Boubrahimi et al. (2017), predicts the occurrence of SEP events of  $>100$  MeV based on time series correlations among GOES X-ray flux and several proton flux channels using an interpretable decision tree model. A classification decision tree model maps observation attributes as branches to class labels at the leaves. In this model, two class labels are considered: the positive class is composed of X-ray and proton channel time series that led to a  $>100$  MeV SEP event, and the negative class are those data which did not lead to such an event. The SEP event list used for training the model is from Núñez (2011) and consists of 47 impulsive events from the period between 1997 and 2013. Another 47 X-ray events which did not produce any associated SEP event were selected for the negative class, producing a balanced dataset. The observations used to train the model are the GOES XRS, Energetic Particle Sensor (EPS) and High Energy Proton and Alpha Detector (HEPAD) channels – eight in total. As a distinction from previous work (e.g., Núñez, 2011), this model considers not only the correlations between X-ray and energetic proton flux time series, but also correlations across different proton channels. Correlations are expressed using the Vector Autoregression Model (VAR), a stochastic process model used to capture the linear interdependencies among multiple time series. The model considers time windows (called “spans”) before the start of the X-ray event, and each time point within a span is expressed as a linear function of  $l$  previous time

Table 4  
GOES X-ray and Proton Instruments and Channels used in Boubrahimi Model.

Instrument	Channel	Description
SX1.	xs	Short wavelength channel irradiance (0.5–0.3 nm)
SX1	xl	Long wavelength channel irradiance (0.1–0.8 nm)
EPS	p6_flux	Proton Channel 80.0–165.0 MeV
EPS	p7_flux	Proton Channel 165.0–500.0 MeV
HEPAD	p8_flux	Proton Channel 350.0–420.0 MeV
HEPAD	p9_flux	Proton Channel 420.0–510.0 MeV
HEPAD	p10_flux	Proton Channel 510.0–700.0 MeV
HEPAD	p11_flux	Proton Channel >700.0 MeV

points (called “lags”). The  $\text{VAR}(l)$  correlation coefficients of the linear function describing the time series are used as the observation attributes for the decision tree. A study was done to determine the optimal span duration (from 3 to 30 h) and number of lags  $l$  (from  $l = 3$  to  $l = 9$ ) using classification accuracy as the metric for success. This work used the Classification And Regression Trees (CART) decision tree algorithm and the Gini impurity and information gain metrics as the splitting criteria for evaluating class separation.

**Inputs:** The model inputs are times series of eight channels from the GOES X-ray and proton instruments, and are summarized in Table 4.

**Outputs:** The model output is a binary flag of the occurrence of a >100 MeV proton event or non-event.

**Free parameters:** This is a machine learning model and it does not contain free parameters in the same sense as a physical model. However, for training the model must set the span window and the number of lag points  $l$  in the  $\text{VAR}(l)$  model for the span time series, as well as choose a metric (e.g. Gini purity or information gain) to use as a splitting criterion. Once the model is trained, no other “free parameters” are provided to the model.

**Limitations and caveats:** The model prediction is a binary flag indicating whether an SEP event will occur in a period immediately following the “span” segment that is analyzed. It is important to emphasize that the model is trained on X-ray and proton channel data that is *prior to an observed X-ray flare*. Therefore, this model does not use the flare event itself as a precursor, but rather the relatively quiet period prior to the flare. The forecast lead time for this model, though unspecified, would be expected to be typical of the time between the onset of a flare and an SEP event.

**Access to model output or forecasts:** This model is under development and is not available publicly.

**Model validation:** The model was trained and evaluated with a 10-fold cross-validation using stratified sampling. The dataset ( $N = 47 \times 2 = 94$  samples) is randomly divided into 10 subsamples (or folds), and then 10 tests are done where 9 of the folds are used for training and 1-fold is used for testing. Evaluation metrics for the testing portion are averaged over the 10 tests. The metrics presented are accuracy, recall, precision, the F1 metric (har-

monic mean of recall and precision), and Area Under the Curve (AUC) of the Receiver Operator Characteristic (ROC), which is statistically consistent and more discriminating than accuracy. Models trained using the largest span considered, 30 h, and with intermediate lag,  $l = 5$ , performed the best. Of the models with those parameters, the model trained with information gain as the splitting criteria outperformed that trained using the Gini index. For this best model, accuracy = 0.78, recall = 0.73, precision = 0.86, F1 = 0.82, and AUC = 0.77. The accuracy is comparable (3% better) to the University of Malaga Solar Energetic Particles (UMASEP) model (Núñez, 2011) trained using the same data.

### 3.6. COMESEP SEPForecast - Coronal Mass Ejections and Solar Energetic Particles

**Model developers:** Mark Dierckxsens (Royal Belgian Institute for Space Aeronomy (BIRA-IASB)), Michael Marsh (UK Met Office), Silvia Dalla (University of Central Lancashire), Norma Crosby (BIRA-IASB).

**Model description:** CORonal Mass Ejections and Solar Energetic Particles (COMESEP) is an operational alert system that runs without human intervention and contains tools for forecasting geomagnetic storms and SEP radiation storms (<https://www.comesep.eu>). The system is triggered by solar phenomena - Solar Flare (SF) and CMEs. After the automatic detection in solar data of SF and CMEs, alerts are sent through the system to the relevant modules that need the information. The SEPForecast tool within COMESEP produces SEP predictions. SEPForecast is composed of a statistical model (Dierckxsens et al., 2015), which predicts >10 and >60 MeV SEP probability of occurrence and peak fluxes, and a tool to query a run database produced using the physics-based model SPARX Marsh et al. (2015) to make time profile predictions for >10 and >60 MeV.

An extensive statistical analysis of SEP events observed during SC23 was performed to derive the probability and peak flux relationships implemented in SEPForecast (Dierckxsens et al., 2015). The SEPEM<sup>5</sup> reference proton

<sup>5</sup> <https://www.sepem.eu>.

dataset (Crosby et al., 2015) from European Space Agency (ESA) was used to calculate SEP values. Predictors studied were flare intensity and location for flares  $\geq M1$ , CME speed and width, and various combinations of these parameters. A flare list was generated from the NOAA GOES X-ray solar flare catalog. A flare-CME list was compiled from the GOES X-ray solar flare catalog and the Coordinated Data Analysis Workshop (CDAW) SOHO/LASCO CME catalog, linking the two phenomena using temporal and spatial criteria.

COMESSEP predictions are derived from combinations of parameters to allow for the potential (un) availability of data after measuring the flare magnitude. In this vein, the probability of SEP occurrence and  $>10$  MeV and  $>60$  MeV peak proton flux values were derived from both the flare only and flare-CME lists. To calculate the integral peak fluxes for  $>10$  MeV and  $>60$  MeV from the SEP differential channels, the authors assume a Weibull function to describe the spectral shape of the SEP peak. The flare and CME values are used to directly generate  $>10$  MeV and  $>60$  MeV peak proton fluxes. SEPForecast does not consider the ESP peak due to a passing CME - only the peak prior to the ESP.

All COMESSEP forecasts are triggered following an observation of a soft solar X-ray flare with magnitude  $\geq M1$ . A first prediction is derived from the statistical model using the flare intensity as derived by the Flaremail tool in combination with the flare location provided by the Solar Dimming and EUV Wave Monitor (DEMON) tool and the CME speed and width provided by Computer Aided CME Tracking catalog (CACTus) for observed CMEs with a width  $>150^\circ$ . If the location or CME parameters are available after the flare intensity, the alert is subsequently updated. Via this methodology, the likelihood of SEP occurrence and peak flux are quickly provided from statistical relationships.

The SEP time profile is forecast from a previously generated database of runs by the physics-based SPARX model (see Section 3.31), which is queried to produce profiles at Earth for ten-minute averaged  $>10$  MeV and  $>60$  MeV (Marsh et al., 2015). SPARX assumes a broad acceleration region located at a radius of  $2R_{Sun}$  with a standard width  $48^\circ \times 48^\circ$ . The injection region can be increased or decreased by combining a set of  $6^\circ \times 6^\circ$  tiles. With this approach, SPARX does not need any information about the associated CME and can be triggered solely by flare observations. SPARX is triggered by the automated detection of a flare by the Flaremail tool and the measurement of flare location from Solar DEMON. The injection region is centered around the flare location. The time of particle injection is taken to be the flare peak time. The flare X-ray peak flux value is used to normalize the simulated flux profiles into physical flux units (Marsh et al., 2015). The time to maximum intensity, event start and end times are derived from the predicted profiles by applying the thresholds

of  $>10$  MeV exceeds 10 pfu and  $>60$  MeV exceeds  $7.9 \times 10^{-2}$  pfu<sup>6</sup>.

#### Inputs:

1. Flaremail - whenever an M- or X-class flare is detected in the GOES X-ray data, an alert is sent to the COMESSEP system.
2. Solar DEMON - Capable of providing information on flares (location, time, and relative intensity) automatically and in real time using Solar Dynamics Observatory (SDO)/Atmospheric Imaging Assembly (AIA) data.
3. CACTus - autonomously detects CMEs in image sequences from SOHO/LASCO and STEREO/COR2. For the COMESSEP alert system, only the LASCO detections are used. Whenever a CME with angular width larger than 150 degrees is detected, an alert is sent to the COMESSEP system.
4. Ground-Level Event (GLE) Alert - this tool monitors the GLE Alert web page provided by NKUA<sup>7</sup> and sends an alert to the COMESSEP alert system when a new GLE Alert is issued.

#### Outputs:

- The probability of occurrence of radiation storms with proton energies  $E > 10$  MeV and  $E > 60$  MeV
- Peak flux of proton energies  $E > 10$  MeV and  $E > 60$  MeV
- Time to maximum intensity, event start and end times based on flux thresholds of  $E > 10$  MeV exceeds 10 pfu and  $> 60$  MeV exceeds  $7.9 \times 10^{-2}$  pfu

**Free parameters:** None.

**Limitations and caveats:** Flare magnitude must reach M1 to trigger the SEPForecast tool.

Subsequent updates of the alert will be issued if additional information becomes available after the initial SEPForecast alert has been issued. To predict the probability of occurrence, these combinations of input parameters are used depending on the available information:

- Flare intensity
- Flare intensity + flare location
- Flare intensity + CME and width
- Flare intensity + flare location + CME and width
- GLE Alert: probability is set to 1

To predict the peak intensity, these combinations of input parameters are used:

- Flare intensity
- Flare intensity + CME speed

<sup>6</sup> <https://www.comesep.eu/index.php/tools-description>.

<sup>7</sup> <https://swe.ssa.esa.int/anemos-federated>.

- GLE Alert (regardless of other info): the expected peak flux is set to the average peak value of GLEs over SC23

When both flare intensity and location are available, the SPARX model is run to provide a prediction of the onset & peak time and duration.

Users should be aware that there are large uncertainties in the SEPForecast predictions, in particular when only flare information is used. Introducing CME information improves predictions, but these measurements are not always available on a useful timescale. Additionally, it should be noted that the CME relationships developed for SEPForecast were calculated using values from the CDAW LASCO CME Catalog, while the model uses CME measurements from the automated CME database CACTus. The parameters in these two catalogs show large differences in derived CME width and speed.

**Access to model output or forecasts:** Forecasts are available through the ESA Space Weather Service Network at <https://swe.ssa.esa.int/bira-comesep-federated>.

**Model validation:** Model validation for COMESEP has been performed for SC23 events and reported in an internal report that was generated upon delivery of the model as part of the project, however this work has not yet been published. The COMESEP team is working to extend the validation period to the full SC24, as well as perform a validation of the operational performance since Nov 2013 (Mark Dierckxsens, personal communication).

### 3.7. EPREM - Energetic Particle Radiation Environment Module

**Model developers:** Nathan Schwadron, Kamen Kozarev, Matthew Gorby, Philip Quinn, Matthew Young (developed at Boston University and University of New Hampshire (UNH)).

**Model description:** The Energetic Particle Radiation Environment Module (EPREM) is a 3-dimensional, time-dependent, physics-based model of particle transport anywhere in the heliosphere. EPREM is the core particle transport code of such models as Earth-Moon-Mars Radiation Environment Module (EMMREM), Predictions of radiation from REleASE, EMMREM, and Data In-641 incorporating CRaTER, COSTEP, and other SEP measurements (PREDICCS), EPREM + ENLIL + Cone, and SPE Threat Assessment Tool (STAT).

EPREM simulates particle transport by solving the Focused Transport Equation (FTE) (Skilling, 1971; Ruffolo, 1995; Kóta et al., 2005) and convection–diffusion equation (Jokipii et al., 1977; Lee and Fisk, 1981). The transport effects included in the FTE and convection–diffusion equation are convection, diffusive streaming, adiabatic cooling, adiabatic focusing, pitch-angle scattering, perpendicular diffusion, particle drift, and stochastic acceleration. The formalization of these equations within EPREM can be found in Schwadron et al. (2010) and Quinn et al. (2016).

EPREM solves the FTE and convection–diffusion equation by using a Lagrangian grid with nodes that spawn on the inner boundary. For most cases, the inner boundary is the surface of the sun unless specified elsewhere by the user. The nodes are then convected out with the solar wind. The inner boundary then rotates. This naturally creates a Parker spiral configuration. The nodes continue with the solar wind until the outer boundary of the domain is reached. The user implicitly sets the outer boundary by choosing a total number of nodes to span the simulation domain. Fig. 2 shows an example of the unperturbed EPREM grid in physical coordinates. EPREM distributes nodes over nested spherical surfaces and the connections between equivalent nodes on neighboring surfaces produce velocity path lines. In the steady-state case, these lines are formal streamlines; in the frozen-in ideal MHD case, these lines also represent magnetic field lines.

Users may specify the resolution of energy and pitch-angle bins via a runtime configuration file. In uncoupled mode (see below), the user may also specify the temporal resolution; simulation runs that use output from an MHD simulation will use the corresponding times. Users may specify the values of parameters in the initial flux spectrum based on observed values of some particle species,  $\sigma$ , or chosen theoretical values. This spectrum has the analytic form

$$J_s(E, r) = \frac{J_{0s}}{\xi_{\sigma,s}} \left(\frac{r}{r_0}\right)^{-\beta} \left(\frac{E}{E_0}\right)^{-\gamma} \exp\left(-\frac{E}{E_c}\right) \quad (4)$$

where  $J_s(E, r)$  [counts  $\text{cm}^{-2} \text{s}^{-1} \text{sr}^{-1} (\text{MeV}/\text{nuc})^{-1}$ ] is the flux of simulated species  $s$  at radial distance  $r$  [au] and energy  $E$  [MeV];  $J_{0s}$  is the flux of reference species  $\sigma$  at a reference radial distance,  $r_0$ , and reference energy,  $E_0$ ;  $\xi_{\sigma,s}$  is the solar-wind abundance of  $\sigma$  relative to  $s$ ;  $\beta$  is the power-law dependence on radial distance;  $\gamma$  is the power-law dependence on energy; and  $E_c$  is a cutoff or roll-over energy. EPREM currently assumes that  $\beta$  and  $\gamma$  are the same for all simulated species. It also currently uses fixed values of  $r_0 = 1.0$  au and  $E_0 = 1.0$  MeV. The remaining free parameters,  $J_{0s}$ ,  $\xi_{\sigma,s}$ ,  $\beta$ ,  $\gamma$ , and  $E_c$  determine the initial distribution at all pitch-angles for species  $s$ , which EPREM discretizes into energy bins and assigns to all nodes at the first time step. The nodes carry the distribution information – which changes during transport according to the FTE, convection–diffusion equation, and any heliospheric structures – to the outer boundary.

Computing the evolution of the particle distribution(s) requires knowledge of the magnetic field,  $B$ , plasma velocity,  $V$ , and plasma density,  $\rho$ , at each node. EPREM currently provides a simple internal (i.e., uncoupled) model that computes values of  $B$ ,  $V$ , and  $\rho$  appropriate to a Parker spiral. The user may choose to include an idealized cone-style shock by setting a flag and specifying shock parameters in the runtime configuration file.

EPREM can include more physically realistic MHD quantities (i.e., from a CME) when coupled to either the

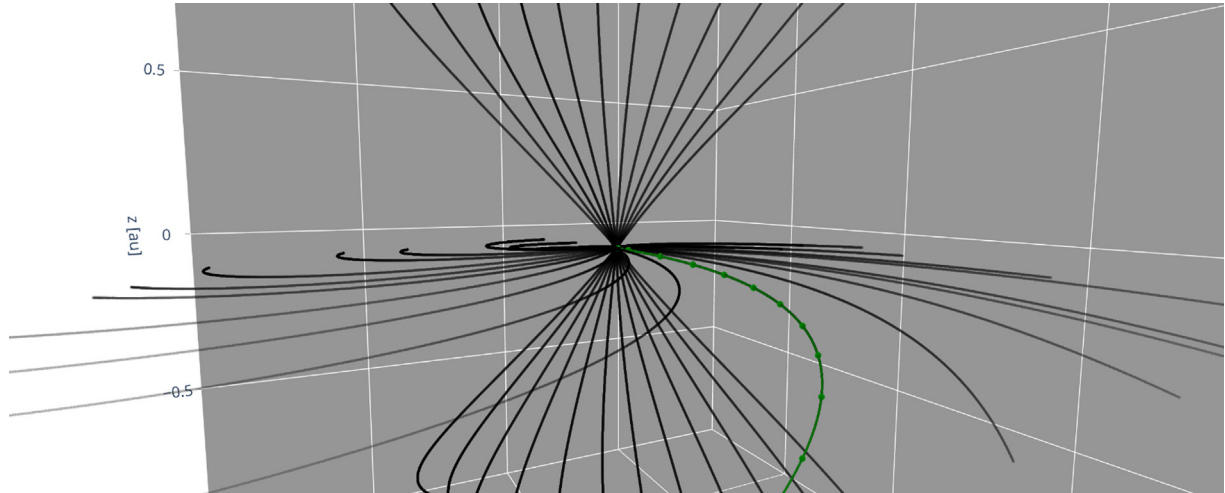


Fig. 2. A representation of the EPREM grid in physical coordinates. Logically connected nodes form velocity path lines throughout the computational domain. This image shows a subset of node lines at the poles and in the ecliptic plane for demonstration purposes; full simulation runs would use enough streams to span the domain. The green line further highlights a subset of nodes along its path.

ENLIL + Cone model or the MAS model. When coupled to either model, EPREM solves the FTE using magnetic field, plasma velocity, and plasma density from the corresponding model. EPREM then pushes the nodes around according to the new plasma parameters. One issue so far is the ENLIL + Cone model uses a spatially limited grid whereas EPREM's grid extended everywhere in the heliosphere. Therefore there are EPREM nodes outside the cone's grid that receive no information. This makes cross-field diffusion and particle drift inaccurate since the EPREM nodes need to communicate with nearby nodes. If there are nodes that exist with no information, then EPREM will give bad results. A non-uniform EPREM grid for use when coupled to the ENLIL + Cone model is currently in development.

**Inputs:** EPREM requires an energy spectrum for a given particle species at a desired location. As described above, the user can provide values of parameters to the initial spectrum (Eq. 4) or use default values. Default values are set to produce a physically reasonable initial spectrum. The user may wish to tailor this spectrum to a particular event by deriving parameter values from observations leading up to the event (for example, by fitting the analytic form to an observed fluence spectrum) or to perform a parameter study by varying input values. If coupled to an MHD model, EPREM treats the model's derived MHD parameters as input at each time step to push the nodes around.

**Outputs:** By default, each stream file contains the following quantities:

- radial ( $r$ ), polar ( $\theta$ ), and azimuthal ( $\phi$ ) position of all nodes as a function of time
- the solar wind velocity components in spherical coordinates at all nodes as a function of time

- the magnetic field components in spherical coordinates at all nodes as a function of time
- the solar wind density at all nodes as a function of time
- the particle distribution at all nodes as a function of time, species, energy, and pitch-angle

The file also includes time and pitch-angle arrays, the mass and charge of each simulated species, and per-species arrays of speed and energy bins. A runtime configuration option allows the user to request that EPREM precompute pitch-angle averaged flux from the pitch-angle resolved distribution and include the flux in the output file instead of the distribution.

Since EPREM treats the particles as an ensemble (kinetic description), the main result is the distribution function, or phase-space density – the number of particles per location and velocity. It has units of  $s^3/km^6$ . The distribution function is a function of time, location, velocity, and pitch-angle, or  $f(t, x, y, z, v_x, v_y, v_z, \mu)$ .

**Free parameters:** The free parameters in EPREM include the injected source distribution (i.e., seed population spectrum), the particle mean free path at 1 AU, and the choice of particle transport effects to include in the simulation.

**Limitations and caveats:** Unless coupled to an MHD model, EPREM assumes a nominal Parker spiral with optional idealized shock, as described above. This is an ideal scenario and does not include the typical variations within the IMF. Since EPREM uses a Lagrangian grid, the nodes may not fall directly at Earth's location and therefore relies on interpolating between the nodes to derive the distribution function at Earth.

**Access to model output or forecasts:** There was work to build EPREM at the CCMC, but runs-on-request are not available. Contact UNH for requesting model runs.



**Model validation:** To date, there has been no rigorous validation performed for EPREM. The majority of studies using EPREM have only made qualitative comparisons (Schwadron et al., 2010; Kozarev et al., 2010; Dayeh et al., 2010; Chen et al., 2015; Quinn et al., 2016; Quinn et al., 2017; Quinn et al., 2018; Quinn et al., 2019; Young et al., 2021).

### 3.8. ESPERTA - Empirical Model for Solar Proton Event Real Time Alert

**Model developers:** Monica Laurenza (National Institute for Astrophysics (INAF)), Edward W. Cliver (National Solar Observatory (NSO)), Alan G. Ling (Atmospheric Environmental Research), Tommaso Alberti (INAF), Mirko Stumpo (Università di Roma Tor Vergata, INAF), Simone Benella (INAF).

**Model description:** The Empirical model for Solar Proton Event Real Time Alert (ESPERTA) forecast tool predicts whether SEP events will exceed S1 or S2 levels (Laurenza et al., 2009; Laurenza et al., 2018) in the NOAA Solar Radiation Storms Scale (<https://www.swpc.noaa.gov/noaa-scales-explanation>). A main focus of the ESPERTA model is to quickly produce an SEP intensity forecast. For this reason, ESPERTA relies primarily on flare characteristics: location, 1–8 Å SXR fluence, and ~1 MHz radio fluence corresponding to Type III radio bursts. Additionally, the model requires that a flare reaches M2 class or higher to produce a forecast.

The  $\geq S1$  ESPERTA forecast is produced within 10 min following the SXR of a flare (Laurenza et al., 2009). ESPERTA was derived from a database of GOES measurements between 1995–2005, selecting time periods for which  $>10$  MeV proton fluxes exceeded 10 pfu for three consecutive 5-min intervals. Each proton flux increase was associated with its solar flare source, resulting in a list of 93 SEP events. For the  $\geq S2$  ESPERTA model (Laurenza et al., 2018),  $\geq S2$  events were selected from  $\geq S1$  lists spanning 1995–2005 and 2006–2014 from Laurenza et al. (2009) and Alberti et al. (2017), respectively. As was done for the previous version of the model,  $>10$  MeV proton intensity was required to exceed 100 pfu for three consecutive 5-min intervals, resulting in a list of 59 SEP events. SXR fluence values were derived from GOES 1-min 1–8 Å data using an empirical prescription to estimate the fluence at 10 min following the flare peak. The SXR fluence is calculated from the 1/3 power point on the rise of the SXR burst before the peak to the 1/3 power point after. The 1/3 power point is defined as 1/3 of the flare peak X-ray flux. If the X-ray intensity drops by a factor of 3 within 10 min of the peak, the integration stops, otherwise an exponential fit of the flare is used to extrapolate the intensity curve to the 1/3 power point. The fit is based on the intensity values from 6 to 10 min after the peak and it is a reasonable tool to take into account the flare profile. The ~1 MHz radio values were

compiled from the Wind/Radio and Plasma Wave Experiment (WAVES) instrument and integrated from 10 min prior to the flare integration start time to 10 min after the peak (Laurenza et al., 2018; Alberti et al., 2017).

Between 1995 and 2005, there were 704  $\geq M2$  flares. This increased to 980  $\geq M2$  flares when the data set was extended up to 2014. To derive  $\geq S1$  and  $\geq S2$  forecasts, ESPERTA developers compared SXR fluence to 1 MHz radio fluence for all flares and identified probability contours in parameter space that contained flares associated with  $\geq S1$  and  $\geq S2$  SEP events. The probability contours were derived using a logistic regression analysis by McCullagh and Nelder (1983) that allows one to compute the probability that an event will occur by using a parametric space with two variables. The probability ( $P$ ) can be expressed in terms of the X-ray fluence ( $X$ ) and 1 MHz radio fluence ( $R$ ) as:

$$P(\log X, \log R) = \frac{e^\eta}{1 + e^\eta} \quad (5)$$

where  $\eta = \eta(\log X, \log R)$ .

First, the flares were grouped within three different longitudinal bands, effectively taking magnetic connectivity into account: 1) E 120° - E 41°, 2) E 40° - W 19°, 3) W 20° - W 120°. Probability contours were found for each longitudinal range individually and a probability threshold for each one was selected by maximizing POD and minimizing FAR. Then, a yes/no  $\geq S1$  and  $\geq S2$  forecast was produced by identifying which side of the probability contour threshold a flare was located. Final probability contours were selected by maximizing POD and minimizing FAR.

The  $\geq S1$  contours were derived using data up to 2005 with the corresponding values:

1.  $\eta_1 = -6.07 - 1.75 \log(X) + 1.14 \log(R) + 0.56 \log(X) \log(R)$
2.  $\eta_2 = -7.44 - 2.99 \log(X) + 1.21 \log(R) + 0.69 \log(X) \log(R)$
3.  $\eta_3 = -5.02 - 1.74 \log(X) + 0.64 \log(R) + 0.40 \log(X) \log(R)$

The associated probability levels were 28%, 28%, and 23% for the three longitudinal ranges, respectively (Alberti et al., 2017).

The  $\geq S2$  contours were derived from the full 1995 to 2014 data set following the same approach. The eastern and central probability thresholds remained the same, however the W 20° - W 120° probability contour was adjusted to 35%. An additional criterion was added such that  $\geq S2$  alerts are only issued for events that cross S1 levels within 30/15/6 h for eastern/central/western events, therefore ESPERTA also monitors  $>10$  MeV proton intensity levels. This modification results in a delay of  $\geq S2$  forecasts compared to  $\geq S1$  forecasts, but with a significant improvement in  $\geq S2$  forecast performance.

#### Inputs:

- Flare location
- Flare SXR fluence (X-ray peak threshold  $\geq M2$ )

- Flare  $\sim 1$  MHz radio fluence (time-integrated Wind/GOES type III intensity)
- $>10$  MeV proton flux (for  $\geq S2$  forecast)

**Outputs:** Alert for  $>10$  MeV proton fluxes  $\geq S1$  and  $\geq S2$ .

**Free parameters:** None.

**Limitations and caveats:**

- A forecast will only be issued in the case that the model determines a threshold will be crossed. If it is determined that a threshold will not be crossed, then no forecast is produced.
- Model will not trigger for flares below M2
- $\geq S2$  forecasts are delayed until S1 levels are crossed (Laurenza et al., 2018)
- $\geq S2$  alerts will not be issued for a flare if the pre-flare background proton flux level already exceeds 100 pfu (Laurenza et al., 2018).

**Access to model output or forecasts:** ESPERTA is not currently available to the public.

**Model validation:** The  $\geq S1$  ESPERTA tool was developed using data between 1995–2005 and initially validated over the same data set (Laurenza et al., 2009). Moreover, it was validated using an independent data set from 2006–2014 (Alberti et al., 2017). Increases in intensity above S1 levels due to the passage of a shock or compression region at Earth were not counted in the development or validation of the model. A total of 36  $\geq S1$  events with reliable flare source associations were identified in the 2006–2014 time period. These were broken into three categories: 23 SEP events with  $\geq M2$  flares, 9 with  $<M2$  flares, and 4 farside events with no available flare data.

Forecast performance was organized into four categories:

- Hit: correct prediction (19)
- Miss: SEP associated with  $\geq M2$  front-side flares that were not predicted (4)
- MISS: SEP associated with front-side  $<M2$  flares (no prediction possible by definition, 9)
- not counted: SEP associated with backside flares  $<M2$  (data gaps, 4)

The performance resulted in a  $POD = Hits/(Hits + Misses + MISSES) = 59\%$  ( $19/(19 + 4 + 9)$ ),  $FAR = FAs/(Hits + FAs) = 30\%$  ( $8/(19 + 8)$ ),  $HSS = 0.55$  ( $44/80$ ), and  $Percent\ Correct\ (PC) = 87\%$  ( $240/276$ ) (Alberti et al., 2017). The validation over the whole dataset from 1995 to 2014 led to the results:  $POD = 63\%$  ( $69/69 + 20 + 21$ ), and  $FAR = 38\%$  ( $42/69 + 42$ ) (Laurenza et al., 2018; Alberti et al., 2019). More recently, Stumpo et al. (2021) reinterpreted the ESPERTA model for  $\geq S1$  events in the framework of machine learning. These authors performed a cross validation, leading to a comparable performance. They also demonstrated that a quite high FAR is a natural

consequence of the small size of the SPE sample with respect to the SPE non-associated flares, which is a critical issue of any statistical approach.

In Laurenza et al. (2009), the Advance Warning Time (AWT) was calculated by comparing the time that the ESPERTA forecast was issued with the onset in the SOHO/Electron Proton and Helium Instrument (EPHIN) 31–50 MeV energy channel published by Posner (2007). This choice was made because GOES  $>10$  MeV intensities are not accurate at the onset of SEP events due to electron and proton contamination and post-processing effects (Posner, 2007). Nevertheless, in order to allow a comparison with other forecasting techniques, Alberti et al. (2017) chose to assess the ADWT by calculating the difference between the time that the forecast was issued and the time that the GOES  $>10$  MeV proton intensity reached the S1 threshold (Alberti et al., 2017). For the data between 2006–2014, the median (average) ADWT was  $\sim 2$  h ( $\sim 7$  h) ranging from 0.4 to 35.9 h. For the full 20-year interval, the median (average) ADWT was 4.8 h (9 h) with a range from 0.4 to 52.8 h for the 66 hit events (Alberti et al., 2017).

The  $\geq S2$  ESPERTA tool was derived from data between 1995–2014 and metrics were calculated based on performance for the same set of events (Laurenza et al., 2018). In this case, increases above the S2 level due to a passing shock are counted in the statistics. Forecasts performance was organized into the four categories described above with the results: 41 Hits, 8 Misses, 6 MISSES, and 4 not counted.

The  $\geq S2$  tool shows improvement over the  $\geq S1$  tool with a  $POD = 41/(41 + 8 + 6) = 75\%$  and  $FAR = 13/(41 + 13) = 24\%$ . The median ADWT for the 41 hits is 1.7 h with a minimum of 0.2 h.

### 3.9. FORSPEF - Forecasting Solar Particle Events and Flares

**Model developers:** Anastasios Anastasiadis (National Observatory of Athens (NOA)), Athanasios Papaioannou (Ingmar Sandberg (SPARC)), Ingmar Sandberg (SPARC), Manolis K. Georgoulis (RCAAN of the Academy of Athens).

**Model description:** FORECASTING SOLAR PARTICLE EVENTS AND FLARES (FORSPEF) is an operational tool that is composed of three modules that aim to forecast and nowcast 1) the likelihood of upcoming Solar Flare (SF) eruptions, 2) the occurrence of SEPs by making a prediction of the time before onset, and 3) the SEP characteristics of an upcoming event (Papaioannou et al., 2015; Anastasiadis et al., 2017; Papaioannou et al., 2018). In forecasting mode, the model makes predictions when no solar event (flare or CME) has yet taken place. In nowcasting mode, the model will use SF and CME information to predict SEP event characteristics (Anastasiadis et al., 2017).

To develop the flare and CME forecasting module (Anastasiadis et al., 2017), a database of active region (AR) s was compiled from SDO/HMI full-disk magne-

tograms. The ARs were selected between longitudes of 70° E/W on the solar disk and the effective magnetic field ( $B_{eff}$ ) was calculated for each. Due to limb effects, a proxy was used to find  $B_{eff}$  between 50° to 70° E/W. The probability of flare occurrence from C, M, and X-class flares was derived for each  $B_{eff}$ . The likelihood of a flare of a particular peak SXR flux to erupt with a CME was inferred from Yashiro et al. (2005). Folding the two probability functions gives the likelihood an AR will produce a CME. Additionally, the CME speed is predicted using a relationship with  $B_{eff}$  derived in Georgoulis (2008):  $V_{CME} = 87.3B_{eff}^{0.38}$  [km/s].

A separate SEP forecasting module was derived from a database of SEPs (>10, >30, >60, and >100 MeV), flares, CMEs and radio fluxes compiled by Papaioannou et al. (2016) spanning three decades from 1984 to 2013. The solar disk was divided into five longitudinal bins and 4000 flares in each bin were used to derive the probability of SEP occurrence per SF magnitude at each longitude:  $P(SEP_{flare})_i = (N_{SEP})_i / (N_{all,i})$ . For each AR location, the probability that an SEP will occur per SF magnitude is multiplied by the probability distribution output by the flare forecasting module that a flare of a given magnitude will be produced by the AR. This produces the final output from the forecasting module: the maximum probability of SEP occurrence for each AR (Anastasiadis et al., 2017).

After a SF has occurred, the FORSPEF flare nowcasting module uses information from Solar DEMON to make SEP predictions. Probability distribution functions for the observed flare longitude are calculated from the FORSPEF database and the SEP probability of occurrence is identified following a similar approach to the forecasting mode. The module also reports the expected SEP values derived from the SXR peak flux, e.g., proton peak flux, time of peak, duration, and fluence for each energy channel (Papaioannou et al., 2016).

FORSPEF also forecasts SEP characteristics from CMEs observed by the automated real time CACTus CME catalog. CACTus is the only near real-time solution that provides reliable and continuous outputs that can be used for SEP nowcasting (Anastasiadis et al., 2017; Papaioannou et al., 2018). To develop the CME to SEP nowcasting tool, however, SEP event information from the FORSPEF database (Papaioannou et al., 2016) was paired with CME information from the CDAW CME Catalog<sup>8</sup>. Data from 1997–2013 were used, representing the overlapping time period between the two catalogs, comprising a total of 1905 CMEs and 158 SEP events (>10 MeV).

The CMEs were sorted into a matrix of nine subgroups according to their speed and width. The speed ranges were divided into slow ( $400 \text{ km/s} \leq V < 1000 \text{ km/s}$ ), moderate ( $1000 \text{ km/s} \leq V < 1500 \text{ km/s}$ ) and fast ( $V \leq 1500 \text{ km/s}$ ) and the Angular Width (AW) ranges divided into full halo

( $AW = 360^\circ$ ), partial halo ( $120^\circ \leq AW \leq 359^\circ$ ) and non halo ( $AW < 120^\circ$ ). The probability that an SEP event is produced by a CME in each subgroup was calculated along with the correspond 68% confidence level. For each CME angular width category, curves were fitted to the SEP probabilities to derive continuous functions of SEP probability with velocity for halo, partial halo, and non halo CMEs (Papaioannou et al., 2018).

To calculate the relationship between the CME parameters and SEP peak flux and total fluence, linear regressions were performed between the CME speed and peak flux or fluence in each energy channel ( $E > 10, > 30, > 60$ , and  $> 100 \text{ MeV}$ ). Separate linear regressions were found for halo, partial halo, and non-halo CMEs with each GOES energy channel. Tables specifying the linear regressions and their standard error are specified in (Papaioannou et al., 2018).

A third nowcasting module incorporates the ESPERTA model (Section 3.8) approach to predict whether an SEP event will exceed S1 on the NOAA Solar Storm Scale. Radio data at 0.944 MHz from the Wind/WAVES instrument were compiled and calculations of the radio and SXR data were refined. Revised versions of the SEP occurrence equations in ESPERTA were produced. However, the Wind/WAVES data or an appropriate substitute is not available in near-real-time, so this module cannot presently be used in the operational version of FORSPEF.

#### Inputs:

**Forecasting:** 1) SDO/HMI full-disk magnetograms, 2) AR number from NOAA/SWPC, 3) FORSPEF database for SEPs, SFs, CMEs (Papaioannou et al., 2016).

**Nowcasting:** 1) near real-time SF data from Solar DEMON<sup>9</sup>, 2) near real-time CME identifications obtained from the automated CACTus CME catalog<sup>10</sup>, 3) integrated radio flux at 1 MHz for the ESPERTA Model (not available in real-time).

Both forecasting and nowcasting modes use the FORSPEF database for SEPs, SFs, CMEs (Papaioannou et al., 2016).

**Outputs:** Forecasts on the FORSPEF web page provide the AR NOAA number, AR heliographic and device-coordinate location, the corresponding  $B_{eff}$  value, the 24-h cumulative flare probabilities for each of the 28 GOES flare classes (from C1.0 to X10.0) and their peak photon fluxes, the respective eruptive-flare or CME likelihoods, the projected CME velocity, and the probability of SEP occurrence.

Nowcasts report the probability of SEP occurrence and SEP characteristics - onset time, peak time, decay time, peak flux, and fluence for ( $E > 10, > 30, > 60$ , and  $> 100 \text{ MeV}$ ) in table and graphical outputs.

**Free parameters:** None.

<sup>8</sup> [https://cdaw.gsfc.nasa.gov/CME\\_list/](https://cdaw.gsfc.nasa.gov/CME_list/).

<sup>9</sup> <http://solardemon.oma.be/flares.php>.

<sup>10</sup> <https://wwwbis.sidc.be/cactus/>.

**Limitations and caveats:** FORSPEF makes predictions for all  $\geq C1$  flares reported by the Solar DEMON service.

There is a higher level of uncertainty when forecasting flares from ARs near the limbs between  $50^\circ$  to  $70^\circ$  E/W. No forecasts can be made from ARs beyond  $70^\circ$  E/W.

SEP and CME relationships applied in FORSPEF were derived using values from the CDAW CME catalog, which are determined by hand, however the model runs using CME parameters reported in the CACTus catalog and are derived through an automated detection algorithm.

**Access to model output or forecasts:** The FORSPEF system has been online since April 2015 and may be accessed at <http://tromos.space.noa.gr/forspef/main/> where it provides continuous forecasts of SFs and SEPs. The system will inform registered users when an SEP event is expected to take place. All forecasts are stored in a fully accessible archived database.

**Model validation:** Anastasiadis et al. (2017) performed a validation of the FORSPEF tool focusing on the POD, FAR, HSS, Overall Accuracy (OA), Critical Success Index (CSI), PCOR, and TSS. For the post-event nowcasting mode, FORSPEF was validated as follows: from the SFs, CMEs and SEPs of SC23 (Papaioannou et al., 2016), 90% of the SFs were selected as the control sample, and the rest (10%) were treated as the test sample, with the selection of the test and control samples being completely random. This procedure was repeated for 10 times and consequently ten different – completely independent – control and test samples were created. For each sample categorical scores were implemented for all test samples with the categorical measures calculated as a function of a Probability Threshold (pt) using SF, CME, and the integrated radio and SXR flux information as independent inputs. As a result, a  $pt = 0.25$  was identified as the optimal one for the SF and CME modules and a  $pt = 0.28$  for the ESPERTA module. Mean values of selected categorical scores are reported in Table 5, reproduced from Anastasiadis et al. (2017).

Papaioannou et al., 2018 evaluated the performance of the CME nowcasting model using all CMEs from the CDAW catalog between April 2013 to 2015, 43 of which were associated with SEP events recorded by GOES satellite in the  $>10$  MeV energy channel. A probability threshold of 0.3 maximized the HSS derived from the data set. POD, FAR, PCOR, and HSS as a function of probability threshold are plotted in Papaioannou et al. (2018). With a threshold of 0.3, POD is 65% and FAR is 58% for  $>10$  MeV events, POD is 70% and FAR is 15% for

$>30$  MeV events, and POD is 67% and FAR is 63% for  $>100$  MeV events.

As a next step, Papaioannou et al. (2018) extended the FORSPEF database until the end of 2015, aiming at utilizing the whole time span from the beginning of SC23, *i.e.*, 1997 until 2015. Similar to Anastasiadis et al. (2017), out of the whole sample 85% of all SFs, CMEs, SEPs was chosen as the control sample and the rest 15% as the test sample. This procedure was repeated ten times, and ten different completely independent control and test samples were obtained. For all paired samples (control and test) categorical scores were obtained. The mean POD – out of the 10 different pairs of samples – was 70% and the mean FAR was 44%, which is consistent with the results presented in Anastasiadis et al. (2017).

Papaioannou et al., 2018 assessed the performance of the peak flux prediction using the same set of 43 SEP events. They found significant scatter between the forecasts and observations, but most of the forecasts ( $\approx 75\%$ ) were within an order of magnitude of the observed value. The corresponding correlation coefficients per energy were  $E > 10$  MeV: 0.198 ( $n = 42$ ),  $E > 30$  MeV: 0.235 ( $n = 33$ ), and  $E > 100$  MeV: 0.173 ( $n = 15$ ).

### 3.10. Georgia State Model

**Model developers:** Berkay Aydin, Manolis K. Georgoulis, Anli Ji, Dustin Kempton, Chetraj Pandey, Rafal Angyk, and Petrus Martens (developed at Georgia State University).

**Model description:** This model is a work in progress, but is intended to become an operational SEP event watch and warning system that runs without human intervention. In its current state, the system provides an All-Clear SEP event forecast, and is composed of a set of connected space weather event forecasting modules, working in different modes. The All-Clear SEP event forecast places emphasis on precise and sensitive prediction of non-flaring (CBN; labeling as 'non-flaring' active regions hosting C-, B- or lower-class flares) active regions in order to identify periods where the occurrence of an SEP event is highly unlikely. In such cases, SEP events of  $>10$  MeV proton flux are not likely to exceed 10 pfu. Later phases of development will implement the SEP Watch, where conditions are likely to lead to an SEP triggering event, and an SEP Warning, where a triggering event has occurred and an SEP event is likely imminent. The connected modules of the system are constructed as ensembles of different learning algo-

Table 5  
Mean values of the HSS, POD, FAR, and pt for the ten independent test samples.

FORSPEF nowcasting based on	HSS	POD	FAR	pt
Solar flare data	$0.37 \pm 0.011$	0.40	0.57	0.25
CME data	$0.65 \pm 0.007$	0.71	0.41	0.25
Radio and SXR fluence data	$0.47 \pm 0.04$	0.55	0.42	0.28

rithms, producing binary, probabilistic, and regression-based prediction models for flare, eruptive-flare, and CME speed predictors. All predictions are designated for and deployed on individual active regions. All reports are aggregated for a final probabilistic ‘All-Clear’ output based on a set of user-defined thresholds. The All-Clear SEP predictor utilizes Near-Real Time (NRT) HMI Active Region Patch (HARP) data described in [Hoeksema et al. \(2014\)](#) to produce Multivariate Time Series (MVTs) of active-region metadata, with many of the metadata parameter calculation algorithms being the same as the Spaceweather HMI Active Region Patch (SHARP) of [Bobra et al. \(2014\)](#). All models are trained for a 12-h observation window, meaning that a complete prediction result can be issued only after 12 h’ worth of high-quality data has been collected. The prediction window (forecast validity period) for all the models is 24 h with a zero latency (i.e., forecasts are effective immediately). For a discussion of these intervals on flare prediction, see [Angryk et al. \(2020\)](#).

The predictive process follows three distinct paths. First, it determines the probability of a sizable flare (i.e.,  $\geq M1.0$ ) occurrence within the next 24 h. This path uses three base learners (i.e., SOHO-FP, DSDO-FP, NSDO-FP) and a meta learner (which uses the output of base learners), described in [Ji et al. \(2020\)](#), where each base learner is a multivariate Time Series Classifier (TSC) based on the Time Series Forest algorithm from [Deng et al. \(2013\)](#). The second path predicts the probability of an eruptive flare occurrence within the next 24 h. This path also uses the AR MVTs and issues probabilities for occurrence of eruptive (P(ER)) vs. non-eruptive (P(NE)) events. Note here that an eruption may originate from X-, M-, or C-class flares, but not all flares are eruptive. A- and B-class flares are not considered in this framework. The third path uses the outputs of base learners (i.e., the occurrence probability of major flares  $\geq M1.0$ ) to predict the occurrence probability of X-, M-, C-class flares and Flare-Quiet (FQ) regions. This is a quaternary meta-learner with its outputs fed into a regressor seeking to project a CME speed.

As the prediction algorithms of this system are trained on individual active regions, the results of individual forecasts must then be aggregated. The active region all-clear probability is issued for individual active regions using the following formula:

$$P_{AR-AC} = 1 - [P_{ER}(AR_i) \times \phi_{FL}(P_{FL}(AR_i)) \times \phi_V(V_{CME}(AR_i))]$$

where  $P_{ER}$  is the eruption probability,  $\phi_{FL}$  is the flare probability activation function, and  $\phi_V$  is the CME speed activation function. These activation functions are currently signum functions (thresholded step functions):

$$\phi_{FL} = \begin{cases} 1 & \text{if } P_{FL} > FL_{th} \\ 0 & \text{otherwise} \end{cases} \quad \begin{cases} 1 & \text{if } V_{CME} > V_{th} \\ 0 & \text{otherwise} \end{cases}$$

where the flare probability threshold ( $FL_{th}$ ) and the CME speed threshold ( $V_{th}$ ) are set to a user defined values. The full disk all clear probability ( $P_{AC}$ ) is then calculated as the joint all-clear probability of active region all-clear output. The probabilities of eruptions from active regions are assumed to be statistically independent, making the joint probability a simple product of the observed active regions at the time of model report.

**Inputs:** The current model input consists of the NRT data series of the HARP data product described in [Hoeksema et al. \(2014\)](#). The most recent observations are collected from the source repository at the Joint Science Operations Center (<http://jsoc.stanford.edu/>) for each active region recorded at the report time. The data for each active region is collected at 12 min intervals over the previous 12 h.

#### Outputs:

- The probability of occurrence for the peak proton flux exceeding 10 pfu for proton energies  $E \geq 10\text{MeV}$  over the next 24 h
- A binary all clear flag indicating that the probability of peak proton flux exceeding 10 pfu has exceeded some threshold (currently 25%)

**Free parameters:** This is a combination of several machine learning models and it does not contain free parameters in the same sense as a physical model. However, when deploying the system there are several parameters that can be set to change runtime frequency, as well as assumptions about weighting of intermediary results and thresholds for consideration in calculations.

- Solar maximum climatological eruptive flaring rate for any given active region observation time: used when data for an active region is unreliable and the model is set to assume it is running during solar maximum;
- Solar minimum climatological eruptive flaring rate for any given active region observation time: used when data for an active region is unreliable and the model is set to assume it is running during solar minimum;
- CME Speed Threshold is used to determine when an active region will be included in the All-Clear calculation. The active regions predicted by the CME speed module not to produce a CME exceeding this speed will be assumed to be clear from possibly producing an SEP event and will be excluded from calculation;
- M and X flare Threshold is used to determine when an active region will be included in the All-Clear calculation. The active regions that the flare prediction meta model output of [Ji et al. \(2020\)](#) does not predict will produce an M or X class flare with this probability threshold are excluded from calculation.

**Limitations and caveats:** The All-Clear forecasting heuristic makes two major assumptions to provide conservative All-Clear forecasts: first, it assumes that all predicted

eruptions (CMEs) are directed towards Earth face-on (i.e., they are halo CMEs) and, second, it assumes that all of them can potentially lead to an SEP event. Therefore, if either of these events is expected, an All-Clear forecast will not be issued.

**Access to model output or forecasts:** Model forecasts can be accessed at <https://dmlab.cs.gsu.edu/sep-prediction/>.

**Model validation:** The various sub-models of the system were trained and tested with a set time segmented partitions to enable cross-validation. For instance, the SOHO-FP flare prediction sub-model utilized a SOHO dataset much like the HARP dataset, divided into three partitions allowing a  $\frac{2}{3}$  training vs.  $\frac{1}{3}$  testing split for each iteration. As discussed in Ji et al. (2020), training and testing on the DSDO-FP sub-model utilizes 5 partitions from a machine learning ready dataset for the flare prediction task described in Angryk et al. (2020). Similarly, the NSDO-FP sub-module utilizes the same partitioning strategy on the NRT HARP data to construct the partitions, instead of the definitive data used in Angryk et al. (2020).

### 3.11. *i*PATH - improved Particle Acceleration and Transport in the Heliosphere

**Model developers:** Gang Li, Junxiang Hu, Gary Zank (University of Alabama in Huntsville).

**Model description:** The improved Particle Acceleration and Transport in the Heliosphere (IPATH) model is a 2-D MHD SEP model that simulates Diffusive Shock Acceleration (DSA) at CME-driven shocks and follows the subsequent transport of energetic particles through the inner heliosphere. IPATH models the background solar wind and CME-driven shocks at the ecliptic plane starting at 0.05 AU and produces time profiles of SEP intensity spectra and pitch angle distributions as outputs at selected vantage points (e.g., at Earth or Mars). It considers both perpendicular and parallel diffusive factors of energetic particles, which come from Nonlinear Guiding Center Theory (NLGC) and Quasi-Linear Theory (QLT) respectively. The transport module is a Monte Carlo code which follows test particles through space described by the FTE and is set up for parallel computations. This model is improved over the original PATH model which was 1-D.

IPATH first creates the shock perturbation along the inner boundary, and propagates the CME outward with the forward shock region tracked with a 2-D onion-shell model. For each time step, a new outer shell is created based on the shock speed and all previous shells convect and adiabatically expand with the solar wind. Then accelerated particle distributions are calculated along the whole shock front, based on the diffusive shock acceleration. Accelerated particles are then allowed to diffuse back to the shock complex, and between each parcel behind the shock via parallel and perpendicular diffusion. This gives the distribution function in each shock parcel at each time step, which is important for the ESP phase when the shock

arrives at the observer. Once a particle has moved a certain distance during a single time step, it escapes the shock and is transported through the unperturbed solar wind via a focused transport scheme, which includes terms for weak scattering and cross-field diffusion from the random walk of magnetic field lines. The FTE is solved using a time-backwards stochastic differential equation approach until a steady-state is found where ensemble averages of many test particle paths give the full particle distribution function. The full model description is detailed in Hu et al. (2017).

#### Inputs:

- Background solar wind parameters based on 1 AU observations (solar wind density, speed, temperature, and magnetic field strength)
- CME parameters (CME speed, width, location, and perturbation duration)
- Turbulence parameters (turbulence level, turbulence spectral parameters, and radial dependencies of these parameters)
- Suprathermal seed particle input (suprathermal particle energy spectral parameters)
- Observer locations (radius, longitude)

#### Outputs:

- Time profiles for energetic proton/heavy ion intensities (differential fluxes) at a wide energy range (from hundreds of keV's to GeV's) at the chosen observer locations
- Time profiles for pitch angle distributions
- Event-integrated fluences (in  $MeV^{-1}cm^{-2}$ )
- Time profiles for integral flux above certain energies (in pfu)

**Free parameters:** None.

**Limitations and caveats:** IPATH as a coupled MHD and acceleration/transport model has many advantages at modeling the underlying physics during a SEP event. For instance, its inclusion of perpendicular diffusion allows for a large longitudinal spread of energetic particles. Thus, it is well suited to model events that are not well-connected from the CME to the observer. It can also generate results at multiple observer locations throughout the inner heliosphere. Using the latest developments in the modeling of seed particles, IPATH is able to approximate the solar wind's background pre-event particles that are to be injected into the DSA. Additionally, as distribution functions of particles trapped in the shock downstream are also tracked, IPATH is capable of modeling the ESP phase.

Like other models using CME information as inputs, IPATH's performance as a prediction model relies on how early we can acquire good quality CME parameters from observations. As the inner boundary is set at 0.05 AU ( $10 R_{sun}$ ) and the shock is formed even further in, it cannot capture the SEP acceleration happening in the low corona and does not produce output for the first

couple of hours of the events. IPATH is not able to fully capture the effects of previous CMEs without modifications on the model so the operational version is best suited for single CME events. The background solar wind used in IPATH is a simple homogeneous Parker spiral model, which cannot capture some complex solar wind geometries in a specific event. But this simplification is efficient for general prediction purposes.

**Access to model output or forecasts:** iPATH is in the process of implementing the model at CCMC for Runs on Request and the developers are in the process of developing a real-time forecasting module for the SEP Scoreboards.

**Model validation:** Originally IPATH was only used as a research model for historic SEP events (see Ding et al., 2020 as an example), so no large validation study has been done with the model. More recently, IPATH has been involved with the International Space Weather Action Teams (ISWAT)/Solar Heliospheric and INterplanetary Environment workshop (SHINE) community SEP model validation challenge.

The next steps for IPATH include:

- Coupling with a coronal model to account for acceleration before the shock reaches 0.1 AU - see coupling of IPATH and AWSOM called SEPcAster (Section 3.24).
- Implementation of a nowcasting mode using real time solar wind inputs and near continuous runs for real events, as part of the SEP Scoreboards.

### 3.12. Lavasa Model

**Model developers:** Eleni Lavasa (National and Kapodistrian University of Athens) and Giorgos Giannopoulos (Information Management Systems Institute (IMSI) - "Athena" Research Center).

**Model description:** A consistent ML framework for the binary prediction of SEP events, based on SF and CME observational data has been implemented. A thorough investigation for optimal solutions was performed under our proposed approach, across diverse classification algorithms and extended hyper-parameter spaces. A thorough experimental evaluation, with the twofold purpose to uncover informative combinations of the selected SXR flare and/or CME input variables, as well as to establish the proper setting for the inherently imbalanced problem at hand was performed. Random Forest (RF), a tree-based ensemble model is found to be the best performing and more robust solution in our evaluation setting, running on both flare and CME data to achieve a POD = 0.76 ( $\pm 0.06$ ), a FAR = 0.34 ( $\pm 0.10$ ), TSS = 0.75 ( $\pm 0.05$ ) and HSS = 0.69 ( $\pm 0.04$ ). Post-hoc analysis was performed, to relate the recovered ML models to the underlying physics of SEP drivers. CME speed and width, along with flare SXR fluence are highlighted as the features with the strongest discriminatory capabilities in our setting.

The prediction of SEP events was treated as a supervised binary classification task. Solar eruptive events (*i.e.* flares, CMEs and their combination) can be allocated to one of two possible classes, depending on whether these are associated with an SEP event ( $>10$  MeV) or not. Thereby, two classes are defined (*i.e.*, 0/1 – no/yes). The models that were constructed include: Logistic Regression (LR), Support Vector Machines with Linear kernels (linSVM) and Non-Linear kernels (SVM), NN, RF, Extremely Randomized Trees (ET) and Extreme Gradient Boosting (XGB) (see details in Lavasa et al., 2021).

#### Inputs:

##### Depend on the dataset used

Characteristics of solar flares and CMEs features were extracted from the source database (Papaioannou et al., 2016), in order to construct the input variable space to all models. These *features* include:

- i Solar-flare heliographic longitude in degrees
- ii The log<sub>10</sub> value of flare peak intensity (W/m<sup>2</sup>) in SXR (1 – 8 Å)
- iii The log<sub>10</sub> value of SXR flare time-integrated flux in J/m<sup>2</sup>
- iv Duration of SXR flare in minutes
- v Rise time of SXR flare in minutes
- vi CME apparent angular width in the sky-plane projection in degrees
- vii CME linear speed in km/s
- viii Cycle index was created as a simple numerical feature, indicative to the magnitude of solar activity at the time when an event occurred

Then *datasets* were created as follows:

1. **Flare dataset** (includes i-v & viii features)
2. **CME dataset** (includes vi-viii features)
3. **Flare & CME dataset** (includes all i-viii features)

In addition, these *datasets* were treated as *Imbalanced* and *Balanced* in two parallel experimental settings, depending on whether all (*i.e.*, negative and positive) class instances were included, or a subset of negative class instances was kept via undersampling, so that the dataset contained an equal number of positive and negative instances. Finally, another condition was imposed based on the treatment applied to Missing Value (MV) s. Thereby, *Noiseless* datasets are the ones where all entries having at least one MV were eliminated and *Noisy* datasets are those for which MVs were filled with the feature's median value.

#### Outputs:

Binary classification includes SEP-associated eruptive events that are assigned a label of + 1, hence the positive class, while the negative class includes eruptive events without SEP association that are assigned a label of –1. All of

the above models (see SubSection 3.12) provided outputs for all of the created datasets (see SubSection 3.12).

#### Free parameters:

The free parameters (hyper-parameters) for each of the examined ML models, are tuned in the inner loop of the adopted nested cross-validation scheme. In this process, each model is built for 1000 randomly chosen hyper-parameter configurations within an extended hyper-parameter grid. The optimal configuration is selected based on mean validation scores. For the best-performing and more robust amongst the examined models, RF, optimized with respect to Precision (=1-FAR), the optimal hyper-parameter set recovered in all five folds is:

- Number of estimators = 800
- Split criterion = Entropy
- Minimum samples per split = 5
- Minimum samples per leaf = 2
- Maximum depth = 50
- Maximum number of features = sqrt(number of features)
- Class weight = 0: 1, 1:500

We note however that different hyper-parameter configurations may be recovered in each fold, but still provide consistent predictions, as is the case when we optimize

RF by means of the F1-score. In any case, our proposed pipeline recovers the optimal free parameter configurations in each fold, to evaluate the combined performance of (classification model + hyper-parameter grid) on the given data.

**Limitations and caveats:** All models predict the occurrence (or not) of an upcoming SEP event.

**Access to model output or forecasts:** None of the implemented ML models have been set into operation. It is envisioned, however, that a selection of the implemented models will be integrated as an independent module into the ASPECS tool in order to facilitate direct comparison of the predictions in archived and near real-time data.

**Model validation:** All models were validated using probabilistic metrics (i.e., POD, FAR, TSS, HSS, F1-Score) for both the established *Imbalanced* and *Balanced* evaluation settings. The reported results in Lavasa et al., 2021 are calculated on the unseen, test partitions of a nested cross-validation scheme, averaged across folds. Out of the datasets configured and employed, the examined models achieve higher SEP predictability effectiveness, in the real-world *Imbalanced* setting, when applied on the *Flare\_CME\_Noiseless* one. As it can be seen in Fig. 3, RF, a tree-based ensemble model is the best performing and more robust solution in our evaluation setting, running on both flare and CME data, achieving  $POD = 0.76$

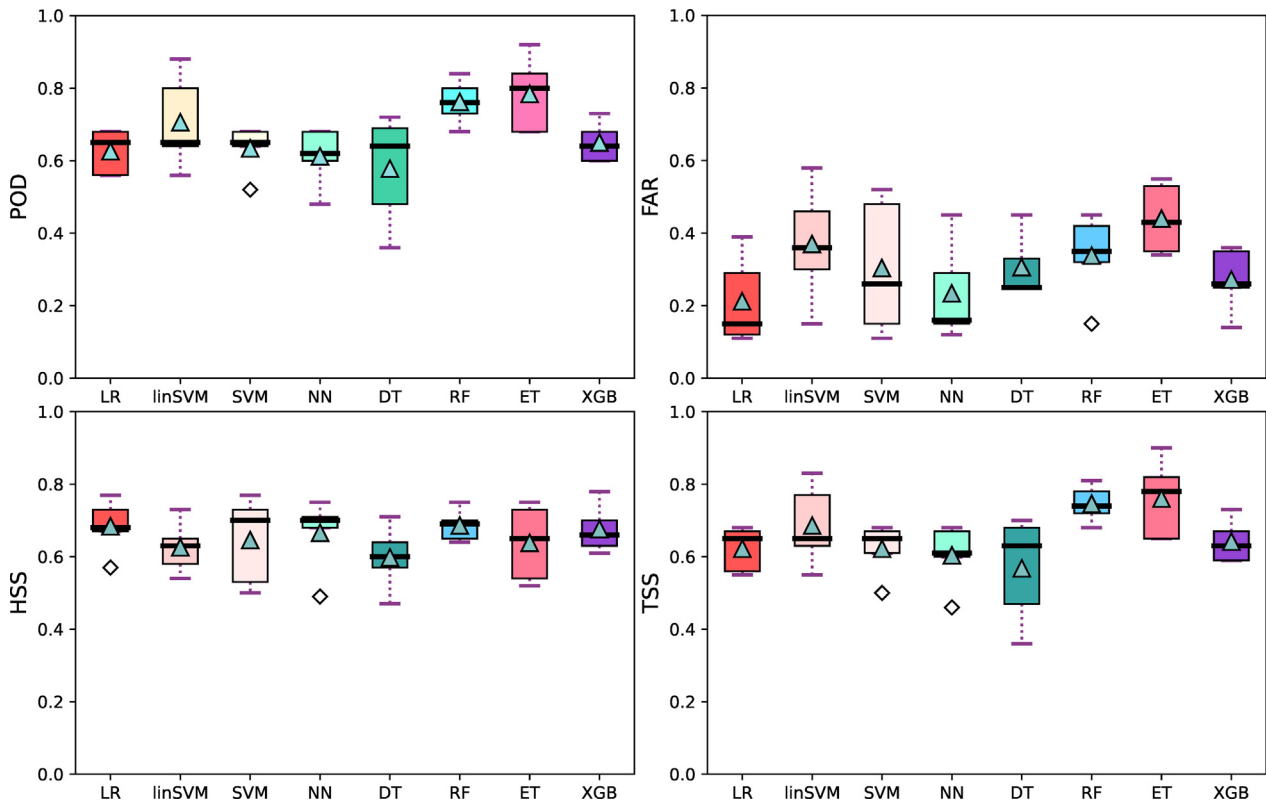


Fig. 3. Lavasa Models' performance plots: POD, FAR, TSS and HSS, on the *Flare\_CME\_Noiseless* dataset configuration. Results obtained by the *Imbalanced* evaluation settings under F1 optimization are displayed. The scores are constructed for each of the eight models employed, which are printed on the x-axis. The mean and median values are indicated by filled triangles and thick horizontal black lines, respectively, while gray diamonds indicate outliers. Figure adapted by Lavasa et al. (2021).



( $\pm 0.06$ ), FAR = 0.34( $\pm 0.10$ ), TSS = 0.75( $\pm 0.05$ ) and HSS = 0.69( $\pm 0.04$ ). As a next step in the evaluation of the ML models the most important features employed in our study that, in turn, would signify the highest prediction capability, were searched for. The average permutation importance scores were calculated, for all models utilizing both flare and CME features in the *Flare\_CME\_Noiseless* dataset signifying that the CME speed, width and SXR fluence are the prime proxies for the identification of an SEP event.

### 3.13. MAG4 - Magnetogram Forecast

**Model developers:** David Falconer (University of Alabama in Huntsville).

**Model description:** Magnetogram Forecast (MAG4) is a probabilistic forecasting tool that is capable of giving probabilities of the following events: M + X-class flares, X-class flares, CMEs, fast CMEs, and SPEs. MAG4 is suited to operational use because it forecasts the probability of  $>10$  MeV protons crossing the 10 Particle Flux Units (1/cm<sup>2</sup>-s-ster) (pfu) threshold prior to observation of the actual event. The model is fully automated, runs in real-time, and is widely used within the forecasting and science communities.

MAG4 starts with magnetograms from SDO/HMI in the form of SHARP data. SHARP data includes an algorithm that identifies an AR on the solar disk. Depending on the forecast mode in MAG4, the model makes use of either the line-of-sight (LOS) or vector magnetograms. Additionally, if Michelson Doppler Imager (MDI) forecast curves are being used, the HMI magnetograms are smoothed to the (lower) MDI resolution.

For each SHARP, MAG4 performs the following steps:

- Use an analytic solution (Alissandrakis, 1981) to calculate the horizontal potential field from the vertical magnetic field at every pixel. In the LOS mode, MAG4 uses the LOS magnetic field to calculate the transverse potential field.
- Use a contour scheme to identify the neutral line. Apply a threshold to the neutral line such that the transverse potential field must be greater than 150 G to capture the neutral line between strong magnetic fields.
- Calculate the following magnetic parameters:
  - Length of the strong-field neutral line.
  - Area with  $|B_z| > 100$  G.
  - Magnetic flux with  $|B_z| > 100$  G.
  - Shear angle between the magnetic field and transverse potential field across each pixel on the neutral line.
  - Gradient of the magnetic field across each pixel on the neutral line.
- Remove any ARs where the length of the neutral line divided by the square root of the area with  $|B_z| > 100$  G is less than 0.75.

- Use the shear angle and gradient along the neutral line to get the event rate per day based on previously derived forecast curves for each event type.
- Use Poisson statistics to convert the event rate per day to a probability. This is done while including the event rates across all ARs currently on the disk.

#### Inputs:

- Magnetograms from one or both of the following instruments:
  - SOHO/ MDI
  - SDO/ HMI
  - Global Oscillation Network Group (GONG) (as a back-up source)
- “MAG4 w/ flaring” model sub-type includes M- and X-class flare history from the previous 24 h for flare productive ARs.

#### Outputs: Probabilities of occurrence of the following:

- M + X-class flares
- X-class flares
- CMEs
- Fast CMEs
- SPEs

MAG4 provides a graphic identifying the locations of each AR identified by the model overlaid on a magnetogram image. A graphical “Threat Gauge” shows the cumulative probability of occurrence for each of the phenomena in the list above.

**Free parameters:** None.

**Limitations and caveats:** MAG4 forecasts are most accurate for ARs within a 45-degree cone from disk center.

**Access to model output or forecasts:** Model is available at CCMC for Runs on Request, as well as on the SEP Probability Scoreboard. Model results can also be viewed on MAG4’s website: <https://www.uah.edu/cspar/research/mag4-page>.

**Model validation:** Model validation has been performed for a version of MAG4 that uses HMI data smoothed to MDI resolution, MDI forecast curves, and previous flare activity Falconer et al. (2014). The study used a monte-carlo technique similar to k-fold cross validation. A fraction of the data set was set aside for testing. The remaining data set was used to train the model, then tested against the training data set. This was repeated many times, and an average skill score was calculated. The results are shown in Table 6 and include a comparison to the model without using previous flare activity.

Space Radiation Analysis Group (SRAG) provided a list of  $>100$  MeV,  $>1$  pfu events and  $>50$  MeV,  $>0.5$  pfu events for verification purposes. Filament eruption events were removed from the event list. Also eliminated from the event list were events with  $>10$  MeV,  $>10$  pfu that

Table 6

Ratios and skill scores for MAG4 with and without flaring. PC = Percent Correct; POD = Probability of Detection; FAR = False Alarm Rate; HSS = Heidke Skill Score; TSS = True Skill Score.

Mode	PC	POD	FAR	HSS	TSS
MAG4 without flaring	95.5 ± 0.5	0.31 ± 0.06	0.50 ± 0.08	0.35 ± 0.05	0.47 ± 0.08
MAG4 with flaring	95.7 ± 0.5	0.38 ± 0.05	0.48 ± 0.06	0.42 ± 0.04	0.49 ± 0.06

had no enhancement at higher energy fluxes. These latter events were deemed to be operationally irrelevant.

### 3.14. MagPy - Magnetogram Forecast in Python

**Model developers:** David Falconer (University of Alabama at Huntsville) and Tilaye Tadesse, Yash Kadadi, and Ian Fernandes (developed at NASA/Johnson Space Center (JSC)/ SRAG).

**Model description:** MagPy is the Python version of MAG4. It is a near real-time large-database program for forecasting an AR's next-day production rate of major flares, CMEs, and SEP events from its free-energy proxy and short-term previous flare productivity. MAG4 is written in Interactive Data Language (IDL) and despite its success, the IDL platform upon which it was built may not serve robust development requirements that are necessary for the model's growth, suggesting a more modern and widespread programming language. With the explosion in popularity of Python, the number of packages and abundant online documentation has grown dramatically, resulting in functions that duplicate and greatly exceed much of IDL's capabilities.

MagPy is designed for the empirical forecasting of M- and X-class flares, CMEs, and SEP events. For each type of event, the algorithm is based on the empirical relationship between the event rate and the free magnetic energy proxy of each AR on the solar disk. The program uses vector magnetograms to measure these free energy proxies, including the gradient of the magnetic field across the neutral line, the magnetic shear angle across the neutral line, and others. These free energy proxies are then related to historically derived event rates, and with Poisson statistics, probabilities of the occurrence of M-class flares, X-class flares, CMEs, Fast CMEs, and SPEs within the next 24 h of a magnetogram are determined.

The proxy of free magnetic energy takes advantage of the observation that non-potential or sheared magnetic fields tend to build up along magnetic neutral lines, as well as the observation that magnetic neutral lines that have strong gradients across them in the vertical magnetic field nearly always have a strongly sheared horizontal field along them. In order to evaluate these proxies, we have to identify the strong field neutral line in the magnetic island. The neutral line (or polarity inversion line) in an AR's magnetogram is the line that separates positive and negative polarity flux, i.e., the zero-Gauss contour. We divide the zero-Gauss contour into segments, each roughly a pixel in length. For each segment, its length, neighbor

segments, the interpolated values of the potential horizontal field at the midpoint of the segment, the vertical gradient of the vertical field at the midpoint, the average positive field nearby, and the average negative field nearby are compiled. A segment is considered if it meets the following two conditions: (1) it has a strong potential horizontal field (greater than optimal potential magnetic field value) and (2) it separates at least moderately strong positive and negative fields (optimally-pixel-smoothed fluxes of both polarities are stronger than optimal field value). The potential horizontal field is calculated from the observed vertical component of an AR's magnetogram. The rules for average positive and negative field strength ensure that the segment separates active region polarities rather than an active region polarity and a quiet Sun polarity. The remaining segments are further checked for whether they have a neighbor segment; isolated segments are discarded. Overall MagPy data processing techniques are shown in Fig. 4.

In order to determine the optimal function relating event rate and total non-potentiality as well as the optimal data selection criteria and magnetic field thresholds to use in the forecasting process, data mining must be performed. The idea behind data mining is that data from many years can be processed and analyzed for their free magnetic energy proxies and other related parameters to determine the most accurate function relating an active region's total non-potentiality to its major solar flare event rate. We run the data mining process with thousands of magnetic field threshold configurations (see optimal thresholds previously mentioned) and compare skill scores across the validation results to determine the best set of magnetic field thresholds for operational use. In doing that, we have succeeded in improving the HSS skill score of 0.32 in MAG4 to 0.48 in MagPy.

For each SHARP, MagPy performs the following steps:

- Use an analytic solution to calculate the transverse potential field from the  $B_z$  magnetic field at every pixel.
- Use a contour scheme to identify the neutral line. Apply a cut to the neutral line such that the transverse potential field must be greater than its optimal field value threshold and the averaged positive and negative field magnitudes must be greater than their optimal threshold to capture the neutral line between strong magnetic fields.
- Calculate the following magnetic parameters:
  - Length of the strong-field neutral line.
  - Area with  $|B_z| > \text{optimal magnetic field value}$ .

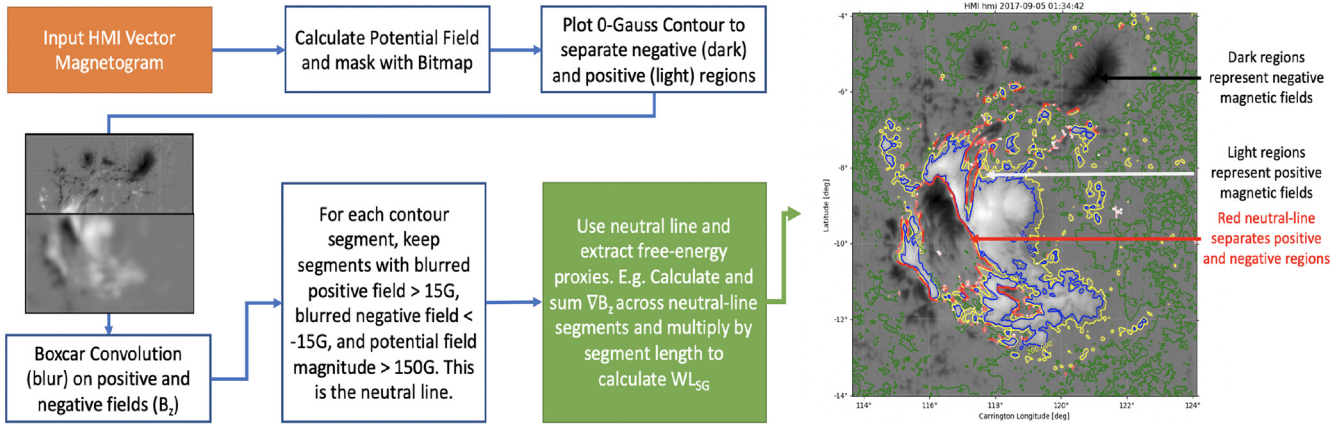


Fig. 4. MagPy Image Processing Pipeline: a succinct summary of the image processing techniques used to extract free-energy proxies.

- Magnetic flux with  $|B_z| > \text{optimal magnetic field value}$ .
  - Shear angle between the magnetic field and transverse potential field across each pixel on the neutral line.
  - Gradient of the magnetic field across each pixel on the neutral line.
- Use the shear angle and gradient along the neutral line to get the event rate per day based on previously derived forecast curves for each event type.
  - Use Poisson statistics to convert the event rate per day to a probability. This is also performed for the aggregate of event rates across all ARs currently on the disk to get a full-disk probability.

#### Inputs:

- Vector magnetograms from the SDO/ HMI
- NOAA Solar Region Summary (SRS)
- CCMC-Database Of Notifications, Knowledge, Information (DONKI) Flare database

**Outputs:** Probabilities of occurrence of the following:

- M + X-class flares
- X-class flares
- CMEs
- Fast CMEs
- SPEs

**Free parameters:** None.

**Limitations and caveats:** Each magnetogram is also subject to multiple quality control checks put in place to increase the fidelity of the data analyzed. MagPy utilizes a 45-degree cone filter to discard magnetograms on the limbs of the solar disk. These magnetograms, distorted by effects like foreshortening, engender high degrees of error in free-energy proxy calculations and spawn false neutral-lines. As these types of magnetograms can severely skew the correlation between proxies and event-rates, they

are left out of the training dataset. MagPy is most accurate within a 45 degree cone from disk center.

**Access to model output or forecasts:** The model will be available at CCMC for Runs on Request, as well as on the SEP Probability Scoreboard.

**Model validation:** MagPy is actively under development, including the addition of SEP forecasting capabilities, and validation will be carried out after the model is finalized.

#### 3.15. MEMPSEP - Multivariate Ensemble of Models for Probabilistic SEP prediction

**Model developers:** Maher A Dayeh (Southwest Research Institute (SWRI), University of Texas San Antonio), Andres Munoz-Jaramillo (SWRI Boulder), Hazel M. Bain (Cooperative Institute for Research in Environmental Sciences (CIRES)), Subhamoy Chatterjee (SWRI Boulder), Kimberly D. Moreland (University of Texas San Antonio, SWRI).

**Model description:** The Multivariate Ensemble of Models for Probabilistic SEP prediction (MEMPSEP) is based on a data-driven Convolutional Neural Network (CNN) (LeCun and Bengio, 1998) architecture that takes both remote images (SOHO/MDI and SDO/HMI full-disk magnetogram sequences for now) and in situ pre-flare to post-SEP parameters as inputs and provides (i) SEP occurrence probability and in the case this probability passes a certain threshold, it then provides (ii) absolute prediction of physical SEP properties (e.g., SEP peak flux), as illustrated in a flowchart (see Fig. 5).

This must be emphasized that the objective here is not to do just a binary classification. Instead, the focus is on estimating true probabilities of SEP occurrence with associated uncertainties (using a model-ensemble). The aim is to provide flexibility for the users of MEMPSEP forecast to determine their own acceptable level of risk, rather than imposing a threshold of detection that optimizes an arbitrary binary classification metric. Furthermore, instead of training a single model, the class imbalance between negative and positive events is utilized to train an ensemble of

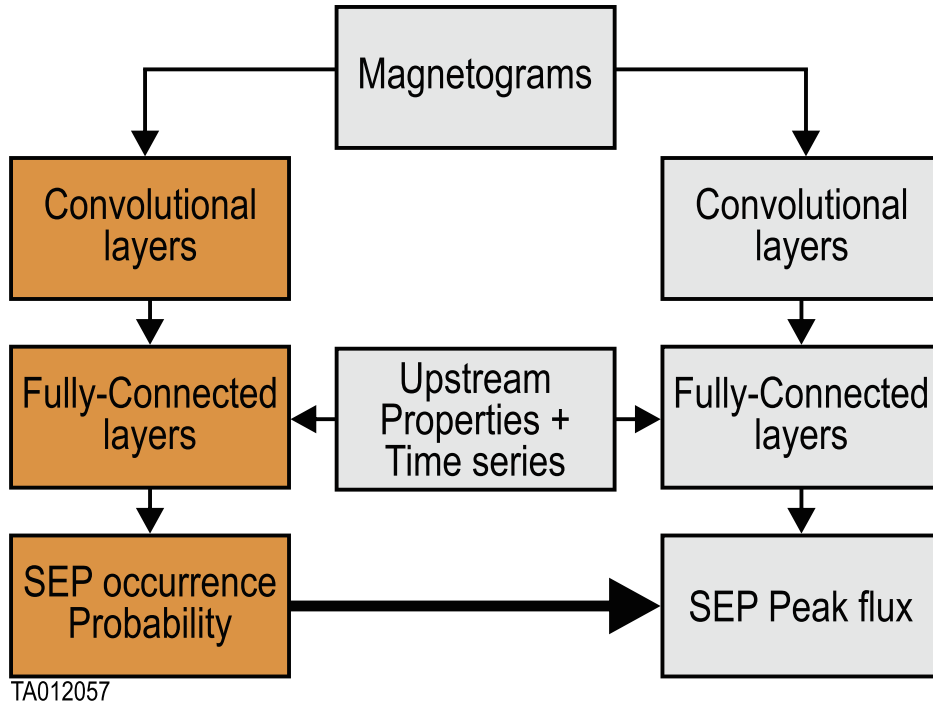


Fig. 5. Architecture of MEMPSEP model.

models. This has the added benefit of providing a clear measure of uncertainty in the forecast. The predicted SEP occurrence probability of each ensemble model is calibrated (Guo et al., 2017) such that the probabilistic forecast is reliable (Bain et al., 2021) to use.

The design of the test set is tailored to be non-modulated by the solar cycle and the model inferences are evaluated with uncertainty for each event within the test set. Based on the median of the ensemble and a probability threshold of 0.5, a few classification metrics (Bain et al., 2021) are estimated, reported at the end of this section.

For SEP peak prediction task, a similar CNN architecture, as in prediction of SEP occurrence probability, is trained. The layers are frozen for probability estimation branch and those probabilities are used to penalize the loss function for training the SEP peak prediction layers (Fig. 5). This coupling is done to ensure tighter prediction of SEP peak for the events with higher predicted probabilities.

The dataset driving MEMPSEP is a multivariate remote and in situ dataset. The main event list is based on the GOES flare list from the Heliospheric Event Knowledgebase (HEK) and contains over 17,000 flare events. For each flare event, remote solar images along with spacecraft measured X-ray, radio, proton, electron, upstream Interplanetary (IP) plasma and magnetic field properties are included, in addition to associated IP coronal mass ejections and IP shock parameters, whenever available. The in situ data comes from multiple instruments onboard different operational missions, including GOES, Advanced Composition Explorer

(ACE), and Wind spacecraft. The remote sensing data, also from various instruments, comprises full-disk magnetograms, EUV, and coronagraph images from STEREO, SOHO, and SDO. Positive SEP events are selected based on a defined threshold using the integrated proton fluxes. Physical SEP properties such as SEP duration, peak flux, elemental composition, and fluence for each event are also derived and included. Averaged elemental composition of the suprathermal particles (Dayeh et al., 2009; Dayeh et al., 2017) prior to each event by up to 3 days is also calculated and included as an input. Special consideration is given to data that is currently obtained in operational real-time or that will be available in real-time on upcoming missions.

**Inputs:** Current form of MEMPSEP ingests the following inputs-

- Full-disc (SOHO/MDI + SDO/HMI) magnetogram sequences spanning over 3 days prior to flare-onset with a temporal resolution of 6 h.
- Pre-flare upstream properties such as solar wind plasma (speed, density), interplanetary magnetic field components and elemental abundances etc.
- GOES X-ray pre-flare time series for 24 h with a temporal resolution of 1 min.
- GOES Electron pre-flare time series for 24 h with a temporal resolution of 5 min.

The model has capability to also seamlessly ingest inputs such as SOHO/Extreme ultraviolet Imaging Telescope (EIT) 171Å + SDO/AIA 171Å image sequences, SOHO/

LASCO-C2 + C3 image sequences and WIND/WAVES data reflecting radio bursts.

**Outputs:** MEMPSEP performs both classification and regression tasks. For every set of (remote + in situ) inputs MEMPSEP produces following outcomes:

- SEP occurrence probability and associated uncertainty
- SEP properties (e.g., peak flux, fluence, event spectrum, time to peak, duration etc.) and associated uncertainty for user defined energy range

**Free parameters:** The prediction model-ensemble does not have tunable parameters that need to be fine-tuned by the user/forecaster. However, it relies on the training of an ensemble of neural networks which involves the creation of training, validation, and test sets; definition of a neural network architecture, and choosing a neural network optimizer with hyperparameters.

**Limitations and caveats:** CNNs are data hungry algorithms, so they need to be trained and deployed very carefully to avoid overfitting. This is marked as the limitation/caveat because there is a series of good practices that need to be followed strictly in order for the results to be meaningful. This includes:

1. a strict separation between training + validation and test sets.
2. a disciplined optimization of the experiments exclusively on training + validation sets.
3. to never make architecture or training decisions based on the final results of deploying on the test set.

Furthermore, MEMPSEP currently comprises of an ensemble of 10 models. However, it is unknown what is the critical number of ensemble members after which the uncertainty in predicted SEP occurrence probability and peak flux converges. MEMPSEP group is currently working on that aspect and also investigating the effect of additional inputs on the prediction.

**Access to model output or forecasts:** The model is currently not available to the public.

**Model validation:** The validation of MEMPSEP is done on a test set comprising of unseen events tied to different flare classes (C, M, X) and spanning over the years 1998–2013. Based on the median of the model-ensemble prediction and a probability threshold of 0.5 (as used in different SEP classification models, [Bain et al., 2021](#)), a few classification metrics are evaluated. The POD (TP/TP + FN) and False Positive Rate (FP/FP + TN) are found to be 0.79 and 0.27 respectively, TSS and HSS are to be 0.52 and 0.43 respectively. The metrics, namely AUC (ROC) and Brier Score (BS), that do not depend on a single classification threshold, are also estimated. AUC and BS are found to be 0.85 and 0.14 respectively. The regression step provides a statistically significant correlation of  $\sim 0.55$  between target and predicted median peaks for positively predicted events.

### 3.16. M-FLAMPA - Multiple-Field-Line-Advection Model for Particle Acceleration

**Model developers:** Igor V. Sokolov, Lulu Zhao, Zhen-guang Huang, Dmitry Borovikov, Iliia Roussev, Aleksandre Taktakishvili, Frederic Effenberger, and Tamas Gombosi (developed at the University of Michigan).

**Model description:** The SEP forecast model, Multiple Field Line Advection Model for Particle Acceleration (M-FLAMPA), is composed of several fully coupled modules in the SWMF developed at the University of Michigan ([Borovikov et al., 2018](#)). There are three components in this SEP forecast model: 1) background solar wind, 2) coronal mass ejections, and 3) particle acceleration and transport. The background solar wind plasma in which the SEPs propagate is modeled by the AWSOM-Realtime (AWSOM(-R)) driven by the near-real-time hourly updated GONG (bihourly Air Force Data Assimilation Photospheric flux Transport (ADAPT)-GONG) magnetogram. In the background solar wind, real/hypothetical CMEs are regularly launched employing the Eruptive Event Generator using Gibson-Low configuration (EEGGL), by inserting a flux rope estimated from the free magnetic energy in the active region. The acceleration and transport processes are then modeled self-consistently by the multiple magnetic field line tracker (MFLAMPA). The three modules are now fully integrated and run faster than real-time, thus providing a forecast capability.

The 3D global solar wind plasma in the Solar Corona ( $1-20R_s$ ), Inner Heliosphere ( $20R_s - 2$  AU) and Middle Heliosphere (2 AU – 20 AU) are modeled by the AWSOM(-R) configuration in SWMF ([Sokolov et al., 2013](#); [Sokolov et al., 2021](#); [Gombosi et al., 2018](#); [Gombosi et al., 2021](#)). AWSOM(-R) is an Alfvén wave-driven, self-consistent solar wind model, in which the coronal plasma is heated by the dissipation of two discrete turbulence populations propagating parallel and antiparallel to the magnetic field ([Sokolov et al., 2013](#)). AWSOM applies a semi-empirical coronal heating function that is based on these aspects of the physics of Alfvén waves. The fully 3D version of AWSOM is computationally expensive. And AWSOM-R is a version that runs faster than real-time by reducing the 3D problem to a 1D problem by bringing boundary conditions up from the solar surface along 1D *threads* and adopting the simplifying assumption that the magnetic field may be considered to be potential within a certain radial distance from the Sun.

The CME/Coronal Mass Ejection (ICME) simulation in this SEP forecast model is driven by the EEGGL module in SWMF ([Jin et al., 2017](#); [Borovikov et al., 2017](#)). The initial conditions of the CME within the solar corona is treated by inserting an unstable (or force imbalanced) flux rope suggested by [Gibson and Low \(1998\)](#) into an active region of the solar corona. The magnetogram from GONG and the observed CME speed (from CDAW catalog and/or DONKI database) are used to calculate the flux rope parameters. This approach offers a relatively simple, and

inexpensive model for CME initiation based on empirical features of pre-event conditions (Gombosi et al., 2021). The EEGGL module is publicly available for download at <http://csem.engin.umich.edu> or can be used through CCMC (<https://ccmc.gsfc.nasa.gov/eeegl/>).

In the proposed SEP forecast model, protons are accelerated at the shocks driven by the CMEs through first order Fermi acceleration mechanism (e.g., Axford et al., 1977; Krymsky, 1977). The original FLAMPA scheme was developed by Sokolov et al. (2004). In this early version the energetic particle distribution function was solved along a single time-evolving magnetic field line. MFLAMPA is a high-performance extension of FLAMPA, enabling us to solve the kinetic equation of SEPs along a multitude of magnetic field lines simultaneously. The line-extracting procedure is augmented with an algorithm designed to interpolate the fields sampled on block adaptive grids (Borovikov et al., 2015) that eliminates spurious distortions near grid resolution interfaces that routinely occur in large-scale MHD grids. Such artifacts could result in unphysical particle acceleration, but they are thus avoided in the model. In addition, novel mathematical methods have been applied to the extracted magnetic field lines to sharpen the shocks thus making the Fermi acceleration process to be more efficient.

MFLAMPA is directly coupled with AWSOM-R and EEGGL within the SWMF. Magnetic field lines are extracted seamlessly from the active region in the solar corona through the inner and middle heliosphere to the observer and are passed to MFLAMPA. MFLAMPA then calculates the evolving energetic particle populations by solving the kinetic equations. MFLAMPA incorporates the effects of the near-Sun field line meandering that affects the perpendicular transport of SEPs and can explain the occurrence of large longitudinal spread observed even in the early phases of such events.

**Inputs:** The input to the model includes the magnetogram that drives the background solar wind simulations, e.g., GONG, HMI, and ADAPT-GONG. The CME speed, together with the magnetogram is needed to calculate the parameters of the flux rope that will be inserted into the corresponding active region.

**Outputs:** Since the MFLAMPA model calculates the distribution function of energetic particles within the energy range of 10 keV to 1 GeV, the model is able to output the time intensity profiles, at energies >10 MeV, >50 MeV, >100 MeV, or otherwise specified by the user, along each individual magnetic field line extracted using MFLAMPA. Moreover, an ensemble average and standard deviation of the intensity profiles on the magnetic field lines around the observational point of interest is also provided. The intensity at the prescribed energies on the longitude and latitude sphere at certain radial distance is also provided.

**Free parameters:** The free parameters of the model consist of the treatment of particles' injection, i.e., seed populations into the shock system. In the current model, we

follow the seed particle setup in Sokolov et al. (2004), assuming a suprathermal tail of protons from the thermal distribution at the local kinetic temperature through the injection energy, which is a free parameter. The injection energy is set to be 10 keV. We are currently working on scaling the suprathermal seed particle distribution observed at 1 AU<sup>11</sup> back to the sun and extract the seed population.

**Limitations and caveats:** The integrated AWSOM(-R), EEGGL and MFLAMPA model is time and computation resource consuming. When the CME propagates in the solar corona domain (SC domain,  $1R_s \sim 20R_s$ ), the integrated model runs as fast as the real time using 4000 cpu cores. The most time consuming component is the MHD simulation of the CME propagation in the SC. When the CME left the SC domain, the integrated model runs much faster than real time. Another limitation of the model is the specification of the injected seed population.

**Access to model output or forecasts:** Users will be able to access MFLAMPA and associated models on CCMC's runs-on-request system (<https://ccmc.gsfc.nasa.gov/requests/requests.php>).

**Model validation:** The background solar wind model is validated by comparing the simulations and observations for both in situ solar wind and the predicted LOS appearance of the corona in different wavelengths. A detailed validation study of the solar wind model can be found in (Sachdeva et al., 2019; Gombosi et al., 2021). The EEGGL model to initialize CMEs and the subsequent CME/ICME evolution has been extensively used and validated (Jin et al., 2017, Manchester et al., 2004, 2005, 2008, 2012, 2014, Manchester et al., 2017, Roussev et al., 2004, Roussev, 2008, van der Holst et al., 2007, 2009). Borovikov et al. (2018) showed a proof-of-concept demonstration of AWSOM-R, EEGGL, and MFLAMPA for the January 23, 2012 SEP event. The simulated >10 MeV time profile is plotted alongside GOES, however, no further analysis is performed.

### 3.17. PARADISE - Particle Radiation Asset Directed at Interplanetary Space Exploration

**Model developers:** Nicolas Wijsen (Katholieke Universiteit (KU) Leuven), Angels Aran (Universitat de Barcelona), Stefaan Poedts (KU Leuven, University of Maria Curie-Skłodowska).

**Model description:** PArTicle Radiation Asset Directed at Interplanetary Space Exploration (PARADISE; Wijsen, 2020) is a physics-based model aimed at simulating the acceleration and transport of energetic particles in the inner heliosphere. This is done by evolving energetic particle distributions through a solar wind configuration generated by the time-dependent three-dimensional MHD model named EUropean Heliospheric FORecasting Information

<sup>11</sup> [https://ccmc.gsfc.nasa.gov/assessment/topics/SEP/campaign2020/seed\\_population.php](https://ccmc.gsfc.nasa.gov/assessment/topics/SEP/campaign2020/seed_population.php).

Asset (EUHFORIA; Pomoell and Poedts, 2018). The coupling of PARADISE to EUHFORIA allows the model to simulate the effect of large-scale solar wind structures on the transport of energetic particles in the heliosphere. For example: [1] Wijsen et al. (2019b) and Wijsen et al. (2019a) studied how a high speed stream and a Co-rotating Interaction Region (CIR) can affect the transport and energization of impulsive SEP events. [2] Wijsen et al. (2022) simulated the particle transport and acceleration in an CME-driven shock wave, to reproduce the ESP event on 14 July 2012. An example PARADISE simulation for 9 October 2021 is shown in Fig. 6.

PARADISE is a Monte Carlo code that solves the five-dimensional Focused Transport Equation (FTE, e.g., le Roux and Webb, 2009) by integrating an equivalent set of stochastic differential equations forward in time using the Itô calculus (Gardiner, 2004). The FTE accounts for the particles' pitch-angle and momentum changes in compressional, shear, and accelerating solar wind flows, which are omni-present in EUHFORIA solar wind simulations. In addition, the FTE solved in PARADISE models the effect of small-scale turbulence on the energetic particle transport by including a spatial diffusion process perpendicular to the IMF and a pitch-angle diffusion process. Various different pitch-angle and perpendicular diffusion theories are available for use in PARADISE, which is made possible by its modular implementation structure (see Wijsen, 2020, for a full overview). The modular implementation of the code makes it also straightforward to add new diffusion theories to the model in the future. Moreover, the energetic particle's guiding center drifts due to magnetic gradients and the curvature of the IMF can be

included in the PARADISE simulations (e.g., Wijsen et al., 2020; van den Berg et al., 2021). Finally, we note that Chapter 3 of Wijsen (2020) describes the implementation of the PARADISE model in detail.

**Inputs:** PARADISE requires three different kinds of inputs:

1. EUHFORIA data files, which contain the solar wind velocity and magnetic field vectors on a spherical grid. As input, EUHFORIA simulations use synoptic magnetograms provided by the GONG. In addition, imaging observations can be used to constrain the input parameters of the CMEs that can be injected into the EUHFORIA simulation.
2. Particle injection distribution: To run PARADISE, the user needs to provide a particle injection distribution which can have both a spatial and a temporal dependence. Moreover, the injection distribution can depend on the properties of the background solar wind. For example, in Wijsen et al. (2021) and Wijsen et al. (2022), the particle injection distribution was assumed to be non-zero only at some of the interplanetary shock waves present in the simulation and, in addition, the injection distribution was scaled proportionally to the divergence of the solar wind velocity vector.
3. A configuration file which contains the information about the particle type (electrical charge and rest mass), the particle diffusion conditions, and the resolution of the output grid.

**Outputs:** PARADISE provides the directional particle intensities as a function of time on a five-dimensional grid.

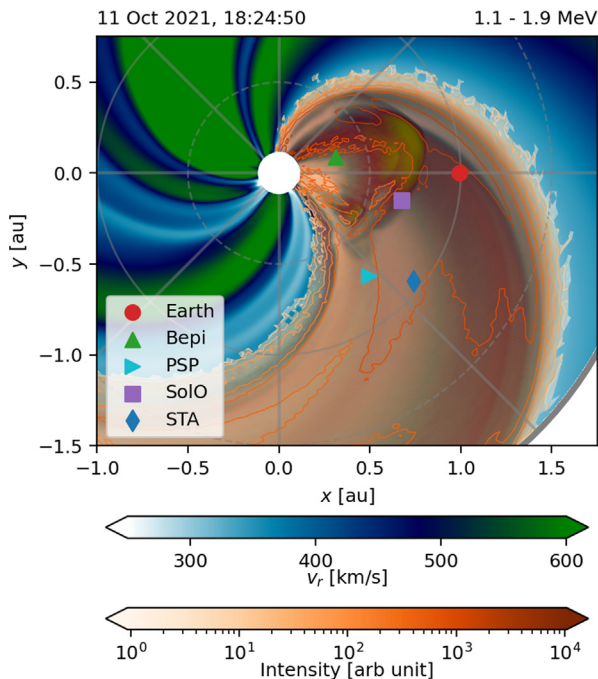


Fig. 6. An example of a PARADISE simulation for the 9 October 2021 event. The left panel shows, in orange shades, a snapshot of the 1.1 – 1.9 MeV proton intensities. The background shows the radial speed profile of a EUHFORIA solar wind simulation, including a CME. The right panel shows the simulated time-intensity profiles (top panel), solar wind speed (middle panel), and solar wind magnetic field (bottom panel) at the location of Solar Orbiter.

The first three dimensions of the grid correspond to the spatial dimensions and cover the inner heliosphere. The two remaining dimensions of the grid correspond to the energy and the pitch-angle coordinate of the energetic particles. The resolution of the output grid and the energy coverage is defined by the user in the configuration file.

The model also provides the directional particle intensities, the first-order parallel anisotropies, and the omnidirectional particle intensities at the location of the planets and most spacecraft, including the STEREO spacecraft, PSP, SO, and BepiColombo. In addition, the user can add additional virtual spacecraft to the simulations.

Finally, PARADISE contains python scripts and Jupyter Notebooks which can be used to visualize the simulation output.

**Free parameters:** PARADISE incorporates several different diffusion theories, which all have various free parameters. For example, the implemented pitch-angle diffusion theories are derived from Quasi-Linear Theory (QLT; Jokipii, 1966), and require the user to specify the properties of the slab component of the solar wind magnetic turbulence. As a default, the slab spectrum is assumed to follow a Kolmochorov dependence in the inertial range and the level of turbulence is assumed to be a fraction of the large-scale background magnetic field. Alternatively, the level of pitch-angle diffusion can be fixed by assuming that the energetic particles have a constant radial or parallel mean free path. Similarly, PARADISE includes different perpendicular diffusion theories. The simplest model assumes that the particles' have a constant perpendicular mean free path. More advanced models, like e.g., the non-linear guiding center theory (Matthaeus et al., 2003), require the user to specify the properties of the 2D component of the solar wind magnetic turbulence.

Apart from the diffusion theories, the particle injection distribution introduces several free parameters in PARADISE. In fact, the user has the freedom to provide its own injection function with an associated set of free parameters (e.g., Wijzen et al., 2019b). This particle injection distribution can, for example, depend on the MHD variables of the EUHFORIA solar wind simulation (e.g., Wijzen et al., 2021; Wijzen et al., 2022). Other parameters include the description of the injection energy spectrum, which can be, for example, a mono-energetic or a (broken) power law (e.g., Wijzen et al., 2020). The initial pitch-angle distribution can also be specified to be (an) isotropic.

**Limitations and caveats:** When using the PARADISE model, the following limitations should be taken into account:

1. In PARADISE, the energetic particles are assumed to propagate as test particles through the solar wind. As a result, PARADISE does not capture the turbulence generated by energetic particles in the foreshock regions of CMEs, although this turbulence can be added in an ad hoc fashion (see Wijzen et al., 2022).

2. PARADISE provides a default particle injection function at CME-driven shock waves, which scales proportionally to the local divergence of the solar wind velocity. However, this injection function has not yet been calibrated to in situ data, which limits the capabilities of PARADISE as a SEP forecasting tool. In the future, this limitation will be addressed by using results from the SOLAR Particle Acceleration in Coronal Shocks (SOLPACS; Afanasiev et al., 2015) model, which simulates particle acceleration at oblique shock waves, hereby taking into account the generation of Alfvén waves in the upstream shock region by the energetic particles.

**Access to model output or forecasts:** The PARADISE model is currently being implemented in the Virtual Space Weather Modelling Centre (VSWMC; Poedts et al., 2020) of the ESA. Once implemented, users will be able to perform PARADISE simulations through a front-end Graphical User Interface (GUI). In addition, the model repository is made available upon request.

**Model validation:** The validation of PARADISE is an actively ongoing process. The implementation of the model was first tested by performing simulations in a synthetic solar wind configuration containing a CIR (see Wijzen et al., 2019b; Wijzen et al., 2019a; Wijzen et al., 2020). More recently, the validation effort of the model has been focused on reproducing in situ observed energetic particle events. In Wijzen et al. (2021), PARADISE was used to successfully reproduce an energetic particle event associated with a CIR, which was observed in September 2019 by both PSP and STEREO-A. This simulation captured both the acceleration and the transport of the energetic protons associated to the CIR. In Wijzen et al. (2022), PARADISE was used to reproduce the ion intensity-time profiles observed near Earth on 14 July 2012. The CME generating this ESP event was simulated by using the spheromak model of EUHFORIA. For energies below  $\sim 1$  MeV, the simulation results were shown to agree well with both the upstream and downstream components of the ESP event observed by ACE. In the future, we plan to extend our study by modelling several of the recently observed multi-spacecraft SEP events of SC25.

### 3.18. PCA (Papaioannou) Model - Principal Component Analysis

**Model developers:** Athanasios Papaioannou (NOA), Anastasios Anastasiadis (NOA), Athanasios Kouloumvakos (Institut de Recherche en Astrophysique et Planétologie (IRAP)), Miikka Paassilta (University of Turku (UTU)), Rami Vainio (UTU), Eino Valtonen (UTU), Anatoly Belov (Pushkov Institute of Terrestrial Magnetism, Ionosphere and Radio Wave Propagation (IZMIRAN)), Eugenia Eroshenko (IZMIRAN), Maria Abunina (IZMIRAN), Artem Abunin (IZMIRAN).



**Model description:** The Papaioannou Model (Papaioannou et al., 2018) is a post-eruption model that uses Principal Component Analysis (PCA) to forecast the probability of SEP occurrence.

PCA is a dimension-reduction method typically used to reduce the number of correlated variables in large data sets. The method transforms the variables into orthogonal components called Principal Component (PC). The PCOMs are composed of uncorrelated variables in terms of the original correlated variables.

In the case of the Papaioannou Model, PCA is used to reduce the number of features and to create a combination of the uncorrelated features in order to calculate a probability of SEP occurrence. The features included here are the log of the flare peak flux, flare longitude, flare rise time, flare duration, CME velocity, and CME width. A sigmoid function is used to relate the combination of features to a probability.

$$P(x) = \frac{1}{1 - \exp[-\theta^T g(x)]} \quad (6)$$

Here,  $g(x)$  is a function of the PCOMs, and  $\theta^T$  are the coefficients. The function  $\theta^T g(x)$  depends on the type of logistic regression used. The following are the types of regression considered:

- One-parameter linear:  $\theta^T g(x) = \theta_0 + \theta_1 x$
- Multiple linear:  $\theta^T g(x) = \theta_0 + \theta_1 x^{(1)} + \theta_2 x^{(2)}$
- Multiple non-linear:  $\theta^T g(x) = \theta_0 + \theta_1 x^{(1)} + \theta_2 x^{(2)} + \theta_3 x^{(1)} x^{(2)}$

where  $x$  can be any combination of PCOMs such as PCOM1, PCOM2, PCOM1 + PCOM2, etc. The coefficients were estimated by using the Broyden-Fletcher-Goldfarb-Shanno (BFGS) quasi-Newton method to reduce the negative log-likelihood function. This function reached a minimum for a probability threshold of 50% for event occurrence.

**Inputs:**

- Log of the flare peak flux
- Flare longitude

- Flare rise time
- Flare duration
- CME velocity
- CME width

**Outputs:**

- Probability of SEP occurrence

**Free Parameters:** None.

**Limitations and Caveats:** Model predictions are very straight forward. The model outputs the probability of SEP occurrence where an event is defined as >10 MeV protons above 10 pfu. A probability below 50% should be interpreted as no event will occur, while a probability above 50% should be interpreted as an event will occur.

**Access to model output or forecasts:** The PCA model is incorporated into FORSPEF. See Section 3.9 for access to forecasts.

**Model validation:** Validation included two methods: single variable logistic regression and multivariate logistic regression. Both methods used an optimized probability threshold (pt) of 50% for SEP occurrence. An event was defined as > 10 MeV protons above 10 pfu. For single variable logistic regression, 3598 predictions were made (34 true positive, 27 false positive, 3510 true negative, and 34 true positive). For multivariate logistic regression, 3663 predictions were made (69 true positives, 57 false negatives, 3507 false negatives, and 30 false positives). The table below summarizes the resulting POD, FAR, and HSS for all validations. The highest scoring method was a type of multivariate logistic regression with a POD of 58.73%, FAR of 24.49%, and HSS of 0.6502.

The best skill scores were I(3) and I(3 + O2) (see Table 7). As a result, their categorical measures were calculated as a function of the probability threshold. That is, the pt was treated as an independent parameter (not set to 50%) ranging between 0.0 to 1.0 with a step of 0.1. For both schemes, the optimal skill score was achieved at a range of pth from 25% to 40%. The optimal HSS is observed at pth = 0.33 (HSS = 0.6411) for I(3) and at pth = 0.25 (HSS = 0.6579) for I(3 + O2). In turn, this results in a POD = 65.87% and an FAR = 35.16% as well as a POD = 77.78% and an FAR = 40.96%, respectively.

Table 7  
Results of validation from single variable and multivariate logistic regression applied in the Papaioannou (PCA) Model.

index	Form (Scheme)	POD (%)	FAR (%)	HSS
$I^{(1)}$	[PC1]	26.98	44.26	0.3490
$I^{(2)}$	[PC1,PC2]	54.76	30.30	0.6013
$I^{(3)}$	[PC1,PC2,PC3]	55.56	28.57	0.6134
$I^{(4)}$	[PC1,PC2,PC3,PC4]	53.97	29.17	0.6007
$I^{(5)}$	[PC1,...,PC5]	53.17	29.47	0.5943
$I^{(6)}$	[PC1,...,PC6]	53.17	28.72	0.5973
$I^{(2+\sigma^2)}$	[PC1,PC2,PC1 <sup>2</sup> ,PC2 <sup>2</sup> ,PC1·PC2]	56.35	31.07	0.6080
$I^{(3+\sigma^2)}$	[PC1,PC2,PC3,PC1 <sup>2</sup> ,PC2 <sup>2</sup> ,PC3 <sup>2</sup> ,PC1·PC2]	58.73	24.49	0.6502

### 3.19. PHSVM

**Model developers:** Pouya Hosseinzadeh, Soukaina Filali Boubrahimi (Utah State University).

**Model description:** Support Vector Machine (SVM) is a machine learning model that finds a hyperplane that best divides the dataset into different classes. PHSVM is an SVM model that follows the same idea described in Boubrahimi et al. (2017), in order to predict >100 MeV SEP events and non-SEP events.

The data used to train PHSVM is composed of GOES X-ray flux and proton flux channels as multivariate time series that led to >100 MeV events, considered as the positive class, and multivariate time series proton data that did not lead to >100 MeV events, which are considered as the negative class. Specifically, PHSVM considers X-ray channel (xl) and proton channel P8 (p8\_flux) as a multivariate time series to classify specific events into SEP and non-SEP events.

One of the model's hyperparameters is the span window, which is defined as the number of hours that constitute the observation period prior to an X-ray event. A span of 120 time steps has been found to be optimal for training our model. Each time step corresponds to a 5-min average of X-ray or proton flux channels, which makes our span equivalent to 10 h. PHSVM considers each SEP or non-SEP sample as a 2x120 matrix that is composed of 120 X-ray and 120 proton flux channel data points.

The input training data for training the model is composed of a balanced number of samples, 50 (2 × 25) samples for the positive and negative classes that are collected from GOES measurements from the period between 1997 and 2002.

**Inputs:** The model inputs are multivariate times series of two channels from the GOES X-ray and proton instruments.

**Outputs:** The model output is a binary flag for >100 MeV SEP event or non-SEP event.

**Free parameters:** This is a machine learning model and it does not contain free parameters in the same sense as a physical model. However, the span window and SVM kernel are set during the model's hyper-parameter search.

**Limitations and caveats:** This is an "all clear" evaluation indicating whether there is >100 MeV SEP event or non-SEP events. Therefore, predicting the exact intensity is missing since other energy channels are ignored. Furthermore, the training and validation sets used in this study are not adequate for providing a general and robust result. One may consider more events for training and testing the model.

**Access to model output or forecasts:** Output from this model is not currently available to the public.

**Model validation:** The model was trained on 50 events including both classes. The evaluation process was performed on 10 non-SEP and 6 SEP events. The result was as follows: accuracy = 0.86, recall = 0.83, precision = 0.83, F1 = 0.83. Furthermore, we added a lag time of 5 h before

the solar flare onset time to provide the stakeholders with extra time to make decisions. The accuracy dropped to 0.83.

### 3.20. PROTONS

**Model developers:** Christopher C. Balch (NOAA SWPC).

**Model description:** The PROTONS model is the operational SEP proton prediction model currently used by the NOAA SWPC forecast office (Balch, 1999; Balch, 2008). It predicts >10 MeV SEP occurrence and maximum flux from ≥C2.4 flares derived from time-integrated SXR flux, peak SXR flux, the occurrence or non-occurrence of metric radio type II and type IV sweeps, and the location of the flare.

The probability prediction is based on the GOES XRS maximum X-ray flux, the X-ray flux integrated from the flare onset until the flux decays to half of the maximum flux value, and the occurrence of Type II or Type IV radio bursts reported from the USAF Solar Electro-Optical Observatory Network (SEON). The probability model was trained with 88 proton events and 1334 control events between 1986 to 2004. These events were classified into groups defined by integrated X-ray flux, maximum X-ray flux, and radio sweep values, generating a 5 × 5 × 4 parameter space. For each point in parameter space, the number of proton events was divided by the total number of events to estimate the probability of proton event occurrence. One dimension of the parameter space was removed as necessary when the sample size for a particular point in parameter space was too small (Balch, 1999; Balch, 2008).

The proton maximum flux model is based primarily on a statistical relationship between the log of the >10 MeV peak flux of the proton events and the log of the integrated X-ray flux of the associated X-ray event (Balch, 2008). The prediction is also informed by the integrated X-ray flux of the most recent previous event that occurred in the same active region. The prediction is given by the formula:

$$\Phi_{P10} = 10\alpha_{PF} \times \left[ \frac{X_{int}}{0.00987} \right]^{0.82} \quad (7)$$

where  $\Phi_{P10}$  is the predicted maximum flux for >10 MeV,  $X_{int}$  is the integrated X-ray flux for the associated flare, and

$$\alpha_{PF} = \begin{cases} \left( \frac{X_{pfmt}}{0.167} \right)^{1.146} & \text{if } X_{pfmt} > 0.08, \\ 1 & \text{if } X_{pfmt} \leq 0.08 \end{cases} \quad (8)$$

where  $X_{pfmt}$  is the integrated X-ray flux of the previous flare event.

The rise time is defined as the time difference between the X-ray maximum and proton maximum. The prediction of this value is derived from the location of the associated flare on the solar disk using the formula:

$$t_{rise} = t_{min} + \left[ \frac{longitude - l_{SE}}{\lambda} \right]^2 \quad (9)$$

where  $l_{SE}$  is the optimal sub-Earth longitude (78 degrees west),  $\lambda$  is the longitudinal scaling factor (18.1 degrees), and  $t_{min}$  is the minimum rise time (9.4 h).

#### Inputs:

- Peak SXR flux
- Time-integrated SXR flux
- Flare location
- Occurrence or non-occurrence of metric Type II and Type IV radio bursts.

#### Outputs:

- Probability of proton event occurrence
- Maximum proton flux
- Rise time (time difference between the X-ray max and proton max)

**Free parameters:** None.

**Limitations and Caveats:** An analysis found the model overforecasts in the 0.55–0.65 probability range and underforecasts in the 0.25–0.35 probability range (Balch, 2008).

**Access to model output or forecasts:** This model is used internally by NOAA SWPC and is not available to the public.

**Model validation:** Balch (2008) describes the validation of the model along with an explanation of each of the metrics used. The validation was extensive and a selected set of results are included here.

The proton data set was rederived with corrections applied to GOES data prior to 1990, resulting in a list of 165 events from 1986–2004. Instead of strictly using the >10 MeV, 10 pfu definition, cases where an “event” was due to multiple injections in a row, each injection was treated as a separate SEP event and associated with its flare source.

For their analysis, flares occurring behind the limb automatically counted as a miss. About 17% of the source originated behind the west limb and two events were behind the east limb. 5.4% (9) qualified as events in the ESP phase. These events were treated as a priori missed events. These excluded events places an upper limit on the probability of detection at 77%.

For the remaining 127 events, analysis of the event parameters showed that all were associated with an XRS event with peak flux in the 1–8 Å band of greater than  $2.44 \times 10^{-6}$  Watts  $m^{-2}$ , integrated X-ray flux greater than  $9.93 \times 10^{-3}$  Joules  $m^{-2}$ , and background-subtracted integrated X-ray flux greater than  $5.95 \times 10^{-3}$  Joules  $m^{-2}$ . All XRS events that satisfied these conditions but did not produce a proton event resulted in a list of 3656 negative events from 1986 to 2004.

They presented a forecast reliability diagram and skill scores calculated by applying varying thresholds to convert the probabilistic score to a binary forecast. The optimum threshold of 20–30% probability results in a POD of 0.57, FAR of 0.55, PCOR of 96%, and HSS of 0.48. For the peak flux forecast, the correlation coefficient was 0.524 and the mean absolute log error for peak flux forecast was 0.87. The mean error for rise time prediction was 12.6 h.

#### 3.21. REleASE and HESPERIA/REleASE - Relativistic Electron Alert system for Exploration

**Model developers:** Arik Posner (NASA HQ), Olga E. Malandraki (NOA), Bernd Heber (Institute of Experimental and Applied Physics (IEAP)), Johannes Labrenz (IEAP), Patrick Kühl (IEAP), R. Du Toit Strauss (North-West University).

*Initial development of the RELEASE model is described in Posner (2007). Further development of what is now called the HESPERIA/RELEASE model has been performed in the context of the HESPERIA HORIZON 2020 EU program, as described in Malandraki and Crosby (2018)*

**Model description:** The current High Energy Solar Particle Events foRecastIng and Analysis (HESPERIA)/Relativistic Electron Alert System for Exploration (REleASE) model takes advantage of promptly arriving near-relativistic as well as relativistic electrons as an early indicator of a solar energetic particle event. It uses 175–315 keV electron measurements from ACE/Electron, Proton, and Alpha Monitor (EPAM) and 0.25–1 MeV electrons measured by SOHO/Comprehensive Suprathermal and Energetic Particle Analyzer (COSTEP) to predict 15.6–39.8 MeV and 28.2–50.1 MeV proton fluxes in the 30, 60 and 90 min future windows. Relativistic electrons ~1 MeV always arrive at 1 AU prior to the ~30–100 MeV protons (Posner, 2007). For a nominal Parker Spiral of 1.2 AU from the Sun to the Earth, 1 MeV electrons would arrive 30.4 min earlier than 30 MeV protons, 21.8 min earlier than 50 MeV protons, and 13.3 min ahead of 100 MeV protons, but would lag behind 300 MeV protons by more than 5 min (Posner, 2007). While this method does not provide early warning for the highest energy SEP protons arriving at Earth, it does provide advance warning for the bulk of SEP events as well as acts as an indicator of magnetic connectivity between the Sun and Earth, i.e., if energetic electrons arrive at Earth, it is clear that a magnetic connection exists between the Earth and active region and energetic protons are expected. A unique aspect of this forecast method is inherent in the use of in situ particle measurements (i.e., electrons at L1) as opposed to reliance on remote solar observations (e.g., X-rays). HESPERIA/RELEASE can therefore forecast SEP events associated with solar eruptions behind the western solar limb, an expansion of capabilities beyond those offered by models relying on remote sensing observations only available for the visible solar disc.

The RELEASE project combined data and knowledge from 9 European partners and several collaborating parties from the US and Russia. The HESPERIA project produced two novel forecasting tools based upon proven concepts: HESPERIA/UMASEP-500 (Section 3.35) and HESPERIA/RELEASE. The RELEASE model uses the relationship between the propagation speeds of relativistic electrons and ions during transport from the sun to 1 AU. This could plausibly be extended to other locations for the observer, such as Mars. The relativistic electrons from Solar Particle Event (SPE) s, highly abundant and easy to detect outside the magnetosphere, can be used as messengers for the later arriving ions (predominantly protons) energetic enough to affect humans and technology in space. Superposed epoch and statistical analyses revealed that 1) the behaviors of the electron and proton increase parameters are very similar and 2) the maximum flux intensity between protons and electrons has a clear ordering over a broad range of SPEs. It is therefore feasible to forecast proton fluxes based on electron onset observations.

A list of solar proton events, defined as  $>10$  MeV exceeds 10 pfu, measured by GOES-8 from 1996–2002 serves as a basis to derive the fundamentals of the forecasting method with statistical and superposed epoch techniques. To derive the intensity relationship between electrons and protons during event onset, the slope of the rise in electron flux, called the electron increase parameter, and the slope in the rise of the proton flux were derived. The authors found that the rise characteristics were similar for both electrons and protons. Making use of this information, a forecasting matrix was generated with the electron increase parameter on one axis and electron intensity on the other axis. For each element in the matrix, the predicted proton flux was derived (See Figure 8 in Posner (2007)).

HESPERIA/RELEASE also accounts for the delay between electron and proton arrival at 1 AU. It was found that the average time delay between the arrival of electrons and  $<50$  MeV protons was 63.3 min. Due to varying magnetic connectivity conditions, most protons arrived within 30–90 min of electron arrival. To account for the possible magnetic connectivity of any given SEP event, the model issues three separate predictions of exactly the same proton fluxes, but with 30-, 60-, and 90-min delays applied. These forecasts can be considered to represent the range of possible proton arrivals at Earth resulting from the most statistically likely connectivities. Which of the three turns out to be the most accurate forecast will depend on the magnetic connectivity of the specific event. The current HESPERIA/RELEASE version builds on the work of the original RELEASE model, relying on the created empirical matrices to develop a prediction 30, 60, and 90 min into the future. The matrices are based on historic measurements of proton flux, observed 30, 60, and 90 min after the electrons, as a function of both the electron flux and the slope of the electron flux increase.

HESPERIA/RELEASE issues a warning if the following conditions are met:

- The average proton flux for the previous two hours is below the hazard level (20 pfu)
- The predicted proton flux exceeds the hazard level by 50% (30 pfu)
- The predicted value at the time of the warning is required to be the maximum predicted value over the previous 2 h

Fig. 7 illustrates the HESPERIA REleASE tool's panel with the forecasting results for the successfully predicted SEP event on the 28th of March 2022. The upper panel on both sides shows real time proton fluxes measured by SOHO/EPHIN. The proton flux in the energy range of 15.8 to 39.8 MeV is shown in red and the proton flux in the energy range of 28.2 to 50.1 MeV is shown in green. The next three panels show the proton flux forecasts obtained with the HESPERIA REleASE forecasting scheme. From top to bottom the panels show expected proton fluxes in 30, 60, and 90 min (time-shifted). On the left and right sides, the forecasts are based on electron measurements by SOHO/EPHIN and ACE/EPAM, respectively. All forecasts use the same color code as the real-time proton flux in the top panel. The bottom panels on both sides show the measured real-time electron fluxes used for the forecasts. The SOHO/EPHIN and ACE/EPAM electron fluxes cover the energy range of 0.25 to 1.0 MeV and 0.175 to 0.315 MeV, respectively. Also, the first dashed line at  $0.1 \text{ flux}/(\text{cm}^2 \text{ s sr MeV})^{-1}$ , is the HESPERIA REleASE proton flux intensity threshold. The second dashed line is shown to guide the eye of the user about the peak intensity of the event and whether this crosses the threshold of  $10 \text{ flux}/(\text{cm}^2 \text{ s sr MeV})^{-1}$ . Furthermore, the vertical grey shaded areas indicate the time periods during which the electron input data for the ACE/EPAM and SOHO/EPHIN experiments is available, respectively. It can be observed that the ACE/EPAM provides full coverage concerning the electron input data for the time period where the SEP event occurred.

Fig. 8 presents the actual SOHO COSTEP/EPHIN proton fluxes observations (blue curve) along with the forecasted proton fluxes in 60 min, produced by the HESPERIA REleASE tool utilizing the ACE/EPAM electron input data (red curve). The actual and the forecasted proton fluxes are assessed for the energy range of 28.2 to 50.1 MeV, essentially the critical energy range for human spaceflight. Also, to determine the advanced warning time (AWT), note that there is no time shift applied to the 60 min forecast and the red points are plotted at the time that the forecast was issued. The red curve, i.e., the forecasted proton fluxes produced by the HESPERIA REleASE scheme, crosses the threshold on 12:00:00 and generates a proton alert, while from the actual measured proton fluxes (blue curve) the threshold is crossed on 13:53:02. This gives an important AWT of 113.03 min, concerning the SEP

event. Therefore, astronauts performing EVA activities have ample time to take shelter.

**Inputs:**

Original Version:

- Energetic electron measurements from COTSEP

HESPERIA Version:

- Relativistic electron ( $v > 0.9c$ ) measurements from SOHO/ COTSEP/ EPHIN
- Near-relativistic electron ( $v < 0.8c$ ) measurements from ACE/ EPAM

**Outputs:**

Original Version:

- Proton fluxes at the following four COTSEP energy bands to facilitate direct model and data comparison/performance evaluation: 4–9 MeV; 9–15.8 MeV; 15.8–39.8 MeV; 28.2–50.1 MeV.
- Proton flux alerts at 15.8–39.8 MeV and 28.2–50.1 MeV.

HESPERIA Version:

- Proton flux alerts at 15.8–39.8 MeV and 28.2–50.1 MeV (COTSEP input).
- Proton flux alerts at 15.8–39.8 MeV and 28.2–50.1 MeV (EPAM input).

**Free parameters:** None.

**Limitations and caveats:** HESPERIA/RELEASE relies on data availability and measurement quality. Current detectors are not ideal for predicting extreme events.

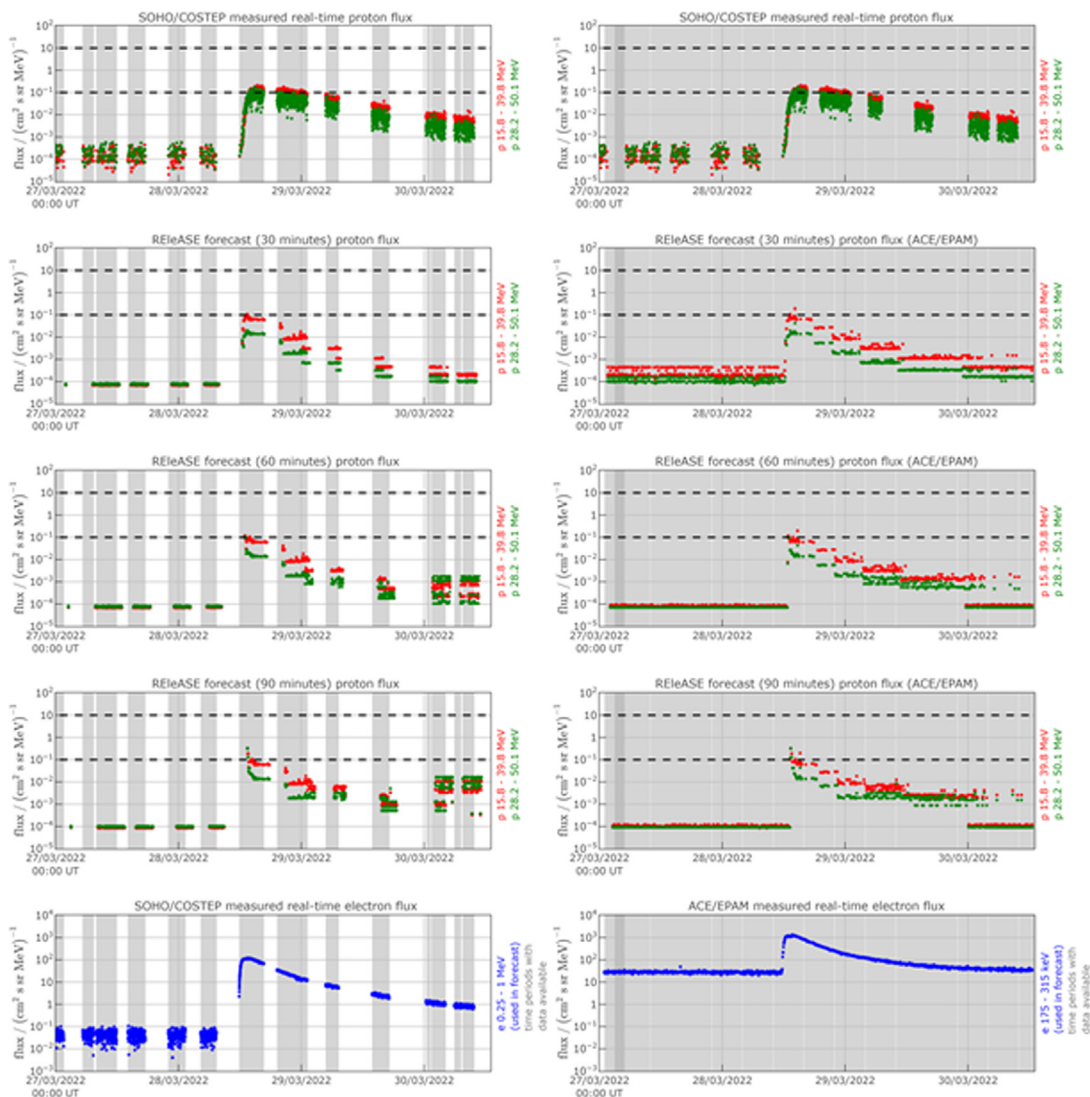


Fig. 7. HESPERIA REleASE results for the SEP event on 28 March 2022.

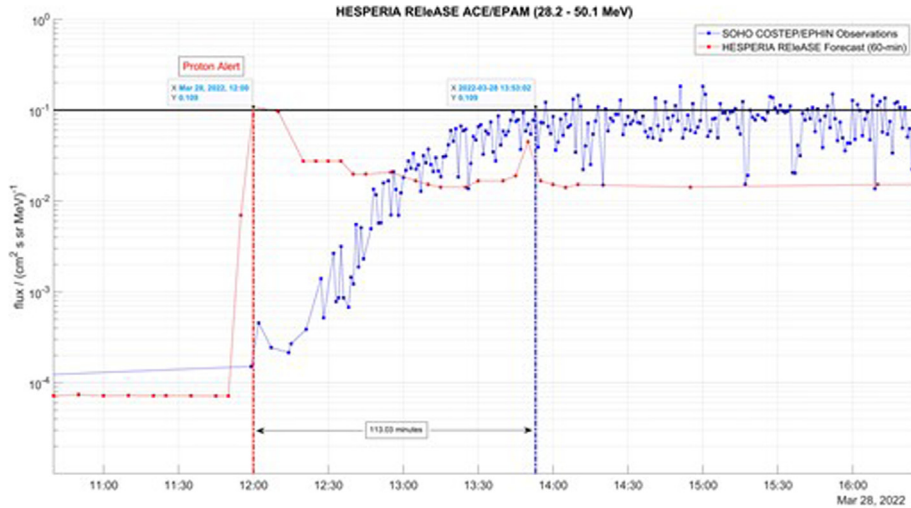


Fig. 8. HESPERIA REleASE AWT for the SEP event on the 28th of March 2022.

**Access to model output or forecasts:** Real-time SEP predictions are publicly available via the HESPERIA project website: <https://www.hesperia.astro.noa.gr/index.php/results/real-time-prediction-tools/release>. Projections are also available on the publicly-facing SEP scoreboards in addition to the iSWA interface hosted by CCMC.

**Model validation:** Analysis of historic data from 2009 to 2016 has shown the HESPERIA/RELEASE tools have a low FAR ( $\approx 30\%$ ) and a high POD (63%). (Malandraki et al., 2020). In Posner (2007), RELEASE was derived from a list of proton events, defined as  $>10$  MeV exceeds 10 pfu, measured by GOES-8 from 1996–2002. The model was derived from COTSEP/EPHIN electron and proton measurements. At the time of the paper, the model had been running in real-time for 11 months in 2003. This time period was used for evaluation of the model. During this time, RELEASE issued nine series of SEP hazard warnings. ADWT, defined as the time of the issued forecast and the onset of the proton event (ons) or from proton intensity reaching the hazard level (haz), was also assessed.

Over the 11-month time period, 9 warnings were issued. 4 were correct warnings for SPEs that exceeded the hazard levels with an ADWT of 27, 18, 7, and 74 min (31.5 min average). Two false warnings were for SPE that did not cross the hazard thresholds with 30 and 7 min advance warning. The remaining 3 were false warnings which were due to increases in electron flux due to interplanetary shocks or occurred during the declining phase of an SPE. No mention was made about whether the model missed SPEs.

### 3.22. Sadykov et al. (2021) Model

**Model developers:** Viacheslav M. Sadykov, Alexander G. Kosovichev, Irina N. Kitiashvili, Vincent Oria, Gelu M. Nita, Egor Illarionov, Patrick M. O’Keefe, Yucheng Jiang, Sheldon H. Ferreira, Aatiya Ali (collaboration of

Georgia State University, New Jersey Institute of Technology, and NASA Ames Research Center).

**Model description:** The ML research model represents the artificial NN of a custom architecture designed for daily whole-Sun prediction of  $>10$  MeV,  $>10$  pfu SPEs. The model is trained and evaluated on the SC24 data and events. The NN architecture implemented in Sadykov et al. (2021) for the whole-Sun daily SPE prediction is schematically illustrated in Fig. 9. The key idea of this custom architecture is to pre-process the characteristics of sunspot groups and active regions (such as properties of SHARPS, Bobra et al., 2014) within so-called “AR Blocks” before combining them with other whole-Sun characteristics. The network parameters within the AR blocks (weights and biases of connections between neurons) are shared among all AR blocks, providing exactly the same preprocessing for each AR. Also, the outputs of the AR blocks are summed up before propagating to the main part of the network. This strategy allows one to (1) add the physics knowledge, that the ARs should be processed in the exact same way based on their characteristics and position on the solar disk, into the machine learning algorithm, and (2) significantly reduce the number of network parameters to tune while training the NN. The dark blue rectangles in Fig. 9 represent the fully-connected NN layers. The number of layers and neurons in each layer depends on the implementation and type of input. For example, the numbers of neurons in the subsequent layers were 30–15 - 8–4 - 2 for the AR blocks and 21–15 - 10–5 - 2 for the main network in Sadykov et al. (2021).

While the architecture demonstrated in Fig. 9 can be adapted to various settings of the whole-Sun SEP forecasts (particle energy and flux thresholds, prediction time windows, etc), Sadykov et al. (2021) considered it for daily prediction of the  $>10$  MeV,  $>10$  pfu proton events for the SC24. These particular energy and flux thresholds correspond to the least-strength S1 events on the scale of

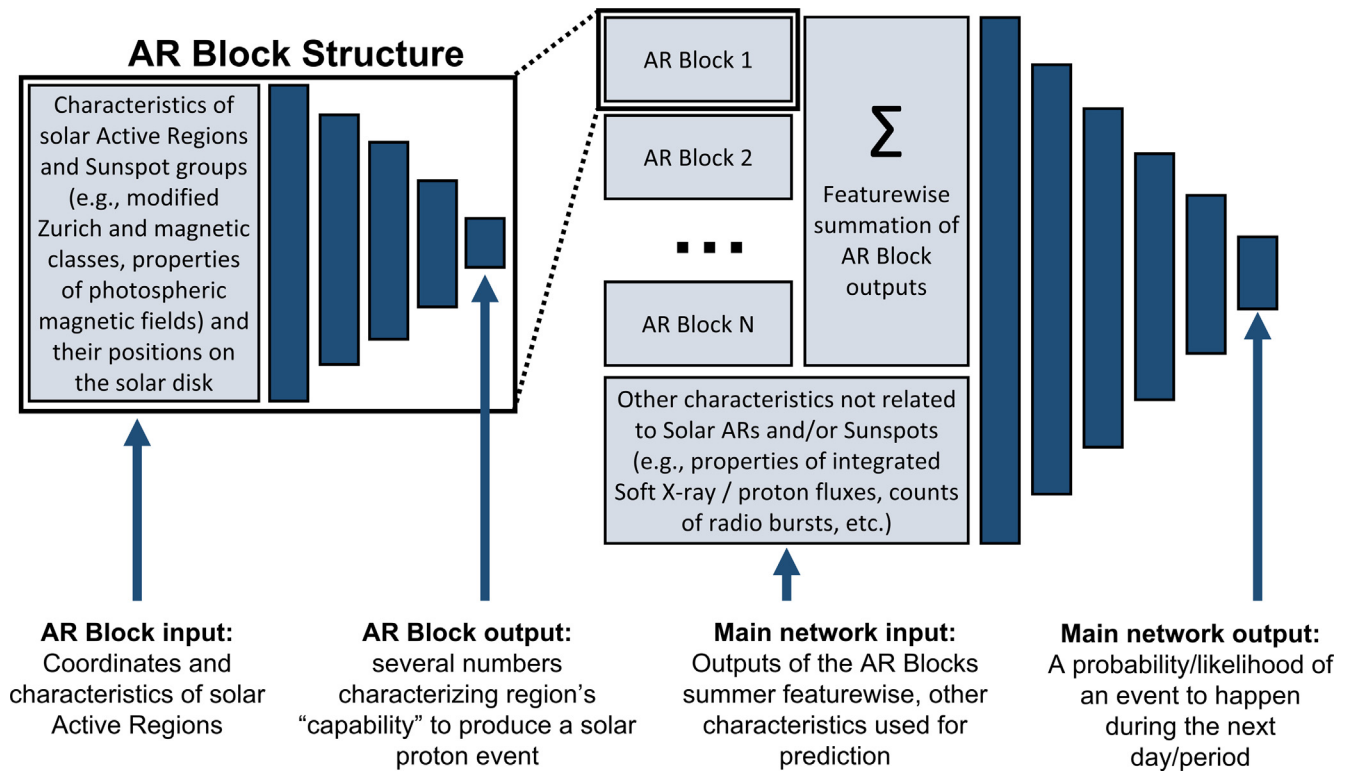


Fig. 9. A schematic representation of a neural network architecture for a daily whole-Sun prediction of SPEs based on properties of individual sunspot groups/ ARs and whole-Sun integrated properties implemented in Sadykov et al. (2021) model. The neuron connections in AR Blocks share the weights, and the biases.

NOAA/SWPC<sup>12</sup>. In addition, this allows one to compare the prediction issued by machine learning algorithm with the operational daily probabilities of the S1 SPEs issued by NOAA/SWPC.

**Inputs:** The prediction is constructed based on the daily characteristics of the SXR and proton fluxes (e.g., the daily mean and median values), the daily median values of SHARP parameters in ARs (Bobra et al., 2014), and the daily counts of type-II, type-III, and type-IV radio bursts (Winter and Ledbetter, 2015). To account for the ARs near the western solar limb and at the far side of the Sun, the developers extrapolated the ARs for 10 days forward after the ARs pass the 68deg west longitude assuming the Carrington rotation rate and unchanged SHARP parameters. The importance of the ARs near the western limb and related asymmetry of SEP events was demonstrated, for example, by Cliver et al. (2020) and was confirmed by the developers. The ratio of the number of samples in the train and test subsets was  $\sim 2/1$ , the class-imbalance ratio was kept  $\sim 1/34$  in both subsets. Also, both subsets consisted of significantly-long temporal intervals to avoid temporal coherence problem (Ahmadzadeh et al., 2021).

**Outputs:** The model can provide both the binary and probabilistic (likelihood) predictions of the SPE to happen

during the next day (starting at 00:00 AM UT) based on the data available at or before 22:00 PM UT.

**Free parameters:** One can select the probability/ likelihood threshold to optimize the binary prediction with respect to a particular score (TSS, HSS, etc) or forecast setting (e.g. "all-clear").

**Limitations and caveats:** The model developers noted that one of the problems in their approach is the relatively small data set used for model training and evaluation. The developers are currently expanding the "all-clear" prediction approach to the data and events of the SC22 and 23 based on the SXR and proton flux characteristics, as well as to the SC23 data and events based on the modified Zurich and magnetic classes of sunspot groups and ARs. Also, the non-operational (definitive) SHARP parameters (Hoeksema et al., 2014) were used. The performance of the model on near-real-time SHARP data has yet to be evaluated.

**Access to model output or forecasts:** For information on how to access the data set, the model, and related Jupyter Notebooks illustrating the data preparation and model training procedures, please see Sadykov et al. (2021).

**Model validation:** The model developers examined their prediction on the test data set in terms of several binary classification metrics, including traditionally used TSS and HSS, as well as binary cross-entropy, and the area under the ROC curve. The key results of their analysis are the following:

<sup>12</sup> [https://www.swpc.noaa.gov/sites/default/files/images/NOAA\\_scales.pdf](https://www.swpc.noaa.gov/sites/default/files/images/NOAA_scales.pdf).

- The designed architecture of the NN performs better with respect to the fully connected architecture and with respect to the architecture distinguishing between different ARs.
- It is very important to evaluate the binary prediction based on the set of different metrics rather than focusing on a single one; the forecast may perform differently with respect to the baseline for different metrics.
- Inclusion of proxies characterizing ARs on the western limb and the far side improves the prediction built only on the AR characteristics.
- The most valuable characteristics for daily whole-Sun prediction of SPEs are the properties of the preceding 10 MeV proton flux. The addition of the SXR flux characteristics and the AR characteristics is equally-valuable for the forecast, while the radio burst counts do not improve the forecast performance.
- The constructed machine-learning-based forecast is very promising in situations when missing events is very undesirable. In particular, the ROC curve of the ML forecast is above the ROC curve of the operational forecast in the region of high true positive rate (for details, see Figure 3 in [Sadykov et al., 2021](#)).

The last key result is of special interest in terms of the development of the “all-clear” prediction of SPEs (i.e., the situation when having an event missed by the prediction algorithm is significantly more undesirable with respect to having a false alarm). In addition to the analysis of ROC curves, the developers introduced a score named the Weighted True Skill Statistic (WTSS):

$$WTSS(\alpha) = 1 - \frac{2}{\alpha + 1} \left( \alpha \frac{FN}{TP + FN} + \frac{FP}{TN + FP} \right) \quad (10)$$

In this equation, the TP is the number of correctly predicted SPEs, TN is the number of correctly-predicted no-SPEs, FN is the number of SPEs predicted as no-SPEs, FP is the number of no-SPEs predicted as SPEs,  $\alpha$  is the parameter that indicates how strongly the missed event rate ( $FN/TP + FN$ ) is penalized with respect to the false alarm rate ( $FP/TN + FP$ ). The model developers concluded that WTSS score is larger for ML-based predictions with respect to operational forecasts for  $\alpha > 1$  (i.e., for the situations when the missed event rate is penalized more with respect to the false alarm rate).

### 3.23. SAWS-ASPECS - SEP Advanced Warning System, Advanced Solar Particle Events Casting System

**Model developers:** The SEP Advanced Warning System (SAWS)-Advanced Solar Particle Events Casting System (ASPECS) forecasting system was developed by a consortium headed by A. Anastasiadis, through an ESA contract. The main developers of the ASPECS modules are as follows:

- Forecasting of SFs, CME likelihood and maximum CME speed per active region (Manolis K. Georgoulis, Evangelos Paouris)
- Forecasting of SEPs based on the prediction of SFs (Sigiava Aminalragia-Giamini)
- Nowcasting of SEPs based on SF, CME characteristics and combinations of both thereof (Athanasios Papaioannou)
- Nowcasting/Forecasting of the expected peak flux of SEP events (Athanasios Papaioannou)
- Nowcasting/Forecasting of the SEP time profile (Rami Vainio, Miikka Paasilta, Angels Aran)

**Model description:** The SEP Advanced Warning System (SAWS) is an ESA modular framework for forecasting SEP events, their characteristics and profiles. ASPECS is the first realization of this operational tool that collates and combines outputs from different modules providing predictions of SF and CME likelihood of occurrence, SEP event occurrence, expected peak flux and SEP time profile, all of which evolve with time. The system achieves this through the use of 3 modules. The predictions start with the SF forecasting based on near real-time SHARP ([Bobra et al., 2014](#)) outputs and continuously evolve through updates based on near-real time inputs (e.g., SF and CME data/characteristics) received by the system. Finally, for the first time the complete time profile of the SEP event at respective energies is provided in near real-time, utilizing both simulations and observations.

ASPECS incorporates two modes of operation. The *forecasting* and the *nowcasting*. The *forecasting* mode is the pre-event one, meaning that no event has actually taken place on the Sun, yet. The only input is the identification of an AR. The *nowcasting* mode is the post-event mode. In this case a SF, a CME, or a combination of both have taken place.

*Forecasting mode:* The input used is the SHARP output from the processing of the SDO/HMI data. Based on these, ASPECS delivers conditional flare probabilities complemented by information on CME probabilities and expected maximum CME speeds. Flare probabilities rely on the “effective connected magnetic field strength” ( $B_{eff}$ ) prediction metric ([Georgoulis and Rust, 2007](#)). The CME likelihood relies on the published flare-to-CME association rates ([Yashiro et al., 2005](#)) and the maximum CME speed is directly defined by a relation between the  $B_{eff}$ -values and the recorded near-Sun CME velocities ([Georgoulis, 2008](#)). See also details on this approach in [Anastasiadis et al. \(2017\)](#). The statistics of flare prediction for ASPECS have been inferred from historical data covering the period September 2012 – December 2018, (2313 days in total), using the Flare Likelihood And Region Eruption forecasting (FLARECAST) property service ([Georgoulis et al., 2021](#)). Moreover, the statistics are built for a set of forecasting windows, namely for the next 6, 12, 24, 48 and 72 h. The outputs of ASPECS, for each AR, include



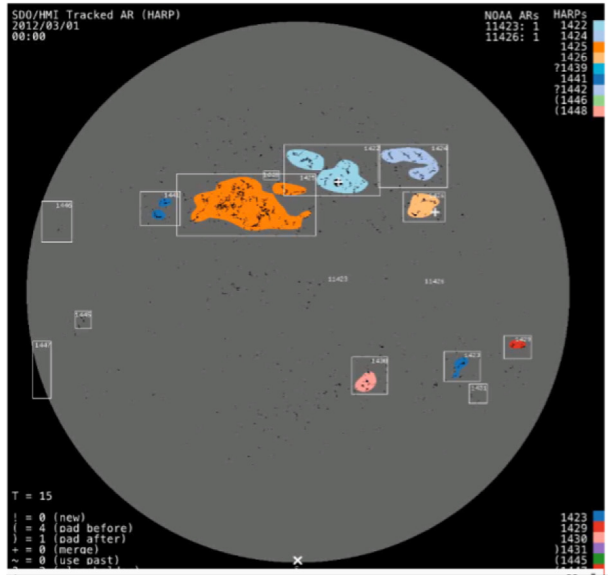
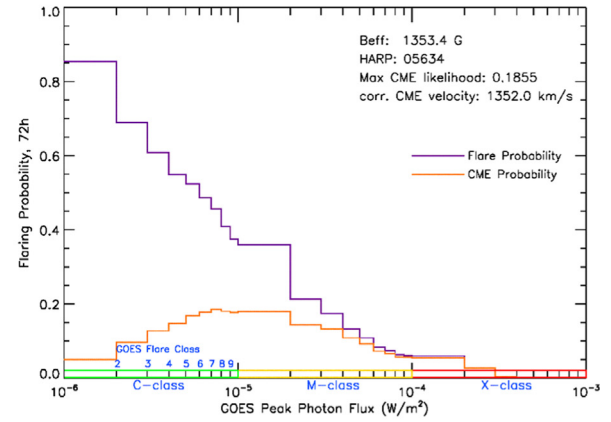


Fig. 10. An SDO/HMI magnetogram processed with SHARP (panel on the left hand side) and the corresponding outputs of ASPECS (panel on the right hand side). See text for details.

the a) cumulative flare probability as a function of SF magnitude distributed over 28 classes (9 for each of the C, M and X-class flares and another one for X10+), b) the corresponding CME likelihood which is the product of the flare probabilities with the CME-flare association rate and the c) maximum CME speed. An example is presented in Fig. 10. The left panel shows SDO/HMI magnetogram processed with SHARP where ARs are clearly identified. The right panel incorporates all ASPECS's outputs: flare probabilities (purple line), CME likelihood (orange line) and maximum CME speed. Moreover, the maximum CME likelihood is also provided.

The next step is to provide the probability of SEP occurrence ( $P(\text{SEP})$ ) based on the information delivered by the SF forecasting (i.e., the cumulative SF probabilities). The work flow is the following: for a given location of an AR, the SF forecasting module provides a Cumulative Distribution Function (CDF) over all 28 GOES SF classes (see Fig. 10). For this given AR location, the nearest historical SF events are identified. Then a probability distribution function for SEP occurrence is derived from these historical data. This forecasting module derives a  $P(\text{SEP})$  which is essentially a conditional probability given that a flare with magnitude within a given range has also occurred. The product of the flare and SEP probabilities produces the final output per bin and the final  $P(\text{SEP})$  is the sum of all binned probabilities.

**Nowcasting mode:** In the nowcasting mode, ASPECS incorporates the Probabilistic Solar Particle Event foRecasting (PROSPER) Model (Papaioannou et al., 2022). PROSPER applies a novel, data-driven methodology to predict SEP events probabilistically. The model comes with three modes of operation depending on the inputs available: (a) CME characteristics (width, speed);



(b) SF characteristics (longitude, magnitude) and (c) combinations of both CME and SF characteristics. The output is the corresponding  $P(\text{SEP})$ . The next step is to further infer the expected peak flux at two confidence levels, set to 50% and 90%, respectively. Following this, the SEP time profile is predicted and then scaled to the estimated peak flux values.

The SEP time profile is estimated based on the interplay of two solutions: (a) the Kahler-Ling (KL) (Kahler and Ling, 2017) fitting in which purely empirical fits to the time-intensity profiles or injection function convoluted with Green's functions were explored (i.e., the method mentioned in the ADEPT model description in Section 3.1). In principle, Kahler and Ling (2017) used 14 SEP events and applied a modified Weibull function in order to fit the SEP time profile. We performed this investigation applying the function

$$F(t) = -I_0(\alpha/\beta)((t-t_0)/\beta)^{\alpha-1} \exp\{-[(t-t_0)/\beta]^\alpha\} \quad (11)$$

where  $t$  is time (measured in hours) from the listed event onset,  $I_0$  is a scaling parameter,  $t_0$  is an offset from the time of the peak soft X-ray flux of the associated SF, and  $\alpha$  and  $\beta$  are parameters controlling the shape of the function. The dependence of the parameter's fits ( $\alpha, \beta$ ) with respect to solar longitude for a total of 217 SEP events has been explored. It seems that both parameters can be represented by simple, reproducible fits. In turn, these fits can be used to produce predicted (simulated) time-intensity SEP profiles (see Fig. 11, left panel). (b) A database of synthetic integral intensity SEP time profiles for a set of pre-defined test cases obtained by using the SOLAR Particle ENgineering Code 2 (SOLPENCO2, see Section 3.29) software tool of the Universitat de Barcelona (Crosby et al., 2015; Aran et al., 2017). SOLPENCO2 is derived from

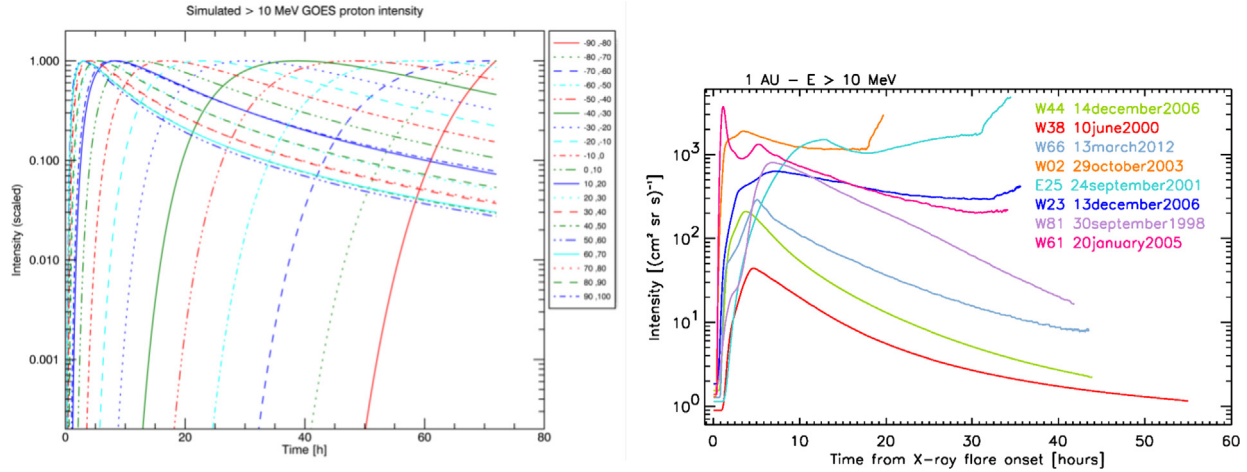


Fig. 11. SAWS-ASPECS examples of different simulated SEP time-profiles at  $E > 10$  MeV for parent solar events (e.g., SFs) distributed from  $-90$  to  $100$  degrees, in longitude (panel on the left) and  $> 10$  MeV synthetic proton intensity-time profiles provided by SOLPENCO2 for selected SEP events (panel on the right).

the physics-based Shock-and-Particle (SaP) transport model (Aran et al., 2007; Pomoell et al., 2015) and uses the semi-empirical  $Q(VR)$  -relation (e.g., Aran et al.,

2006; Rodríguez-Gasén et al., 2014) to characterize the particle source function at the associated travelling shock. The outputs of this tool are simulated proton differential

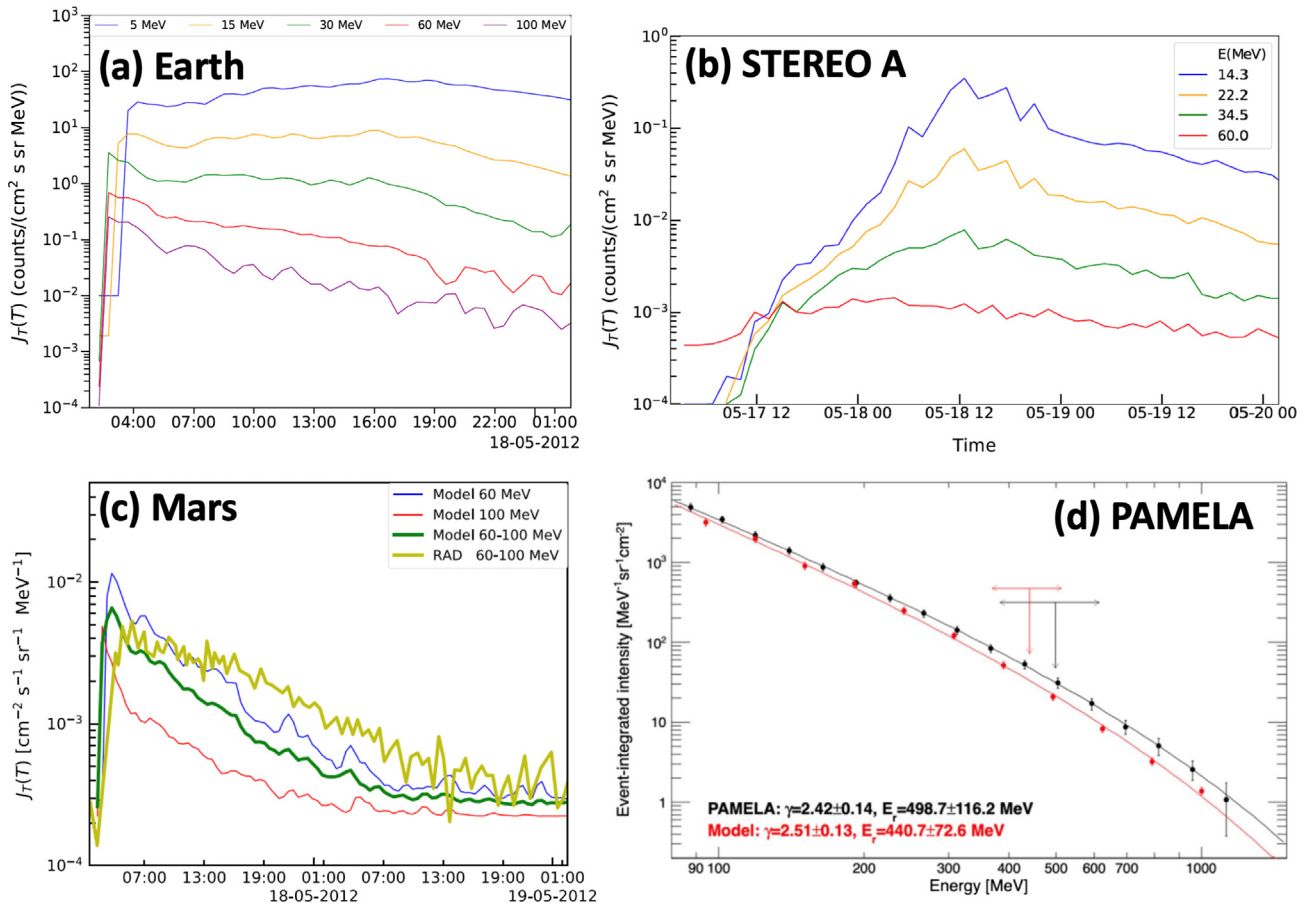


Fig. 12. An example of SEPcaster model output. (a)-(c) Modeled time intensity profiles at three points of interests: Earth, STEREO A, and Mars. The thick-brown curve in (c) shows MAVEN/RAD flux of 60–100 MeV. (d) The modeled (red) and Payload for Antimatter Matter Exploration and Light-nuclei Astrophysics (PAMELA) observed (black) spectrum at 1 AU. The arrows indicate the roll-over energies. The figure is adapted from Li et al. (2021).

intensity-time profiles at selected locations in the inner interplanetary space. SOLPENCO2 furnishes ASPECS with predictions based on 10 SEP reference events<sup>13</sup>, three of which have been re-modeled to reach an integral energy of  $E > 300$  MeV (by using GOES/HEPAD data) and 2 new modeled cases. The right panel of Fig. 11 shows the  $> 10$  MeV profiles for a group of events (indicated in the inset).

#### Inputs:

##### Forecasting mode:

- SDO/HMI SHARP magnetogram
- SF (magnitude, longitude)

##### Nowcasting mode:

- SF (magnitude, longitude)
- CME (speed, width)
- Particle flux

#### Outputs:

##### Forecasting mode:

- Beff
- Probabilities of SF occurrence,
- CME likelihood
- Maximum CME speed
- Probability of SEP occurrence
- Peak flux estimation at 50% and 90% CL
- SEP time profile

##### Nowcasting mode:

- Probability of SEP occurrence
- Peak flux estimation at 50% and 90% CL
- SEP time profile

#### Free parameters: None.

**Limitations and caveats:** ASPECS is a modular tool and incorporates several different modules. The final outcome is the SEP time profile, which evolves with time. The predictions are directly related to the probability of SEP occurrence. Once an SEP is expected to take place, the peak flux and the time profile are also predicted. The SEP time profile is provided for a set of integral energies from  $>10$  to  $>300$  MeV. For each integral energy ASPECS outputs the upper (90% CL) and the lower (50% CL) SEP time profiles. From these SEP time profiles, the peak fluxes can be estimated.

**Access to model output or forecasts:** ASPECS is a web-based tool directly accessible via <http://phobos-srv.space.noa.gr/>. There are several options for the users: real-time predictions under the forecasting and the nowcasting

mode, run-on-demand functionalities that the user can utilize and test the performance of the tool and its modules on archived data. The only required input is a date. The interface then searches the backend database, obtains the relevant inputs and triggers the tool, and displays the obtained outputs. JavaScript Object Notation (JSON) files are produced and thus all outputs are directly reproducible. SAWS-ASPECS is also available on the CCMC SEP Scoreboards.

**Model validation:** Each module has been validated against an independent test sample. For PROSPER and the SEP time profiles the NASA/CCMC SEP challenge events<sup>14</sup> were utilized. The results for PROSPER show a robust identification of the P(SEP) and the expected peak flux at CL of 50% and 90% in each module, while the SEP time profiles seem to bound well the actual SEP time profile.

### 3.24. SEPCaster

**Model developers:** Gang Li (UAH), Meng Jin (LMSAL/SETI).

**Model description:** SEPCaster is a new SEP model which couples the solar wind and CME model AWSOM with the particle acceleration and transport model IPATH. By coupling these two models together, the goal is to provide knowledge of the physics of the dynamics of an SEP event from the upper chromosphere of the Sun outward into the heliosphere and at Earth and beyond. SEPCaster is proposed to have two modes, one running in an automatic forecasting mode, and a mode for user-input data.

SEPCaster has been presented as a proof of concept in the paper Li et al. (2021). The model starts with modelling the upper chromosphere and coronal environment with AWSOM (van der Holst et al., 2014), where a steady state solar wind solution is found, using the Potential Field Source Surface (PFSS) as an initial condition and relaxed to MHD solution with local time-stepping. A CME is then initiated using a Gibson-Low (GL) flux rope (Gibson and Low, 1998). The GL flux rope parameters are calculated using EEGGL (Jin et al., 2017). This CME flux rope is then superposed onto the steady state background, and advanced through time. At each time step, a 2-D shock surface is obtained, with each point along the shock having its own shock parameters (compression ratio, obliquity angle, Mach number, and shock speed) and plasma information, which is then fed into the IPATH modules.

In the IPATH section of this paper (3.11), we discuss the three modules of that model. In the case of SEPCaster, the first module, the MHD module, is replaced with AWSOM, and the second module now takes information from the outputs of AWSOM. As these outputs are more complex, IPATH was modified to a 3-D cell structure from its 2-D parcel structure. The rest of the module functions in the same manner as the original IPATH, where each time step

<sup>13</sup> [http://www.sepem.eu/help/solpenco2\\_intro.html](http://www.sepem.eu/help/solpenco2_intro.html).

<sup>14</sup> <https://ccmc.gsfc.nasa.gov/assessment/topics/SEP/campaign2020.php>.

particles diffuse between nearby cells and some escape the shock complex - to be transported via the transport module. The transport is handled by a backward stochastic differential equation method. Cross-field diffusion can be included as a part of this process, but has been excluded to add in an ensemble simulation. This type of simulation, instead of assuming the observer is located at a singular point, it instead is located uniformly within a small angular region  $\sim 5^\circ$  to  $10^\circ$ . The results for the model show little differences between considering either the perpendicular diffusion or ensemble simulation approach for cases when the observer is magnetically connected to the shock for extended periods of time.

A special case is made for the proposed forecasting mode, where EEGGL will determine flux rope location and flux rope parameters for all active regions, which will then all be initiated in separate runs. For each region, three CME options will be run: slow ( $v_{cme} = 800 \text{ km s}^{-1}$ ), normal ( $v_{cme} = 1000 \text{ km s}^{-1}$ ), and fast ( $v_{cme} = 1200 \text{ km s}^{-1}$ ). These runs are passed into IPATH to provide a first-order prediction of a CME event's or SEP event's occurrence, as an "all-clear" measurement. Once a particular flare eruption has been observed, the model will accept a specific CME speed from an empirical relationship between flare class and CME speed.

#### Inputs:

- GONG diachronic magnetic maps (source region, erupting location, CME speed)
- Proton and electron temperatures ( $T_i = T_e = 50,000\text{K}$ )
- Proton and electron number density ( $n = 2 \times 10^{17} \text{ m}^{-3}$ )
- CME shock width, CME speed, and duration (user mode only)

#### Outputs:

- Time intensity profiles
- Particle Spectra
- All-clear

**Free parameters:** The Aflvén wave coronal heating parameters. Although these parameters could be constrained by the remote-sensing solar EUV observations and in situ solar wind measurements at 1 AU. Under the user mode, CME shock width, speed, and duration can be specified by the users to fine-tune event fitting.

**Limitations and caveats:** Although the standalone AWSOM MHD and IPATH simulations are already capable of running cases from the Sun to 1 AU, the current coupling between AWSOM and IPATH in the SEPCaster is limited to the first 6 h, beyond which a Parker-spiral field is assumed in the IPATH transport module. A fully coupling to cover the entire CME propagation in the heliosphere is being implemented/tested. Preliminary results of this full-scale coupling shows that the resulting particle spectra and intensity profile at certain heliospheric locations can be

different from the current 6-h-only coupling approach. SEPCaster is not fully operational ready at the moment.

**Access to model output or forecasts:** SEPCaster is planned to be hosted on CCMC servers providing 24/7 real-time SEP forecasts.

**Model validation:** SEPCaster has participated in the community modelling validation challenge as part of SHINE and ISWAT, where a few example events were submitted. Once further effort has been made into development of the model, more validation can be done. Fig. 12 shows an example of SEPCaster model output based on a realistic event study of 2012 May 17 event (Li et al., 2021), in which the intensity profiles at different heliospheric longitudes and distances (i.e., Earth, STEREO A, Mars) are provided (Fig. 12a-c). In addition, by including the early-phase shock evolution in the lower corona, the SEPCaster model could provide the particle spectra from 100 keV to GeV. Fig. 12d shows a comparison between the modeled and observed particle spectra by PAMELA (Bruno et al., 2018).

### 3.25. SEPMOD - Solar Energetic Particle MODEL

**Model developers:** Janet Luhmann (UC Berkeley), Christina Lee (UC Berkeley), Erika Palmerio (Predictive Science Inc.).

**Model description:** Solar Energetic Particle MODEL (SEPMOD) (Luhmann et al., 2007; Luhmann et al., 2010) is a physics-based test particle code for modeling SEP proton events, that outputs differential protons flux time profiles in the energy range of 1–1000 MeV. A version modified for Integrated Solar Energetic Particle (Warning System) (ISEP) use also outputs integral proton fluxes in the channels  $>10$ ,  $>30$ ,  $>50$ ,  $>60$ ,  $>100$ ,  $>300$ ,  $>500$ ,  $>750$  MeV. SEPMOD assumes that SEP particles are accelerated at the shock created by a CME as it propagates outwards from the Sun. It requires inputs derived from a MHD solar wind and CME propagation model in the form of time sequences of observer-connected magnetic field lines and shock parameters on those field lines. Currently, SEPMOD uses outputs derived from the WSA-ENLIL coupled solar corona and solar wind model, where the geometrical 'cone' tool is used for parameterizing the CME clouds in ENLIL. SEPMOD then tracks test particles along the connected field lines from the MHD model shock source(s) to the observer. Its output is a SEP flux time profile at the observer's location for the duration of the MHD simulation. Because the magnetic connection to the modeled ICME shock continues to be tracked past the observer to the MHD solar wind model outer boundary (usually 2 AU or 5 AU in ENLIL), periods of sunward-streaming SEPs are occasionally produced. SEPMOD has options to include additional sources of particles, such as those accelerated at a flare source and also ESP flux increases (ESP events) that may accompany the arrival of the shock, the latter of which is typically included in the runs. An example of a

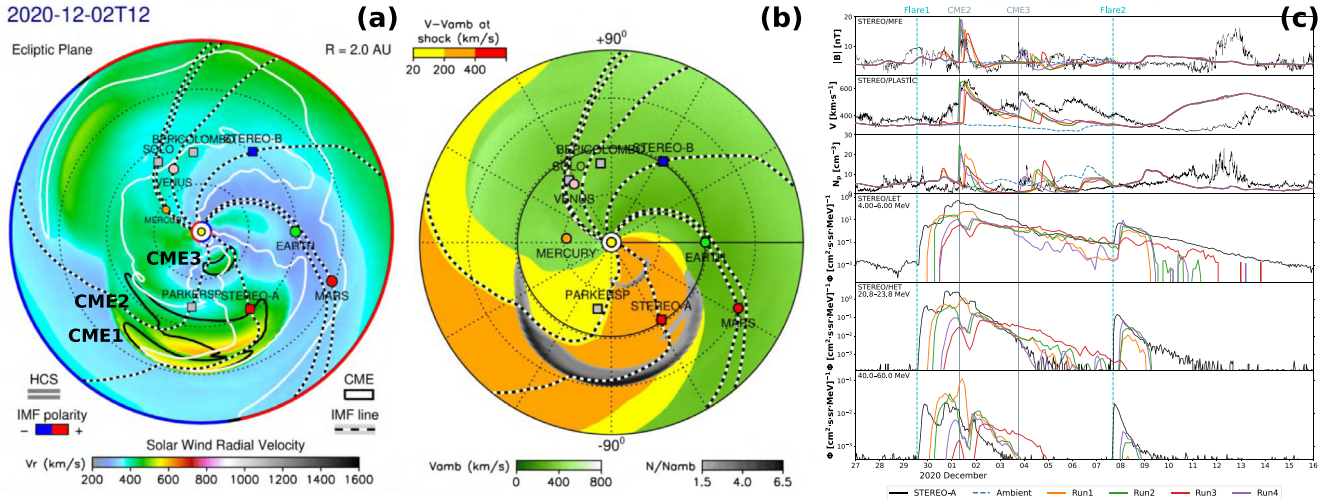


Fig. 13. Example of a WSA-ENLIL-SEPMOD application. (a) Snapshot of a WSA-ENLIL run, showing results for the solar wind radial speed on the ecliptic plane. (b) Corresponding view of a few shock parameters that are used as input for SEPMOD, i.e. the difference between shock and ambient speed and the compression ratio. (c) Example results at the STEREO-A spacecraft compared to spacecraft data, from top to bottom: Magnetic field magnitude, solar wind speed, solar wind density, and SEP fluxes at three sample energies. The plot shows results for four different WSA-ENLIL-SEPMOD runs, and the results reported in panels (a) and (b) correspond to Run4 in panel (c). More details on these simulations and comparisons with observations throughout the inner heliosphere can be found in [Palmerio et al. \(2022\)](#).

recent WSA-ENLIL-SEPMOD application is shown in [Fig. 13](#).

When applying and evaluating SEPMOD results, it is important to consider that the underlying MHD modeled ICME shock and heliospheric field line descriptions are just as critical to the performance of SEPMOD as the treatment details within the SEPMOD code itself. In this case, limitations that have particularly important impacts on the SEPMOD results using ENLIL with cone model CMEs include the location of the ENLIL inner boundary of 21.5 Rs, where below this region (*e.g.*,  $\sim 5$ –10 Rs) the early strong CME shock formation occurs, and the lack of an internal magnetic field description within the cone model CMEs. These limitations affect the modeled SEP time profile onset times and the ICME shock formation and evolution (*e.g.* timing, shape, strength), respectively. In particular, the current 21.5 Rs inner boundary location affects the modeling of GLE events, which are inferred to originate at heights of a few Rs. Future enhancements to SEPMOD will enable the inclusion of surface sources (*e.g.*, flares) and mappings, as well as coronal mirroring of SEPs below the 21.5 Rs boundary.

In SEPMOD itself, protons are injected into the solar wind on the sequence of observer-connected field lines from the MHD model with a prescribed seed population (energy and angular distribution, and flux) that depends on the MHD model shock properties on the field lines. The energy distribution is currently specified by a standard power law for the diffusive acceleration process based on the shock compression ratio, while the injected flux depends on the shock velocity jump according to an empirical result by [Lario et al. \(1998\)](#). The assumed angular distributions of the injected particles are isotropic. This seed population

is then tracked as it adiabatically propagates along the modeled magnetic field without further scattering to the observer site within the MHD simulation domain. Particle propagation includes any mirroring dictated by the field topology along the particle trajectories. Each time a new magnetic connection to a shock is indicated for either the next field line in the MHD model sampling sequence or the appearance of a new ICME shock connection, SEPMOD injects a new burst of test particles, diluted by  $1/r^2$  due to radial expansion of the volume into which the injection occurs. The particles are transported and the results of these impulsive injections are then integrated at the observer location at each time step to achieve the modeled SEP event time profile. SEPMOD includes two additional optional components that 1) represent particles accelerated by the flare source at the Sun at the start of the event and 2) the ESP increase due to the ICME shock passing Earth. If the observer is located within a few tenths of an AU of the shock source and the shock is moving at greater than 300 km/s, an energy-dependent (softer spectrum) ESP flux enhancement is applied that increases as the shock is approached ([Luhmann et al., 2017](#)).

**Inputs:** WSA-ENLIL input parameters:

- Magnetogram
- CME ‘cone’ cloud parameters (angular width, latitude, longitude, speed at 21.5Rs, time at 21.5Rs)

SEPMOD inputs from post-processing of ENLIL:

- Shock information from ENLIL
- Magnetic field connectivity information from ENLIL

**Outputs:** SEPMOD can produce 1–1000 MeV differential proton flux and  $> 10$ ,  $> 30$ ,  $> 50$ ,  $> 60$ ,  $> 100$ ,  $> 300$ ,  $> 500$ ,  $> 750$  MeV time profiles at any spacecraft/planet in the ENLIL domain. SEPMOD also outputs pitch angle distribution (anisotropy) information.

**Free parameters:** Particle injection spectrum parameters.

**Limitations and caveats:** The ENLIL inner boundary starts at 21.5 Rs, so SEPMOD does not necessarily model the onset of a SEP event if the particle acceleration starts within this boundary (i.e., inside the solar corona). SEPMOD performance relies strongly on the performance of the underlying modeling of the solar wind and CME propagation (e.g. by WSA-ENLIL + cone model).

**Access to model output or forecasts:** SEPMOD forecasts are displayed on CCMC’s SEP Scoreboard (<https://sep.ccmc.gsfc.nasa.gov/intensity/>) and archived json files containing forecasts are available for download. SEPMOD may also be run through CCMC’s runs-on-request system (<https://ccmc.gsfc.nasa.gov/requests/requests.php>).

**Model validation:** About 10–15 cases studies have been performed and published, but no systematic validation has been published.

Some preliminary validation work has been carried out through the ISEP project. An unpublished study (performed by Mays, M. L., Whitman, K., Allison, C. Quinn, P., and Bain, H., 2021) of 16 SEP events in SC24 was carried out to test the sensitivity of SEPMOD + ENLIL’s performance with respect to CME characteristics and magnetic connectivity to Earth. Nominal CME parameters were provided by NOAA/SWPC, then the width, speed, latitude, and longitude were varied by  $\pm 30\%$ ,  $\pm 35\%$ ,  $\pm 5^\circ$ , and  $\pm 15^\circ$ , respectively. One combination of CME parameters was selected to maximize the magnetic connectivity and CME speed and width (high) and a second combination of parameters was selected to minimize the magnetic connectivity and CME speed and width (low). This produced three separate outcomes for each SEP event—nominal, high, and low. WSA-ENLIL + SEPMOD was run for each combination and the resulting  $> 10$  MeV and  $> 100$  MeV proton time profiles were compared to GOES observations. The NOAA 10 pfu threshold was applied to the  $> 10$  MeV fluxes and a threshold of 1 pfu used by the SRAG was applied to the  $> 100$  MeV fluxes. The study found that SEPMOD performs best for central and western CMEs that originate closer to the magnetic footpoint of the observer (within  $\approx \pm 40$ ). The runs with the nominal CME parameters were found to best reproduce observations overall. The peak flux predictions resulted in a Mean Log Error (MLE) of  $-0.067$  and Pearson’s correlation coefficient (R) of 0.71 for  $> 10$  MeV and MLE of 0.53 and R of  $-0.27$  for the  $> 100$  MeV. The SEPMOD time profiles were found to start  $\sim 6$ – $7$  h after the observed proton flux threshold crossing for both  $> 10$  and  $> 100$  MeV. These are preliminary findings and a more comprehensive study must be carried out to fully assess the performance of SEPMOD.

The  $\sim 6$ – $7$  h onset delays can, in part, be attributed to the ENLIL inner boundary of 21.5 Rs and initial shock formation time for cone model CMEs, but these known issues have not yet been examined in detail. The ISEP Project analysis found that, in the simulation, CMEs were typically injected onto the ENLIL inner boundary between 11 h before and 2.5 h after the observed  $> 10$  MeV start time (median of 40 min after event start). The remaining  $\sim 5$  to 6 h between the CME injection and the simulated event start was due to a delay in a magnetic connection between the shock and the observer, possibly due to the time for shock formation in the ENLIL simulation. There are currently no readily available options for addressing the ENLIL inner boundary limitation.

Similar conclusions were reached in a recent study by Palmerio et al. (2022), who simulated a sequence of CMEs and their related SEP enhancements that were observed between late November and early December 2020 and compared the results with in situ observations at six well-separated locations. The authors noted that SEPMOD performed best for well-connected observers located up to several tens of degrees away from the corresponding shock apex and that small differences in the ENLIL shock arrival time tend to yield larger differences in magnetic connectivity onset and, thus, in SEP transport. Additionally, the study reported that in about half of the cases, the SEP event onset times measured in situ occurred  $\sim 6$ – $7$  h before the time of insertion of the modeled CME at the ENLIL inner boundary of 21.5 Rs. The study of Palmerio et al. (2022) employed a “mini-ensemble” approach, in which four different WSA-ENLIL + SEPMOD runs were performed with slightly different CME input parameters. Among other results, it was noted that the simulation run for which the ENLIL shock arrival times were adjusted to match those observed in situ did not perform better than the one initiated with input parameters derived in real time.

### 3.26. SEPSTER - SEP prediction derived from STEReo observations

**Model developers:** Ian G. Richardson (NASA Goddard Space Flight Center and University of Maryland, College Park); M. Leila Mays and Barbara J. Thompson (NASA Goddard Space Flight Center).

**Model description:** Solar Energetic Particle STEReo (SEPSTER) is an empirical model that uses CME speed and direction relative to the observer’s magnetic footpoint at the Sun to predict the peak intensity of 14–24 MeV protons at the observer’s location, assumed to be at 1 AU (Richardson et al., 2018). The peak proton intensity/flux in other energy ranges is predicted through extrapolation.

The basis of SEPSTER is a relationship between the peak intensity of an SEP event, the speed of the associated CME, and the observer’s connection angle, defined as the longitudinal angle between the source (e.g., flare) location and the footpoint at the Sun of the magnetic field line con-

nected to the observer (Richardson et al., 2014). This relationship was derived from observations of a sample of 25 SEP events detected by the High Energy Telescopes (von Rosenvinge et al., 2008) on both STEREO spacecraft when widely separated from Earth, and at near-Earth spacecraft, principally by the Energetic and Relativistic Nuclei and Electron (ERNE) (Torsti et al., 1995) and EPHIN (Müller-Mellin et al., 1995) instruments on SOHO. The peak intensities at all three locations for each SEP event were fitted by a Gaussian function of connection angle. The fits are summarized by the relationship:

$$I_p \approx 0.013 \exp\left(0.0036V - \frac{\phi_{CA}^2}{2\sigma^2}\right). \quad (12)$$

Here,  $I_p$  is the peak intensity of 14–24 MeV protons in  $(\text{MeV s cm}^2 \text{ sr})^{-1}$ ,  $V$  is the CME speed in km/s,  $\phi_{CA}$  is the connection angle in degrees, and  $\sigma$  is the average value of the width of the Gaussian functions fitted to the SEP events ( $43^\circ$ ).

Because relating flare observations (to give the source longitude) with the associated CME is not always trivial, and in some cases, the flare associated with a CME may be behind the limb, for operational SEP prediction at Earth, SEPSTER uses the CME speed and direction (as a proxy for the source location) taken from the CCMC DONKI database<sup>15</sup>. When available, these CME parameters are inferred from multi-spacecraft coronagraph observations (e.g., from STEREO and SOHO); see Mays et al. (2015) for further details of the derivation of CME parameters by CCMC. The connection angle is then taken to be the longitudinal difference between the direction of the CME and the magnetic field line footpoint. The footpoint location is obtained by using the solar wind speed measured at the observing spacecraft or other nearby spacecraft, at the time of the CME, if available, or otherwise a default speed of 450 km/s, to map a Parker spiral field line back to the Sun. Field line mapping in the corona is not considered in this case because SEP acceleration is believed to occur predominantly at heights above the source surface, often assumed to be at  $2.5 R_s$ . In addition, the field line connection longitude derived from WSA-ENLIL, which does include coronal field line mapping, is used to give an estimate of the influence of uncertainty in the connection point on the predicted SEP intensity. SEPSTER enters these variables into Eq. 12, then predicts the peak intensity of 14–24 MeV protons at the observing location. For events before April 2010, or other events for which DONKI CME parameters are not available, flare and CME observations may be used to give the source location and CME speed.

The SEPSTER workflow follows the following steps:

1. SEPSTER queries the CCMC DONKI database then copies a list of recent CME parameters to a local file.

2. SEPSTER queries CCMC integrated Space Weather Analysis System (iSWA) for recent solar wind observations from the Deep Space Climate Observatory (DSCOVR) spacecraft and downloads the data for approximately two days before the CME time until the start of the day following the CME, or the end of the available data, if earlier. If no DSCOVR data are available, similar observations from ACE are downloaded, if available. The in situ speed measured closest to CME onset is then selected. If no solar wind data are available, the model assumes a default solar wind speed of 450 km/s.
3. The connection angle is calculated using the equation

$$\phi_{CA} = \frac{1.5 \times 10^8}{u} \frac{360}{86400 \times 27.25} - \phi_{CME} \quad (13)$$

where  $\phi_{CA}$  is the connection angle in degrees, 1 AU is  $\sim 1.5 \times 10^8$  km,  $u$  is the solar wind speed in km/s, 27.25 days is the Carrington rotation period, and  $\phi_{CME}$  is the longitude of the CME direction with respect to the Sun-Earth line.

4. As discussed briefly below and in more detail by Richardson et al. (2018), various types of filtering may be applied to reduce the number of false SEP event predictions, since Eq. 12 can be used to predict the SEP intensity for any CME whereas only a small subset of CMEs are accompanied by SEP events detected at 1 AU. In the operational model, the following simple filters are applied:
  - If the CME speed is below 200 km/s, no prediction is made.
  - If the CME width is below  $10^\circ$ , no prediction is made.
  - If the CME speed  $\times$  width is less than 50000 km/s. deg., an SEP event “all clear” is predicted.
5. For CMEs that are not filtered by the CME speed/width requirements, Equation 12 is used to estimate the peak intensity of 14–24 MeV protons at Earth.
6. Peak proton fluxes equivalent to the standard GOES integral energy ranges of  $> 10$  MeV,  $> 30$  MeV,  $> 50$  MeV, and  $> 100$  MeV are predicted using scaling factors of  $\sim 20I_p$ ,  $\sim 2I_p$ ,  $\sim I_p$ , and  $\sim 0.2I_p$ , respectively, where  $I_p$  is given by Eq. 12 and the fluxes obtained are in pfu. These scaling factors are derived from correlating 14–24 MeV proton intensities from SOHO with simultaneous GOES observations over an extended time interval including multiple SEP events.
7. The time of peak intensity (in hours relative to the CME onset time) for 14–24 MeV protons is estimated using a result from Figure 20 of Richardson et al. (2014):

$$T_{\text{peak}}(\text{h}) \approx 7.32 \exp\left(\frac{\phi_{CA}}{114}\right). \quad (14)$$

<sup>15</sup> <https://kauai.ccmc.gsfc.nasa.gov/DONKI/>.

8. The CME parameters, predicted SEP intensity and peak time, and whether or not the predicted intensity meets the criterion for a GOES event “all clear,” are written to a JSON file. This file is overwritten/updated if the file already exists for a CME with the same time and speed.
9. These steps are repeated for the next CME in the list.
10. The DONKI database is re-checked every minute to see if a new CME has been added, and the above steps are repeated for this CME.
11. For “historical” events, SEPSTER options include using the CDAW list of CMEs and flares associated with type II radio emission<sup>16</sup> or a user-generated CME-source location list in place of the DONKI CME list in step 1.

**Inputs:** The inputs needed for SEPSTER include the CME speed, CME width (optional, used for false-prediction filtering), CME direction longitude or flare/eruption location, SEP-observing spacecraft longitude at  $\sim 1$  AU, and the solar wind speed at the observing spacecraft, if available, otherwise a default speed is used.

**Outputs:** SEPSTER outputs the peak intensity and peak time of 14–24 MeV protons at the observing location (i.e., Earth) which is extrapolated to give GOES-equivalent  $>10$  MeV,  $>30$  MeV,  $>50$  MeV, and  $>100$  MeV proton fluxes.

**Free parameters:** SEPSTER has no free parameters.

**Limitations and caveats:** SEPSTER predicts an SEP event for every reported CME whereas observationally, only a small subset ( $\sim 15\%$ ) of CMEs are accompanied by SEP events detectable at 1 AU (Richardson et al., 2018). Also, because Eq. 12 is derived from widespread “three-spacecraft” SEP events, it tends to overestimate the intensity of the many small SEP events associated with slow, well-connected CMEs. The filters based on CME speed and width listed above help to mitigate these limitations. Richardson et al. (2018) discuss these and other filtering methods, for example, based on spacecraft observations of type II and III radio emissions accompanying CMEs, and their influence on SEPSTER skill scores (see their Table 1). However, since such radio observations are not currently available in near-real time, they are not considered in the operational version of SEPSTER.

SEPSTER relies on measurements of CME speed and width, requiring coronagraph imagery which currently may be only available hours or even days after the CME has occurred. Estimation of the CME parameters also requires several images to be acquired. Hence, SEPSTER predictions are made later than those from similar flare-triggered models. An SEP event may also commence before the associated CME enters the field of view of a spacecraft coronagraph. On the other hand, since SEPSTER predicts the peak intensity, which may not occur until several hours

following CME onset, a modest delay in estimating the CME parameters may not be a critical concern.

Derivation of Eq. 12 was based on plane-of-the-sky CME speeds from the CDAW LASCO CME catalog<sup>17</sup> and flare locations, whereas the operational model uses DONKI CME speeds/directions. As discussed by Richardson et al. (2015), the speeds of SEP-associated CMEs reported in different catalogs can differ significantly. Richardson et al. (2018) discuss the use of this Equation for SEP prediction using both CDAW/LASCO and DONKI CME speeds.

**Access to model output or forecasts:** SEPSTER is housed at the CCMC and available for runs-on-request. The model is also running continuously and predictions are displayed on the SEP Scoreboard (<https://sep.ccmc.gsfc.nasa.gov/intensity/>).

**Model validation:** Richardson et al. (2018) discuss a method of assessing SEPSTER skill scores as a function of a variable (rather than the more usual fixed) SEP event intensity threshold when various filters (as discussed above) are applied. These results clearly show that SEPSTER predictions are most reliable for the larger SEP events that are of space weather interest, while filtering substantially improves the false prediction rate for weaker events. For the larger events, with a peak 14–24 MeV proton intensity exceeding  $0.1$  ( $\text{MeV s cm}^2 \text{ sr}^{-1}$ ), over 80% of the predictions were within an order of magnitude of the observed intensity. Table 1 of Richardson et al. (2018) shows skill scores for these events assuming different filters. For example, applying the CME speed  $\times$  width  $> 50000$  km/s.deg. filter used by SEPSTER decreases the false alarm ratio from 0.67 with no filter to 0.31, with the lowest value of 0.21 obtained by requiring the observation of strong type III radio emission accompanying the CME.

### 3.27. SEPSTER2D - SEP prediction derived from STEREO observations 2D

**Model developers:** Alessandro Bruno (Catholic University of America, NASA Goddard Space Flight Center), Ian G. Richardson (University of Maryland, College Park and NASA Goddard Space Flight Center).

**Model description:** SEPSTER2D (Bruno and Richardson, 2021) is an empirical model to predict SEP event-integrated and peak intensity proton spectra between 10 and 130 MeV at 1 AU. Developed from the SEPSTER model, SEPSTER2D similarly assumes that the SEP intensity can be predicted based on the speed and direction of a CME relative to the observing spacecraft using an empirical formula derived from multi-point spacecraft measurements, specifically from GOES-13/15, STEREO A and B, and the PAMELA satellite experiments (Bruno et al., 2018). The GOES data used are based on the *effective* energies derived by Sandberg et al. (2014) for the P2–P5

<sup>16</sup> [https://cdaw.gsfc.nasa.gov/CME\\_list/radio/waves\\_type2.html](https://cdaw.gsfc.nasa.gov/CME_list/radio/waves_type2.html).

<sup>17</sup> [https://cdaw.gsfc.nasa.gov/CME\\_list/](https://cdaw.gsfc.nasa.gov/CME_list/).



(<80 MeV) proton energy channels, and by Bruno (2017) for the P6–P11 (>80 MeV) channels, based on comparison with the IMP-8/GME and PAMELA data, respectively. SEPSTER2D assumes that the SEP intensity distribution,  $\Phi$ , as a function of energy  $E$  and the (energy-dependent) spherical distance  $\delta$  from the location of peak SEP intensity, can be estimated as

$$\Phi(E, \delta) = \Phi_o(E, V_{cme})G(E, \delta), \quad (15)$$

where

$$\Phi_o(E, V_{cme}) = \Psi_{cme}(E) \exp[\Lambda_{cme}(E)V_{cme}], \quad (16)$$

is the SEP maximum intensity spectrum. Here,  $V_{cme}$  is the parent CME speed, and the functions  $\Psi_{cme}(E)$  and  $\Lambda_{cme}(E)$  account for the energy-dependence of the intensity. The SEP angular distribution is modeled with a periodic Gaussian functional form  $G(E, \delta) = G(E, \delta \pm 2\pi)$  accounting for both the longitudinal and latitudinal magnetic connectivity. The latitudinal angle of the peak of the SEP distribution is assumed to coincide with the estimated CME latitudinal angle based on coronagraph observations. The model parameters are derived by using the 3-spacecraft (STEREO A, B, and near-Earth) measurements of 32 SEP events occurring between 2010 and 2014. The location of the footpoint of the IMF field lines passing the observer (Earth, STEREO-A and -B) is estimated at the CME first appearance time and at a 2.5 Rs radial distance, based on a simple Parker spiral IMF model using measured solar wind speeds. SEP intensity prediction errors are evaluated by accounting for the uncertainties of the different experimental quantities involved in the calculation. Further details can be found in Bruno and Richardson (2021). Future plans include the implementation of a faster prediction scheme based on X-ray flare data.

**Inputs:** CME speed, direction and first appearance time from DONKI; solar wind speed from ACE/DSCOVR/STEREO.

**Outputs:** SEPSTER2D outputs SEP peak and event-integrated intensities (both differential and energy-integrated) at various proton energies, along with corresponding uncertainties, as well as peak intensity times and event end times.

**Free parameters:** None.

**Limitations and caveats:** Predicted intensities are expected to overestimate those observed for relatively slow (<600 km/s) CMEs and narrow SEP events. SEP intensities above 130 MeV are based on spectral extrapolations and are characterized by large uncertainties.

**Access to model output or forecasts:** SEPSTER2D forecasts are available real-time on the SEP Scoreboard (<https://sep.ccmc.gsfc.nasa.gov/intensity/>).

**Model validation:** The model performance, including its extrapolations to lower/higher energies, was tested by comparing with the spectra of 20 SEP events not used to derive the model parameters, showing a reasonable agreement (Bruno and Richardson, 2021).

### 3.28. SMARP Model

**Model developers:** The model developers are Spiridon Kasapis, Lulu Zhao, Xiantong Wang, Yang Chen and Tamas Gombosi who are members of the Solar Storms and Terrestrial Impacts Center (SOLSTICE) team at the University of Michigan Climate and Space Science Department<sup>18</sup>. Monica Bobra from the Hansen Experimental Physics Laboratory in Stanford University provided the Space-Weather MDI Active Region Patches (SMARP) dataset whose predictive capabilities are being explored in this work.

**Model description:** The SMARP Model from Interpretable Machine Learning to Forecast SEP Events for SC23 is a machine learning-based SEP model developed at the University of Michigan. The developers explore how capable two popular groups of ML algorithms (SVM (Cortes and Vapnik, 1995) and Regression Models) are in predicting whether an AR which produces flares will lead to a SEP event. The SVM models use four different kernels: a linear, two polynomial (second and third degree) and the Gaussian Radial Basis Function (RBF) kernel which has been used in similar studies (Inceoglu et al., 2018). In addition to the above, two Regression models are trained: the Ridge and the Logistic Regression models.

Based on the magnetograms measured by the MDI (Scherrer et al., 1995) onboard SOHO, Bobra et al. (2021) derived a new database called SMARPs, which contains characteristics of the active regions on the solar surface. The developers surveyed the SMARP active regions associated with flares that appear on the solar disk between June 5, 1996 and August 14, 2010, label those that produced SEPs as positive and the rest as negative. Three physical keywords, total unsigned flux, mean gradient of the vertical field, and the logarithm of the total unsigned flux near the polarity inversion line are calculated using the pixels in the active region's magnetogram and are used as inputs to the models. In addition, the SMARP dataset also contains four spacial features specifying the location of the corresponding AR on the solar surface: the minimum and maximum longitude and latitude. Using these spacial features, two more inputs were calculated - the angular distance between the AR and the magnetic foot-point of the earth and the size of the active region.

In this 14-year time span, 65 Solar Energetic Particle events have information adequate to label the 6,510 flare-AR couples, a label is therefore assigned to each couple: positive if it led to an SEP and negative if it did not. Consequently, the output of the binary prediction models is a 0 (negative) or 1 (positive) label.

**Inputs:** SMARP files and derived values.

**Outputs:** Binary yes/no forecast of SEP occurrence (>10 MeV), probability of SEP occurrence and quantified uncertainty of the prediction model.

<sup>18</sup> <https://solstice.engin.umich.edu/>

**Free parameters:** Both SVM and Linear models are affected by user-defined constants such as the  $\alpha$  (complexity parameter) and  $C$  (regularization parameter). An embedded grid search using the testing dataset to avoid overfitting is employed varying each free parameter on a range between 0.05 to 20. All the results reported in this work use a probability decision threshold  $pt = 0.5$ .

**Limitations and caveats:** The task of SEP prediction using SMARPs is subject to a number of limitations such as data uncertainties, a vastly unbalanced dataset which only includes a limited amount of positive events and the inherent limitation of the SMARP dataset which is that compared to other data products it provides lower resolution time series (96-min cadence). It is important to acknowledge that the SMARP dataset could not be used alone to reliably forecast SEP events, therefore the aim of this study is to explore the prediction capabilities of the SMARP dataset and the quality of its different physical parameters rather than propose an operational forecasting apparatus.

**Access to model output or forecasts:** Forecasts from the model are not available, however the source code may be accessed at [https://github.com/skasapis/SEP\\_Prediction\\_Using\\_SMARP](https://github.com/skasapis/SEP_Prediction_Using_SMARP).

**Model validation:** The mean accuracy we obtain when validating a Third Degree Polynomial SVM trained on the best two SMARP predictors (unsigned flux and active region distance from the magnetic foot-point of the earth) suggests that 72% of the times ( $\pm 12\%$  for a single run) algorithm can correctly predict whether a flare will lead or not to an SEP. These are the results when training on a balanced data set, however there is a significant reduction in accuracy when training with a more realistic imbalanced data set. These outcomes show that although the SMARP dataset has some ability to make distinctions between flares that produce SEPs and flares that do not, when put in an operational setting where the testing is performed in a vastly imbalanced set of samples, the forecasting model fails to produce meaningful results. This is yet another proof of the initial hypothesis that although the SMARP dataset includes meaningful information which can be proven useful for SEP forecasting if used to augment other existing machine learning models, it cannot be used by itself as a forecasting dataset.

### 3.29. SOLPENCO and SOLPENCO2 - Solar Particle Engineering Code

**Model developers:** SOLPENCO: Angels Aran (main developer, University of Barcelona (UB)), Blai Sanahuja (UB), David Lario (NASA Goddard Space Flight Center). SOLPENCO2: Angels Aran (main developer, UB), Blai Sanahuja (UB), Carla Jacobs (Space Applications Services, Belgium), Stefaan Poedts (KU Leuven).

**Model description:** The original SOLar Particle ENgineering Code (SOLPENCO) was an initial step towards developing an operational tool to rapidly predict proton

intensity-time profiles and fluences for gradual SEP events (Aran et al., 2006; Aran et al., 2008). The SOLPENCO predictions are based on database interpolations from synthetic proton intensity-time profiles pre-computed for a range of CME-driven shock scenarios and associated solar-interplanetary conditions.

The SOLPENCO synthetic proton flux database is computed from a physics-based SAP model (Heras et al., 1992; Lario et al., 1998). The conceptual framework of SOLPENCO is based on the assumption that the proton intensity-time profile of a gradual SEP event is mainly the result of particle acceleration by an IP shock, and the subsequent injection of shock-accelerated particles that takes place at the point on the traveling IP shock front that magnetically connects to the observation location (Lario, 2005). This point on the shock front has been given the name Connecting-with-OBServer-POINT (cobpoint) (Heras et al., 1995).

The shock model determines the propagation of an IP shock from the  $18 R_{\odot}$  inner boundary of a 2.5D (2-dimensions, 3 vector components for the flow velocity and magnetic induction) MHD model to 1.0 AU (Wu et al., 1983). The model numerically solves the ideal adiabatic MHD equations. The shock is introduced into the MHD model at the inner boundary by defining the initial shock speed, the heliolongitude of the origin of the shock disturbance, and the longitudinal width of the shock at the location of origin. The shock perturbation is defined as a finite pulse shape in space and time, and the MHD shock jump conditions are solved separately to determine other state variables (e.g., density and temperature) given the initial shock velocity. The pre-shock IMF is assumed to be a Parker spiral field and homogeneous background solar wind conditions are determined by the pre-shock, steady-state solutions of the MHD equations. The meridional velocity and magnetic field components are adjusted at the inner boundary of the model to maximize agreement with various plasma and field measurements at 1.0 AU.

The particle transport model determines the interplanetary propagation of shock-accelerated energetic particles that are injected at the COBPOINT, by solving the FTE. The physical processes included in the FTE are streaming and convection of energetic particles, adiabatic focusing, pitch-angle scattering, and adiabatic deceleration (Lario et al., 1998). The injection of shock-accelerated energetic protons at the COBPOINT is included as a source term in the FTE. From modeling and analyzing various SEP events, the functional form of the injection rate,  $Q$ , is described by the following empirical relationship (Lario et al., 1998; Aran et al., 2006; Aran, 2007; Aran et al., 2007):

$$\log Q(E, t) = \log Q_0(E) + k \text{VR}(t), \quad (17)$$

where  $\text{VR}(t)$  is the ratio of the downstream to upstream normalized radial plasma velocity jump at the COBPOINT, which is derived from the output results of the time-dependent MHD simulations of the shock propaga-

tion. Thus, the rate at which shock-accelerated particles are injected into interplanetary space is directly related to the dynamical evolution of the shock strength at the COB-POINT. The parameters  $k$  and  $Q_0$  are determined by fitting the shock-and-particle model simulations to proton flux measurements at 1.0 AU at a reference energy for several SEP events. The slope parameter ( $k$ ) is taken as the average value derived from the different SEP events analyzed, and other energies are fit to the proton flux measurements by assuming  $Q_0$  varies as a power-law in energy, i.e.,  $Q_0(E) = Q_0(E_0)(E/E_0)^{-\gamma}$  (Aran et al., 2006; Aran et al., 2008).

The remaining parameter in the interplanetary transport of the shock-accelerated particles is the parallel proton mean free path (perpendicular diffusion across field lines is not included). Along with the parameters  $k$  and  $Q_0$ , the parallel mean free path for 0.5 MeV protons ( $\lambda_{\parallel 0}$ ) was determined by fits to proton flux and first-order anisotropy measurements at 1.0 AU. From the analysis and fits to the SEP events, two values for  $\lambda_{\parallel 0}$  were adopted: 0.2 AU and 0.8 AU (Aran et al., 2006). The parallel scattering lengths at other energies were assumed to scale with rigidity according to a power-law:  $\lambda_{\parallel} = \lambda_{\parallel 0}(R/R_0)^{0.5}$ , where  $R$  is the proton rigidity. To mimic the ESP component of SEP events, a turbulent foreshock is modelled by taking a 0.01 AU region in front of the shock where the proton mean free path scales as  $\lambda_{\parallel c} = 0.01(R/R_0)^{-0.6}$  AU, where  $R_0 = 30.635$  MV. Such foreshock region starts acting 20 h prior the shock arrival to the observer. The values of the parameters defining this foreshock are average values from modelled events (Aran et al., 2006).

The SOLPENCO database of synthetic proton intensity-time profiles contains 448 combined shock-and-particle scenarios (Aran et al., 2005b; Aran et al., 2006). There are eight IP shocks with initial velocities ranging from  $750 \text{ km s}^{-1}$  to  $1800 \text{ km s}^{-1}$ , which translate to shock transit times at 1.0 AU that range from roughly 25 h to 100 h (Aran et al., 2008). The model calculations were also run for 14 heliolongitudes of the associated parent solar event with respect to the observer, from E75 to W90 for observers at 1.0 AU. In addition, for each database shock/heliolongitude combination there are four IP particle transport conditions: parallel scattering lengths of  $\lambda_{\parallel 0} = 0.2$  AU and 0.8 AU, and simulations with and without a turbulent foreshock region. Furthermore, the output results for the shock-and-particle model scenarios are provided at heliocentric radial distances of 0.4 AU and 1.0 AU and at 10 proton energies ranging from 0.125 MeV to 64 MeV, equally distributed in logarithmic space. The software interface allows the user to retrieve the upstream intensity-time profiles at the selected input parameters (among those for the scenarios depicted above) as well as the integral cumulative fluence profiles above the low-energy bound of each differential channel (labelled by using the mean energy of each energy channel). The code also gives the transit time and velocity of the shock from the

Sun to the observer, the maximum proton intensity (peak flux), and the total fluence of the SEP event computed from the onset of the event up to the arrival of the associated transient CME-driven shock. SOLPENCO and its validation are fully documented in Aran (2007).

SOLPENCO2 is based on a version of the University of Barcelona's SAP model that was built in collaboration with the KU Leuven (Aran et al., 2011; Pomoell et al., 2015).

SOLPENCO2<sup>19</sup> furnishes the SEPEM statistical SEP model (e.g., Jiggins et al., 2012) with 5–300 MeV proton peak flux and event differential-fluence heliocentric radial power-law dependences, derived from the modeling of ten reference gradual proton events: 6 March 1989, 4 April 2000, 6 and 10 June 2000, 29 March 2001, 24 September 2001, 29 October 2003, 13 and 14 December 2006 and 13 March 2012. These events were selected as representative of the 243 SEP events in the SEPEM Reference Event List (REL) at 1.0 AU, spanning the period from January 1988 to March 2013. The synthetic proton peak flux and event differential fluence quantities from these ten events were scaled to the observed values at 1.0 AU in order to ensure that the synthetic quantities match the reference data utilized by the SEPEM statistical tools. The scaling is done for each of the eleven energy channels of the SEPEM Reference Data Set (RDS v2.0) (e.g., Jiggins et al., 2018). For each of the ten SEP events, and for each energy channel, the peak proton flux and event fluence quantities are extracted from the simulations at the seven SEPEM reference heliocentric radial distances that lie along the same IMF Parker spiral field line that passes through 1.0 AU (i.e. the Earth's nominal magnetic field line connecting with the Sun). These quantities are then fit to a power-law with the heliocentric radial distance, which provides the means by which the SEPEM tool extends the proton peak flux and event fluence quantities away from 1.0 AU. The events in REL are classified into one of the ten event categories and the corresponding radial scales are applied. The classification depends on the detection of an interplanetary shock at 1.0 AU, the level reached in the proton intensity for  $E > 66$  MeV, the heliolongitude of the parent solar activity, and for the largest events, the peak intensity level reached 8.7 MeV and 79.5 MeV protons (Crosby et al., 2015; Aran et al., 2017). The design of this classification was performed in collaboration with P. Jiggins from ESA. Currently, SOLPENCO2 provides SEPEM with scaled-to-observed (1AU) peak intensity and event fluence ratios for each of the 249 SEP events and for virtual observers located at 0.2, 0.4, 0.6, 0.8, 1.0, 1.3 and 1.6 AU. This allows the inclusion of interplanetary missions in the SEPEM statistical SEP model. ([http://sepem.eu/help/sat\\_radial.html](http://sepem.eu/help/sat_radial.html)).

SOLPENCO2 is designed for the description of gradual solar proton events, originating from the solar western limb to far eastern heliolongitudes, as seen from

<sup>19</sup> [http://sepem.eu/help/solpenco2\\_intro.html](http://sepem.eu/help/solpenco2_intro.html).

virtual observers located within 0.2 AU and 1.6 AU. For any modeled event, the tool provides the 5–300 MeV proton differential intensity-time profiles for the eleven energy channels of RDS v2.0. SOLPENCO2 consists of two main parts: (i) A database of simulated interplanetary shocks and (ii) a database of ten modeled SEP events. These data bases are generated from the physics-based SAP model (Aran et al., 2011; Pomoell et al., 2015). The underlying 2D MHD component of the SAP model used in SOLPENCO2 was significantly updated with respect to the original SOLPENCO version (Aran et al., 2006; Aran et al., 2011; Jacobs and Poedts, 2011; Pomoell et al., 2015). Its inner boundary is now low in the solar corona at  $1.03 R_{\odot}$  (Aran et al., 2011), enabling the modeling of shock-accelerated proton spectra to be extended from 64 MeV to 300 MeV. The approach taken to specify the pre-shock, background solar wind plasma is to adopt a polytropic solar wind model which is a 1.5D extension to the Parker model that includes both solar rotation and the magnetic field (Aran et al., 2011; Jacobs and Poedts, 2011). Advantages and drawbacks in the use of the polytropic wind with interplanetary shock simulations are discussed by Jacobs and Poedts (2011) and (Pomoell et al., 2015). The propagation of an IP shock is performed by numerically solving the ideal MHD equations with a perturbation in solar wind radial velocity and density superimposed onto the background solar wind plasma state (Aran et al., 2011). The functional form of the radial velocity and density perturbations are exponential pulse profiles, with additional parameters introduced to control the pulse shape and the angular width and radial thickness of the initial shock disturbance (Aran et al., 2011; Pomoell et al., 2015). The functional form and shape parameters of the IP shock were selected to reproduce IP shock transit times and solar wind plasma measurements for various gradual SEP events observed at 1.0 AU. The 2D MHD equations are solved using the Versatile Advection Code (VAC) (Toth, 1996). The more reduced grid spacing of the MHD model has led to noticeable improvements in the numerical representation of IP shock propagation with respect to the MHD model used in SOLPENCO. The database of 2D MHD shocks includes the evolution of the COBPOINT for virtual observers located at different heliolongitudes with respect to the incoming shocks (Aran et al., 2011). Specifically, the simulated shocks and cobpoints are computed for:

- Solar winds extending from  $1.03 R_{\odot}$  to 1.6 AU: a slow wind of  $365 \text{ km s}^{-1}$ , and a fast wind of  $595 \text{ km s}^{-1}$ .
- Eight initial shock conditions (different values in speed and density), centered at  $1.75 R_{\odot}$ , that yield to shocks arriving to 1 AU between 25 h and 66 h, for the shocks evolving in the slow solar wind, and between 17 h and 48 h, for the shocks in the fast solar wind.
- Two longitudinal widths for the initial shocks: narrow and wide.

- 14 virtual observers located at 1.0 AU, at longitudinal positions between W85 and E65.

The shock-finder procedure, to extract the evolution of the COBPOINT and the shock plasma jumps at the COBPOINT was also automated and significantly improved with respect to the previous version used in SOLPENCO (Aran et al., 2011). A adaptation for a 3D geometry is described in (Rodríguez-Gasén et al., 2011). For each modelled shock, SOLPENCO2 provides the COBPOINT position as well as density, magnetic field ratios and normalized speed ratio, VR, in the lab's frame, for the 14 (longitudes)  $\times$  7 (radial distances) virtual observers.

The database of intensity-time profiles are generated with the SAP's transport model (Lario et al., 1998). For the 10 reference events SOLPENCO2 provides:

- The particle source at the COBPOINT,  $Q$ , which is obtained by means of a  $Q(\text{VR})$  relation based on the parameters derived from the modeling of the April 4, 2000 and December 13, 2006 SEP events (Aran et al., 2011; Pomoell et al., 2015).
- The proton intensity-time profiles for the 11 SEP reference energies, for the virtual observers located between 0.2 AU and 1.6 AU. The profiles are obtained by setting constant proton mean free path values (0.35 AU or 1.17 AU for 8.7 MeV protons) and the presence of a turbulent foreshock as in SOLPENCO (Aran et al., 2011). The choice of these transport parameters that leads a better comparison with data is selected.
- The peak intensity and the upstream differential fluence [ $\text{MeV}^{-1} \text{ cm}^{-2}$ ] as a function of the observer's radial distance, and the derived power-law indices.

To account for the post-shock portion of the fluence (i.e., the downstream fluence) of the events time-profiles in the REL list, an observational analysis (including SEP, STEREO and Helios data) of the fluence in the downstream region of the proton intensity-time profiles of gradual SEP events was performed (Aran et al., 2017; Pacheco, 2019). In SOLPENCO2, all fluences are differential fluences. For each event in REL with an IP shock detected, the total fluence at the different radial distances is obtained by adding the scaled upstream fluence and a scaled downstream fluence (values at 1 AU match the observations). The scaling of the downstream fluence is based on an empirical relation found between the downstream-to-total fluence ratio and the longitudinal separation of the observer with respect to the nose of the shock, for each energy channel (Pacheco, 2019). Therefore, in contrast to SOLPENCO, SOLPENCO2 can include a prediction for the downstream fluence of the synthetic events.

The main difference between SOLPENCO and SOLPENCO2 lies in the purpose of the two tools. SOLPENCO is a stand-alone tool ready to be operated by any user with some knowledge of SEP events; and SOLPENCO2 is

designed for providing inputs to the SEPEM interplanetary statistical SEP model. SOLPENCO2 uses scaling factors that are specific for the reference events, in order to match 1.0 AU data, whereas SOLPENCO used a universal scaling factor for its SEP events database. Both, however, share the same modular approach, which would enable the possibility of developing another tool more similar to the first SOLPENCO, using the simulations available in SOLPENCO2. The first attempt for this is the inclusion of SOLPENCO2 outputs in SAWS-ASPECS.

#### Inputs:

For the SOLPENCO tool, the user needs to specify the following parameters:

- Radial distance from the Sun (0.4 AU or 1.0 AU).
- Angular position of the observer from the CME eruption (any value from E75 to W90).
- Shock initial speed at  $18R_{\odot}$  (any value from  $750\text{ km s}^{-1}$  to  $1800\text{ km s}^{-1}$ ).
- Proton energy in MeV (0.125, 0.25, 0.5, 1, 2, 4, 8, 16, 32, or 64).
- The proton mean free path of 0.5 MeV protons (0.2 AU or 0.8 AU).
- Turbulent foreshock region (Yes or No).

For SOLPENCO2, in order to model an event, the transit time of the shock to 1 AU, the longitude of the parent event (the CME or the flare if the first is not known) and the pre-event solar wind speed are needed. To scale the data, the observed peak flux or the upstream fluence is needed, at least for one energy channel.

**Outputs:** For the user's selected input values the SOLPENCO tool gives: the proton flux time profile, the cumulative fluence profile and the shock transit time and speed to the observer's location and total upstream fluence. For a particular event, SOLPENCO2 provides proton differential intensity-time profiles for the 11 energy channels of SEPEM RDS v2.0 data set, with prescribed values for the transport and source function parameters, as described above.

**Free parameters:** For the SOLPENCO tool all parameter values are fixed. For the SOLPENCO2 tool, the values of the parameters describing the particle source function, Eq. 17, change for each reference event. With respect to the FTE of the SAP model (Lario et al., 1998), the free parameters are the parallel proton mean free path, the turbulent foreshock region characteristics which are determined by fitting the observed intensity-time profiles, as well as the particle source function. The solar wind speed is also determined by observations, or by the simulated solar wind. The free parameters of the shock propagation models used to describe the initial perturbation: initial speed, width and duration for (Wu et al., 1983) and density (Aran et al., 2011), which are fixed in the databases of the SOLPENCO tools to obtain different shock transit times to the virtual observers. The solar wind model of SOLPENCO2 has also the polytropic

index as a free parameter to match observations (Jacobs and Poedts, 2011).

**Limitations and caveats:** SOLPENCO and SOLPENCO2 generated databases of SEP time profiles for use in forecasting. The models themselves are not run in real time. The main difficulty for that is to find an appropriate proxy for the initial shock speed. The transport model used assumes an Archimedian IMF, perpendicular diffusion is not included, and transport is simulated only up to the shock arrival to the observer. Another limitation for SOLPENCO is the inner boundary location of the shock propagation model, that prevents the simulation of the particle source function at coronal heights. The two tools depend on 1-D particle transport simulations, and hence perpendicular transport is not considered. In addition, the particle source function depends only on the plasma shock-jump in speed at the COBPOINT, and hence does not consider explicitly other parameters that may be relevant for particle acceleration such as the shock obliquity (Lario et al., 1998; Pomoell et al., 2015). Given the underlying assumption of an Archimedian IMF field in the model, non nominal conditions for the solar wind are not taken into account.

**Access to model output or forecasts:** SOLPENCO is available by request to the main author. SOLPENCO2 time profiles are one of the outputs of the SAWS-ASPECS (Section 3.23) real time forecasting tool. Peak flux and total fluence energy spectra for the 172 events in the SEPEM radial event list (1988–2013) are available for seven heliocentric distances (0.2 AU to 1.6 AU) at the SEPEM application server (sepem.eu).

**Model validation:** SOLPENCO's proton intensity-time profiles outputs have been compared with actual large SEP events (Aran et al., 2005a; Aran et al., 2006; Aran, 2007; Aran et al., 2008). The validation shows good results for  $E < 2\text{ MeV}$  protons, and SOLPENCO fails in predicting the peak intensity for  $E > 5\text{ MeV}$  for events showing a strong prompt component (e.g., Aran et al., 2008). The two main reasons for the mismatch are the impossibility of tracking the COBPOINT (and hence of modelling the source function at the shock) below 0.1 au, and the value of  $k$  in Eq. 17 for high energies. Both are taken into account in the development of SOLPENCO2. SOLPENCO2 time profiles have recently been validated as part of the SAWS-ASPECS system (Section 3.23), however the work is ongoing and has not yet been published.

### 3.30. South African Model

**Model developers:** Du Toit Strauss (principal developer, North-West University), Ruhann Steyn (North-West University), Jabus van den Berg (North-West University, South African National Space Agency).

**Model description:** The South African SEP transport model is a physics-based model aimed at simulating the transport of solar energetic particles, on the pitch-angle level, through the turbulent interplanetary plasma. The

model implements a [Parker \(1958\)](#) magnetic field geometry and focuses on applying transport coefficients that are derived from first principles, also including the perpendicular diffusion of SEPs. The model implements a finite differences numerical scheme, with special flux conservative boundary conditions, that solves the focused transport equations in a reduced geometry (neglecting adiabatic energy losses and only performing simulations in the equatorial plane) in order to speed up computations so that the model can be executed in a real-time operational setting ([Strauss and Fichtner, 2015](#); [Heita, 2018](#)).

Previously, the focus of the model was on simulating SEP electrons ([Strauss et al., 2017](#); [Strauss and le Roux, 2019](#); [Strauss et al., 2020](#)), including the effects of wave generation. The model was also tested for an operational setting by [Steyn et al. \(2020\)](#) where the model was driven using an observationally constrained inner boundary condition in order to simulate historical SEP electron events. As the acceleration of SEP is not simulated self-consistently in this transport model, the time and spatial profile of the accelerated SEP distribution must be specified at the inner numerical boundary (assumed to be the solar source surface). We refer to this as the injection function. Work continues to constrain this function, especially for protons, using historical SEP events. The model is currently being tested and optimized to simulate SEP proton transport, where after it will be moved into a predictive setting.

**Inputs:** The model requires the following inputs:

1. The injection function, i.e., the time and spatial dependence of the accelerated SEP source that propagates into the inner heliosphere. The time dependence can be derived from different proxies, e.g. the SXR flux or the CME speed, and is directly read into the model. The spatial dependence of the injection function, most importantly the width/broadness of the SEP source, also needs to be specified. We generally assume the SEP source to have a Gaussian shape in terms of longitude and only specify the broadness of this Gaussian function.
2. The position of active region that produced the SEP event and the position of the virtual observers where the predicted SEP intensity is required.

**Outputs:** The model provides the pitch-angle dependent particle distribution function as a function of time at all spatial grid points in the equatorial plane. From this the omni-directional SEP intensity and first-order anisotropy, amongst other quantities, can be calculated. [Fig. 14](#) shows an example of a simulated multi-spacecraft event.

**Free parameters:** In the present iteration of the model, the level of perpendicular diffusion is a free parameter. However, work is underway in order to constrain this parameter using historical SEP measurements. The level of pitch-angle scattering is fixed but can be varied if required.

**Limitations and caveats:** When using this SEP model, the following limitations should be taken into account:

1. The model neglects adiabatic energy losses.
2. The model only solves the focused transport equation in the equatorial plane and therefore adopts a 2D spatial geometry. However, a comparison between 2D and 3D models show very good agreement ([Steyn et al., 2020](#)).

**Access to model output or forecasts:** A 1D (i.e. neglecting the cross-field coordinate) version of the model is described in detail by [van den Berg et al. \(2020\)](#) and available at [https://github.com/RDStrauss/SEP\\_propagator](https://github.com/RDStrauss/SEP_propagator). Once the real-time implementation of 2D model is complete, it will be included in the same repository. Interested users can contact the model developers for access to a preliminary version of the model.

**Model validation:** The validation of the model is an actively ongoing process. The model is primarily a research tool and the emphasis in the past was on comparing model results with SEP measurements in order to understand the underlying processes in more detail. The validation of the model's predictive capability is currently underway and we hope to present this to the community in the very near future.

### 3.31. SPARX - Solar Particle Radiation swX

**Model developers:** Michael S. Marsh (Met Office), Silvia Dalla (University of Central Lancashire), Bill Swalwell (University of Central Lancashire), Charlotte Waterfall (University of Central Lancashire).

**Model description:** Solar Particle Radiation SWx (SPARX) is a forecasting system based on a full 3-D physics-based model for simulating SEP propagation for Space Weather forecasting purposes ([Marsh et al., 2015](#)). As SPARX was initially developed as part of the European Union-funded Seventh Framework Programme (FP7) COMESSEP project ([Crosby et al., 2012](#)), a version of the SPARX output is operational within its SEP forecasting component which produces alerts at <https://swe.ssa.esa.int/bira-comesep-federated>. As described in [Figure 1](#) of [Marsh et al. \(2015\)](#), results of earlier runs of a 3D test particle code are used by SPARX in real time to produce a forecast.

The 3D test particle code naturally describes propagation across the magnetic field. High energy SEPs have a strong influence on radiation dose and these particles are affected by drifts due to the gradient and curvature of the Parker spiral, requiring a 3D description ([Dalla et al., 2013](#)). The latter effects are included in the current version (v1.0) of SPARX, while neither drift along the heliospheric current sheet nor magnetic field line meandering are considered at present. SPARX simulates a large number of independent test particles that follow the equation of motion in 3D:

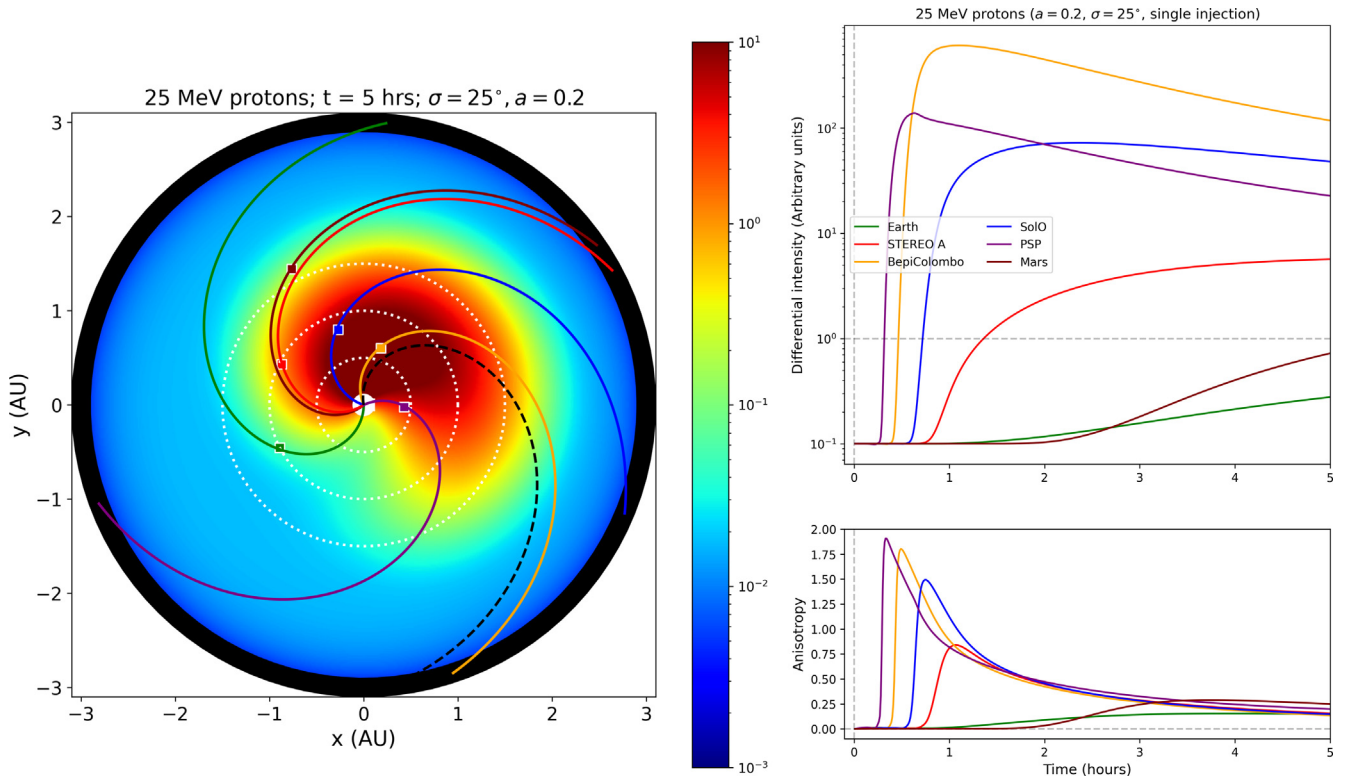


Fig. 14. An example of the South African SEP model applied to a multi-spacecraft event. The left panel shows a contour plot of 25 MeV proton intensities and the position of a number of spacecraft. The right panel shows the simulated differential intensity and anisotropy levels at the position of these spacecraft.

$$\frac{d\mathbf{p}}{dt} = q \left( \mathbf{E} + \frac{1}{c} \frac{\mathbf{p}}{m_0 \gamma} \times \mathbf{B} \right) \quad (18)$$

where  $\mathbf{p}$  is the particle's momentum,  $q$  is the particle charge,  $m_0$  is its rest mass,  $\gamma$  is its Lorentz factor, and  $c$  is the speed of light. The magnetic field  $\mathbf{B}$  is defined by a unipolar Parker Spiral and  $\mathbf{E}$  is the solar wind electric field in a fixed reference frame (Marsh et al., 2015). The field polarity of the IMF used in the SPARX forecast is determined by the hemisphere in which the eruptive event occurs and the  $A^+$  or  $A^-$  phase of the global solar magnetic field, which changes throughout the solar cycle. The particle motion is calculated in a fixed reference frame that sees the solar wind move radially outward and the effects of corotation of magnetic flux tubes anchored at the Sun are included. Turbulence is simulated by introducing isotropic scattering of each particle's pitch angle and gyrophase in the reference frame of the solar wind with a prescribed value of the mean free path. Particle drifts are naturally described by SPARX's approach and play an important role in longitudinal spreading and particle deceleration (Marsh et al., 2013; Dalla et al., 2013).

In the test particle simulations particles are injected instantaneously at  $2R_{sun}$  across a spatially extended source region that represents a CME-driven shock in the corona. The input particle spectrum is assumed to be a power law  $E^{-\gamma}$ . Particles are propagated and every time they cross a

spherical boundary at 1 AU, their parameters are output and used to generate a synthetic particle spectrum.

SPARX is part of the COMESSEP Alert System and its implementation within that system is described in detail in Section 3.6. Running of the 3D test particle code is too time consuming for operational usage, therefore the real-time forecasting tool, SPARX, uses a pre-generated database of outputs of runs with varying proton injection locations. The database contains 30 model runs for each IMF polarity, each run describing a specific  $6^\circ \times 6^\circ$  injection tile at a given central latitude, following the particles for 100 h. In each tile 100,000 protons are injected with energies in the range 10–400 MeV. An extended CME-shock-like injection region is simulated by summing up the outputs of multiple  $6^\circ \times 6^\circ$  tiles. In SPARX v1.0 a default fixed injection width of  $48^\circ \times 48^\circ$  is used. The centre of the shock-like region is the location of the flare associated to the event. A constant particle injection density over the shock is maintained, i.e. it is assumed that the acceleration efficiency is constant across the full injection region. In v1.0 the spectral index of the injection energy spectrum is taken to be  $\gamma = 1.1$  and the mean free path  $\lambda = 0.3$  AU. Because of the symmetric nature of the assumed IMF, only a single strip of injection tiles are required to build up the  $48^\circ \times 48^\circ$  injection region by utilising the rotational symmetry and relative longitude difference between the observer and the detected flare (Marsh et al., 2015). A synthetic particle spectrum is produced at

the observer by integrating over a  $2^\circ \times 2^\circ$  surface area element at 1 AU for a selected period of time. The flux spectrum is normalized by applying the statistical relationships between proton peak flux and flare X-ray peak flux derived by (Dierckxsens et al., 2015), described in detail in Section 3.6.

#### Inputs:

SPARX inputs:

- Flare location
- Flare peak time
- Flare X-ray peak value (input into SPARX as a magnitude, i.e., ‘-4.0’ for M1.0 flare)

3D test particle code inputs: (fixed in current implementation but could be varied in future)

- Solar magnetic field polarity
- Particle species (in v1.0: protons)
- Output flux energy range (in v1.0: >10 MeV, >60 MeV)
- Injection energy spectrum (in v1.0: power law with index 1.1)
- Location in the heliosphere where to generate flux profiles (in v1.0: 1 AU)
- Mean free path

**Outputs:** SPARX v1.0 produces as outputs SEP flux time profiles for  $E > 10$  MeV and  $E > 60$  MeV (see Fig. 15 for an example). Threshold crossing times, proton peak flux and peak time, and SEP event duration are calculated from the time profile. The 3D test particle model can be used to produce new versions of SPARX that output profiles in other energy ranges and a version for >300 MeV protons is currently being developed (Waterfall et al. 2022, in preparation).

#### Free parameters:

- Power law index of input energy spectrum
- Mean free path
- Solar wind speed (which effects the shape of the unipolar Parker Spiral)
- Width of injection region

**Limitations and caveats:** Only flares >M1.0 can be taken as input by SPARX. The analysis that led to this selection (Dierckxsens et al., 2015) was carried out for 5 flare bins, where the last bin is for >X5.0 flares. Any flares >X5.0 will result in the same scaling/normalisation factors in SPARX.

The SPARX 3D test particle code model accounts for the initial acceleration and transport of the particles at the start of an event low in the corona. No evolution of the acceleration region, such as the propagation of a CME out into the inner heliosphere, is considered. Through this approach, this model can predict event onset and evolution of the initially accelerated particles, but does not include the particle populations that are continuously accelerated at a CME shock front following the initial eruption.

**Access to model output or forecasts:** An initial SPARX version is implemented in COMESSEP at <https://swe.ssa.esa.int/bira-comesep-federated>. SPARX is planned to be run operationally at the UK Met Office in future, using the GOES-R XRS flare magnitude and location products as inputs. It will also be possible to run SPARX via the ESA VSWMC (<https://esa-vswmc.eu/>).

**Model validation:** Dalla et al. (2018) assessed model performance using a list of 125 X-class flares between 1 September 1997 and 30 April 2017. For each flare, SPARX was run in forecast mode with a fixed set of model parameters for all events. The output >10 MeV fluxes were

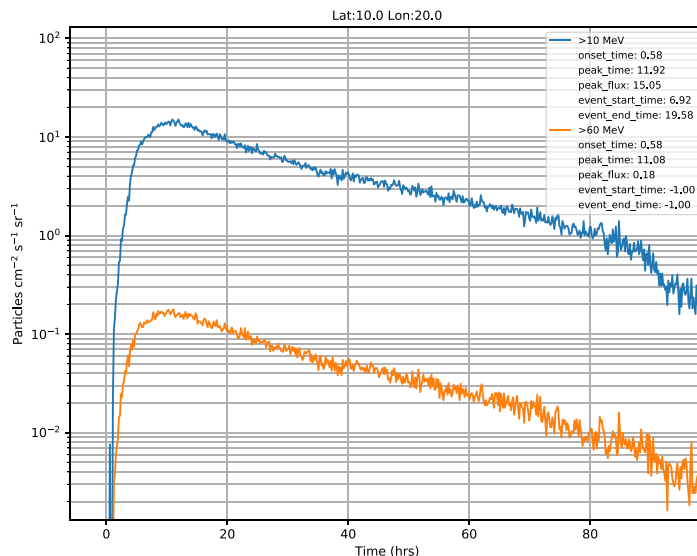


Fig. 15. Example of a SPARX output. Flux profiles of >10 MeV and >60 MeV protons for an X1.0 flare at N10W20 are shown. The legend displays calculated parameters of the flux profiles.



Table 8

Validation of the SPARX model by Dalla et al. (2018). Bias = tendency to under/over forecast; POD = Probability of Detection; FAR = False Alarm Rate; POFD = Probability of False Detection; CSI = Critical Success Index.

	$F_{10}$	$F_1$
<b>Bias</b>	1.18	1.37
<b>POD</b>	0.5	0.77
<b>FAR</b>	0.57	0.44
<b>POFD</b>	0.32	0.43
<b>CSI</b>	0.30	0.48

assessed for event/no event predictions by applying the standard NOAA threshold of 10 pfu ( $F_{10}$ ) and additional lower threshold of 1 pfu ( $F_1$ ). The forecasts were compared to GOES >10 MeV observations with the same thresholds applied.

SPARX performance when applying the 10 pfu threshold resulted in 20 hits, 27 false alarms, 20 misses, and 58 correct negatives. Application of the 1 pfu threshold resulted in 40 hits, 31 false alarms, 12 misses, and 42 correct negatives. The corresponding metrics and skill scores are reported in Table 8.

### 3.32. SPREADFAST - Solar Particle Radiation Environment Analysis and Forecasting – Acceleration and Scattering Transport

**Model developers:** Kamen Kozarev (Institute of Astronomy, Bulgarian Academy of Sciences (IA-BAS)), Mohamed Nedal (IABAS), Rositsa Miteva (IABAS), Momchil Dechev (IABAS), Pietro Zuca (Netherlands Institute for Radio Astronomy (ASTRON)).

**Model description:** Over the last fifteen years, observations and numerical models have confirmed that in their early stages (below 5–10  $R_{Sun}$ ), CMEs often drive shocks (Ontiveros and Vourlidis, 2009; Gopalswamy and Yashiro, 2011), and those shocks may accelerate SEPs to energies up to and beyond 100 MeV/n (Battarbee et al., 2013; Kozarev et al., 2013; Schwadron et al., 2014; Kong et al., 2017). To investigate the particle acceleration and transport in these very early stages of solar eruptions, we have developed a prototype and various scientific aspects of an end-to-end, physics-based, heliospheric SEP modeling and forecasting system —Acceleration and Scattering Transport (SPREADFAST). It allows for producing predictions of SEP fluxes in the inner heliosphere, by modeling the acceleration of protons at CME-driven shocks near the Sun, and their subsequent interplanetary transport. The system prototype incorporates results from our scientific investigations, the modification and linking of existing open-source scientific software, and its adaptation to the goals of the proposed work. SPREADFAST helps fulfill a vital component of ESA’s Space Situational Awareness program by contributing to the capability to protect space assets from solar activity space radiation. A description of the project is available at <https://spreadfast.astro.bas.bg/>.

The modeling framework combines detailed EUV observations of Coronal Bright Front (CBF) events with modeling of the interacting coronal plasma and the resulting SEP production and interplanetary transport. It is a chain of data-driven analytic and numerical models for estimating: coronal plasma conditions, dynamics of large-scale coronal (CME-driven) shock waves; energetic particle acceleration; scatter-based, time-dependent SEP propagation in the heliosphere to specific positions.

To characterize the kinematics of CBFs, we applied to the AIA observations the methodology of the Coronal Analysis of SHocks and Wave (CASHew) framework (Kozarev et al., 2017), updated and implemented in SPREADFAST. Our framework estimates the CBF kinematics in a similar way to Long et al. (2021) and Downs et al. (2021), by following the leading edge of the front on consecutive images. We explicitly measure the kinematics of the front in both the radial and lateral (parallel to the limb) directions, in order to model the CBF shape more realistically. In addition, we calculate the kinematics of the peak and back edge of the CBFs over time, which allows us to estimate their time-dependent mean intensity and thickness. The front observations may be extrapolated to 10–30 solar radii based on some model (Gallagher et al., 2003; Byrne et al., 2013).

Based on the radial and lateral measured front positions over time, a three-dimensional, time-dependent geometric spheroid model - Synthetic Shock Model (S2M) - is developed for all compressive fronts, consisting of a large number of points (>1000), used for the estimation of the dynamic shock upstream coronal parameters. The spheroid remains centered on the eruption source throughout the event, while its aspect ratio varies based on the radial and lateral CBF position measurements and extrapolations. The three-dimensional geometric model describes the shock surface evolution at 24-s intervals from the onset of the CBF to the time when its nose (leading direction’s front position) reaches 10  $R_{Sun}$ . This model shock surface is then propagated through a model solar corona, represented by results of a Magnetohydrodynamic Algorithm outside a Sphere (MAS Mikić et al., 1999) synoptic coronal MHD model run for the Carrington rotation of each simulated event. The shock surface thus samples at discrete points the relevant parameters for coronal shock acceleration of SEPs, determined by the magnetic field lines crossing it consecutively at each point.

After the plasma parameters along the individual shock-crossing field lines have been established, they are fed in a time-dependent manner into the coronal DSA model (Kozarev and Schwadron, 2016; Kozarev et al., 2019) for calculation of the proton acceleration between the low corona and 10 $R_{Sun}$ . The model was specifically developed to take as input remote solar observations and data-driven model output from the CASHEW framework. The model solves for the coronal charged particle acceleration by large-scale CME-driven shocks. The model calculates the minimum shock injection momenta for the particles. It

takes as input a particle distribution function, and provides time-dependent distribution function spectra or fluxes, as output. We use as input to the model averaged and rescaled suprathermal proton spectra from the SOHO/ERNE instrument (Torsti et al., 1995), observed during the 24 h of quiet time preceding each SEP event. We fit power laws to each suprathermal spectrum in the energy range 0.056 – 3.0 MeV, and scale them to  $1.05R_{Sun}$ , assuming a simple inverse square dependence on radial distance (implying flux conservation).

The final step of the modeling chain is the transport of the accelerated SEPs to 1 AU, and subsequent comparison with particle observations with the ERNE instrument. This is achieved by taking the resulting averaged fluxes from the coronal acceleration model for the entire event as input to a modified version of the EPREM focused transport model (Schwadron et al., 2010), and transporting them through a Parker-type static interplanetary medium.

We have so far modeled a set of 62 historical events with typical coronal and interplanetary conditions, with results available at <https://spreadfast.astro.bas.bg/catalog/>. The SPREADFAST system also has a real-time version, which is under development.

#### Inputs:

- SDO/AIA Level 1 full-cadence and full resolution data (EUV channels 94,131,171,193,211,335)
- SOHO/ERNE observations (LEMS120 P1-P8 channels)
- ACE/EPAM hourly observations (channels p1, p3, p5, fp6p, p7)
- Synoptic MAS MHD model results (datacubes freely available from Predictive Science’s website <https://www.predsci.com/mhdweb/home.php>)

#### Outputs:

- 3D models of EUV wave eruptions in the corona (below 10 Rs)
- Modeled shock front plasma parameters below 10 Rs
- Proton fluxes and fluences below 10 Rs for  $\sim 4$  h of events
- Proton fluxes and fluences at 1 au for the first  $\sim 10$  h of events

#### Free parameters:

- Coronal acceleration (DSA) scattering mean free path
- Interplanetary transport parallel scattering mean free path
- Interplanetary transport ratio of perpendicular to parallel diffusion (for model runs with perpendicular transport)

#### Limitations and caveats:

- SPREADFAST is currently set up to run only for protons;

- The model assumes a source spectrum based on quiet-time suprathermal observations (no flare particles);
- Currently, only parallel interplanetary transport is implemented
- No lat/lon dependence of coronal DSA fluxes for interplanetary transport - to be implemented in next version;

#### Access to model output or forecasts:

Results for modeled historical events are available in the SPREADFAST catalog at <https://spreadfast.astro.bas.bg/catalog/>. The near-real time forecasting service is under development. It will be available at <https://spreadfast.astro.bas.bg/>

**Model validation:** Kozarev et al. (2022) modeled 62 events with the SPREADFAST model framework. The modeled time profiles were calculated for the geometric mean of the ERNE energy channels between 3 and 115 MeV and the ERNE pre-event background was added for better comparison with data. The modeled results were plotted on top of ERNE data for May 11, 2011, and were found to have good agreement. The event-integrated fluence was also compared. Similar plots for all 62 events are available in the SPREADFAST catalog.

Kozarev et al., 2022 presented correlation plots between the modeled and observed power-law indices of the fluence spectra as well as the modeled and observed onset times for all 62 events. The power law indices showed significant scatter, but clustered around an index of  $-2.5$  for both SPREADFAST and ERNE. The onset times were strongly correlated for multiple energies, with the modeled times typically within  $\sim 5$  h of the observed onsets.

The paper reports that 2/3 of the modeled events showed good agreement with observations, but there was a discrepancy in the remaining events. It is hypothesized that this is likely due to the existence of additional seed population beyond the quiet-time suprathermal spectra, possibly from flare-accelerated protons.

#### 3.33. SPRINTS - Space Radiation Intelligence System

**Model developers:** Alec Engell (NextGen), Brianna Maze (NextGen), Harold Farmer (NextGen), Thuha Kerber (NextGen), Ben Barnett (NextGen), Jeremy Loomis (NextGen), David Falconer (University of Alabama Huntsville), Ian Richardson (University of Maryland/Goddard Space Flight Center (GSFC)), Maher Dayeh (SWRI), Barbara Thompson (GSFC), Tilaye Tadesse (JSC), Ian Fernandez (JSC, Princeton), Kerry Lee (JSC).

**Model description:** The Space Radiation Intelligence System (SPRINTS) is an empirical and machine-learned forecasting tool that is capable of giving forecasts for solar-driven events covering solar flares, solar particle events (SPEs), and coronal mass ejections (CMEs). SPRINTS uses and independently runs MAG4 (3.13) and extends MAG4 capabilities to make predictions of solar flares out to 48 h, with additional forecast probabilities of the GOES X-ray flare fluence and the peak flare ratio

of the long and short wavelength channels. SPRINTS combines the pre-eruptive forecast probabilities of MAG4 with SPRINTS post-eruptive forecast probabilities to provide continuously-updated and coupled forecast probabilities of SPEs as new phenomena and events are observed. It is designed as an extensible forecast application, where new datasets and new models can be integrated into the system's database and forecast modeling processes. The model currently runs automatically and in real-time on an Amazon Web Services GovCloud environment.

For its SPE primary forecast model, SPRINTS uses MAG4's X-ray flare forecast probabilities and feeds them into a user-defined ML model. The currently running ML model is the Multi-Layer Perceptron (MLP) model but has options to run other models including random forecasts and SVM. The MLP model is trained to predict SPEs at user-defined proton energy channels (e.g., 1, 5, 10, 30, 50, 100 MeV), fluxes, and time resolution (e.g., 12-h) out to 96 h.

To train the SPRINTS models, the data first needed to be labeled. Flare-only events were all labeled as a "zero", while the flare events that led to an SPE were labeled as a "one". The labeling was done per the desired temporal resolution, i.e., if the SPE occurred in the first 24 h after the flare onset, the 24-h bin was labeled as a one, while all other temporal resolutions were labeled as a zero.

As expected, the labeled data was unbalanced and heavily weighted towards flare-only events. For example, the maximum number of flares with SPEs was 152 for the proton events reaching 10 pfu at 50 MeV in a 96-h bin, whereas the number of flare-only events was 19,959. Because the problem of detecting SPEs suffers from the issue of unbalanced data, the selection of the training data is important to ensure the accuracy of the models.

To select the training data, the flares were first subsampled down to only include those flares with an SPE fluence above the minimum threshold for SPEs. This left 10,084 flare-only events. It was also empirically found that a 1 to 3 ratio of SPE to flare events resulted in the best models. For training the models, the SPEs were up sampled to a 1 to 3 ratio. The models were then trained through cross-validation using 4-folds. Results are reported for all flare and SPEs within the catalog.

Prior to an eruption of a flare, SPRINTS takes the MAG4 flare probabilities and feeds them into the MLP model where it then provides the probabilities of the user defined SPEs. As a flare is detected, the forecast transitions from the pre-eruptive forecast mode to the post- (or ongoing) eruptive mode. The flare metadata parameters are captured on-the-fly throughout the course of the flare and feed into the model every 5 min. Once the flare has ended, those parameters are "locked" in and the post-eruptive forecast is final. SPRINTS provides the pre-eruptive (MAG4), post-eruptive, and coupled forecasts through its REST API.

**Inputs:** SPRINTS ingests everything MAG4 needs and GOES X-ray and proton data. An automatic flare event

detection script [Aschwanden and Freeland \(2012\)](#) identifies flare start, peak, and end times. SPE predictions are made by the MLP model based on the metadata from the MAG4 predicted or observed X-ray flare events (peak flux, fluence, peak ratio) and eruptive location provided by the Latest Events Pipeline from Lockheed Martin Solar and Astrophysics Laboratory (LMSAL) or, optionally, NOAA SWPC.

#### Outputs:

- Pre-eruptive (updated MAG4)
  - M- and X-Class Flares (24 and 48 h)
  - X-class Flares (24 and 48 h)
  - X-ray fluences (24 and 48 h)
  - X-ray peak ratio (24 and 48 h)
  - CMEs (24 and 48 h)
  - Fast CMEs (24 and 48 h)
- Post-eruptive and coupled
  - SPEs (96 h at 12-h temporal resolution)
  - \* Currently deployed in real-time for: 10 MeV @ 10 pfu, 10 @ 40, 30 @ 10, 50 @ 10, 100 @ 1
  - \* Configurable to any desired GOES energy channel and flux threshold

**Free parameters:** None.

**Limitations and caveats:** [Fig. 16](#) shows the SPRINTS primary forecast dashboard. X-ray, proton, and solar wind observations are displayed for the past 8 days with 4-day forecast panels directly to the right. For the observed SPE for this time-period you can see what the forecast probabilities were for the five SPE criteria at a 12-h resolution out to 96 h from the peak of the flare.

We note that the red forecast bar in the first 12-h bin is for the 30 MeV channel at 10 pfu and is a higher probability than the 10 MeV channel at 10 pfu. This is because the forecast capability is comprised of multiple MLP models – one for each temporal bin and energy/flux. Therefore, this results in 20 MLP independent models.

As with many ML models the unbalanced nature of the number of flares to SPEs leads to problems during the training of the model. The SPRINTS team is currently developing a time-series ML model to address this issue.

For the forecast example shown for the May 2012 event, the flare occurred close to the western limb. This was well outside of MAG4's optimal active region observation window of 45 heliocentric degrees. This highlights the benefit of combining the MAG4 pre-eruptive capability with a post-eruptive capability within SPRINTS.

**Access to model output or forecasts:** Access to model outputs and supporting dashboards can be obtained by becoming IP whitelisted to NextGen's REST API. Email [aengell@nextgenfed.com](mailto:aengell@nextgenfed.com) to be whitelisted. NextGen is currently deploying the real-time dashboard on a public website and will be available in 2022. Additionally, SPRINTS will be providing forecasts on the SEP Scoreboard.

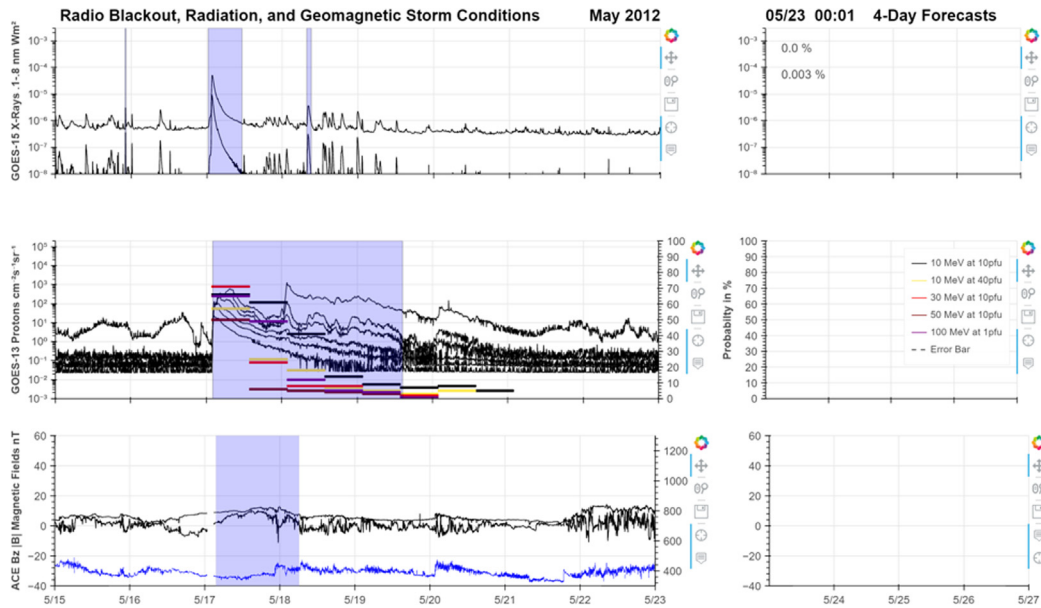


Fig. 16. SPRINTS SPE post-eruptive probabilistic forecasts displayed on top of proton observations. MAG4 flare X and M + X forecast probabilities are displayed.

**Model validation:** Model validation has been performed on the post-eruptive modeling capabilities of SPRINTS. Fig. 17 shows the POD, FAR, and HSS results for 24 h temporal bins. SPRINTS is under consideration for inclusion in a comparative evaluation of several SEP forecasting models being performed by the Air Force Institute of Technology. SPRINTS model validation is a straight-forward process that is baked into model development and deployment cycle.

SPRINTS collaborative JupyterHub environment provides executable code to evaluators and supportive dashboards such the one shown in Fig. 16. Parallel coordinates, 4D plots, and scatterplot matrices are among the plotting tools to support SEP event occurrence and ML modeling understanding.

### 3.34. STAT - Solar Particle Event (SPE) Threat Assessment Tool

**Model developers:** Jon Linker, Ron Caplan, Cooper Downs, Tibor Török, Roberto Lionello, Viacheslav Titov, Erika Palmerio (Predictive Science Inc.).

Nathan Schwadron, Matthew Gorby, Matthew Young (University of New Hampshire).

**Model description:** The SPE Threat Assessment Tool (STAT) (Linker et al., 2019; Young et al., 2021) is developed by Predictive Science Inc (PSI) and University of New Hampshire. STAT combines the Energetic Particle Radiation Environment Module (EPREM, a component of EMMREM Schwadron et al. (2010)) with the Magnetohydrodynamic Algorithm outside a Sphere (MAS, a component of CORona-HELiosphere (CORHEL), Riley et al. (2012)). STAT utilizes precomputed MAS simulations of CMEs to simulate SEP events

and provide diagnostics that can be compared with observations.

MAS is an MHD model that simulates the structure of the plasma in the corona and inner heliosphere. It handles the background corona conditions, CME formation, and CME eruption. MAS integrates the standard viscous and resistive one-fluid MHD equations in 3D spherical coordinates. It solves the thermodynamic MHD equations which extend the standard equations by including terms for thermal conduction, radiative losses, and coronal heating (Lionello et al., 2009; Mikić et al., 2018). In this approach, the plasma density and temperature at the lower boundary are chosen to be uniform and roughly consistent with the upper chromosphere, and the coronal heating specification determines the properties (density, temperature, velocity) of the simulated coronal and solar wind plasma. The coronal heating can either be empirical (Lionello et al., 2009), or based on a Wave-Turbulence Driven model (Downs et al., Dec. 2016).

EPREM (see Section 3.7) is a 3D kinetic model that simulates particle transport anywhere in the heliosphere. It uses a Lagrangian grid scheme such that the nodes where information is stored move with the plasma. EPREM solves the FTE which describes how the distribution of particles changes with time and includes terms for convection, parallel diffusion, adiabatic focusing, adiabatic cooling, and pitch-angle scattering. There is a separate module within EPREM that solves for perpendicular diffusion and particle drift.

STAT starts with a global magnetic map of the sun's radial magnetic field derived from magnetogram observations. The majority of grid cells are concentrated within the AR of interest, which may incorporate a higher resolution vector or LOS magnetogram. The areas around the

AFRL req.	HSS	POD	FAR
10@10	0.58	0.56	0.34
10@40	0.73	0.59	0.00
30@10	0.66	0.56	0.17
50@10	0.80	0.67	0.00
100@1	0.89	0.80	0.00

Fig. 17. Table of SPRINTS validation results.

poles, where no measurements exist or are not reliable, are fitted in the magnetic map using an extrapolation technique (Linker et al., 2013) or using the polar filling provided by observatories (e.g., Sun et al., 2011). The data is interpolated onto the non-uniform numerical grid of the lower boundary using an integral (flux) preserving interpolation scheme, and smoothed to the grid resolution (Linker et al., 2017).

To create the coronal and solar wind background, the thermodynamic MHD equations are solved on a non-uniform spherical mesh that ranges from 1 solar radii to 20–30 solar radii, until the solar wind has fully opened up the field associated with coronal holes, resulting in a steady-state MHD solution. The coronal heating specification is chosen to give a reasonable match to the observed EUV and SXR emission.

To initiate the CME, a stable magnetic flux rope is constructed along the AR's Polarity Inversion Line (PIL) and inserted into the global thermodynamic MHD solution in a way that the original magnetogram is preserved. In practice, the configuration is first relaxed toward a force-free state using a zero-beta MHD solution prior to insertion. Török et al. (2018) described the use of multiple, modified Titov-Démoulin (TDm) flux ropes (Titov et al., 2014) to model the July 14, 2000 flare/CME. In that case, the eruption was triggered by imposing small photospheric flows that canceled flux at the PIL, resulting in a slow rise and successive detachment of the flux rope until it became unstable and erupted. More recent examples use the Regularized Biot-Savart Laws (RBSL) flux rope model (Titov et al., 2018), that preserves the magnetogram flux by construction. The eruption can also be initiated by setting the axial flux of the rope slightly above the stable value, leading to a similar eruptive sequence.

Particle transport and particle energization is handled within STAT by EPREM. To begin, a seed population using a differential flux that scales as a power law in energy with an exponential roll-over is assumed. This injected spectrum is converted into a distribution function and acts

as the source term in the FTE. EPREM's grid nodes spawn on a rotating inner boundary at the surface of the sun. The nodes are then convected out with the solar wind. As the sun rotates, the nodes naturally make a Parker spiral configuration. The structure of the CME and subsequent effects on the IMF push the nodes around according to the MHD equations solved within MAS.

At each time-step within EPREM, the model solves the FTE which describes how the distribution of particles changes with time. The FTE includes terms for convection, parallel diffusion, adiabatic focusing, adiabatic cooling and heating, and pitch-angle scattering. There is a separate module within EPREM that solves for perpendicular diffusion and particle drift; these terms were turned off for the events that have been delivered to CCMC. Each node contains information about the proton flux at the location of the node and its time-history. The user can select a node near Earth or other locations of interest to access the proton flux time-profile.

The STAT model aims to reproduce the complete set of physics governing the coronal eruption and the acceleration and transport of energetic particles. This model is well-suited to testing and improving our understanding of the critical physics associated with the production and distribution of solar energetic particles.

#### Inputs:

- Global magnetic map, either an observatory synoptic map or from a flux transport model
- Coronal heating specification, parameters chosen to specify flux rope and CME eruption
- Seed population, parallel mean free path, perpendicular diffusion

#### Outputs:

- Differential fluxes on a fine energy grid at any node
- >10, >50, and >100 MeV integral proton flux time profile at any node.

## March 7, 2012 Particle Simulation with Focused Transport

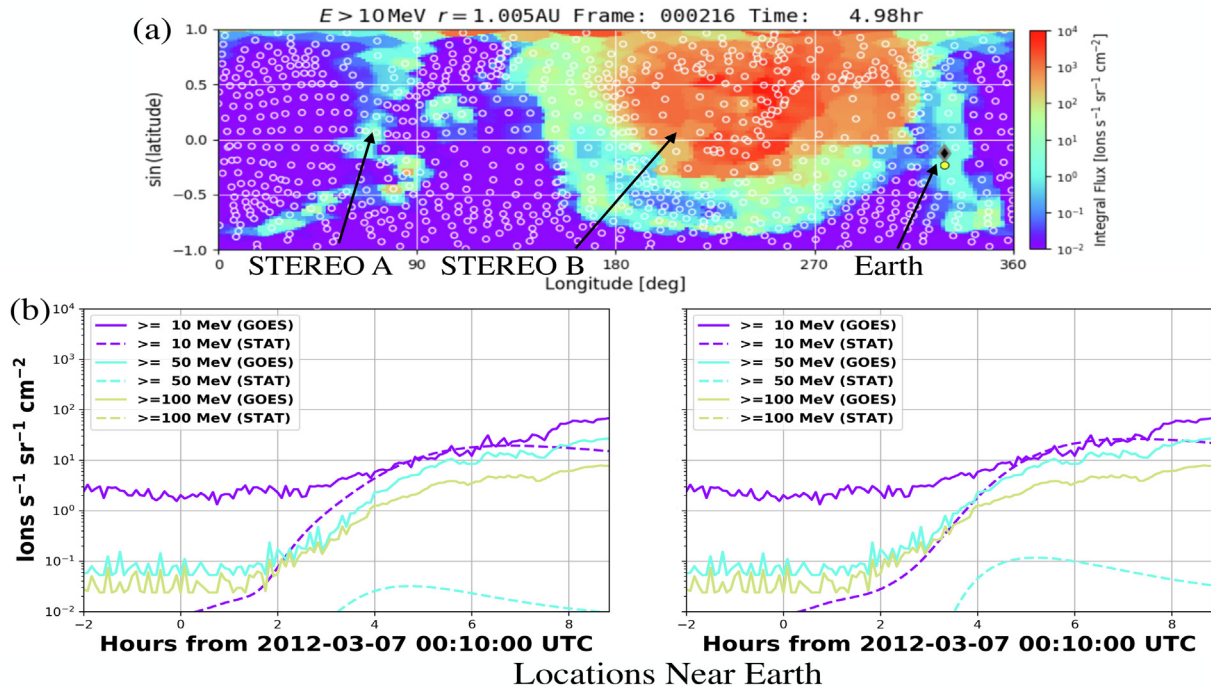


Fig. 18. STAT simulation of the March 7, 2012 CME/SEP event, showing particles widely distributed in longitude. (a) Integrated proton flux  $>10$  MeV as a function of longitude and sine(latitude) at 1 AU. This is a standard output visualization from STAT. The circles indicate the location of EPREM nodes where the calculation is performed. The locations of the two STEREO spacecraft and Earth are shown. (b) Comparison of  $>10$  MeV integrated proton flux with GOES.

- Animated map in longitude and sin(latitude) of  $>10$ ,  $>50$ , or  $>100$  MeV integral proton flux using all nodes at the coronal boundary and at 1 AU.
- Animated map in radius and longitude (slice of the ecliptic plane) of  $>10$ ,  $>50$ , or  $>100$  MeV integral proton flux using all nodes from the sun out to the coronal boundary or 1 AU.

Fig. 18 shows model output for the March 7, 2012 CME, a strong event that produced SEPs that were measured at multiple locations in the heliosphere (Kouloumvakos et al., 2016). Fig. 18(a) shows the  $>10$  MeV integrated proton flux as a function of longitude and latitude at 1 AU. Fig. 18(b) shows a comparison to GOES data for the event.

**Free parameters (MHD):** coronal heating specification, flux rope specification.

**Free parameters (FTE):** Seed population spectral shape and normalization, parallel mean free path, perpendicular diffusion.

**Limitations and caveats:** In terms of forecasting, STAT is a computationally intensive physics model that at present does not run in real time. To use STAT in an operational environment, it may be feasible to follow the approach of other physics-based models, such as SPARX (Section 3.31), and create a database of pre-run historical SEP events that can be accessed to generate a forecast.

At the time of writing, CME propagation within STAT is limited to the boundary of the coronal domain at  $20\text{--}30 R_{\odot}$ . Once the CME has left this domain, particle acceleration from CME propagation in the heliosphere is not modeled, restricting the simulation to only the first few hours of the SEP event (Young et al., 2021).

**Access to model output or forecasts:** STAT may be run on demand using CCMC's runs-on-request system. Some pre-run model simulations produced by PSI are available at <https://ccmc.gsfc.nasa.gov/ISEP/>.

**Model validation:** Young et al. (2021) presented a simulation of the 14 July 2000 Bastille Day event compared to measured GOES-08 fluxes. The comparison included both nominal GOES-08 data provided by NOAA and corrected fluxes produced using recalibrated GOES-08 energy bins derived by Sandberg et al. (2014).

### 3.35. UMASEP - University of Malaga Solar Energetic Particles

**Model developers:** Marlon Nunez (University of Malaga).

**Model description:** The University of Malaga Solar Energetic Particles (UMASEP) models are an empirical suite of tools comprised of multiple independent modules predicting different particle energy ranges: UMASEP-10 (Núñez, 2011) predicts  $>10$  MeV SEP events; UMASEP-

100 (Núñez, 2015) predicts >100 MeV events; and UMASEP-500 (Núñez et al., 2017) predicts the occurrence of a GLE. UMASEP-500 was developed in collaboration with the European Unions's HESPERIA project, which also includes the RELEASE code (Section 3.21). Two additional modules, UMASEP-30 and UMASEP-50, have recently been developed to forecast >30 and >50 MeV events. All model versions use similar underlying algorithms; however, the implementation differs.

The preliminary forecast functionality of UMASEP-10 was originally divided into the Well-Connected (WC) and Poorly-Connected (PC) modules. The WC module assesses the relationship between the time series GOES SXR (X-ray emissions) and an increase in GOES differential proton flux to determine if particles have escaped along the IMF field lines. The PC module, unique to the UMASEP-10 version, compares the characteristics of the current event to similar historical events to determine if it is more likely to surpass the SPE threshold or return to background. The PC module is intended to detect an event when there is no magnetic connection between the parent event and the observer. The preliminary warnings from both the WC and PC modules are passed to the Analysis and Inference module with preference assigned to the WC module; if this preliminary result is accepted, an alert is issued. UMASEP-10 has recently been updated to include the University of Malaga predictor from Solar Data (UMASOD) model, which incorporates radio data (Zucca et al., 2017; Núñez and Paul-Pena, 2020) to enhance the model's ability to provide advance warning of an SEP event.

UMASEP-100 performs in a similar manner to the WC module, but uses a derived instead of real-value time series. The updated algorithm performs a bit-based transformation of the X-ray flux and the GOES differential proton channels P6 to P11, with a focus on strong positive derivatives (1 vs 0). The newer UMASEP-30 and UMASEP-50 modules were developed based on a similar theory as the original UMASEP-10 and UMASEP-100.

UMASEP-500 is very similar to the UMASEP-100 method, with appropriate changes in the model parameters and boundary conditions. For the model developer's work with the HESPERIA/HORIZON 2020 project, the focus of the work transitioned to GLEs to complement the GLE Alert Plus Tool (Souvatoglou et al., 2014). For this version, the model developer has also considered replacing the SXR data input stream with microwave flux density

(Hard X-ray (HXR)); however, this functionality is not available real-time.

**Inputs:** All data streams available from NOAA/SWPC:

- GOES SXR
- GOES differential proton flux
- Radio burst data (UMASOD only) from the USAF RSTN

**Outputs:** Viewer displays real-time forecast, including.

- Observed integral proton flux
- Forecasted integral proton flux
- All-clear period (if applicable)
- Observed X-ray flux
- Magnetic connectivity estimation (proportion representing low/medium/high)
- Real-time forecast
- Model inferences in real-time (includes AR information, if available, from SWPC database)
- Early SEP event fluence projection

**Free parameters:** None.

**Limitations and caveats:** Since the WC UMASEP module algorithm emphasizes connectivity, it is unable to predict behind-limb events. As the PC module only analyzes the evolution of in situ protons, this module is able to predict this type of event. Additionally, to limit false alarms, a flare intensity threshold is integrated into each model version; below this threshold, UMASEP does not run. It is also important for the user to understand that the event intensity provided by the model is intended to be the maximum value during the initial 'x' hours of an event, where 'x' varies by model variation.

**Access to model output or forecasts:** Real-time SEP predictions from UMASEP-10, UMASEP-30, UMASEP-50, UMASEP-100 and UMASEP-500 are available on the SEP Scoreboard (<https://sep.ccmc.gsfc.nasa.gov/intensity/>) and the ISWA interface hosted by CCMC. UMASEP-10 outputs are also available from the University of Malaga. UMASEP-500 outputs are available through the HESPERIA collaboration.

**Model validation:** The model developer used events from SC23 and 24 to validate the results of UMASEP-100 and UMASEP-500; a recent publication detailing updates to UMASEP-10 incorporates solar cycle 22 as well (Table 9). For the UMASEP-10 WC module and the UMASEP-100

Table 9

Validation of UMASEP model as performed by developer. UMASEP-10 was validated for predicting all >10 MeV SEP events from 1996 to 2017. UMASEP-100 was validated for predicting all >100 MeV SEP events from 1994 to 2013. UMASEP-500 was validated for predicting all GLE events from 2000 to 2016. POD = Probability of Detection; FAR = False Alarm Rate; AWT = Average Warning Time.

	UMASEP-10 (Núñez, 2022)	UMASEP-100 (Núñez, 2015)	UMASEP-500 (Núñez et al., 2017)
<b>POD (%)</b>	82.16	80.85	53.8
<b>FAR (%)</b>	21.52	29.62	30.0
<b>AWT (hh:mm)</b>	03:15	01:06	00:08

variation, the POD was incremented and the FAR was minimized by optimizing parameters to maximize forecasting performance (Davis and Goadrich, 2006):

$$w_{precision} * Precision + w_{recall} * Recall \quad (19)$$

where  $Recall = POD$  and  $Precision = 1 - FAR$ .  $w_{precision}$  and  $w_{recall}$  are weights that are set at 0.5 to give both calculations equal priority. For the UMASEP-10 PC variation, the weights (contributions, or “votes”) of the individual model trees were selected to maximize Precision and Recall, as defined above. The Analysis and Interference Module then selected the thresholds  $\tau_1$  and  $\tau_2$ , representing temporal limits of the event, to maximize forecasting performance as defined above. For the UMASEP-500 variation, a successful forecast was defined as whether the model alert preceded neutron monitor alert. A low POD indicated no sign of proton enhancement before neutron monitor alert. The HESPERIA UMASEP-500 tool makes real-time predictions of the occurrence of >500 MeV and GLE events from the analysis of soft X-ray flux and high-energy differential proton flux measured by the GOES satellite network. Regarding the prediction of GLE events for the period 2000–2016, this tool had a POD of 53.8% and a FAR of 30.0%. For this period, the tool obtained an Average Warning Time (AWT) of 8 min taking as reference the alert time from the first neutron monitor station; using the time of the warning issued by the GLE Alert Plus tool for the aforementioned period as reference, the tool obtained an AWT of 15 min.

### 3.36. Zhang Model

**Model developers:** Ming Zhang (Florida Institute of Technology).

**Model description:** The Zhang model is a physics-based SEP model taking a focused transport approach to predicting SEP events. In Zhang and Zhao (2017), the developers use a PFSS model to set up the coronal magnetic field, where NSO GONG’s spherical harmonic coefficients are fit to photospheric magnetogram measurements. The model uses the first available coefficient post-eruption, since CMEs can significantly alter the coronal magnetic field configuration. Above the source surface ( $R_{ss} > 2.5R_s$ ), the solar wind speed and density is modelled after Leblanc et al. (1998) and the magnetic field in the solar wind is a Parker spiral. These become initial conditions to constrain the solution to the transport side of the model. The FTE is a 3-D time-dependent equation with terms for pitch-angle diffusion, magnetic focusing, adiabatic cooling and pitch angle change, particle streaming, perpendicular diffusion, convection with the solar wind, particle drift via gradient and curvature drifts, and particle injection rate. Perpendicular diffusion is modelled after the random walk of field lines, and contributes to the longitudinal spread of particles. From the model developer’s studies, see Zhang and Zhao (2017), Zhao et al. (2020), the value for the perpendicular diffusion can change event-

by-event, but a typical value is  $\sim 10\%$  of the supergranular diffusion rate. The pitch angle diffusion coefficient takes a form from quasi-linear theory, where some nonlinear corrections have been made. Since perpendicular diffusion is included, the FTE becomes a time-dependent parabolic partial differential equation in 5-D phase space that can be solved via a Stochastic Differential Equation (SDE). This model can solve the SDE either in a time-forwards or time-backwards scheme, dependent upon whichever one minimizes computation time.

#### Inputs:

- solar wind speed
- perpendicular diffusion coefficient
- outer boundary (50 AU)
- particle injection profile
- particle mean free path
- For PFSS: spherical harmonic coefficients derived from synoptic magnetograms

#### Outputs:

- Time intensity profile
- SEP distributions

**Free Parameters:** None.

**Limitations and caveats:** Since this model takes advantage of the PFSS, it’s coronal modelling starts deeper down to the solar surface within the corona than other similar models; this also contributes to how accurately the model can capture the magnetic connection to the source location within the corona. However, this comes with the downsides of PFSS, where small scale structures are not modelled well, which shouldn’t affect the overall predictive qualities of the Zhang model as particle transport is not greatly affected by those structures (Zhao and Zhang, 2018).

**Access to model output or forecasts:** There is currently no public access to model output.

**Model validation:** This model has been use for singular events as a research model (see Zhang and Zhao, 2017; Zhao and Zhang, 2018; Zhao et al., 2020 for the most recent case studies). Many of these studies involve looking at particle distributions in the corona and other underlying physics, not comparisons to observations - so no validation studies have been published.

## 4. Conclusions

This paper has summarized the current SEP models produced by the scientific community. Section 3 describes a wide range of models that have been developed for various purposes, often not specifically for SEP prediction, and are in different stages of maturity. Some well-established SEP models are actively providing forecasts in real time in support of operations while others, such as ML models, are pursuing new approaches as a proof of concept. Physics-based SEP models are increasing in sophistication and



Table 10  
Observational measurements used as inputs into SEP models.

Model	Type	Magnetograms	Optical Imaging	EUV Imaging	Soft X-ray Intensity	Ground-based Radio	Space-based Radio	Coronagraph	Solar Wind (n,T,p,v)	Suprathermal Particles	Energetic Protons	Energetic Electrons	Neutron Monitors
ADEPT	Empirical										x		
AFRL PPS	Empirical		x		x	x							
Aminalragia-Giamini model	ML			x	x								
AMPS	Physics-based	x		x				x					
Boubrahimi model	ML				x						x		
COMSEP SEPForecast	Emp. & Physics			x	x			x					x
EPREM	Physics-based	x		x				x		x			
ESPERTA	Emp. & ML			x	x		x				x		
FORSPEF	Empirical	x	x		x		x	x					
GSU	ML	x											
iPATH	Physics-based	x		x				x	x	x			
Lavasa Model	ML		x		x			x					
MAG4	Empirical	x	x		x								
MagPy	Empirical	x	x		x								
MEMPSEP	ML	x		x	x		x	x	x	x	x	x	
M-FLAMPA	Physics-based	x		x				x					
PARADISE	Physics-based	x		x				x					
PCA model	Empirical				x			x					
PHSVM	ML				x						x		
PROTONS	Empirical				x	x							
REleASE	Empirical											x	
Sadykov's Model	ML	x			x	x					x		
SAWS-ASPECS	Empirical	x	x		x			x			x	x	x
SEPCaster	Physics-based	x		x				x	x				
SEPMOD	Physics-based	x		x				x					
SEPSTER	Empirical			x				x	x				
SEPSTER2D	Empirical			x				x	x				
SMARP Model	ML	x											
SOLPENCO	Physics-based			x				x					
SOLPENCO(2)	Physics-based			x				x	x		x		
South African model	Physics-based			x	x			x					
SPARX	Physics-based			x	x								
SPREAdFAST	Physics-based	x		x				x		x	x		
SPRINTS	ML	x		x	x						x		
STAT	Physics-based	x		x				x		x			
UMASEP	Empirical				x	x					x		
Zhang model	Physics-based	x		x				x	x				
<b>Total</b>		19	6	21	19	4	3	21	7	5	11	3	2

aim to partially or fully model the heliophysics system, coupling coronal, heliospheric, and particle acceleration/transport models together. The model summaries explicitly identify the observational inputs for each model, demonstrating the range of critical observational infrastructure that is required for effective SEP forecasting. Models generally have limitations as well as caveats that should be understood to accurately interpret model output. Finally,

model validation efforts are summarized in order to understand the current state of the art of SEP model performance as well as to emphasize that all models and model types can benefit from thorough, quantitative validation.

In the remaining sections, we will draw conclusions from this comprehensive look at the current state of SEP modeling. We will highlight the critical measurements used by models, describe forecasting coverage and identify any

gaps, highlight models already running in real time, and discuss what is needed to ensure all models are appropriately validated.

#### 4.1. Critical measurements

In Table 10, the observations required for input into each model are specified. The bottom row shows the total number of models that use each kind of observation. For models that ingest CME parameters produced by forecasters or extracted from a database, we specify the observations required to produce these parameters. CME parameters are derived using as many coronagraph vantage points as possible, as well as EUV imagery from the SDO or STEREO to view the eruption source region (Millward et al., 2013). For models that use output from another model to run, we identify the observations required as input into the first model in the chain. Physics-based models often run on top of MHD solar wind models with propagating CMEs (e.g. WSA-ENLIL + Cone and SEPMod, MAS + CORHEL and EPREM, AWSOM + EEGGL and MFLAMPA) and these require magnetograms and CME parameters as input. Some models ingest and report NOAA AR information, which is derived from the SOON<sup>20</sup> by the USAF (Robert Steenburg, NOAA/SWPC forecaster, private communication). H-alpha imagery from SOON is also used to identify solar flare locations. Databases such as the Solar DEMON derive solar flare location from real time EUV imagery from SDO. Other flare databases, such as Hinode/EUV Imaging Spectrometer (EIS)<sup>21</sup> provide flare locations derived from X-ray imagery, which are valuable for model training but are not available as real time inputs. The GOES-R XRS product on the NOAA website<sup>22</sup> provides flare location from the XRS quad diodes (Machol et al., 2021). Until recently, this location product was not available in real time. For the models described in this paper, flare locations are derived in real time from H-alpha or EUV imagery, however the GOES XRS locations services may provide an alternative now that they are available.

Table 10 clearly demonstrates the heavy current utilization of magnetograms, EUV imaging, coronagraph observations and energetic particle observations for SEP prediction. *Therefore, we emphasize that such data streams must be supported operationally to ensure that SEP models can be used for forecasting – this includes the continuity of existing data streams and development of new ones to enhance or replace them.* However, it should be noted that those observations that are less widely used also provide valuable inputs into SEP prediction and should also be supported operationally. In particular, neutron monitors provide *confirmation* of the onset of an extremely high-

energy SEP event (e.g., He and Rodriguez, 2018), while energetic electrons provide *direct observational* forewarning of an SEP event (Posner, 2007). Also, currently only a few models are listed as using suprathermal ions as input, but continuing research into characterizing suprathermal ions would also benefit other physics-based models that need to specify a “seed spectrum” as a starting point for acceleration at shocks. The limited use of space-based radio emissions reflects the fact that such observations are not currently available in near-real time, notwithstanding their demonstrated strong association with historical SEP events (e.g., Gopalswamy et al., 2005; Cane et al., 2002; Winter and Ledbetter, 2015; Miteva et al., 2017). There is a tendency for radio emission to be weak or absent when a solar event is not accompanied by a significant SEP event (e.g., Richardson et al., 2018; Lario et al., 2020) and therefore, the presence of strong radio emission has been included as a predictor in some SEP models (e.g., Laurenza et al., 2009; Richardson et al., 2018). As described in Section 2.1, critical radio frequencies are not accessible from the ground, which argues in favor of operational space-based, near-real time, solar radio monitoring capability.

Finally, observations of the type that are most widely utilized for SEP prediction along the Sun-Earth line would have greatly enhanced value if obtained from the L4 Lagrange point, where the observed central meridian lies at W60° (Posner et al., 2021). Magnetograms, EUV imagery, coronagraph images, and in situ particles and fields measurements from this vantage point would cover locations on the Sun with the highest degree of magnetic connectivity to the Earth-Moon system and points along minimum-energy transfer (Hohmann) orbits to Mars. SEP events from these well-connected source locations have the highest potential impact, thus posing the largest risk for human radiation and space hardware concerns. This includes locations that are beyond the Earth-Sun west limb that our present set of observatories do not cover, therefore limiting our ability to produce a complete All Clear forecast.

#### 4.2. Model coverage for SEP forecasting

In operations, space weather forecasters are asked to answer the following questions:

- Will there be an SEP event (or can an All Clear be issued)?
- When will it occur?
- How intense will it be?
- How long will it last?

Table 11 identifies the predicted quantities output by the models discussed in this paper and whether each model produces output before (“Pre”) a flare or CME or after (“Post”) the eruptive event. The specific meaning of each field is indicated in the table caption. Most are self-explanatory, but “Flux Point” indicates that a model pre-

<sup>20</sup> [https://www.wbdg.org/FFC/AF/AFMAN/149XX5\\_Solar\\_Observing\\_Optical\\_Network1.pdf](https://www.wbdg.org/FFC/AF/AFMAN/149XX5_Solar_Observing_Optical_Network1.pdf).

<sup>21</sup> <http://solarb.mssl.ucl.ac.uk/SolarB/eisflare2017.jsp>.

<sup>22</sup> <https://www.ngdc.noaa.gov/stp/satellite/goes-r.html>.

Table 11

Outputs produced by the SEP models summarized in this paper. Pre/Post: Pre indicates pre-eruptive forecast prior to the flare or CME, Post indicates a forecast issued after an eruptive event (flare, CME) has occurred; All Clear: binary yes/no forecast for an SEP event or specific threshold crossing; Probability: probability of occurrence; Flux Point: forecast of proton intensity levels for a single time point or a single flux value within a specific time window in the future (see main text for further description); Onset time: time of threshold crossing or SEP event start; Peak: peak intensity; Peak time: time of the peak intensity; End time: event end time or decay time; Fluence: total event time-integrated fluence; Time profile: produces intensity with time; Multi loc.: capable of producing forecasts for multiple locations in the heliosphere; 3D: produces 3D environmental data and particle info, such as pitch angle distributions.

Model	Proton Energy [MeV]	Pre/Post	All Clear	Probability	Flux Point	Onset time	Peak	Peak time	End time	Fluence	Time profile	Multi loc.	3D
ADEPT	>10, >30, >50, >100	Post					x	x	x	x	x		
AFRL PPS	>5, >10, >50	Post				x	x	x	x	x	x		
Aminalragia-Giamini model	≥5	Post	x	x									
AMPS	eV to GeV	Post				x	x	x	x	x	x	x	x
Boubrahimi model	>100	Post	x										
COMESSEP SEPFforecast	>10, >60	Post		x		x	x	x	x				
EPREM	5 - 1000**	Post				x	x	x	x	x	x	x	x
ESPERTA	>10	Post	x										
FORSPEF	>10, >30, >60, >100	Pre/Post		x		x	x	x	x	x			
GSU	>10	Pre	x	x									
iPATH	100 keV - GeV	Post	x			x	x	x	x	x	x	x	x
Lavasa Model	>10	Pre	x										
MAG4	>10	Pre	x	x									
MagPy	>10, >100	Pre	x	x									
MEMPSEP	9-15, >5, >10, >30, >60, >100	Post		x		x	x	x	x	x			
M-FLAMPA	10 keV - 1 GeV	Post				x	x	x	x	x	x	x	x
PARADISE	keV - GeV	Post				x	x	x	x	x	x	x	x
PCA model	>10	Post		x									
PHSVM	>100	Post	x										
PROTONS	>10	Post		x			x	x					
REleASE	4-9; 9-15.8; 15.8-39.8; 28.2-50.1	Post		x	x								
Sadykov et al.	>10	Pre	x	x									
SAWS-ASPECS	>10 to >300	Pre/Post	x	x		x	x	x	x	x	x		
SEPCaster	100 keV - GeV	Post	x			x	x	x	x	x	x	x	x
SEPMOD	1 - 1000	Post					x	x	x		x	x	x
SEPSTER	14 - 24; >10, >30, >50, >100	Post					x	x				x	
SEPSTER2D	10 - 130; >130	Post					x	x	x	x		x	
SMARP Model	>10	Pre	x	x									
SOLPENCO(2)	0.125 - 64; 5 - 300	Post				x	x	x		x	x	x	
South African model	keV - GeV	Post				x	x	x	x	x	x	x	x
SPARX	>10, >60, >300	Post				x	x	x	x	x	x	x	x
SPREAdFAST	2 - 115	Post				x	x	x			x	x	x
SPRINTS	1, 5, 10, 30, 50, 100	Pre/Post	x	x									
STAT	1 - 1000	Post				x	x	x			x	x	x
UMASEP	>10, >30, >50, >100, >500	Post	x		x	x	x	x		x			
Zhang model	MeV - GeV	Post				x	x	x	x	x	x	x	x

dicts the particle flux for a specific time or time range into the future. For example, UMASEP forecasts the maximum flux in the next 3 to 24 h (depending on energy channel and magnetic connectivity) and this forecasted flux value may not necessarily correspond to the peak flux, which could occur outside of the time window for very gradual events. RELEASE forecasts the differential proton intensity 30,

60, or 90 min in the future. The “3D” label indicates that a wide range of information calculated by many physics-based models describing the energetic particle distributions and magnetic field environment in 3-dimensional space, such as pitch-angle distributions and magnetic field line locations, is provided. If a model outputs a time profile, then it is indicated that the model predicts onset time, peak

flux and time, end time, and fluence as applicable. There are some time profile models that cannot currently simulate the full duration of the event and for these, only the predictions that are possible to derive from their time profiles are indicated.

It is important to consider whether the model outputs together can answer all the above questions or if there are clear gaps in our current capabilities. All 35 models generate predictions for protons in the  $\sim 10$  MeV energy range. This is not surprising as the NOAA definition of an SEP event is  $>10$  MeV proton flux exceeds 10 pfu, and modelers have focused on providing predictions that are consistent with this definition. In terms of human space exploration,  $>10$  MeV particles pose a danger for astronauts outside of a vehicle during an EVA in space or on the lunar surface. Higher energy particles that can penetrate spacecraft shielding are a danger for astronauts throughout a mission, particularly exploration missions outside of Low-Earth Orbit (LEO). SRAG at NASA/JSC applies a threshold of  $>100$  MeV proton flux exceeding 1 pfu to indicate when the particle environment is of concern. About half of the models provide predictions in that energy range, but many of those are physics-based models that face challenges in running in real time. Developing (and validating) empirical and machine learning models to make high energy proton predictions is also a challenge since SEP events that reach such energies are relatively rare. From a space radiation operations perspective, Table 11 demonstrates a need to expand forecasting to higher energies, particularly by “fast and light” models that can produce results ahead of an eruption or quickly following an eruptive event.

Table 10 shows that many of the models rely on flare or CME information to make their predictions, thus it is not surprising that most models in Table 11 provide post-eruption forecasts. The models that do make a prediction ahead of an eruption typically provide an All Clear and/or probability of occurrence. These models rely on information derived from magnetograms and take empirical or machine learning approaches. Indeed, pre-eruptive forecasting capabilities may be an area where machine learning algorithms can make advances over more traditional empirical models. This will remain to be seen until the application of ML to space weather forecasting matures.

Table 10 also indicates the current limited use of energetic electrons as model input and identifies an opportunity for future models to take advantage of their potential to provide an early warning of a proton event or as an effective discriminator to reduce false alarms. The detection of energetic electrons may be particularly important for space exploration missions as external electron detectors could be mounted on board the vehicle to create an early warning system at the spacecraft. Posner et al. (2020) have shown that electron measurements at Earth-L1 and Mars-L1 used with the RELEASE forecasting system could provide advanced warning of proton events throughout most of a mission to Mars.

Overall, Table 11 shows that the models, taken as a whole, provide good coverage of all listed quantities with high redundancy that could be used to address the above forecaster questions. However, a major current restriction is that most of the model outputs are not available to forecasters in real time. In some cases, this is due to the latency in observations, e.g., coronagraph images of CMEs. In other cases, models are not yet robust enough to run continuously or cannot produce output faster than real time. Space agencies around the world have developed forecasting dashboards for individual or a small number of SEP models, but the opportunity remains to make use of the diverse set of models that exist within the research community. Increased Research-to Operations (R2O) efforts are needed to prepare and onboard SEP models into operational settings.

#### 4.3. Models running operationally or in real time

Significant effort is required to move a model from the development phase to running robustly in real time. Twelve of the SEP models discussed in this paper have undertaken these steps and are running in a real time or operational environment. Here, operational models are defined as those being served through the ESA Space Weather Service Network (<https://swe.ssa.esa.int/>) for its space weather users or utilized by the USAF or NOAA SWPC for space weather forecasting. These models have undergone a vetting process for robustness, stability, and performance by their respective operational agencies and have external users that monitor their forecasts for decision-making purposes. Five models satisfy these criteria: AFRL PPS, COMESEP<sup>23</sup>, PROTONS, REleASE, and UMASEP.

An additional seven models are defined as running in real time: FORSPEF<sup>24</sup>, MAG4, SAWS-ASPECS<sup>25</sup>, SEP-MOD, SEPSTER, SEPSTER2D, and SPRINTS. These models have done the key work to ensure stability and are deployed on public-facing environments, like the applications developed at CCMC. Model forecasts are monitored by users on an experimental basis.

The ESA Space Weather Service Network provides a dashboard of forecasts to support a wide variety of end-users in order to mitigate the effects of space weather on their systems (Kruglanski et al., 2016). The Network is organized around five Expert Service Centres that each have an individual focus on Solar Weather, Heliospheric Weather, Space Radiation Environment, Ionospheric Weather and Geomagnetic Conditions.

The USAF Space Weather Operations Center (SpWOC) is the only Department of Defense (DoD) unit delivering 24/7 space weather information for the Total Force,

<sup>23</sup> SPARX predictions are used in COMESEP forecasting in the form of a pre-run database.

<sup>24</sup> The PCA Model provides probabilistic forecasts within FORSPEF.

<sup>25</sup> SOLPENCO2 predictions are used in SAWS-ASPECS forecasting in the form of a pre-run database.

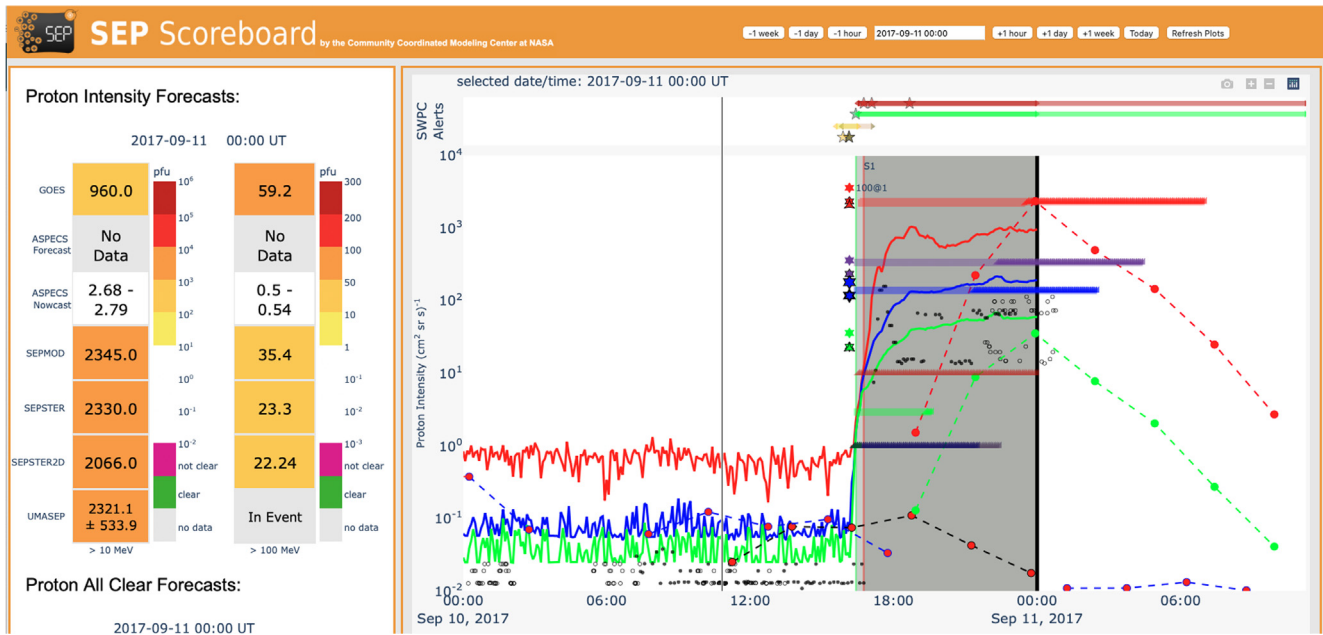


Fig. 19. The intensity SEP Scoreboard displaying forecasts for the 2017–09-10 SEP event. GOES proton measurements are shown as lines for  $>10$  MeV (red),  $>50$  MeV (blue), and  $>100$  MeV (green). Forecasts from SEPSTER (stars), SEPSTER2D (triangles), SEPMOD (circles with dashed lines), and UMASEP (horizontal bars) for the same energies are in corresponding colors. HESPERIA/RELeASE forecasts are shown as black circles. The heat map on the left displays the observed GOES flux values and the peak flux predictions for  $>10$  and  $>100$  MeV from the various models. The SWPC Alerts bar at the top shows warnings, alerts, and event summaries issued by SWPC for X-ray fluxes, radio bursts, and protons.

Defense, and Intelligence Community Agencies. They provide forecasts and tailored products at multiple classification levels through the Air Force Air Force Weather Enterprise (AFW-WEBS).

NOAA SWPC (<https://www.swpc.noaa.gov>) is a service center of the U.S. National Weather Service and provides official space weather forecasting services to industries in the United States and global users. SWPC's wide array of customers include the U.S. power grid, commercial airline industries, NASA, satellite operators, and others.

CCMC runs many of its models, including SEP models, continuously/real-time based on whether it is possible to do so and if the model is robust enough (<https://ccmc.gsfc.nasa.gov/tools/continuous-run/>). Real-time run outputs are primarily served via CCMC's integrated Space Weather Analysis (iSWA) web application which also displays space weather observations. All SEP models that are running in real-time at CCMC are available both via iSWA and the SEP Scoreboard (see Fig. 19). The SEP Scoreboard is one of many community-driven "Scoreboards" facilitated by the CCMC. Each scoreboard gathers, displays, and serves (via API) real-time forecasts in order to test the community's predictive capabilities before event onset. The SEP Scoreboard project (<https://ccmc.gsfc.nasa.gov/scoreboards/sep/>) began in 2016 as an international effort and started receiving input from SRAG in 2018 in support of upcoming human space exploration missions. The SEP scoreboard captures SEP onset, duration, peak flux, probability, all-clear, and overall profile within three separate web applications: probability heat map and time-series, intensity heat-map and time-series, and all-clear.

Current forecasting methods participating in the SEP Scoreboard include: SAWS-ASPECS, MAG4, RELeASE, SEPMOD, SEPSTER, SEPSTER2D, SPRINTS, SWPC, and UMASEP. The GSU and iPATH models are currently being onboarded. The time series plots also show relevant SWPC alerts and MLSO K-Cor automatic CME detections or CME all-clear. The SEP Scoreboard is being monitored by SRAG operators as a test-case ahead of NASA's planned Artemis missions to the Moon. Table 12 lists each of the operational or real time models, the year that they were first implemented, the location of the model forecasts, and the end users. The model implementation history was collected through personal communication with the model developers and historical literature.

About 1/3 of the models summarized in this paper have performed the required work to transition their models to systems external to their home institutions where they have been configured to run continuously and robustly, regardless of data outages, corrupted observations, or other complicating factors. Significant effort is required on the part of model developers and the staff at the hosting institutions to onboard the models. This type of work does not typically fall within the scope of traditional funding opportunities, however it is necessary and important work for models that demonstrate benefit in the context of forecasting. Many model developers in the research community have expressed interest in working towards implementing their models in real time and are in the very early stages of this process. This worthwhile effort will require support from the various institutions that hold stake in space weather forecasting.

Table 12  
SEP models that are running in operational and real time environments.

Operational Models			
Model	Date of Implementation	Location	End Users
AFRL PPS	1987 (as early as 1976)	USAF Space Weather Analysis and Forecast System (SWAFS)	USAF Space Weather Operations Center (SpWOC)
COMESSEP	2013 (real time), 2016 (operations)	<a href="#">ESA Space Weather Service Network</a>	ESA space weather stakeholders, PECASUS global center for aviation users
PROTONS	1998 (earlier version running from at least 1983)	NOAA SWPC	NOAA SWPC
HESPERIA REleASE	real time since 2008, operational since 2016	<a href="#">ESA Space Weather Service Network</a> , <a href="#">HESPERIA</a> , <a href="#">CCMC iSWA</a> , <a href="#">SEP Scoreboard</a>	ESA space weather stakeholders, NASA SRAG, public
UMASEP	real time since 2011, operational since 2016	<a href="#">ESA Space Weather Service Network</a> , <a href="#">HESPERIA</a> , <a href="#">University of Malaga</a> , <a href="#">CCMC iSWA</a> , <a href="#">SEP Scoreboard</a>	ESA space weather stakeholders, NASA SRAG, public
Real Time Models			
Model	Date of Implementation	Location	End Users
FORSPEF	2015	<a href="#">NOA</a>	registered users
MAG4	2019 (various real time locations from 2011)	<a href="#">SEP Scoreboard</a>	NASA SRAG, public
SAWS- ASPECS	2022	<a href="#">SEP Scoreboard</a> , <a href="#">NOA</a>	NASA SRAG, public
SEPMOD	2020	<a href="#">SEP Scoreboard</a>	NASA SRAG, public
SEPSTER	2020	<a href="#">SEP Scoreboard</a>	NASA SRAG, public
SEPSTER2D	2021	<a href="#">SEP Scoreboard</a>	NASA SRAG, public
SPRINTS	2022	<a href="#">SEP Scoreboard</a>	NASA SRAG, public

#### 4.4. Validation

Validation of SEP models has been non-uniform across the community. Validation efforts have ranged from subjective comparisons between model and data “by eye” for a few selected events, to thorough efforts that assess a variety of metrics and skill scores for a statistical sample of events. This non-uniformity is generally a consequence of the different computational needs and level of automation of each model. As the SEP modeling field matures, all SEP models should pursue a quantitative comparison to observations.

A number of steps can be taken to improve the quality, consistency, and ease of validation within the community. The creation of a standard set of SEP event definitions and the identification of community-accepted metrics would facilitate consistent validation and cross-model comparison. The curation of a shared data set of all observations required as input into the models (e.g., linked flare, CME, radio, and energetic electron measurements) and for comparison with model output (e.g., in situ particle data) would significantly reduce the workload for individual modelers and minimize duplicated efforts, and also remove disparities between model predictions that are due to the use of different input parameters. Lastly, a service with the ability to validate all types of SEP forecasts could be developed and made available to the community in a system such as CCMC’s Comprehensive Assessment of Models and Events using Library Tools (CAMEL) Framework (Rastätter et al., 2019).

Validation performed with the intent to demonstrate operational performance should aim to reproduce real-time operational scenarios as closely as possible, such as through participation in CCMC’s SEP Scoreboard <sup>26</sup>. Model forecasts should be issued without any tuning after the fact, and use only information available in real time as input into the model. It is also important to produce forecasts for time periods when no SEP event was observed, to assess false alarms and the validity of All Clear forecasts. Multi-point validation of 3D models for time periods when multiple spacecraft SEP observations are available at different locations can provide additional constraints and important insight into model performance. Lastly, forecasts should be output in energy ranges that match observational capabilities to ensure a meaningful comparison between model and observational data.

High-quality validation requires high-quality observational measurements to provide the “ground truth”, but the current spacecraft instruments that provide important SEP data sets have limitations that degrade their accuracy. In particular, the proton detectors on the operational GOES series of spacecraft have known problems with cross-talk between energy channels and contamination issues that impact the measurements, particularly during the onset of SEP events (Posner, 2007; Sandberg et al., 2014; Bruno, 2017; Rodriguez et al., 2017). The SOHO experiment has two science-quality detectors, EPHEM (Müller-Mellin et al., 1995), which only extends up to pro-

<sup>26</sup> <https://ccmc.gsfc.nasa.gov/challenges/sep.php>.

ton energies of 50 MeV, and ERNE (Torsti et al., 1995), which extends up to higher energies, but saturates during the highest intensity SEP events (Valtonen et al., 2009). These instruments (and also, for example, the High Energy Telescope (HET) s on the STEREO spacecraft) also have much lower backgrounds than the GOES proton detectors, and so can detect many more SEP events that do not meet the NOAA definition of an SEP event based on GOES data (e.g., Richardson et al., 2014), raising the question of how to define an “SEP event” for use in model validation. In the future, it would be valuable to fly operationally supported proton detectors near the Earth and at other locations (e.g., L4, see Section 4.1) that can overcome the limitations of the current instruments. For a detector to appropriately characterize SEP events, Vourlidas et al. (2021) specify that energy coverage for protons should extend from 1 to 1000 MeV. Kühl et al. (2020) describe such a detector that would build on the design of SOHO/EPHIN, but use lessons learned to envision a more capable detector across extended energy ranges and intensity levels. However, developing new SEP observatories and gathering event statistics from them will take considerable time. Therefore, near-term validation efforts should be aware of the limitations of the existing data archives, and further work should be done to correct the deficiencies to the greatest extent possible.

In conclusion, the SEP modeling community has developed a rich and diverse set of SEP models that exhibit a wide array of capabilities but currently have significant limitations, in particular arising from the gaps in real-time observations. If supported with the necessary observations, and with further developments, for example in computational capabilities and the application of artificial intelligence and machine learning, the field is poised for continued growth with a great potential to contribute significantly both to space weather operations and advances in the understanding of the physics of SEP events.

### Declaration of Competing Interest

The authors declare that they have no known competing financial interests or personal relationships that could have appeared to influence the work reported in this paper.

### Acknowledgements

The ISEP project is supported by the Advanced Exploration Systems Division under the Human Exploration and Operations Mission Directorate of NASA and performed in support of the Human Health and Performance Contract for NASA (NNJ15HK11B).

The HESPERIA project was funded through the European Union’s HORIZON 2020 research and Innovation Programme (Contract No 637324) and coordinated by the National Observatory of Athens in Greece.

PARADISE has received funding from the European Union’s Horizon 2020 research and innovation programme

under grant agreement No 870405 (EUHFORIA 2.0) and the ESA project “Heliospheric modelling techniques” (Contract No. 4000133080/20/NL/CRS). The code was developed in the framework of the projects C14/19/089 (C1 project Internal Funds KU Leuven), G.0D07.19N (FWO-Vlaanderen), SIDC Data Exploitation (ESA Prodex-12), and Belpo project B2/191/P1/SWiM.

Predictive Science Inc. was supported by NASA grants 80NSSC19K0067 and 80NSSC20K0285, and NSF grant ICER1854790.

The development of the Sadykov et al. model was supported by NASA ESI grant 80NSSC20K0302 and NSF FDSS grant 1936361.

JGL and COL acknowledge support for the SEP MOD model development for CCMC under National Aeronautics and Space Administration (NASA) Grant/Cooperative Agreement 80NSSC20K1873 from GSFC to UCB/SSL, with additional support to COL from AFOSR Grant FA9550-16-1-0418.

SEPSTER was supported by the NASA Living With a Star Program (grants NNX15AB80G and NNG06EO90A), and by the CCMC/SRAG ISEP project.

SEPSTER2D was funded by the NASA/HSR program NNH19ZDA001NHSR, the Goddard Space Flight Center / Internal Scientist Funding Model (ISFM) grant HISFM18, and the Johnson Space Center / Space Radiation Analysis Group (SRAG) under the Integrated Solar Energetic Proton Alert/Warning System (ISEP) project.

SOLPENCO was funded by the ESA contract 14098/99/NL/MM and its validation by the Spanish Ministerio de Educación y Ciencia under the project AYA2004-03022.

SOLPENCO2 was developed under ESA’s SEP EM project (Crosby et al., 2015) and updated during ESA’s SOL2UP project (Aran et al., 2017), both projects under ESA’s contract n. 20162/06/NL/JD and 4000114116/15/NL/HK, respectively.

SPARX was initially developed as part of the European Union-funded Seventh Framework Programme (FP7) COMESSEP project.

The development of the SPREADFAST framework has been funded by a contract to the ESA.

SD and CW acknowledge support from NERC via grant NE/V002864/1.

### Appendix A. Acronyms

An extensive list of acronyms used throughout this paper and their meanings have been compiled here for clarity and organized into multiple tables. General acronyms including physics terminology, instruments, and institutions are listed in Table A.13. Acronyms related to Machine Learning are described in Table A.14 and those related to validation are in Table A.15. Acronyms for the SEP models reviewed in this paper are found in Table A.16 while those related to other space weather models are found in Table A.17.

Table A.13  
General acronyms.

Acronym	Meaning
ACE	Advanced Composition Explorer
ACE/EPAM	Electron, Proton, and Alpha Monitor
AFRL	Air Force Research Laboratory
API	Application Programming Interface
AR	Active Region
ASTRON	Netherlands Institute for Radio Astronomy
AU	Astronomical Unit
AW	Angular Width
BIRA-IASB	Royal Belgian Institute for Space Aeronomy
CACTus	Computer Aided CME Tracking catalog
CAMEL	Comprehensive Assessment of Models and Events using Library Tools
CBF	Coronal Bright Front
CCMC	Community Coordinated Modeling Center
CCOR	Compact Coronagraph
CDAW	Coordinated Data Analysis Web
CIR	Corotating Interaction Region
CIRES	Cooperative Institute for Research in Environmental Sciences
CME	Coronal Mass Ejection
Cobpoint	Connecting-with-Observer point
DONKI	Space Weather Database of Notifications, Knowledge, Information
DSA	Diffusive Shock Acceleration
DSCOVR	Deep Space Climate Observatory
ESA	European Space Agency
ESP	Energetic Storm Particles
EU	European Union
EUV	Extreme Ultraviolet
FTE	Focused Transport Equation
FQ	Flare-Quiet
GLE	Ground Level Event
GOES	Geostationary Operational Environment Satellite
GOES/EPS	Energetic Particle Sensor
GOES/EPEAD	Energetic Proton Electron and Alpha Detector
GOES/HEPAD	High Energy Proton and Alpha Detector
GOES/XRS	X-ray Sensor
GONG	Global Oscillation Network Group
GSFC	NASA Goddard Space Flight Center
GUI	Graphical User Interface
HARP	HMI Active Region Patch
HEK	Heliospheric Event Knowledgebase
HESPERIA	High Energy Solar Particle Events forecasting and Analysis
Hinode/EIS	EUV Imaging Spectrometer
IA-BIS	Institute of Astronomy, Bulgarian Academy of Sciences
ICME	Interplanetary Coronal Mass Ejection
IDL	Interactive Data Language
IEAP	Institute of Experimental and Applied Physics
IMF	Interplanetary Magnetic Field
IMP	Interplanetary Monitoring Platform (series of satellites)
INAF	National Institute for Astrophysics
IP	Interplanetary
IRAP	Institut de Recherche en Astrophysique et Planetologie
ISEP	Integrated Solar Energetic Proton Event Alert/Warning System
iSWA	integrated Space Weather Analysis System
ISWAT	International Space Weather Action Teams
IZMIRAN	Pushkov Institute of Terrestrial Magnetism, Ionosphere and Radio Wave Propagation
JSC	NASA Johnson Space Center
JSOC	Stanford Joint Science Operations Center
KU	Katholieke Universiteit
L1, L4	Langrangian point 1, 4
LEO	Low Earth Orbit
LMSAL	Lockheed Martin Solar and Astrophysics Laboratory
LOS	Line of Sight
MDI	Michelson Doppler Imager

(continued on next page)



Table A.13 (continued)

Acronym	Meaning
MHD	Magnetohydrodynamic
NASA	National Aeronautics and Space Administration
NKUA	National and Kapodistrian University of Athens
NLGC	Nonlinear Guiding Center theory
NM	Neutron Monitor
NOA	National Observatory of Athens
NOAA	National Oceanics and Atmospheric Administration
NRT	Near Real Time
NSO	National Solar Observatory
PAMELA	Payload for Antimatter Matter Exploration and Light-nuclei Astrophysics (satellite experiment)
PC	Principal Components
PCA	Principal Component Analysis
pfu	Particle Flux Unit
PIL	Polarity Inversion Line
PSI	Predictive Science Inc
PSP	Parker Solar Probe
QLT	Quasi-linear Theory
R2O	Research to Operations
RSTN	Radio Solar Telescope Network
SC	Solar Cycle
SDE	Stochastic Differential Equation
SDO	Solar Dynamics Observatory
SDO/AIA	Advanced Imaging Assembly
SDO/HMI	Helioseismic Magnetic Imager
SECCHI	Sun Earth Connection Coronal and Heliospheric Investigation
SEON	Solar Electro-Optical Observatory Network
SEP	Solar Energetic Particles
SEPEM	ESA's Solar Energetic Particle Environment Modelling
SEPEM RDS	SEPEM Reference Data Set
SF	Solar Flare
sfu	Solar flux unit
SHARP	Space-weather HMI Active Region Patch
SHINE	Solar Heliospheric and Interplanetary Environment workshop
SMARP	Space-Weather MDI Active Region Patches
SO	Solar Orbiter
SOHO	Solar and Heliospheric Observatory
SOHO/COSTEP	Comprehensive Suprathermal and Energetic Particle Analyzer
SOHO/EPHIN	Electron Proton and Helium Instrument
SOHO/EIT	Extreme-Ultraviolet Imaging Telescope
SOHO/ERNE	Energetic and Relativistic Nuclei and Electron
SOHO/LASCO	Large Angle and Spectrometric Coronagraph Experiment
SOHO/MDI	Michelson Doppler Imager
Solar DEMON	Solar Dimming and EUV wave Monitor
SOLSTICE	Solar Storms and Terrestrial Impacts Center
SOON	Solar Observing Optical Network
SPARC	Space Applications and Research Consultancy
SPE	Solar Particle Event, Solar Proton Event
SRAG	Space Radiation Analysis Group
SRS	Solar Region Summary
STEREO	Solar Terrestrial Relations Observatory (A & B)
STEREO/LET	Low-Energy Telescope
STEREO/HET	High-Energy Telescope
SWFO-L1	Space Weather Follow On - L1
SWPC	Space Weather Prediction Center
SWRI	Southwest Research Institute
SXR	Soft X-rays
USAF	United States Air Force
UTU	University of Turku
VSWMC	Virtual Space Weather Modelling Centre
WAVES	Radio and Plasma Wave Experiment

Table A.14  
Acronyms related to machine learning.

Acronym	Meaning
AI	Artificial Intelligence
CART	Classification And Regression Trees
CNN	Convolutional Neural Network
DT	Decision Trees
ET	Extremely Randomized Trees
LR	Logistic Regression
ML	Machine Learning
MLE	Mean Log Error
MLP	Multi-layer Perceptron
MV	Missing Values
MVTS	multivariate time series
NN	Neural Network
RF	Random Forest
RBF	Radial Basis Function
SVM	Support Vector Machines
TSC	Time Series Classifier
VAR	Vector Autoregression model
XGB	Extreme Gradient Boosting

Table A.15  
Acronyms related to validation.

Acronym	Meaning
AUC	Area Under the Curve
AWT	Advanced Warning Time
AWT	Average Warning Time
BS	Brier Score
CDF	Cumulative Distribution Function or Cumulative Probability Function
CSI	Critical Success Index
FAR	False Alarm Rate
FN	False Negative
FP	False Positive
HSS	Heidke Skill Score
OA	Overall Accuracy
PC	Percent Correct
pt or PT	Probability Threshold
POD	probability of Detection
POFD	Probability of False Detection
ROC	Receiver Operator Characteristic
TN	True Negative
TP	True Positive
TSS	True Skill Statistic
WTSS	Weighted True Skill Statistic

Table A.16  
Acronyms for the SEP models reviewed in this paper.

Acronym	Meaning
ADEPT	Air Force Dynamic Energetic Particle Tool
AFRL PPS	Air Force Research Laboratory Proton Prediction System
AMPS	Adaptive Mesh Particle Simulator
COMSEP	COronal Mass Ejections and Solar Energetic Particles
EPREM	Energetic Particle Radiation Environment Module
ESPERTA	Empirical model for Solar Proton Event Real Time Alert
FORSPEF	FOrecasting Solar Particle Events and Flares
iPATH	improved Particle Acceleration and Transport in the Heliosphere
MAG4	Magnetogram Forecast
MagPy	Magnetogram Forecast in Python
MEMPSEP	Multivariate Ensemble of Models for Probabilistic SEP prediction
M-FLAMPA	Multiple-Field-Line-Advection Model for Particle Acceleration
PARADISE	PARticle Radiation Asset Directed at Interplanetary Space Exploration
PCA	Principal Component Analysis model
REleASE	Relativistic Electron Alert System for Exploration
SAWS-ASPECS	SEP Advanced Warning System, Advanced Solar Particle Events Casting System
SEPMOD	Solar Energetic Particle MODel
SEPSTER	SEP prediction derived from STEReo observations
SOLPENCO	SOLAR Particle ENgineering Code
SPARX	Solar PArticle Radiation swX
SPREAdFAST	Solar Particle Radiation Environment Analysis and Forecasting – Acceleration and Scattering Transport
SPRINTS	Space Radiation Intelligence System
STAT	Solar Particle Event (SPE) Threat Assessment Tool
UMASEP	University of Malaga Solar Energetic Particles

Table A.17

Acronyms related to space weather models.

Acronym	Meaning
ADAPT	Air Force Data Assimilative Photospheric flux Transport
AWSOM	Alfven-Wave driven sOLar wind Model
CASHeW	Coronal Analysis of Shocks and Waves
CORHEL	Corona-Heliosphere model
EEGGL	Eruptive Event Generator Gibson-Low
EMMREM	Earth-Moon-Mars Radiation Environment Module
EUHFORIA	European Heliospheric Forecasting Information Asset
FLARECAST	Flare Likelihood And Region Eruption foreCASTing
GL	Gibson-Low
MAS	Magnetohydrodynamic Algorithm outside a Sphere
NLGC	Nonlinear Guiding Center Theory
PFSS	Potential Field Source Surface
PREDICCS	Predictions of Radiation from RELEASE, EMMREM, and Data Incorporating the CRaTER, COSTEP, and other SEP measurements
PROSPER	Probabilistic Solar Particle Event forecasting
RBSL	Regularized Biot-Savart Laws
REL	Reference Event List
SaP	Shock and Particle
SOLPACS	SOLar Particle Acceleration in Coronal Shocks
S2M	Synthetic Shock Model
SWMF	Space Weather Modeling Framework
TDm	Titov-Démoulin
UMASEP/PC	Poorly Connected module
UMASEP/WC	Well Connected module
UMASOD	University of Malaga predictor from Solar Data
WSA	Wang-Sheeley-Arge model

## References

- Afanasyev, A., Battarbee, M., Vainio, R., 2015. Self-consistent Monte Carlo simulations of proton acceleration in coronal shocks: Effect of anisotropic pitch-angle scattering of particles. *Astron. Astroph.* 584, A81.
- Ahmadzadeh, A., Aydin, B., Georgoulis, M.K., Kempton, D.J., Mahajan, S.S., Angryk, R.A., 2021. How to Train Your Flare Prediction Model: Revisiting Robust Sampling of Rare Events. *Astrophys. J. Suppl* 254 (2), 23.
- Alberti, T., Laurenza, M., Cliver, E.W., 2019. Forecasting solar proton events by using the ESPERTA model. *Nuovo Cimento C* 42 (1), 40.
- Alberti, T., Laurenza, M., Cliver, E.W., Storini, M., Consolini, G., Lepreti, F., 2017. Solar Activity from 2006 to 2014 and Short-term Forecasts of Solar Proton Events Using the ESPERTA Model. *Astrophys. J.* 838 (1), 59.
- Alissandrakis, C.E., 1981. On the computation of constant alpha force-free magnetic field. *Astron. Astroph.* 100 (1), 197–200.
- Aminalragia-Giamini, S., Raptis, S., Anastasiadis, A., Tsigkanos, A., Sandberg, I., Papaioannou, A., Papadimitriou, C., Jiggins, P., Aran, A., Daglis, I.A., 2021. Solar Energetic Particle Event occurrence prediction using Solar Flare Soft X-ray measurements and Machine Learning. *J. Space Weather Space Climate* 11, 59.
- Anastasiadis, A., Papaioannou, A., Sandberg, I., Georgoulis, M., Tziotziou, K., Kouloumvakos, A., Jiggins, P., 2017. Predicting Flares and Solar Energetic Particle Events: The FORSPEF Tool. *Sol. Phys.* 292 (9), 134.
- Angryk, R.A., Martens, P.C., Aydin, B., Kempton, D., Mahajan, S.S., Basodi, S., Ahmadzadeh, A., Cai, X., Filali Boubrahimi, S., Hamdi, S. M., Schuh, M.A., Georgoulis, M.K., 2020. Multivariate time series dataset for space weather data analytics. *Sci. Data* 7 (1), 227.
- Aran, A., 2007. Synthesis of proton flux profiles of SEP events associated with interplanetary shocks. The tool SOLPENCO. Ph.D. thesis, Universitat de Barcelona, Barcelona, Spain.
- Aran, A., Lario, D., Sanahuja, B., Marsden, R.G., Dryer, M., Fry, C.D., McKenna-Lawlor, S.M.P., 2007. Modeling and forecasting solar energetic particle events at Mars: the event on 6 March 1989. *Astron. Astroph.* 469 (3), 1123–1134.
- Aran, A., Pacheco, D., Agueda, N., Sanahuja, B., 2017. Updating SOLPENCO2 and New Analysis on Downstream FLuence (SOL2UP) Project. Final Report, ESA/ESTEC Contract 4000114116/15/NL/HK, 1–90.
- Aran, A., Rodriguez-Gasen, R., Sanahuja, B., Jabos, C., Poedts, S., 2011. Wp410: Initial and boundary conditions for the shock-and-particle model. SEPTEM Technical Report, ESA/ESTEC Contract 20162/06/NL/JD, 1–58.
- Aran, A., Sanahuja, B., Lario, D., 2005a. A first step towards proton flux forecasting. *Adv. Space Res.* 36 (12), 2333–2338.
- Aran, A., Sanahuja, B., Lario, D., 2005b. Fluxes and fluences of SEP events derived from SOLPENCO. *Ann. Geophys.* 23 (9), 3047–3053.
- Aran, A., Sanahuja, B., Lario, D., 2006. SOLPENCO: A solar particle engineering code. *Adv. Space Res.* 37 (6), 1240–1246.
- Aran, A., Sanahuja, B., Lario, D., 2008. Comparing proton fluxes of central meridian SEP events with those predicted by SOLPENCO. *Adv. Space Res.* 42 (9), 1492–1499.
- Arge, C.N., Pizzo, V.J., 2000. Improvement in the prediction of solar wind conditions using near-real time solar magnetic field updates. *J. Geophys. Res.* 105 (A5), 10465–10479, URL <https://agupubs.onlinelibrary.wiley.com/doi/abs/10.1029/1999JA000262>.
- Aschwanden, M.J., Freeland, S.L., 2012. Automated Solar Flare Statistics in Soft X-Rays over 37 Years of GOES Observations: The Invariance of Self-organized Criticality during Three Solar Cycles. *Astrophys. J.* 754 (2), 112.
- Axford, W.I., Leer, E., Skadron, G., Jan. 1977. The Acceleration of Cosmic Rays by Shock Waves. In: International Cosmic Ray Conference. Vol. 11 of International Cosmic Ray Conference. p. 132.
- Bain, H.M., Mays, M.L., Luhmann, J.G., Li, Y., Jian, L.K., Odstrcil, D., 2016. Shock Connectivity in the August 2010 and July 2012 Solar

- Energetic Particle Events Inferred from Observations and ENLIL Modeling. *Astrophys. J.* 825 (1), 1.
- Bain, H.M., Steenburgh, R.A., Onsager, T.G., Stitely, E.M., 2021. A Summary of National Oceanic and Atmospheric Administration Space Weather Prediction Center Proton Event Forecast Performance and Skill. *Space Weather* 19 (7), e2020SW002670.
- Balch, C.C., 1999. SEC proton prediction model: verification and analysis. *Radiat. Meas.* 30 (3), 231–250.
- Balch, C.C., 2008. Updated verification of the Space Weather Prediction Center's solar energetic particle prediction model. *Space Weather* 6 (1), S01001.
- Barouch, E., Gros, M., Masse, P., 1971. The Solar Longitude Dependence of Proton Event Delay Time. *Sol. Phys.* 19 (2), 483–493.
- Battarbee, M., Vainio, R., Laitinen, T., Hietala, H., 2013. Injection of thermal and suprathermal seed particles into coronal shocks of varying obliquity. *Astron. Astroph.* 558, A110.
- Bobra, M.G., Sun, X., Hoeksema, J.T., Turmon, M., Liu, Y., Hayashi, K., Barnes, G., Leka, K.D., 2014. The Helioseismic and Magnetic Imager (HMI) Vector Magnetic Field Pipeline: SHARPs - Space-Weather HMI Active Region Patches. *Sol. Phys.* 289 (9), 3549–3578.
- Bobra, M.G., Wright, P.J., Sun, X., Turmon, M.J., 2021. SMARPs and SHARPs: Two Solar Cycles of Active Region Data. *Astrophys. J. Suppl.* 256 (2), 26.
- Borovikov, D., Sokolov, I.V., Manchester, W.B., Jin, M., Gombosi, T.I., 2017. Eruptive event generator based on the Gibson-Low magnetic configuration. *J. Geophys. Res.: Space Phys.* 122 (8), 7979–7984.
- Borovikov, D., Sokolov, I.V., Roussev, I.I., Taktakishvili, A., Gombosi, T.I., 2018. Toward a Quantitative Model for Simulation and Forecast of Solar Energetic Particle Production during Gradual Events. I. Magnetohydrodynamic Background Coupled to the SEP Model. *Astrophys. J.* 864 (1), 88.
- Borovikov, D., Sokolov, I.V., Tóth, G., 2015. An efficient second-order accurate and continuous interpolation for block-adaptive grids. *J. Comput. Phys.* 297, 599–610.
- Boubrahimi, S.F., Aydin, B., Martens, P., Angryk, R., 2017. On the prediction of >100 mev solar energetic particle events using goes satellite data. In: 2017 IEEE International Conference on Big Data (Big Data). pp. 2533–2542.
- Bruno, A., 2017. Calibration of the GOES 13/15 high-energy proton detectors based on the PAMELA solar energetic particle observations. *Space Weather* 15 (9), 1191–1202.
- Bruno, A., Bazilevskaia, G.A., Boezio, M., Christian, E.R., de Nolfo, G. A., Martucci, M., Merge', M., Mikhailov, V.V., Munini, R., Richardson, I.G., Ryan, J.M., 2018. Solar Energetic Particle Events Observed by the PAMELA Mission. *Astrophys. J.* 862 (2), 97.
- Bruno, A., Richardson, I.G., 2021. Empirical Model of 10–130 MeV Solar Energetic Particle Spectra at 1 AU Based on Coronal Mass Ejection Speed and Direction. *Sol. Phys.* 296 (2), 36.
- Byrne, J.P., Long, D.M., Gallagher, P.T., Bloomfield, D.S., Maloney, S. A., McAtter, R.T.J., Morgan, H., Habbal, S.R., 2013. Improved methods for determining the kinematics of coronal mass ejections and coronal waves. *Astron. Astroph.* 557, A96.
- Cane, H.V., Erickson, W.C., Prestage, N.P., 2002. Solar flares, type III radio bursts, coronal mass ejections, and energetic particles. *J. Geophys. Res.* 107 (A10), 1315.
- Cane, H.V., Lario, D., 2006. An Introduction to CMEs and Energetic Particles. *Space Sci. Rev.* 123 (1–3), 45–56.
- Cane, H.V., Reames, D.V., von Roseninge, T.T., 1988. The role of interplanetary shocks in the longitude distribution of solar energetic particles. *J. Geophys. Res.* 93 (A9), 9555–9567.
- Cane, H.V., Richardson, I.G., von Roseninge, T.T., 2010. A study of solar energetic particle events of 1997–2006: Their composition and associations. *J. Geophys. Res.* 115 (A8), A08101.
- Chen, J.H., Schwadron, N.A., Möbius, E., Gorby, M., 2015. Modeling interstellar pickup ion distributions in corotating interaction regions inside 1 AU. *J. Geophys. Res.: Space Phys.* 120 (11), 9269–9280.
- Cliver, E.W., Kahler, S.W., Reames, D.V., 2004. Coronal Shocks and Solar Energetic Proton Events. *Astrophys. J.* 605 (2), 902–910.
- Cliver, E.W., Mekhaldi, F., Muscheler, R., 2020. Solar Longitude Distribution of High-energy Proton Flares: Fluences and Spectra. *Astrophys. J. Lett.* 900 (1), L11.
- Cortes, C., Vapnik, V., 1995. Support-vector networks. *Mach. Learn.* 20 (3), 273–297.
- Crosby, N., Heynderickx, D., Jiggins, P., Aran, A., Sanahuja, B., Truscott, P., Lei, F., Jacobs, C., Poedts, S., Gabriel, S., Sandberg, I., Glover, A., Hilgers, A., 2015. SEP-EM: A tool for statistical modeling the solar energetic particle environment. *Space Weather* 13 (7), 406–426.
- Crosby, N.B., Veronig, A., Robbrecht, E., Vrsnak, B., Vernerstrom, S., Malandraki, O., Dalla, S., Rodriguez, L., Srivastava, N., Hesse, M., Odstrcil, D., Comesep Consortium, Nov. 2012. Forecasting the space weather impact: The COMESEP project. In: Hu, Q., Li, G., Zank, G. P., Ao, X., Verkhoglyadova, O., Adams, J.H. (Eds.), *Space Weather: the Space Radiation Environment: 11th Annual International Astrophysics Conference*. Vol. 1500 of American Institute of Physics Conference Series. pp. 159–164.
- Dalla, S., Marsh, M.S., Kelly, J., Laitinen, T., 2013. Solar energetic particle drifts in the Parker spiral. *J. Geophys. Res.: Space Phys.* 118 (10), 5979–5985.
- Dalla, S., Swalwell, B., Battarbee, M., Marsh, M.S., Laitinen, T., Proctor, S.J., Aug. 2018. Application of Test Particle Simulations to Solar Energetic Particle Forecasting. In: Foullon, C., Malandraki, O.E. (Eds.), *Space Weather of the Heliosphere: Processes and Forecasts*. vol. 335. pp. 268–271.
- Davis, J., Goadrich, M., 2006. The Relationship between Precision-Recall and ROC Curves. In: Cohen, W.W., Moore, A. (Eds.), *Proceedings of the 23rd International Conference on Machine Learning, ICML '06*. Association for Computing Machinery, New York, NY, USA, p. 233–240.
- Dayeh, M.A., Desai, M.I., Dwyer, J.R., Rassoul, H.K., Mason, G.M., Mazur, J.E., 2009. Composition and Spectral Properties of the 1 AU Quiet-Time Suprathermal Ion Population During Solar Cycle 23. *Astrophys. J.* 693 (2), 1588–1600.
- Dayeh, M.A., Desai, M.I., Kozarev, K., Schwadron, N.A., Townsend, L. W., PourArsalan, M., Zeitlin, C., Hatcher, R.B., 2010. Modeling proton intensity gradients and radiation dose equivalents in the inner heliosphere using EMMREM: May 2003 solar events. *Space Weather* 8 (9), S00E07.
- Dayeh, M.A., Desai, M.I., Mason, G.M., Ebert, R.W., Farahat, A., 2017. Origin and Properties of Quiet-time 0.11–1.28 MeV Nucleon-1 Heavy-ion Population near 1 au. *Astrophys. J.* 835 (2), 155.
- Deng, H., Runger, G., Tuv, E., Vladimir, M., 2013. A time series forest for classification and feature extraction. *Inf. Sci.* 239, 142–153.
- Desai, M., Giacalone, J., 2016. Large gradual solar energetic particle events. *Living Rev. Sol. Phys.* 13 (1), 3.
- Desai, M. I., Mitchell, D. G., Szalay, J. R., Roelof, E. C., Giacalone, J., Hill, M. E., McComas, D. J., Christian, E. R., Schwadron, N. A., McNutt, R. L., J., Wiedenbeck, M. E., Joyce, C., Cohen, C. M. S., Ebert, R. W., Dayeh, M. A., Allen, R. C., Davis, A. J., Krimigis, S. M., Leske, R. A., Matthaeus, W. H., Malandraki, O., Mewaldt, R. A., Labrador, A., Stone, E. C., Bale, S. D., Pulupa, M., MacDowall, R. J., Kasper, J. C., Feb. 2020. Properties of Suprathermal-through-energetic He Ions Associated with Stream Interaction Regions Observed over the Parker Solar Probe's First Two Orbits. *Astrophys. J. Suppl.* 246 (2), 56.
- Dierckx, M., Tziotziou, K., Dalla, S., Patsou, I., Marsh, M.S., Crosby, N.B., Malandraki, O., Tsiropoula, G., 2015. Relationship between Solar Energetic Particles and Properties of Flares and CMEs: Statistical Analysis of Solar Cycle 23 Events. *Sol. Phys.* 290 (3), 841–874.
- Ding, Z.-Y., Li, G., Hu, J.-X., Fu, S., 2020. Modeling the 2017 September 10 solar energetic particle event using the iPATH model. *Res. Astron. Astrophys.* 20 (9), 145.
- Downs, C., Lionello, R., Mikić, Z., Linker, J.A., Velli, M., Dec. 2016. Closed-field Coronal Heating Driven by Wave Turbulence. *Astrophys. J.* 832 (2), 180.

- Downs, C., Warmuth, A., Long, D.M., Bloomfield, D.S., Kwon, R.-Y., Veronig, A.M., Vourlidas, A., Vršnak, B., 2021. Validation of Global EUV Wave MHD Simulations and Observational Techniques. *Astrophys. J.* 911 (2), 118.
- Eastwood, J.P., Biffis, E., Hapgood, M.A., Green, L., Bisi, M.M., Bentley, R.D., Wicks, R., McKinnell, L.A., Gibbs, M., Burnett, C., 2017. The Economic Impact of Space Weather: Where Do We Stand? *Risk Anal.* 37 (2), 206–218.
- Engell, A.J., Falconer, D.A., Schuh, M., Loomis, J., Bissett, D., 2017. SPRINTS: A Framework for Solar-Driven Event Forecasting and Research. *Space Weather* 15 (10), 1321–1346.
- Erickson, W.C., 1997. The Bruny Island Radio Spectrometer. *Pub. Astron. Soc. Aust.* 14 (3), 278–282.
- Falconer, D., Barghouty, A.F., Khazanov, I., Moore, R., 2011. A tool for empirical forecasting of major flares, coronal mass ejections, and solar particle events from a proxy of active-region free magnetic energy. *Space Weather* 9 (4), S04003.
- Falconer, D.A., Moore, R.L., Barghouty, A.F., Khazanov, I., 2014. MAG4 versus alternative techniques for forecasting active region flare productivity. *Space Weather* 12 (5), 306–317.
- Gallagher, P.T., Lawrence, G.R., Dennis, B.R., 2003. Rapid Acceleration of a Coronal Mass Ejection in the Low Corona and Implications for Propagation. *Astrophys. J. Lett.* 588 (1), L53–L56.
- Gardiner, C.W., 2004. *Handbook of Stochastic Methods for Physics, Chemistry and the Natural Sciences*. Springer-Verlag, Berlin.
- Georgoulis, M.K., 2008. Magnetic complexity in eruptive solar active regions and associated eruption parameters. *Geophys. Res. Lett.* 35 (6), L06S02.
- Georgoulis, M.K., Bloomfield, D.S., Piana, M., Massone, A.M., Soldati, M., Gallagher, P.T., Pariat, E., Vilmer, N., Buchlin, E., Baudin, F., Csillaghy, A., Sathiapal, H., Jackson, D.R., Alingery, P., Benvenuto, F., Campi, C., Florios, K., Gontikakis, C., Guennou, C., Guerra, J.A., Kontogiannis, I., Latorre, V., Murray, S.A., Park, S.-H., von Stachelski, S., Torbica, A., Vischi, D., Worsfold, M., May 2021. The flare likelihood and region eruption forecasting (FLARECAST) project: flare forecasting in the big data & machine learning era. *J. Space Weather Space Clim.* 11, 39.
- Georgoulis, M.K., Rust, D.M., 2007. Quantitative Forecasting of Major Solar Flares. *Astrophys. J. Lett.* 661 (1), L109–L112.
- Gibson, S.E., Low, B.C., 1998. A Time-Dependent Three-Dimensional Magnetohydrodynamic Model of the Coronal Mass Ejection. *Astrophys. J.* 493 (1), 460–473.
- Gombosi, T.I., Chen, Y., Glocer, A., Huang, Z., Jia, X., Liemohn, M.W., Manchester, W.B., Pulkkinen, T., Sachdeva, N., Al Shidi, Q., Sokolov, I.V., Szente, J., Tennishev, V., Toth, G., van der Holst, B., Welling, D. T., Zhao, L., Zou, S., 2021. What sustained multi-disciplinary research can achieve: The space weather modeling framework. *J. Space Weather Space Clim.* 11, 42.
- Gombosi, T.I., van der Holst, B., Manchester, W.B., Sokolov, I.V., 2018. Extended MHD modeling of the steady solar corona and the solar wind. *Living Rev. Sol. Phys.* 15 (1), 4.
- Gopalswamy, N., Aguilar-Rodriguez, E., Yashiro, S., Nunes, S., Kaiser, M.L., Howard, R.A., 2005. Type II radio bursts and energetic solar eruptions. *J. Geophys. Res.* 110 (A12), A12S07.
- Gopalswamy, N., Yashiro, S., 2011. The Strength and Radial Profile of the Coronal Magnetic Field from the Standoff Distance of a Coronal Mass Ejection-driven Shock. *Astrophys. J. Lett.* 736 (1), L17.
- Guarnieri, V., Tamburini, V., Cougnet, C., Pia, M.G., Spillantini, P., Perino, M.A., Eckersley, S., Heynderickx, D., 2005. REMSIM - Final Report. Alenia Spazio Technical Note. URL: <http://www.hep.man.ac.uk/u/johna/pub/Geant4/G4AI/ESA-AO-6765/final%20report%20REMSIM.PDF>.
- Guo, C., Pleiss, G., Sun, Y., Weinberger, K.Q., 2017. On calibration of modern neural networks. In: *Proceedings of the 34th International Conference on Machine Learning - Volume 70. ICML'17. JMLR.org*, pp. 1321–1330.
- He, J., Rodriguez, J.V., 2018. Onsets of Solar Proton Events in Satellite and Ground Level Observations: A Comparison. *Space Weather* 16 (3), 245–260.
- Heita, P.K.N., 2018. Numerical investigation of solar energetic particle transport between the Sun, Earth, and Mars. Master's thesis, North-West University, South Africa. URL: <https://dspace.nwu.ac.za/handle/10394/33865>.
- Heras, A.M., Sanahuja, B., Lario, D., Smith, Z.K., Detman, T., Dryer, M., 1995. Three Low-Energy Particle Events: Modeling the Influence of the Parent Interplanetary Shock. *Astrophys. J.* 445, 497.
- Heras, A.M., Sanahuja, B., Smith, Z.K., Detman, T., Dryer, M., 1992. The Influence of the Large-Scale Interplanetary Shock Structure on a Low-Energy Particle Event. *Astrophys. J.* 391, 359.
- Hilberg, R.G., 1969. Radiation Protection for Apollo Missions - Case 340. URL: [https://www.lpi.usra.edu/lunar/documents/NTRS/collection3/NASA\\_CR\\_106949.pdf](https://www.lpi.usra.edu/lunar/documents/NTRS/collection3/NASA_CR_106949.pdf).
- Hoeksema, J.T., Liu, Y., Hayashi, K., Sun, X., Schou, J., Couvidat, S., Norton, A., Bobra, M., Centeno, R., Leka, K.D., Barnes, G., Turmon, M., 2014. The Helioseismic and Magnetic Imager (HMI) Vector Magnetic Field Pipeline: Overview and Performance. *Sol. Phys.* 289 (9), 3483–3530.
- Hu, J., Li, G., Ao, X., Zank, G.P., Verkhoglyadova, O., 2017. Modeling Particle Acceleration and Transport at a 2-D CME-Driven Shock. *J. Geophys. Res.: Space Phys.* 122 (11), 10938–10963.
- Huang, X., Wang, H.-N., Li, L.-P., 2012. Ensemble prediction model of solar proton events associated with solar flares and coronal mass ejections. *Res. Astron. Astrophys.* 12 (3), 313–321.
- Inceoglu, F., Jeppesen, J.H., Kongstad, P., Hernández Marcano, N.J., Jacobsen, R.H., Karoff, C., 2018. Using Machine Learning Methods to Forecast if Solar Flares Will Be Associated with CMEs and SEPs. *Astrophys. J.* 861 (2), 128.
- Iucci, N., Levitin, A.E., Belov, A.V., Eroshenko, E.A., Ptitsyna, N.G., Villoresi, G., Chizhenkov, G.V., Dorman, L.I., Gromova, L.I., Parisi, M., Tyasto, M.I., Yanke, V.G., 2005. Space weather conditions and spacecraft anomalies in different orbits. *Space Weather* 3 (1), 01001.
- Jacobs, C., Poedts, S., 2011. A polytropic model for the solar wind. *Adv. Space Res.* 48 (12), 1958–1966.
- Jeong, E.-J., Lee, J.-Y., Moon, Y.-J., Park, J., 2014. Forecast of Solar Proton Events with NOAA Scales Based on Solar X-ray Flare Data Using Neural Network. *J. Korean Astron. Soc.* 47 (6), 209–214.
- Ji, A., Aydin, B., Georgoulis, M.K., Angryk, R., 2020. All-clear flare prediction using interval-based time series classifiers. In: *2020 IEEE International Conference on Big Data (Big Data)*, pp. 4218–4225.
- Jiggins, P., Heynderickx, D., Sandberg, I., Truscott, P., Raukunen, O., Vainio, R., 2018. Updated Model of the Solar Energetic Proton Environment in Space. *J. Space Weather Space Climate* 8, A31.
- Jiggins, P.T.A., Gabriel, S.B., Heynderickx, D., Crosby, N., Glover, A., Hilgers, A., 2012. ESA SEPEM Project: Peak Flux and Fluence Model. *IEEE Trans. Nucl. Sci.* 59 (4), 1066–1077.
- Jin, M., Manchester, W.B., van der Holst, B., Sokolov, I., Tóth, G., Mullinix, R.E., Taktakishvili, A., Chulaki, A., Gombosi, T.I., 2017. Data-constrained Coronal Mass Ejections in a Global Magnetohydrodynamics Model. *Astrophys. J.* 834 (2), 173.
- Jokipii, J.R., 1966. Cosmic-Ray Propagation. I. Charged Particles in a Random Magnetic Field. *Astrophys. J.* 146, 480.
- Jokipii, J.R., Levy, E.H., Hubbard, W.B., 1977. Effects of particle drift on cosmic-ray transport. I. General properties, application to solar modulation. *Astrophys. J.* 213, 861–868.
- Jones, J.B.L., Bentley, R.D., Hunter, R., Iles, R.H.A., Taylor, G.C., Thomas, D.J., 2005. Space weather and commercial airlines. *Adv. Space Res.* 36 (12), 2258–2267.
- Kahler, S.W., 1982. The role of the big flare syndrome in correlations of solar energetic proton fluxes and associated microwave burst parameters. *J. Geophys. Res.* 87 (A5), 3439–3448.
- Kahler, S.W., Cliver, E.W., Ling, A.G., 2007. Validating the proton prediction system (PPS). *J. Atmos. Solar-Terr. Phys.* 69 (1–2), 43–49.
- Kahler, S.W., Ling, A.G., 2017. Characterizing Solar Energetic Particle Event Profiles with Two-Parameter Fits. *Sol. Phys.* 292 (4), 59.

- Kahler, S.W., Sheeley, N.R., J., Howard, R.A., Michels, D.J., Koomen, M.J., McGuire, R.E., von Roseninge, T.T., Reames, D.V., 1984. Associations between coronal mass ejections and solar energetic proton events. *J. Geophys. Res.* 89 (A11), 9683–9694.
- Kahler, S.W., White, S.M., Ling, A.G., 2017. Forecasting  $E > 50$ -MeV proton events with the proton prediction system (PPS). *J. Space Weather Space Climate* 7, A27.
- Kasapis, S., Zhao, L., Chen, Y., Wang, X., Bobra, M., Gombosi, T., 2022. Interpretable Machine Learning to Forecast SEP Events for Solar Cycle 23. *Space Weather* 20 (2), e2021SW002842.
- Kim, K.N., Sin, S.A., Song, K.A., Kong, J.H., 2018. A technique for prediction of SPEs from solar radio flux by statistical analysis, ANN and GA. *Astro-phys. Space Sci.* 363 (8), 170.
- Kim, M.-H.Y., De Angelis, G., Cucinotta, F.A., 2011. Probabilistic assessment of radiation risk for astronauts in space missions. *Acta Astronaut.* 68 (7), 747–759.
- Klein, K.-L., Dalla, S., 2017. Acceleration and Propagation of Solar Energetic Particles. *Space Sci. Rev.* 212 (3–4), 1107–1136.
- Kong, X., Guo, F., Giacalone, J., Li, H., Chen, Y., 2017. The Acceleration of High-energy Protons at Coronal Shocks: The Effect of Large-scale Streamer-like Magnetic Field Structures. *Astrophys. J.* 851 (1), 38.
- Kóta, J., Manchester, W.B., Gombosi, T.I., Jan. 2005. SEP Acceleration at Realistic CMEs: Two Sites of Acceleration? In: 29th International Cosmic Ray Conference (ICRC29), Volume 1. Vol. 1 of International Cosmic Ray Conference. p. 125.
- Kouloumvakos, A., Patsourakos, S., Nindos, A., Vourlidis, A., Anastasiadis, A., Hillaris, A., Sandberg, I., 2016. Multi-viewpoint Observations of a Widely distributed Solar Energetic Particle Event: The Role of EUV Waves and White-light Shock Signatures. *Astrophys. J.* 821 (1), 31.
- Kozarev, K., Nedal, M., Miteva, R., Dechev, M., Zucca, P., Feb. 2022. A Multi-Event Study of Early-Stage SEP Acceleration by CME-Driven Shocks—Sun to 1 AU. *Frontiers in Astronomy and Space Sciences* 9. URL: <https://www.frontiersin.org/article/10.3389/fspas.2022.801429>.
- Kozarev, K., Schwadron, N.A., Dayeh, M.A., Townsend, L.W., Desai, M.I., PourArsalan, M., 2010. Modeling the 2003 Halloween events with EMMREM: Energetic particles, radial gradients, and coupling to MHD. *Space Weather* 8, S00E08.
- Kozarev, K.A., Davey, A., Kendrick, A., Hammer, M., Keith, C., 2017. The Coronal Analysis of SHocks and Waves (CASHw) framework. *J. Space Weather Space Clim.* 7, A32.
- Kozarev, K.A., Dayeh, M.A., Farahat, A., 2019. Early-stage Solar Energetic Particle Acceleration by Coronal Mass Ejection-driven Shocks with Realistic Seed Spectra. I. Low Corona. *Astrophys. J.* 871 (1), 65.
- Kozarev, K.A., Evans, R.M., Schwadron, N.A., Dayeh, M.A., Opher, M., Korreck, K.E., van der Holst, B., 2013. Global Numerical Modeling of Energetic Proton Acceleration in a Coronal Mass Ejection Traveling through the Solar Corona. *Astrophys. J.* 778 (1), 43.
- Kozarev, K.A., Schwadron, N.A., 2016. A Data-driven Analytic Model for Proton Acceleration by Large-scale Solar Coronal Shocks. *Astrophys. J.* 831 (2), 120.
- Kruglanski, M., Crosby, N., Devos, A., Perry, C., Borries, C., Martini, D., Luntama, J.-P., 07 2016. Services for space mission support within the esa space situational awareness space weather service network.
- Krymsky, G.F., 1977. A regular mechanism for the acceleration of charged particles on the front of a shock wave. *Soviet Physics-Doklady* 234, 1306.
- Kühl, P., Heber, B., Gómez-Herrero, R., Malandraki, O., Posner, A., Sierks, H., 2020. The Electron Proton Helium Instrument as an example for a Space Weather Radiation Instrument. *J. Space Weather Space Clim.* 10, 53.
- Lario, D., 2005. Advances in modeling gradual solar energetic particle events. *Adv. Space Res.* 36 (12), 2279–2288.
- Lario, D., Kwon, R.Y., Balmaceda, L., Richardson, I.G., Krupar, V., Thompson, B.J., Cyr, O.C.S., Zhao, L., Zhang, M., 2020. Fast and Wide CMEs without Observed  $>20$  MeV Protons. *Astrophys. J.* 889 (2), 92.
- Lario, D., Sanahuja, B., Heras, A.M., 1998. Energetic Particle Events: Efficiency of Interplanetary Shocks as 50 keV  $< E < 100$  MeV Proton Accelerators. *Astrophys. J.* 509 (1), 415–434.
- Laurenza, M., Alberti, T., Cliver, E.W., 2018. A Short-term ESPERTA-based Forecast Tool for Moderate-to-extreme Solar Proton Events. *Astrophys. J.* 857 (2), 107.
- Laurenza, M., Cliver, E.W., Hewitt, J., Storini, M., Ling, A.G., Balch, C. C., Kaiser, M.L., 2009. A technique for short-term warning of solar energetic particle events based on flare location, flare size, and evidence of particle escape. *Space Weather* 7 (4), S04008.
- Lavasa, E., Giannopoulos, G., Papaioannou, A., Anastasiadis, A., Daglis, I.A., Aran, A., Pacheco, D., Sanahuja, B., 2021. Assessing the Predictability of Solar Energetic Particles with the Use of Machine Learning Techniques. *Sol. Phys.* 296 (7), 107.
- le Roux, J.A., Webb, G.M., 2009. Time-Dependent Acceleration of Interstellar Pickup Ions at the Heliospheric Termination Shock Using a Focused Transport Approach. *Astrophys. J.* 693 (1), 534–551.
- Leblanc, Y., Dulk, G.A., Bougeret, J.-L., 1998. Tracing the Electron Density from the Corona to 1au. *Sol. Phys.* 183 (1), 165–180.
- LeCun, Y., Bengio, Y., 1998. Convolutional networks for images, speech, and time series. In: Arbib, M.A. (Ed.), *The Handbook of Brain Theory and Neural Networks*. MIT Press, Cambridge, MA, USA, pp. 255–258.
- Lee, M.A., Fisk, L.A., 1981. The role of particle drifts in solar modulation. *Astrophys. J.* 248, 836–844.
- Li, G., Jin, M., Ding, Z., Bruno, A., de Nolfo, G.A., Randol, B.M., Mays, L., Ryan, J., Lario, D., 2021. Modeling the 2012 May 17 Solar Energetic Particle Event Using the AWSoM and iPATH Models. *Astrophys. J.* 919 (2), 146.
- Liemohn, M.W., Shane, A.D., Azari, A.R., Petersen, A.K., Swiger, B.M., Mukhopadhyay, A., 2021. RMSE is not enough: Guidelines to robust data-model comparisons for magnetospheric physics. *J. Atmos. Solar-Terr. Phys.* 218, 105624.
- Linker, J.A., Caplan, R.M., Downs, C., Riley, P., Mikić, Z., Lionello, R., Henney, C.J., Arge, C.N., Liu, Y., Derosa, M.L., Yeates, A., Owens, M.J., 2017. The Open Flux Problem. *Astrophys. J.* 848 (1), 70.
- Linker, J.A., Caplan, R.M., Schwadron, N., Gorbby, M., Downs, C., Torok, T., Lionello, R., Wijaya, J., 2019. Coupled MHD-Focused Transport Simulations for Modeling Solar Particle Events. *J. Phys. Conf. Ser.* 1225, 012007.
- Linker, J.A., Mikić, Z., Riley, P., Downs, C., Lionello, R., Henney, C., Arge, C.N., Jun. 2013. Coronal and heliospheric modeling using flux-evolved maps. In: Zank, G.P., Borovsky, J., Bruno, R., Cirtain, J., Cranmer, S., Elliott, H., Giacalone, J., Gonzalez, W., Li, G., Marsch, E., Moebius, E., Pogorelov, N., Spann, J., Verkhoglyadova, O. (Eds.), *Solar Wind 13*. Vol. 1539 of American Institute of Physics Conference Series. pp. 26–29.
- Lionello, R., Linker, J.A., Mikić, Z., 2009. Multispectral Emission of the Sun During the First Whole Sun Month: Magnetohydrodynamic Simulations. *Astrophys. J.* 690 (1), 902–912.
- Long, D.M., Reid, H.A.S., Valori, G., O’Kane, J., 2021. Localized Acceleration of Energetic Particles by a Weak Shock in the Solar Corona. *Astrophys. J.* 921 (1), 61.
- Luhmann, J.G., Ledvina, S.A., Krauss-Varban, D., Odstrcil, D., Riley, P., 2007. A heliospheric simulation-based approach to SEP source and transport modeling. *Adv. Space Res.* 40 (3), 295–303.
- Luhmann, J.G., Ledvina, S.A., Odstrcil, D., Owens, M.J., Zhao, X.P., Liu, Y., Riley, P., 2010. Cone model-based SEP event calculations for applications to multipoint observations. *Adv. Space Res.* 46 (1), 1–21.
- Luhmann, J.G., Mays, M.L., Odstrcil, D., Li, Y., Bain, H., Lee, C.O., Galvin, A.B., Mewaldt, R.A., Cohen, C.M.S., Leske, R.A., Larson, D., Futaana, Y., 2017. Modeling solar energetic particle events using ENLIL heliosphere simulations. *Space Weather* 15 (7), 934–954.
- Machol, J., Codrescu, S., Peck, C., 2021. User’s Guide for GOES-R XRS L2 Products. URL: [https://data.ngdc.noaa.gov/platforms/solar-space-observing-satellites/goes/goes16/l2/docs/GOES-R\\_XRS\\_L2\\_Data\\_Users\\_Guide.pdf](https://data.ngdc.noaa.gov/platforms/solar-space-observing-satellites/goes/goes16/l2/docs/GOES-R_XRS_L2_Data_Users_Guide.pdf).

- Mäkelä, P., Gopalswamy, N., Akiyama, S., Xie, H., Yashiro, S., 2015. Estimating the Height of CMEs Associated with a Major SEP Event at the Onset of the Metric Type II Radio Burst during Solar Cycles 23 and 24. *Astrophys. J.* 806 (1), 13.
- Malandraki, O., Heber, B., Kuehl, P., Núñez, M., Posner, A., Karavolos, M., Milas, N., May 2020. Solar Particle Radiation Storms Forecasting and Analysis - The HESPERIA tools. In: EGU General Assembly Conference Abstracts. EGU General Assembly Conference Abstracts. p. 8298.
- Malandraki, O.E., Crosby, N.B. (Eds.), Jan. 2018. Solar Particle Radiation Storms Forecasting and Analysis: The HESPERIA HORIZON 2020 Project and Beyond. Vol. 444 of *Astrophysics and Space Science Library*.
- Manchester, W.B., I., Gombosi, T.I., De Zeeuw, D.L., Sokolov, I.V., Roussev, I.I., Powell, K.G., Kóta, J., Tóth, G., Zurbuchen, T.H., Apr. 2005. Coronal Mass Ejection Shock and Sheath Structures Relevant to Particle Acceleration. *Astrophys. J.* 622 (2), 1225–1239.
- Manchester, W.B., I., van der Holst, B., Lavraud, B., Jun. 2014. Flux rope evolution in interplanetary coronal mass ejections: the 13 May 2005 event. *Plasma Phys. Control. Fusion* 56 (6), 064006.
- Manchester, W.B., I., van der Holst, B., Tóth, G., Gombosi, T.I., 2012. The Coupled Evolution of Electrons and Ions in Coronal Mass Ejection-driven shocks. *Astrophys. J.* 756 (1), 81.
- Manchester, Ward, I., Van Der Holst, B., 2017. The Interaction of Coronal Mass Ejections with Alfvénic Turbulence. *J. Phys. Conf. Ser.* 900, 012015.
- Manchester, Ward B., I., Vourlidas, A., Tóth, G., Lugaz, N., Roussev, I. I., Sokolov, I.V., Gombosi, T.I., De Zeeuw, D.L., Opher, M., 2008. Three-dimensional MHD Simulation of the 2003 October 28 Coronal Mass Ejection: Comparison with LASCO Coronagraph Observations. *Astrophys. J.* 684 (2), 1448–1460.
- Manchester, W.B., Gombosi, T.I., Roussev, I., de Zeeuw, D.L., Sokolov, I.V., Powell, K.G., Tóth, G., Opher, M., 2004. Three-dimensional MHD simulation of a flux rope driven CME. *J. Geophys. Res.* 109 (A1), A01102.
- Marsh, M.S., Dalla, S., Dierckxsens, M., Laitinen, T., Crosby, N.B., 2015. SPARX: A modeling system for Solar Energetic Particle Radiation Space Weather forecasting. *Space Weather* 13 (6), 386–394.
- Marsh, M.S., Dalla, S., Kelly, J., Laitinen, T., 2013. Drift-induced Perpendicular Transport of Solar Energetic Particles. *Astrophys. J.* 774 (1), 4.
- Martens, P.C., Angryk, R.A., Aug. 2018. Data Handling and Assimilation for Solar Event Prediction. In: Foullon, C., Malandraki, O.E. (Eds.), *Space Weather of the Heliosphere: Processes and Forecasts*. Vol. 335. pp. 344–347.
- Matthaeus, W.H., Qin, G., Bieber, J.W., Zank, G.P., 2003. Nonlinear Collisionless Perpendicular Diffusion of Charged Particles. *Astrophys. J. Lett.* 590 (1), L53–L56.
- Mays, M.L., Taktakishvili, A., Pulkkinen, A., MacNeice, P.J., Rastätter, L., Odstrcil, D., Jian, L.K., Richardson, I.G., LaSota, J.A., Zheng, Y., Kuznetsova, M.M., 2015. Ensemble Modeling of CMEs Using the WSA-ENLIL+Cone Model. *Sol. Phys.* 290 (6), 1775–1814.
- McCullagh, P., Nelder, J.A., 1983. *Generalized Linear Models*. Chapman and Hall, London.
- Mikić, Z., Downs, C., Linker, J.A., Caplan, R.M., Mackay, D.H., Upton, L.A., Riley, P., Lionello, R., Török, T., Titov, V.S., Wijaya, J., Druckmüller, M., Pasachoff, J.M., Carlos, W., 2018. Predicting the corona for the 21 August 2017 total solar eclipse. *Nat. Astron.* 2, 913–921.
- Mikić, Z., Linker, J.A., Schnack, D.D., Lionello, R., Tarditi, A., 1999. Magnetohydrodynamic modeling of the global solar corona. *Phys. Plasmas* 6 (5), 2217–2224.
- Millward, G., Biesecker, D., Pizzo, V., de Koning, C.A., 2013. An operational software tool for the analysis of coronagraph images: Determining CME parameters for input into the WSA-Enlil heliospheric model. *Space Weather* 11 (2), 57–68.
- Miteva, R., Samwel, S.W., Krupar, V., 2017. Solar energetic particles and radio burst emission. *J. Space Weather Space Clim.* 7, A37.
- Müller-Mellin, R., Kunow, H., Fleißner, V., Pehlke, E., Rode, E., Röschmann, N., Scharmberg, C., Sierks, H., Rusznyak, P., McKenna-Lawlor, S., Elenndt, I., Sequeiros, J., Meziat, D., Sanchez, S., Medina, J., Del Peral, L., Witte, M., Marsden, R., Henrion, J., 1995. COSTEP - Comprehensive Suprathermal and Energetic Particle Analyser. *Sol. Phys.* 162 (1–2), 483–504.
- National Science & Technology Council, 2019. National Space Weather Strategy and Action Plan. URL: <https://trumpwhitehouse.archives.gov/wp-content/uploads/2019/03/National-Space-Weather-Strategy-and-Action-Plan-2019.pdf>.
- Neergaard Parker, L., Zank, G.P., 2012. Particle Acceleration at Quasi-parallel Shock Waves: Theory and Observations at 1 AU. *Astrophys. J.* 757 (1), 97.
- Nelson, G.J., Melrose, D.B., 1985. Type II bursts. In: McLean, D.J., Labrum, N.R. (Eds.), *Solar Radiophysics: Studies of Emission from the Sun at Metre Wavelengths*. pp. 333–359.
- Núñez, M., 2011. Predicting solar energetic proton events ( $E > 10$  MeV). *Space Weather* 9 (7), S07003.
- Núñez, M., 2015. Real-time prediction of the occurrence and intensity of the first hours of  $>100$  MeV solar energetic proton events. *Space Weather* 13 (11), 807–819.
- Núñez, M., 2022. Evaluation of the UMASEP-10 Version 2 Tool for Predicting All  $>10$  MeV SEP Events of Solar Cycles 22, 23 and 24. *Universe* 8 (1), 35.
- Núñez, M., Paul-Pena, D., 2020. Predicting  $>10$  MeV SEP Events from Solar Flare and Radio Burst Data. *Universe* 6 (10), 161.
- Núñez, M., Reyes-Santiago, P.J., Malandraki, O.E., 2017. Real-time prediction of the occurrence of GLE events. *Space Weather* 15 (7), 861–873.
- Odstrcil, D., 2003. Modeling 3-d solar wind structure. *Advances in Space Research* 32 (4), 497–506, heliosphere at Solar Maximum. URL: <https://www.sciencedirect.com/science/article/pii/S0273117703003326>.
- Odstrcil, D., Riley, P., Zhao, X.P., 2004. Numerical simulation of the 12 May 1997 interplanetary cme event. *J. Geophys. Res.: Space Phys.* 109 (A2), URL <https://agupubs.onlinelibrary.wiley.com/doi/abs/10.1029/2003JA010135>.
- Ontiveros, V., Vourlidas, A., 2009. Quantitative Measurements of Coronal Mass Ejection-Driven Shocks from LASCO Observations. *Astrophys. J.* 693 (1), 267–275.
- Opgenoorth, H.J., Wimmer-Schweingruber, R.F., Belehaki, A., Berghmans, D., Hapgood, M., Hesse, M., Kauristie, K., Lester, M., Lilensten, J., Messerotti, M., Temmer, M., 2019. Assessment and recommendations for a consolidated European approach to space weather - as part of a global space weather effort. *J. Space Weather Space Clim.* 9, A37.
- Pacheco, D., 2019. Analysis and modelling of the solar energetic particle radiation environment in the inner heliosphere in preparation for Solar Orbiter. Ph.D. thesis, Universitat de Barcelona, Barcelona, Spain. URL: <http://hdl.handle.net/10803/667033>.
- Palmerio, E., Lee, C.O., Mays, M.L., Luhmann, J.G., Lario, D., Sánchez-Cano, B., Richardson, I.G., Vainio, R., Stevens, M.L., Cohen, C.M.S., Steinvall, K., Möstl, C., Weiss, A.J., Nieves-Chinchilla, T., Li, Y., Larson, D.E., Heyner, D., Bale, S.D., Galvin, A.B., Holmström, M., Khotyaintsev, Y.V., Maksimovic, M., Mitrofanov, I.G., 2022. CMEs and SEPs During November–December 2020: A Challenge for Real-Time Space Weather Forecasting. *Space Weather* 20 (5), e2021SW002993.
- Papaioannou, A., Anastasiadis, A., Kouloumvakos, A., Paassilta, M., Vainio, R., Valtonen, E., Belov, A., Eroshenko, E., Abunina, M., Abunin, A., 2018. Nowcasting Solar Energetic Particle Events Using Principal Component Analysis. *Sol. Phys.* 293 (7), 100.
- Papaioannou, A., Anastasiadis, A., Sandberg, I., Georgoulis, M.K., Tsiropoula, G., Tziotziou, K., Jiggins, P., Hilgers, A., 2015. A Novel Forecasting System for Solar Particle Events and Flares (FORSPF). *J. Phys. Conf. Ser.* 632, 012075.
- Papaioannou, A., Sandberg, I., Anastasiadis, A., Kouloumvakos, A., Georgoulis, M.K., Tziotziou, K., Tsiropoula, G., Jiggins, P., Hilgers,

- A., 2016. Solar flares, coronal mass ejections and solar energetic particle event characteristics. *J. Space Weather Space Clim.* 6, A42.
- Papaioannou, A., Vainio, R., Raukunen, O., Jiggins, P., Aran, A., Dierckxsens, M., Mallios, S.A., Paassilta, M., Anastasiadis, A., 2022. The probabilistic solar particle event forecasting (PROSPER) model. *J. Space Weather Space Clim.* 12, 24.
- Parker, E.N., 1958. Dynamics of the Interplanetary Gas and Magnetic Fields. *Astrophys. J.* 128, 664.
- Parker, E.N., 1965. Dynamical Theory of the Solar Wind. *Space Sci. Rev.* 4 (5–6), 666–708.
- Poedts, S., Kochanov, A., Lani, A., Scolini, C., Verbeke, C., Hosteaux, S., Chané, E., Deconinck, H., Mihalache, N., Diet, F., Heynderickx, D., De Keyser, J., De Donder, E., Crosby, N.B., Echim, M., Rodriguez, L., Vansintjan, R., Verstringe, F., Mampaey, B., Horne, R., Glauert, S., Jiggins, P., Keil, R., Glover, A., Deprez, G., Luntama, J.-P., 2020. The Virtual Space Weather Modelling Centre. *J. Space Weather Space Clim.* 10, 14.
- Pomoell, J., Aran, A., Jacobs, C., Rodríguez-Gasén, R., Poedts, S., Sanahuja, B., 2015. Modelling large solar proton events with the shock-and-particle model. Extraction of the characteristics of the MHD shock front at the cobpoint. *J. Space Weather Space Clim.* 5, A12.
- Pomoell, J., Poedts, S., 2018. EUHFORIA: European heliospheric forecasting information asset. *J. Space Weather Space Clim.* 8, A35.
- Posner, A., 2007. Up to 1-hour forecasting of radiation hazards from solar energetic ion events with relativistic electrons. *Space Weather* 5 (5), 05001.
- Posner, A., Arge, C.N., Staub, J., StCyr, O.C., Folta, D., Solanki, S.K., Strauss, R.D.T., Effenberger, F., Gandorfer, A., Heber, B., Henney, C. J., Hirzberger, J., Jones, S.I., Kühl, P., Malandraki, O., Sterken, V.J., 2021. A Multi-Purpose Heliophysics L4 Mission. *Space Weather* 19 (9), e2021SW002777.
- Posner, A., Strauss, R.D., 2020. Warning Time Analysis From SEP Simulations of a Two-Tier REleASE System Applied to Mars Exploration. *Space Weather* 18 (4), e2019SW002354.
- Quinn, P.R., Schwadron, N.A., Möbius, E., 2016. Transport of Helium Pickup Ions within the Focusing Cone: Reconciling STEREO Observations with IBEX. *Astrophys. J.* 824 (2), 142.
- Quinn, P.R., Schwadron, N.A., Möbius, E., 2019. Inner Source Pickup Ions from Chondritic Smooth Interplanetary Dust Particles. *Astrophys. J.* 877 (2), 156.
- Quinn, P.R., Schwadron, N.A., Möbius, E., Taut, A., Berger, L., 2018. Inner Source C<sup>+</sup>/O<sup>+</sup> Pickup Ions Produced by Solar Wind Recycling, Neutralization, Backscattering, Sputtering, and Sputtering-induced Recycling. *Astrophys. J.* 861 (2), 98.
- Quinn, P.R., Schwadron, N.A., Townsend, L.W., Wimmer-Schweingruber, R.F., Case, A.W., Spence, H.E., Wilson, J.K., Joyce, C.J., 2017. Modeling the effectiveness of shielding in the earth-moon-mars radiation environment using PREDICCS: five solar events in 2012. *J. Space Weather Space Clim.* 7, A16.
- Rastätter, L., Wiegand, C.P., Mullinix, R.E., MacNeice, P.J., 2019. Comprehensive Assessment of Models and Events Using Library Tools (CAMEL) Framework: Time Series Comparisons. *Space Weather* 17 (6), 845–860.
- Reames, D.V., 2004. Solar energetic particle variations. *Adv. Space Res.* 34 (2), 381–390.
- Reames, D.V., 2017. *Sol. Energetic Particles.* 932.
- Richardson, I.G., Mays, M.L., Thompson, B.J., 2018. Prediction of Solar Energetic Particle Event Peak Proton Intensity Using a Simple Algorithm Based on CME Speed and Direction and Observations of Associated Solar Phenomena. *Space Weather* 16 (11), 1862–1881.
- Richardson, I.G., von Rosenvinge, T.T., Cane, H.V., 2015. The Properties of Solar Energetic Particle Event-Associated Coronal Mass Ejections Reported in Different CME Catalogs. *Sol. Phys.* 290 (6), 1741–1759.
- Richardson, I.G., von Rosenvinge, T.T., Cane, H.V., Christian, E.R., Cohen, C.M.S., Labrador, A.W., Leske, R.A., Mewaldt, R.A., Wiedenbeck, M.E., Stone, E.C., 2014. > 25 MeV Proton Events Observed by the High Energy Telescopes on the STEREO A and B Spacecraft and/or at Earth During the First Seven Years of the STEREO Mission. *Sol. Phys.* 289 (8), 3059–3107.
- Riley, P., Linker, J.A., Lionello, R., Mikić, Z., 2012. Corotating interaction regions during the recent solar minimum: The power and limitations of global MHD modeling. *J. Atmos. Solar-Terr. Phys.* 83, 1–10.
- Rodríguez, J.V., Sandberg, I., Mewaldt, R.A., Daglis, I.A., Jiggins, P., 2017. Validation of the effect of cross-calibrated GOES solar proton effective energies on derived integral fluxes by comparison with STEREO observations. *Space Weather* 15 (2), 290–309.
- Rodríguez-Gasén, R., Aran, A., Sanahuja, B., Jacobs, C., Poedts, S., 2011. Why should the latitude of the observer be considered when modeling gradual proton events? An insight using the concept of cobpoint. *Adv. Space Res.* 47, 2140–2151.
- Rodríguez-Gasén, R., Aran, A., Sanahuja, B., Jacobs, C., Poedts, S., 2014. Variation of Proton Flux Profiles with the Observer's Latitude in Simulated Gradual SEP Events. *Sol. Phys.* 289 (5), 1745–1762.
- Roelof, E.C., 1969. Propagation of Solar Cosmic Rays in the Interplanetary Magnetic Field. In: Ögelman, H., Wayland, J.R. (Eds.), *Lectures in High-Energy Astrophysics.* p. 111.
- Roussev, I., 2008. Eruptive events in the solar atmosphere: new insights from theory and 3-D numerical modelling. *Contemp. Phys.* 49 (4), 237–254.
- Roussev, I.I., Sokolov, I.V., Forbes, T.G., Gombosi, T.I., Lee, M.A., Sakai, J.I., 2004. A Numerical Model of a Coronal Mass Ejection: Shock Development with Implications for the Acceleration of GeV Protons. *Astrophys. J. Lett.* 605 (1), L73–L76.
- Ruffolo, D., 1995. Effect of Adiabatic Deceleration on the Focused Transport of Solar Cosmic Rays. *Astrophys. J.* 442, 861.
- Sachdeva, N., van der Holst, B., Manchester, W.B., Tóth, G., Chen, Y., Lloveras, D.G., Vázquez, A.M., Lamy, P., Wojak, J., Jackson, B.V., Yu, H.-S., Henney, C.J., 2019. Validation of the Alfvén Wave Solar Atmosphere Model (AWSOM) with Observations from the Low Corona to 1 au. *Astrophys. J.* 887 (1), 83.
- Sadykov, V., Kosovichev, A., Kitiashvili, I., Oria, V., Nita, G.M., Illarionov, E., O'Keefe, P., Jiang, Y., Ferreira, S., Ali, A., 2021. Prediction of Solar Proton Events with Machine Learning: Comparison with Operational Forecasts and “All-Clear” Perspectives. arXiv:2107.03911.
- Sandberg, I., Jiggins, P., Heynderickx, D., Daglis, I.A., 2014. Cross calibration of NOAA GOES solar proton detectors using corrected NASA IMP-8/GME data. *Geophys. Res. Lett.* 41 (13), 4435–4441.
- Scherrer, P.H., Bogart, R.S., Bush, R.I., Hoeksema, J.T., Kosovichev, A. G., Schou, J., Rosenberg, W., Springer, L., Tarbell, T.D., Title, A., Wolfson, C.J., Zayer, I., MDI Engineering Team, 1995. The Solar Oscillations Investigation - Michelson Doppler Imager. *Sol. Phys.* 162 (1–2), 129–188.
- Schwadron, N.A., Gorby, M., Török, T., Downs, C., Linker, J., Lionello, R., Mikić, Z., Riley, P., Giacalone, J., Chandran, B., Germaschewski, K., Isenberg, P.A., Lee, M.A., Lugaz, N., Smith, S., Spence, H.E., Desai, M., Kasper, J., Kozarev, K., Korreck, K., Stevens, M., Cooper, J., MacNeice, P., 2014. Synthesis of 3-D Coronal-Solar Wind Energetic Particle Acceleration Modules. *Space Weather* 12 (6), 323–328.
- Schwadron, N.A., Townsend, L., Kozarev, K., Dayeh, M.A., Cucinotta, F., Desai, M., Golightly, M., Hassler, D., Hatcher, R., Kim, M.Y., Posner, A., PourArsalan, M., Spence, H.E., Squier, R.K., 2010. Earth-Moon-Mars Radiation Environment Module framework. *Space Weather* 8 (10), S00E02.
- Shea, M.A., Smart, D.F., 1990. A Summary of Major Solar Proton Events. *Sol. Phys.* 127 (2), 297–320.
- Skilling, J., 1971. Cosmic Rays in the Galaxy: Convection or Diffusion? *Astrophys. J.* 170, 265.
- Smart, D.F., Shea, M.A., 1979. PPS76: A computerized event mode solar proton forecasting technique. In: Donnelly, R.F. (Ed.), *NOAA Solar-Terrestrial Predictions Proceedings. Volume 1.* Vol. 1. pp. 406–427.
- Smart, D.F., Shea, M.A., 1989. PPS-87: A new event oriented solar proton prediction model. *Adv. Space Res.* 9 (10), 281–284.



- Smart, D.F., Shea, M.A., 1992. Modeling the time-intensity profile of solar flare generated particle fluxes in the inner heliosphere. *Adv. Space Res.* 12 (2–3), 303–312.
- Sokolov, I.V., Holst, B.v.d., Manchester, W.B., Su Ozturk, D.C., Szente, J., Taktakishvili, A., Tóth, G., Jin, M., Gombosi, T.I., 2021. Threaded-field-line Model for the Low Solar Corona Powered by the Alfvén Wave Turbulence. *Astrophys. J.* 908 (2), 172.
- Sokolov, I.V., Roussev, I.I., Gombosi, T.I., Lee, M.A., Kóta, J., Forbes, T.G., Manchester, W.B., Sakai, J.I., 2004. A New Field Line Advection Model for Solar Particle Acceleration. *Astrophys. J. Lett.* 616 (2), L171–L174.
- Sokolov, I.V., van der Holst, B., Oran, R., Downs, C., Roussev, I.I., Jin, M., Manchester, Ward B., 2013. Magnetohydrodynamic Waves and Coronal Heating: Unifying Empirical and MHD Turbulence Models. *Astrophys. J.* 764 (1), 23.
- Souvatzoglou, G., Papaioannou, A., Mavromichalaki, H., Dimitroulakos, J., Sarlanis, C., 2014. Optimizing the real-time ground level enhancement alert system based on neutron monitor measurements: Introducing GLE Alert Plus. *Space Weather* 12 (11), 633–649.
- Steyn, R., Strauss, D.T., Effenberger, F., Pacheco, D., 2020. The soft X-ray Neupert effect as a proxy for solar energetic particle injection. A proof-of-concept physics-based forecasting model. *J. Space Weather Space Clim.* 10, 64.
- Strauss, R.D., Dresing, N., Kollhoff, A., Brüder, M., 2020. On the Shape of SEP Electron Spectra: The Role of Interplanetary Transport. *Astrophys. J.* 897 (1), 24.
- Strauss, R.D., Fichtner, H., 2015. On Aspects Pertaining to the Perpendicular Diffusion of Solar Energetic Particles. *Astrophys. J.* 801 (1), 29.
- Strauss, R.D., le Roux, J.A., 2019. Solar Energetic Particle Propagation in Wave Turbulence and the Possibility of Wave Generation. *Astrophys. J.* 872 (2), 125.
- Strauss, R.D.T., Dresing, N., Engelbrecht, N.E., 2017. Perpendicular Diffusion of Solar Energetic Particles: Model Results and Implications for Electrons. *Astrophys. J.* 837 (1), 43.
- Stumpo, M., Benella, S., Laurenza, M., Alberti, T., Consolini, G., Marcucci, M.F., 2021. Open Issues in Statistical Forecasting of Solar Proton Events: A Machine Learning Perspective. *Space Weather* 19 (10), e2021SW002794.
- Sun, X., Liu, Y., Hoeksema, J.T., Hayashi, K., Zhao, X., 2011. A New Method for Polar Field Interpolation. *Sol. Phys.* 270 (1), 9–22.
- Tenishev, V., Roussev, I., Sokolov, I., Tylka, A., Gombosi, T., 2005. An Integrated CME-SEP Numerical Investigation of the 1998 May 1–2 CME Events Part III: SEP Abundance and Variability at IAU. In: AGU Fall Meeting Abstracts. Vol. 2005. pp. SH23A–0327.
- Tenishev, V., Shou, Y., Borovikov, D., Lee, Y., Fougere, N., Michael, A., Combi, M.R., 2021. Application of the Monte Carlo Method in Modeling Dusty Gas, Dust in Plasma, and Energetic Ions in Planetary, Magnetospheric, and Heliospheric Environments. *J. Geophys. Res.: Space Phys.* 126 (2), e2020JA028242.
- Titov, V.S., Downs, C., Mikić, Z., Török, T., Linker, J.A., Caplan, R.M., 2018. Regularized Biot-Savart Laws for Modeling Magnetic Flux Ropes. *Astrophys. J. Lett.* 852 (2), L21.
- Titov, V.S., Török, T., Mikić, Z., Linker, J.A., 2014. A Method for Embedding Circular Force-free Flux Ropes in Potential Magnetic Fields. *Astrophys. J.* 790 (2), 163.
- Török, T., Downs, C., Linker, J.A., Lionello, R., Titov, V.S., Mikić, Z., Riley, P., Caplan, R.M., Wijaya, J., 2018. Sun-to-Earth MHD Simulation of the 2000 July 14 “Bastille Day” Eruption. *Astrophys. J.* 856 (1), 75.
- Torsti, J., Valtonen, E., Lumme, M., Peltonen, P., Eronen, T., Louhola, M., Riihonen, E., Schultz, G., Teittinen, M., Ahola, K., Holmlund, C., Kelh , V., Lepp , K., Ruuska, P., Str mmer, E., 1995. Energetic Particle Experiment ERNE. *Sol. Phys.* 162 (1–2), 505–531.
- Toth, G., 1996. A General Code for Modeling Mild Flows on Parallel Computers: VersatileAdvection Code. In: Uchida, Y., Kosugi, T., Hudson, H.S. (Eds.), *IAU Colloq. 153: Magnetodynamic Phenomena in the Solar Atmosphere - Prototypes of Stellar Magnetic Activity*. p. 471.
- Tylka, A.J., Lee, M.A., 2006. A model for spectral and compositional variability at high energies in large, gradual solar particle events 646 (2), 1319–1334. <https://doi.org/10.1086/505106>.
- Valtonen, E., Riihonen, E., Lehtinen, I.-V., 2009. Solar energetic particle fluences from SOHO/ERNE. *Acta Geophys.* 57 (1), 116–124.
- van den Berg, J., Strauss, D.T., Effenberger, F., 2020. A Primer on Focused Solar Energetic Particle Transport. *Space Sci. Rev.* 216 (8), 146.
- van den Berg, J.P., Engelbrecht, N.E., Wijzen, N., Strauss, R.D., 2021. On the Turbulent Reduction of Drifts for Solar Energetic Particles. *Astrophys. J.* 922 (2), 200.
- van der Holst, B., Jacobs, C., Poedts, S., 2007. Simulation of a Breakout Coronal Mass Ejection in the Solar Wind. *Astrophys. J. Lett.* 671 (1), L77–L80.
- van der Holst, B., Manchester, W., I., Sokolov, I.V., Tóth, G., Gombosi, T.I., DeZeeuw, D., Cohen, O., 2009. Breakout Coronal Mass Ejection or Streamer Blowout: The Bugle Effect. *Astrophys. J.* 693 (2), 1178–1187.
- van der Holst, B., Sokolov, I.V., Meng, X., Jin, M., Manchester, W.B., I., Tóth, G., Gombosi, T.I., 2014. Alfvén Wave Solar Model (AWSoM): Coronal Heating. *Astrophys. J.* 782 (2), 81.
- Van Hollebeke, M.A.I., Ma Sung, L.S., McDonald, F.B., 1975. The Variation of Solar Proton Energy Spectra and Size Distribution with Heliolongitude. *Sol. Phys.* 41 (1), 189–223.
- von Rosenvinge, T.T., Reames, D.V., Baker, R., Hawk, J., Nolan, J.T., Ryan, L., Shuman, S., Wortman, K.A., Mewaldt, R.A., Cummings, A. C., Cook, W.R., Labrador, A.W., Leske, R.A., Wiedenbeck, M.E., 2008. The High Energy Telescope for STEREO. *Space Sci. Rev.* 136 (1–4), 391–435.
- Vourlidas, A., Turner, D., Biesecker, D., Coster, A., Engell, A., Ho, G., Immel, T., Keys, C., Lanzerotti, L., Lu, G., Lugaz, N., Luhmann, J., Mays, L., O’Brien, P., Semones, E., Spence, H., Upton, L., White, S., 2021. Space Weather Science and Observation Gap Analysis for the National Aeronautics and Space Administration (NASA): A Report to NASA’s Space Weather Science Application Program. Tech. rep., Johns Hopkins University Applied Physics Laboratory. URL: [https://science.nasa.gov/science-pink/s3fs-public/atoms/files/GapAnalysisReport\\_full\\_final.pdf](https://science.nasa.gov/science-pink/s3fs-public/atoms/files/GapAnalysisReport_full_final.pdf).
- Wijzen, N., 2020. Paradise: a model for energetic particle transport in the solar wind. Ph.D. thesis, KU Leuven (Belgium) and Univ. Barcelona (Spain). URL: <https://lirias.kuleuven.be/retrieve/573330>.
- Wijzen, N., Aran, A., Pomoell, J., Poedts, S., 2019a. Interplanetary spread of solar energetic protons near a high-speed solar wind stream. *Astron. Astroph.* 624, A47.
- Wijzen, N., Aran, A., Pomoell, J., Poedts, S., 2019b. Modelling three-dimensional transport of solar energetic protons in a corotating interaction region generated with EUHFORIA. *Astron. Astroph.* 622, A28.
- Wijzen, N., Aran, A., Sanahuja, B., Pomoell, J., Poedts, S., 2020. The effect of drifts on the decay phase of SEP events. *Astron. Astroph.* 634, A82.
- Wijzen, N., Aran, A., Scolini, C., Lario, D., Afanasiev, A., Vainio, R., Sanahuja, B., Pomoell, J., Poedts, S., 2022. Observation-based modelling of the energetic storm particle event of 14 July 2012. *Astron. Astroph.* 659, A187.
- Wijzen, N., Samara, E., Aran, A., Lario, D., Pomoell, J., Poedts, S., 2021. A Self-consistent Simulation of Proton Acceleration and Transport Near a High-speed Solar Wind Stream. *Astrophys. J. Lett.* 908 (2), L26.
- Wild, J.P., Smerd, S.F., Weiss, A.A., 1963. Solar Bursts. *Annu. Rev. Astron. Astrophys.* 1, 291.
- Winter, L.M., Ledbetter, K., 2015. Type II and Type III Radio Bursts and their Correlation with Solar Energetic Proton Events. *Astrophys. J.* 809 (1), 105.
- Wu, S.T., Dryer, M., Han, S.M., 1983. Non-Planar Magnetohydrodynamic Model for Solar Flare Generated Disturbances in the Heliospheric Equatorial Plane. *Sol. Phys.* 84 (1–2), 395–418.
- Yashiro, S., Gopalswamy, N., Akiyama, S., Michalek, G., Howard, R.A., 2005. Visibility of coronal mass ejections as a function of flare location and intensity. *J. Geophys. Res.* 110 (A12), A12S05.

- Young, M.A., Schwadron, N.A., Gorby, M., Linker, J., Caplan, R.M., Downs, C., Török, T., Riley, P., Lionello, R., Titov, V., Mewaldt, R. A., Cohen, C.M.S., 2021. Energetic Proton Propagation and Acceleration Simulated for the Bastille Day Event of 2000 July 14. *Astrophys. J.* 909 (2), 160.
- Zhang, M., 2006. Theory of energetic particle transport in the magnetosphere: A noncanonical approach. *J. Geophys. Res.* 111 (A4), A04208.
- Zhang, M., Zhao, L., 2017. Precipitation and Release of Solar Energetic Particles from the Solar Coronal Magnetic Field. *Astrophys. J.* 846 (2), 107.
- Zhao, L., Zhang, M., 2018. Effects of Coronal Magnetic Field Structures on the Transport of Solar Energetic Particles. *Astrophys. J. Lett.* 859 (2), L29.
- Zhao, L., Zhang, M., Lario, D., 2020. Modeling the Transport Processes of a Pair of Solar Energetic Particle Events Observed by Parker Solar Probe Near Perihelion. *Astrophys. J.* 898 (1), 16.
- Zucca, P., Núñez, M., Klein, K., 2017. Exploring the potential of microwave diagnostics in SEP forecasting: The occurrence of SEP events. *J. Space Weather Space Clim.* 7, A13.